Quantized vortices in superfluid ^{3}He

M. M. Salomaa

Low Temperature Laboratory, Helsinki University of Technology, SF-02150 Espoo 15, Finland

G. E. Volovik

L. D. Landau Institute for Theoretical Physics, U.S.S.R. Academy of Sciences, 117334 Moscow, Union of Soviet Socialist Republics

The first measurements on vortices in rotating superfluid ^{3}He have been conducted in the Low Temperature Laboratory at Helsinki University of Technology during the past five years. These experiments have revealed unique vortex phenomena that are not observed in any other known superfluids. In this review, the concept of broken symmetry is applied to investigate the quantized vortex lines in superfluid ^{3}He. In the superfluid A phase, vorticity can be supported by a continuous winding of the order parameter; this gives rise to continuous "coreless" vortices with two flow quanta. Novel vortices with a half-integer number of circulation quanta may also exist in ^{3}He-A due to a combined symmetry of the superfluid state. In the superfluid B phase, the vortices have a complicated core structure. The vortex-core matter is ferromagnetic and superfluid, and it displays broken parity. The ferromagnetism of the core is observed in NMR experiments due to a gyromagnetic effect. The calculated core structures exhibit an experimentally observed first-order phase transition. This vortex-core transition in rotating ^{3}He-B may be understood in terms of a change in the topology for flaring-out of the vortex singularity into higher dimensions; the topological identification further suggests that the phase transition manifests a spontaneous bifurcation of vorticity—involving half-quantum vortices in ^{3}He-B. These recent advances of interest in quantum liquids are also of general relevance to a wide range of fields beyond low-temperature physics.

CONTENTS

I. INTRODUCTION

In the superfluid phases of liquid ^{3}He occur the most complicated known vacuum states of condensed matter, in which many symmetries are simultaneously broken. These broken symmetries are manifested, especially, in the exciting physical properties of the quantized vortex lines in superfluid ^{3}He under rotation. In the A phase these properties include the occurrence of continuous vorticity in the liquid-crystal-like vortex textures and the possible occurrence of vortices with a half-integer number of circulation quanta. In both the A and B phases they include the existence of vortices in which new superfluid phases nucleate within the vortex cores, the spontaneous magnetic and electric moments of the vortices, the magnetic anisotropy of the vortices, and several other intriguing and unprecedented physical properties of the quantized vortex lines and lattices formed in superfluid ^{3}He that follow from the broken symmetries of the liquid, in conjunction with the broken symmetries of the vortex states.

In particular, the topology of quantized vortex lines in superfluid ^{3}He is fundamentally different from that of the vortex lines in superfluid ^{4}He (He II) (for reviews on vortices in He II, see, for example, Vinen, 1961; Feynman, 1964; Andronikashvili and Mamaladze, 1966). For example, the topological charge N of vortices in ^{3}He-A obeys the algebra $1+1=0$ (instead of $1+1=2$ for the He II vortices), which governs a reversible binary reaction: it may be interpreted as describing the coalescence of one singular vortex line ($N=1$) with another ($N=1$), in order to generate a continuous vortex texture ($N=0$), or the reverse "chemical" process for the dissociation of a "neutral" continuous vortex texture to emit a pair of "radicals," i.e., singular vortex lines. Moreover, in contrast to the single topological invariant that can only exist for vortices in He II—the quantum of circulation of the vortex line—in superfluid ^{3}He there can emerge several different kinds of distinct topological charges associated simultaneously with a given vortex line. This circumstance is also a consequence of the peculiar breaking of symmetry that occurs in the superfluid low-temperature phases of liquid ^{3}He.

In superfluid ^{3}He, the complicated hierarchy of interaction phenomena—such as magnetic field anisotropy, nuclear magnetic dipole-dipole interaction, competition of the superfluid condensation energy density with the gradient energy, boundary effects, and rotation-induced superflow—contributes to new possibilities for the simultaneous occurrence of a corresponding hierarchy of vortex-core structures. This means that there will emerge a rich variety of several core regimes with different length scales for vortices in ^{3}He, including regions of the hard core, the soft core, and the dipole-locked and/or dipole-unlocked vortex cores.

Vortex phenomena in superfluid ^{3}He are also rendered quite interesting from a broader point of view in physics due to the occurrence of several types of mechanisms for topological confinement, exemplified by the generation of the soliton glue that holds together the pairs of half-quantum vortex disclinations—like quarks. Another nontrivial connection to quantum field theory is provided by the hedgehog in the l-vector field (the orbital anisotropy axis in the A phase): a vortex can terminate in the bulk superfluid at an l-vector hedgehog, which forms a monopolelike object. In this context, confinement means that it is impossible to separate the hedgehog from its tail, which is a quantized vortex line attached to the monopole. This vortex line is the string that couples the two monopoles. The superflow velocity field around this object is analogous to the gauge-field distribution around the Dirac magnetic monopole (Dirac, 1931).

The complicated core structures of the ^{3}He vortices lead to the possibility of several phase transitions inside the vortex cores. These transitions can take place not only in the hard vortex core—which in ^{3}He is very large in comparison with that of the ^{4}He vortex—but also in the even more extended soft-core region of the vortex structure. This leads to several possible new phase transitions of the vortex-core matter; an interesting one has

been observed (see Fig. 1 and Sec. VII) in the NMR experiments carried out on the rotating bulk B phase of superfluid ^{3}He; it is explained in Sec. VIII.

The nontrivial vacuum state leads to a wealth of intriguing new possibilities for physical effects displayed by the elementary excitations in superfluid ^{3}He. For example, the reversal of the spin quantization axis (the **d** vector) for the ^{3}He quasiparticles encircling a half-quantum vortex line provides an analog to the transformation of a particle into its antiparticle upon circling a singular line like those postulated to exist in the grand unified theories (Schwarz, 1982). For the half-quantum vortices, analogs to the Aharonov-Bohm effect exist. Moreover, superfluid ^{3}He exemplifies the nonconservation of charge; e.g., the topological charge of a hedgehog in the magnetic anisotropy **d**-vector field in ^{3}He-A is not conserved. There also is an analog to the chiral anomaly, which leads to nonconservation of the ^{3}He quasiparticle momentum in moving vortex textures.

A new type of intercoupling of vortices in the usual three-dimensional (3D) real (**r**) and momentum (**k**) spaces occurs in superfluid ^{3}He; the superfluid can escape the real-space singularity at the vortex axis by flowing out into a higher-dimensional space (for **k** on the Fermi sphere, this space is in general five dimensional). The flaring-out of vorticity from the **r** space into the **k** space is associated with a change in the topological structure of the superfluid energy gap: point vortices appear on the Fermi surface. These "boojums on the Fermi sphere" closely resemble the point vortices (boojums) on the surface of a container at the termination point of a continuous vortex, and they play an analogous role in the dissipation of superfluid flow. Hence, vortices in superfluid ^{3}He serve to combine the order-parameter space with the topology of the Fermi surface.

Violations of parity in the cores of vortices in ^{3}He produce, as consequences, new physical properties for the vortices, such as the electric dipole moments of the vortex lines and the spontaneous mass and spin supercurrents along the vortex axis. These properties result in the emergence of corresponding new Ising-type variables for the vortices. Usually these "Ising" variables, which indicate the direction of the spontaneous electric dipole moment or the direction of the mass superflow, would be orientated up or down in the vortex lattice, at random, so that the bulk liquid would appear neutral. However, it is possible—in some cases spontaneously, in some cases through the application of certain external orientating effects—to align such Ising variables, which results in their "ferromagnetic" ordering: in this situation the bulk liquid will display broken-symmetry properties.

Combined with the broken axisymmetry of vortices, this "ferromagnetic" order can lead to a twist, such that the vortex lattice resembles cholesteric liquid crystals. The violation of parity and the breaking of axisymmetry of the vortices also lead to a distortion of the vortex lattice, such that it is not simply square or hexagonal. Due to the confinement of half-quantum vortices into pairs, or "vortex molecules," the primitive lattice cell for these vortices possesses a nontrivial basis with an internal structure, thus leading to new possible modes of oscillation for the vortex lattice.

In Sec. II we discuss the stationary superfluid phases of liquid ^{3}He: the nature of the order parameter in superfluid ^{3}He, the broken symmetries in the ordered states, and the classification of the "inert" bulk-liquid superfluid phases. The superfluidity of the A phase is considered in Sec. III, with special emphasis on the combined gauge-orbital symmetry, which leads to the intrinsic coupling of superfluid and liquid-crystal-like properties, resulting in continuous vorticity.

The topology of the A-phase vortices is described in Sec. IV, while the further symmetry classification of the vortices in ^{3}He-A within given topological classes is explained in Sec. V. The observable physical properties of the vortices are related to the breaking of discrete and axial symmetry. In particular, vortices with several core regions are discussed, and the half-quantum vortices in ^{3}He-A are introduced; the observable NMR properties of the ^{3}He-A vortices are discussed in Sec. VI.

The special physical properties of superfluid ^{3}He-B are presented in Sec. VII; the degenerate states of the order parameter are specified, the gyromagnetism of the Cooper pairs is discussed, and the NMR spectroscopy of the ^{3}He-B vortex textures is explained. This section is illustrated by experimental results and the calculated properties of textures and textural spin waves, which are modified due to the vortices, since vortices produce a magnetic anisotropy in the liquid, as well as a net spontaneous magnetization.

The novel core structures of quantized vortex lines in superfluid ^{3}He-B are treated in Sec. VIII; the breaking of parity as a discrete vortex symmetry leads to the occurrence of superfluid-core vortices with large magnetic moments and to magnetic anisotropy concentrated in the vortex core. The nontrivial superfluid core structure of the ^{3}He-B vortices results in the appearance of point vortices in the **k** space, i.e., realizations of the "boojums on the Fermi surface," thus providing examples of singular lines where vorticity escapes from real space to momentum space.

In addition, axisymmetry of the quantized vortex lines in superfluid ^{3}He-B is broken: at low pressures vortices with broken axisymmetry have been found to be energetically more favorable than any of the axisymmetric ones (see Fig. 2). Broken axisymmetry generates a new Goldstone mode for the quantized vortex line, new features of anisotropy in the vortex parameter λ (associated with the magnetic anisotropy of the vortex core), and a new topology for the flaring-out of vorticity in higher dimensions. Such new properties lead to predictions that are measurable with the use of NMR and ultrasonic techniques. These nonaxisymmetric vortices have been identified as topologically confined pairs of half-quantum vortices, analogous to quarks inside nucleons. Provided that experiments confirm this identification, vortices with half-integer circulation—initially expected to be observed in ^{3}He-A—have in fact first been found in rotating super-

fluid ^{3}He-B.

An interesting "cosmological" experiment on liquid helium was put forward recently (Zurek, 1985); the proposal consists of cooling liquid ^{4}He rapidly from normal to the superfluid state. Hereby vorticity is expected to be generated at the interfaces of the superfluid condensation fronts. It was suggested that such vortex lines may be analogous to the cosmic strings (Zel'dovich, Kobzarev, and Okun, 1974; Vilenkin, 1985) that are expected to have nucleated at the phase transitions of the early Universe. The vortices in superfluid ^{3}He are much easier to observe because of the NMR effect than those in He II, which has no net nuclear spin (vortices in He II can be observed directly only during equilibrium rotation conditions; see Packard, 1982). It is therefore possible to measure the density of vortices not only in the steady state (equilibrium rotating container), but also in the dissipative states (Paalanen and Osheroff, 1980; Hall and Hook, 1986; Sonin, 1987).

The "cosmological" experiment may be realized in superfluid ^{3}He-A and ^{3}He-B, as well. Because the A-phase vacuum has many features in common with the Higgs vacuum—and also because the vortices in ^{3}He are observable—such experiments are much more intriguing, though necessarily more difficult, to carry out on superfluid ^{3}He, which provides a more relevant analog system to grand unified theories than ^{4}He. We note that the same idea of testing cosmological theory in a condensed-matter analog experiment was first advanced in connec-

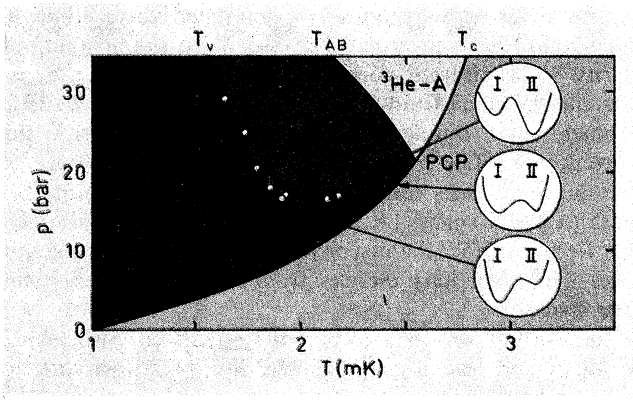

FIG. 1. Phase diagram of ^{3}He (Ahonen, Haikala, Krusius, and Lounasmaa, 1974). The intersection of the T_{AB} curve, separating the A and B phases, and the T_c curve is called the polycritical point (PCP). When superfluid ^{3}He-B was rotated in an open-volume NMR cell, a first-order vortex-core transition was observed (Ikkala, Volovik, Hakonen, Bun'kov, Islander, and Kharadze, 1982) upon crossing the dashed T_v line in the (p,T) plane. ○, $H=284$ G; ●, $H=568$ G. Note that at high pressures the core-transition temperature is roughly parallel to the A-B transition, but curves towards T_c below the polycritical pressure (Pekola, Simola, Hakonen, Krusius, Lounasmaa, Nummila, Mamniashvili, Packard, and Volovik, 1984). The first-order vortex-core transition can possibly be associated with two distinct vortex free-energy minima, illustrated schematically in the insets and identified tentatively in Fig. 54.

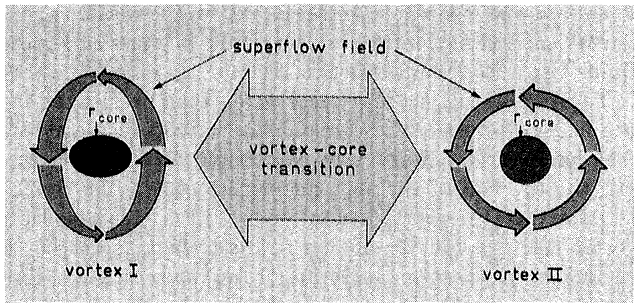

FIG. 2. Tentative identification of the two free-energy minima involved in the vortex-core transition of Fig. 1. At low pressures the nonaxisymmetric v vortex I with axi-planar core provides the free-energy minimum, while at high pressures the axisymmetric v vortex II with A-phase core becomes more advantageous. Circulation quantization escapes from real **r** space into momentum **k** space at the hard-core radius r_{core}. The axisymmetric v vortex has a round core, while the nonaxisymmetric v-vortex core is a "molecule," consisting of two half-quantum vortices. The vortex-core transition is a topological change between two inequivalent ways of accommodating vorticity (Volovik and Mineev, 1982; Salomaa and Volovik, 1986c). See Figs. 53 and 54.

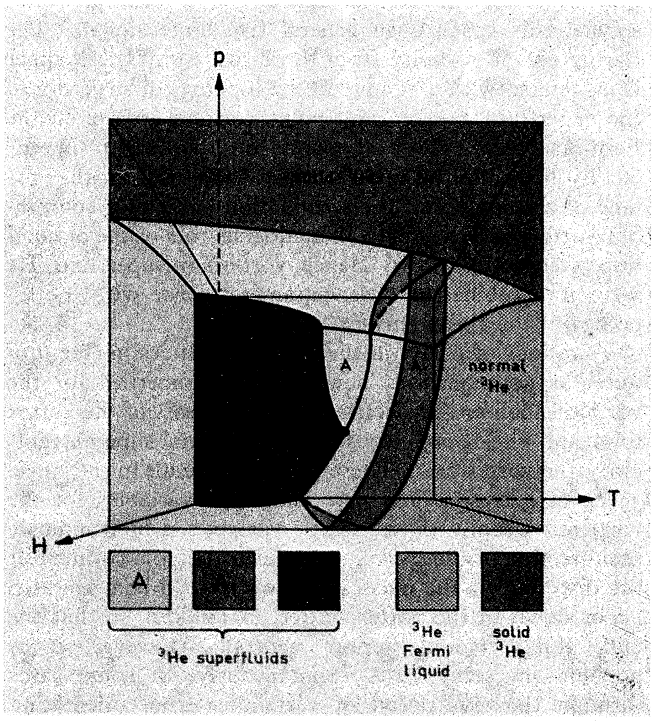

FIG. 3. Phase diagram of the low-temperature phases of stationary ^{3}He (Osheroff, Richardson, and Lee, 1972; Mermin and Lee, 1976). The zero-field cross section coincides with that in Fig. 1. Superfluid ^{3}He-B occurs at low temperatures and/or pressures, while superfluid ^{3}He-A is stabilized in a small region at high temperatures and pressures. With increasing magnetic field H, the A-phase regime increases at the expense of the B phase. In addition, the nonunitary superfluid ^{3}He-A_1 phase appears in a magnetic field between the A phase and the normal Fermi liquid in a narrow temperature regime. New superfluid phases nucleate inside the cores of quantized vortex lines in superfluid ^{3}He under rotation.

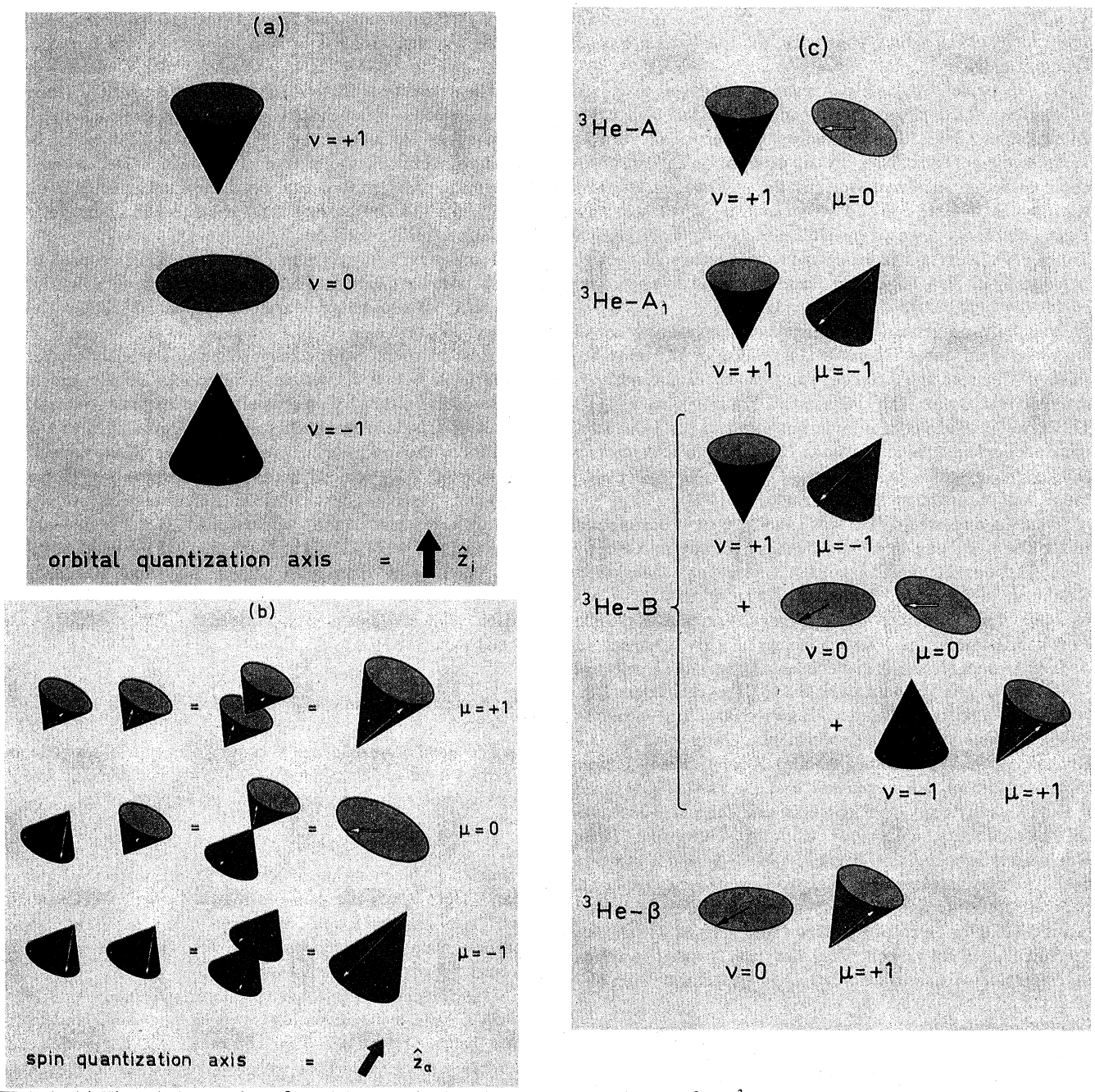

FIG. 4. (a) The relative motion of particles constituting the Cooper pairs in superfluid ^{3}He corresponds to a relative p-wave state ($L^{\rm int}=1$), with the pair orbital angular-momentum projection $L_z^{\rm int}$ obtaining the three possible values $\nu=\pm1$ and 0. The orbital angular-momentum quantization axis is denoted by $\hat{z}_i$. (b) The Cooper-pair spins in superfluid ^{3}He are in a total triplet state ($S=1$). The projection S_z on the spin quantization axis $\hat{z}_\alpha$ may obtain the values $\mu=\pm1,0$. (c) The Cooper-pair structure in the superfluid A, A_1, B, and β phases of ^{3}He may be visualized as follows. In ^{3}He-A, the pair orbital-momentum projection is $\nu=+1$, while the pair spin projection is $\mu=0$; thus, the order parameter equals $\Psi=Y_{1,+1}\,|\uparrow\downarrow+\downarrow\uparrow\rangle$, where the first and second entries refer to the orbital and spin degrees of freedom, respectively, and $Y_{1,\nu}$ denote spherical harmonic eigenfunctions of $L^{\rm int}=1$, with $L_z^{\rm int}=\nu$. The direction of the pair orbital momentum defines the $\boldsymbol{l}$ vector in the A phase. The spin degrees of freedom are described by the magnetic anisotropy vector $\mathbf{d}$, on which the projection of the Cooper-pair spin is zero: $\mathbf{S}\cdot\mathbf{d}=0$. In ^{3}He-$A_1$, $\Psi=Y_{1,+1}\,|\uparrow\uparrow\rangle$, the pair orbital momentum projection $\nu=+1$, and only one spin projection is present, resulting in ferromagnetic nuclear spin alignment. In ^{3}He-B, $\Psi=Y_{1,+1}\,|\downarrow\downarrow\rangle+Y_{1,0}\,|\uparrow\downarrow+\downarrow\uparrow\rangle+Y_{1,-1}\,|\uparrow\uparrow\rangle$, the three possible orbital and spin projections occur with equal weight. Because of the broken relative spin-orbit symmetry, the quantization axes are coupled in equilibrium ^{3}He-B through an order-parameter matrix of rotation: $\hat{z}_\alpha=R_{\alpha i}\hat{z}_i$. In the spontaneously ferromagnetic β phase, $\Psi=Y_{1,0}\,|\uparrow\uparrow\rangle$, the roles of the orbital and spin degrees of freedom are conjugate to those in the A phase. This β phase has not been found to exist in the stationary bulk superfluid ^{3}He, but is theoretically found to nucleate in the axisymmetric v-vortex core in rotating ^{3}He-B. (See Fig. 38.)

tion with linear defects in liquid crystals (Khlopov and Obukhov, 1982), where these disclination lines are easily seen optically.

In the present review we restrict ourselves to a consideration of the static equilibrium properties of vortices in superfluid ^{3}He. The dynamical properties of vortices, such as their contribution to the dissipation of superflow, their processes of creation, and their transformations to each other, are beyond the scope of this paper (see, however, the recent reviews by Hall and Hook, 1986, and by Sonin, 1987; the static equilibrium properties of vortices in superfluid ^{3}He have also been discussed in the recent review by Fetter, 1986).

We shall not discuss experimental techniques at ultralow temperatures (Lounasmaa, 1974c) or the construction of the rotating ^{3}He cryostats in the Laboratory of Atomic and Solid State Physics at Cornell University (J. D. Reppy, private communications) and in the Low Temperature Laboratory at Helsinki University of Technology (Hakonen, Ikkala, Islander, Markkula, Roubeau, Saloheimo, Garibashvili, and Tsakadze, 1983).

Rotating superfluid ^{3}He was investigated experimentally for the first time in 1981 (Crooker, Hebral, and Reppy, 1981; Hakonen, Ikkala, Islander, Lounasmaa, Markkula, Roubeau, Saloheimo, Volovik, Andronikashvili, Garibashvili, and Tsakadze, 1982; Ikkala, Volovik, Hakonen, Bun'kov, Islander, and Kharadze, 1982). By now, several different measurements have been conducted on rotating ^{3}He-A and ^{3}He-B, including (i) NMR experiments (e.g., Hakonen, Ikkala, Islander, Lounasmaa, and Volovik, 1983), (ii) persistent-flow experiments (Gammel, Hall, and Reppy, 1984; Hall, Gammel, and Reppy, 1984; Pekola, Simola, Nummila, Lounasmaa, and Packard, 1984; Gammel, Ho, and Reppy, 1985; Pekola and Simola, 1985), and (iii) experiments with ions (Simola, Nummila, Hirai, Korhonen, Schoepe, and Skrbek, 1986). It is not our purpose to review experiments; however, in order to make the paper self-contained, we briefly mention the most important NMR data on rotating ^{3}He-A and ^{3}He-B, which have been instrumental in achieving progress in the theoretical investigation of quantized vortices in superfluid ^{3}He.

II. SUPERFLUID PHASES OF LIQUID ^{3}He

The phase transitions of liquid ^{3}He into the superfluid states, discovered by Osheroff, Richardson, and Lee (1972; see Fig. 3), are accompanied by a spontaneous breaking of symmetry (Landau and Lifshitz, 1980), like any other phase transitions of condensed matter into ordered states.

Above the critical phase-transition temperature T_c, liquid ^{3}He has all the symmetries allowed in condensed matter. This total symmetry group G of physical laws in condensed matter contains the following subgroups:

$$G=(t\times SO_3^{(L)}\times P)\times SO_3^{(S)}\times(T\times U(1)) . \tag{2.1}$$

Here t is the group of translations, while $SO_3^{(L)}$ denotes the group of space rotations, and P abbreviates the space parity transformation. These three groups form the Euclidian group which is broken in crystals and liquid crystals.

The separate spin rotations of the group $SO_3^{(S)}$ may be considered as independent symmetry operations in those substances in which the spin-orbital coupling is small enough. This is the situation in liquid ^{3}He, where the magnetic dipole interaction between nuclear spins is negligibly small in comparison with the energies characterizing the superfluid transition.

Time-inversion symmetry T is broken in ordered magnets, both antiferromagnets and ferromagnets, while the breaking of the gauge symmetry group U(1) gives rise to superfluidity.

Most of these symmetries are simultaneously broken in liquid ^{3}He below T_c, where there spontaneously appears a Bose condensate of Cooper pairs that display internal degrees of freedom for both spin and orbital motion. This results in the unique and varied behavior of the superfluid phases of ^{3}He, which combine the properties of liquid crystals, ferromagnets, and antiferromagnets, or "spin liquid crystals," and superfluids (for reviews, see Lounasmaa, 1974a, 1974b; Leggett, 1975; Wheatley, 1975; Anderson and Brinkman, 1978; Lee and Richardson, 1978; Wölfle, 1979; Mineev, 1983; Volovik, 1984b; Mineev, Salomaa, and Lounasmaa, 1986; Wölfle and Vollhardt, 1987).

A. The order parameter in superfluid ^{3}He

The Bose condensate of Cooper pairs in a homogeneous Fermi liquid is described by the off-diagonal pair correlator (see, for example, the review by Leggett, 1975):

$$F_{ab}(\mathbf{k})=\langle a_{\mathbf{k}a}a_{-\mathbf{k}b}\rangle , \tag{2.2}$$

which has the meaning of a wave function for the Cooper pair. Here $a_{\mathbf{k}a}$ is the annihilation operator for the particle with momentum $\mathbf{k}$ and with spin index a. The Cooper pairing occurs between particles with opposite momenta, $\mathbf{k}$ and $-\mathbf{k}$, on the Fermi surface.

The correlator $F_{ab}(\mathbf{k})$ is the order parameter in superfluid Fermi systems, which vanishes above T_c and is finite below T_c. The "gap" function $\Delta_{ab}(\mathbf{k})$, which describes the quasiparticle energy spectrum, is expressed through $F_{ab}(\mathbf{k})$ by the pair potential $V(\mathbf{k},\mathbf{k}')$:

$$\hat{\Delta}(\mathbf{k})=\sum_{\mathbf{k}'}V(\mathbf{k},\mathbf{k}')\hat{F}(\mathbf{k}') , \tag{2.3}$$

and the quasiparticle energy spectrum $E_{\mathbf{k}}$ is determined by the eigenvalues of the Bogoliubov matrix

$$\begin{bmatrix} \varepsilon_{\mathbf{k}} & \hat{\Delta}(\hat{k}) \\ \hat{\Delta}^{\dagger}(\hat{k}) & -\varepsilon_{\mathbf{k}} \end{bmatrix} , \tag{2.4a}$$

where $\varepsilon_{\mathbf{k}}$ is the quasiparticle energy in the normal Fermi liquid, counted from the Fermi surface $\varepsilon_{\mathbf{k}}\approx v_F(k-k_F)$. In the so-called unitary phases (Leggett, 1975), where $\hat{\Delta}$ is proportional to the unitary matrix, $(\hat{\Delta}^{\dagger}\hat{\Delta})_{ab}\propto\delta_{ab}$, one

finds for the quasiparticle energy spectrum

$$E_{\mathbf{k}}=\{\varepsilon_k^2+\tfrac{1}{2}\mathrm{Tr}[\hat{\Delta}^\dagger(\hat{k})\hat{\Delta}(\hat{k})]\}^{1/2} . \tag{2.4b}$$

The simplest expression for the gap function is obtained near T_c, in the Ginzburg-Landau (GL) region. According to the Landau theory of phase transitions (Landau and Lifshitz, 1980), the order parameter near T_c is defined by only one of the irreducible representations of the total group G. Contributions from all the other representations are relatively smaller in proportion to the parameter $1-T/T_c \ll 1$.

The relevant representation for superfluid ^{3}He is characterized by the quantum numbers $S=1$ and $L^{\mathrm{int}}=1$ (see, for example, Leggett, 1975), where L^{int} is the internal angular momentum of the Cooper pairs, describing the relative orbital motion of the ^{3}He atoms in a pair, and S is the nuclear spin of a pair (see Fig. 4).

Dictated by the dimension (3×3) of this representation, the order parameter $\Delta_{ab}(\mathbf{k})$ is defined by nine complex values. These are the pair amplitudes $a_{\mu\nu}$ of the eigenstates for the pair spin and orbital momentum projections with the eigenvalues $S_z=\mu$ and $L_z^{\mathrm{int}}=\nu$ in the wave function $\hat{\Delta}$ of the Cooper pair:

$$\Delta_{ab}(\mathbf{k})=\sum_{\mu\nu} a_{\mu\nu}Y_{1,\nu}(\hat{k})(\chi_{1,\mu})_{ab},\quad \hat{k}\equiv\frac{\mathbf{k}}{k_F} . \tag{2.5}$$

Here $Y_{1,\nu}$ and $\chi_{1,\mu}$ are the eigenfunctions of the states with $L^{\mathrm{int}}=1$, $L_z^{\mathrm{int}}=\nu$, and $S=1$, $S_z=\mu$, respectively:

$$\hat{L}_z^{\mathrm{int}}Y_{1,\nu}=\nu Y_{1,\nu},\quad Y_{1,0}=\hat{k}_z ,\qquad Y_{1,\pm1}=\frac{1}{\sqrt{2}}(\hat{k}_x\pm i\hat{k}_y) , \tag{2.6a}$$

$$\hat{S}_z\chi_{1,\mu}=\mu\chi_{1,\mu},\quad \chi_{1,0}=g\sigma_3 ,\qquad \chi_{1,\pm1}=\frac{g}{\sqrt{2}}(\sigma_1\pm i\sigma_2) . \tag{2.6b}$$

Above, g denotes the antisymmetric 2×2 matrix

$$g=\begin{bmatrix}0 & 1\\ -1 & 0\end{bmatrix} , \tag{2.6c}$$

while σ_1, σ_2, and σ_3 are the Pauli spin matrices.

Usually it is more convenient to use linear combinations of these eigenfunctions, which have more transparent transformation properties; these are the vector $\hat{k}$ in the orbital space and the vector $g\boldsymbol{\sigma}$ in the spin space. The corresponding amplitudes $A_{\alpha i}$ of the order parameter,

$$\Delta_{ab}(\mathbf{k})=A_{\alpha i}(g\sigma^\alpha)_{ab}\hat{k}_i , \tag{2.7}$$

form a 3×3 matrix, which transforms as a vector under a spin rotation for given orbital index (i)—and as a vector under an orbital rotation for given spin index (α).

B. Broken symmetries in superfluid ^{3}He

Below the superfluid transition temperature T_c, the symmetry group G in Eq. (2.1) is spontaneously broken. This means that the "vacuum" states of the superfluid phases, described by the order parameter $a_{\mu\nu}$ (or $A_{\alpha i}$), are not invariant under the total symmetry group G of the physical laws. This order parameter transforms under the action of the various elements of the group (2.1) in the following fashion:

$$\hat{\mathbf{L}}=\hat{\mathbf{L}}^{\mathrm{ext}}+\hat{\mathbf{L}}^{\mathrm{int}},\quad \hat{\mathbf{L}}^{\mathrm{ext}}A_{\alpha i}=\frac{1}{i}\mathbf{r}\times\frac{\partial}{\partial\mathbf{r}}A_{\alpha i} ,$$

$$\hat{L}_k^{\mathrm{int}}A_{\alpha i}=-ie_{kil}A_{\alpha l},\quad \hat{\mathbf{L}}^{\mathrm{ext}}a_{\mu\nu}=\frac{1}{i}\mathbf{r}\times\frac{\partial}{\partial\mathbf{r}}a_{\mu\nu} , \tag{2.8a}$$

$$\hat{L}_z^{\mathrm{int}}a_{\mu\nu}=\nu a_{\mu\nu} ,$$

$$\hat{S}_\beta A_{\alpha i}=-ie_{\beta\alpha\gamma}A_{\gamma i},\quad \hat{S}_z a_{\mu\nu}=\mu a_{\mu\nu} , \tag{2.8b}$$

$$U_\phi A_{\alpha i}=e^{i\phi}A_{\alpha i} ,\quad U_\phi A_{\alpha i}^*=e^{-i\phi}A_{\alpha i}^*,\quad U_\phi a_{\mu\nu}=e^{i\phi}a_{\mu\nu} , \tag{2.8c}$$

$$\hat{P}A_{\alpha i}(\mathbf{r})=-A_{\alpha i}(-\mathbf{r}),\quad \hat{P}a_{\mu\nu}(\mathbf{r})=-a_{\mu\nu}(-\mathbf{r}) , \tag{2.8d}$$

$$\hat{T}A_{\alpha i}=A_{\alpha i}^*,\quad \hat{T}a_{\mu\nu}=a_{-\mu,-\nu}^* , \tag{2.8e}$$

$$t_{\mathbf{b}}A_{\alpha i}(\mathbf{r})=A_{\alpha i}(\mathbf{r}-\mathbf{b}),\quad t_{\mathbf{b}}a_{\mu\nu}=a_{\mu\nu}(\mathbf{r}-\mathbf{b}) . \tag{2.8f}$$

The angular momentum operator $\hat{\mathbf{L}}$ in (2.8a) is the generator of the group $\mathrm{SO}_3^{(L)}$ for space rotations. It includes both the center-of-mass rotational motion ($\hat{L}^{\mathrm{ext}}$) and the internal rotations of the Cooper pairs ($\hat{L}^{\mathrm{int}}$). Even for homogeneous superfluids, in which $L^{\mathrm{ext}}=0$, the vacuum state changes under rotations: $\hat{\mathbf{L}}A_{\alpha i}\neq 0$. This means, in particular, that the symmetry $\mathrm{SO}_3^{(L)}$ is broken for any superfluid phase of liquid ^{3}He, which is a direct consequence of the nonzero internal orbital momentum ($L^{\mathrm{int}}=1$) of the Cooper pairs.

Due to the spin triplet nature ($S=1$) of the Cooper pairing in superfluid ^{3}He, the $\mathrm{SO}_3^{(S)}$ symmetry is also broken [Eq. (2.8b)]. The transformation U_ϕ from the group U(1) changes the phase factor of the order parameter (2.8c), thus manifesting the breaking of gauge symmetry. Space parity P is broken even for the homogeneous liquid, since the order parameter changes sign under this transformation (2.8d); this is an immediate consequence of pairing with an odd value of pair orbital angular momentum: $L^{\mathrm{int}}=1$. The time-inversion symmetry T (2.8e) is conserved only for real order-parameter amplitudes $A_{\alpha i}$; this is possible for ^{3}He-B, but not for ^{3}He-A. Thus the only symmetry group that is not broken in ^{3}He below T_c is translational symmetry: a translation $t_{\mathbf{b}}$ through the vector $\mathbf{b}$ in (2.8f) does not change the order parameter of homogeneous superfluids.

C. The most symmetric superfluid phases

For a given vacuum state (with a given form of the order parameter $A_{\alpha i}$), however, there exist elements of the group G—besides translations—which do not change the Bose condensate. These elements form the group H of the symmetry of the vacuum, which is a subgroup of G. All the most important physical properties of a given vac-

uum state, which distinguish it from the other vacuum states, are completely determined by the group H. Thus there are different types of vacuum states, or different superfluid phases, and the symmetry classification of the possible superfluid phases must enumerate all the possible subgroups H of the group G.

This enumeration of the different classes of superfluids is not yet completed [though significant progress was recently reported by Bruder and Vollhardt (1986)], but the most symmetric vacuum states—the so-called "inert" phases (Barton and Moore, 1974a, 1974b)—are known. Due to their extreme symmetry (they belong to the maximal subgroups H of the group G: that is, only the normal state is more symmetric), they have a very useful property: they are always solutions of the Gor'kov equations (or the Ginzburg-Landau equations near T_c) for the order parameter. Therefore an inert phase has a fair chance of providing the absolute minimum of energy.

There are eight inert phases (Barton and Moore, 1974b) described by the order parameters $A_{\alpha i}$ (or $a_{\mu\nu}$) in Table I, where $\hat{x}_i$, $\hat{y}_i$, $\hat{z}_i$, and $\hat{x}_\alpha$,$\hat{y}_\alpha$,$\hat{z}_\alpha$ are unit vectors in the orbital and spin frames, which may be chosen to be different (see Fig. 4). These vectors also give the transformation from the matrix $A_{\alpha i}$ to the pair amplitudes $a_{\mu\nu}$:

$$A_{\alpha i}=\sum_{\mu,\nu}\lambda_\alpha^\mu\lambda_i^\nu a_{\mu\nu}\ ,$$
$$\lambda^0_{\alpha(i)}=\hat{z}_{\alpha(i)},\quad \lambda^{\pm}_{\alpha(i)}=\frac{1}{\sqrt{2}}(\hat{x}_{\alpha(i)}\pm i\hat{y}_{\alpha(i)})\ . \tag{2.9}$$

The first six superfluid phases in Table I belong to symmetry groups H, which contain one or two continuous subgroups. These are either subgroups of the broken groups $SO_3^{(S)}$ and $SO_3^{(L)}$, with generators $\hat{S}_z$ and $\hat{L}_z$ of rotations around one axis $\hat{z}$, or combined groups with the generators $\hat{\mathbf{J}}=\hat{\mathbf{L}}+\hat{\mathbf{S}}$, $\hat{S}_z-\hat{I}$, $\hat{L}_z-\hat{I}$, or $\hat{L}_z+\hat{S}_z$. Here $\hat{I}$ denotes the generator of the gauge group U(1):

$$\hat{I}A_{\alpha i}=A_{\alpha i},\quad \hat{I}A^*_{\alpha i}=-A_{\alpha i}\ . \tag{2.10}$$

The bipolar and α phases only display discrete symmetry. However, their discrete groups H are also maximal, so that these phases are also most symmetric. The discrete symmetry is also important for the planar phase, serving to make it an inert phase, too.

The order parameter for a given superfluid phase, i.e., for a given group H, may be found from the solution of symmetry equations. For example, the superfluid A phase, or the Anderson-Brinkman-Morel state (see Anderson and Morel, 1961; Anderson and Brinkman, 1973), corresponds to a symmetry group H_A, which contains the two generators $\hat{S}_z$ and $\hat{L}_z^{\rm int}-\hat{I}$. Thus the A-phase order parameter, which should be invariant with respect to H_A, is obtained as a solution of the following two symmetry equations:

$$\hat{S}_z a_{\mu\nu}=0,\quad (\hat{L}_z^{\rm int}-1)a_{\mu\nu}=0\ . \tag{2.11}$$

This, according to Eqs. (2.8a) and (2.8b), gives all $a_{\mu\nu}=0$, except for the a_{0+} component; the corresponding $A_{\alpha i}$ is obtained from Eq. (2.9):

$$A_{\alpha i}=\frac{1}{\sqrt{2}}\hat{z}_\alpha(\hat{x}_i+i\hat{y}_i)a_{0+}\ . \tag{2.12}$$

Cooper pairing in the A phase thus occurs in the state with the quantum numbers $S=1$, $S_z=0$, $L_z^{\rm int}=1$, and $L^{\rm int}=1$. However, far from T_c, all other odd representations (with odd $L^{\rm int}$, but with the same quantum numbers $S_z=0$, $L_z^{\rm int}=1$) should appear, since $L^{\rm int}$ is not a good

TABLE I. The most symmetric (inert) superfluid phases with $L=1$ and $S=1$. Of these eight possible superfluid phases for liquid ^{3}He, only the A and B phases occur in zero magnetic field (see Fig. 1). In an applied magnetic field, the A_1 phase is also stabilized in the close vicinity of T_c. Several of the other superfluid phases appear in the cores of quantized vortex lines in rotating ^{3}He-A and ^{3}He-B. The bipolar and α phases possess discrete symmetry only; hence there exist no continuous symmetries, i.e., no good quantum numbers for the Cooper-pair wave function.

Maximally symmetric phase	Vector order parameter $A_{\alpha i}$	Nonzero pairing amplitudes $a_{\mu\nu}$	Quantum numbers of the Cooper pairs
B phase	$\delta_{\alpha i}$	$a_{+-}=a_{00}=a_{-+}$	$J=0$
A phase	$\hat{z}_\alpha(\hat{x}_i+i\hat{y}_i)$	a_{0+}	$S_z=0,\ L_z=1$
	or	or	or
	$\hat{x}_\alpha(\hat{x}_i+i\hat{y}_i)$	$a_{++}=a_{-+}$	$S_z=1,\ L_z=1$ and $S_z=-1,\ L_z=1$
β phase	$(\hat{x}_\alpha+i\hat{y}_\alpha)\hat{z}_i$	a_{+0}	$S_z=1,\ L_z=0$
Polar phase	$\hat{z}_\alpha\hat{z}_i$	a_{00}	$S_z=L_z=0$
A_1 phase	$(\hat{x}_\alpha+i\hat{y}_\alpha)(\hat{x}_i+i\hat{y}_i)$	a_{++}	$S_z=L_z=1$
Planar phase	$\hat{x}_\alpha\hat{x}_i+\hat{y}_\alpha\hat{y}_i$	$a_{+-}=a_{-+}$	$J_z=0$
Bipolar phase	$\hat{x}_\alpha\hat{x}_i+i\hat{y}_\alpha\hat{y}_i$	$a_{--}=a_{++}=ia_{-+}=ia_{+-}$	None
α phase	$\hat{z}_\alpha\hat{z}_i+\hat{x}_\alpha\hat{x}_i e^{2\pi i/3}$ $+\hat{y}_\alpha\hat{y}_i e^{-2\pi i/3}$	$a_{00}=-2a_{++}=-2a_{--}$ $=i\frac{2}{\sqrt{3}}a_{+-}=i\frac{2}{\sqrt{3}}a_{-+}$	None

quantum number in the nonlinear Gor'kov or Ginzburg-Landau equations—as distinct from S_z and $L_z^{\rm int}$, which are conserved due to the symmetry equation (2.11).

An alternative representation for the A phase may be obtained by choosing the spin quantization axis in $A_{\alpha i}$ of Eq. (2.12) along $\hat{x}$ (or $\hat{y}$) (Leggett, 1975). In this case, since $\hat{x}=\frac{1}{2}[(\hat{x}+i\hat{y})+(\hat{x}-i\hat{y})]$, there exist two nonzero amplitudes $a_{++}=a_{-+}$; i.e., the A phase may as well be considered as the equal solution of two superfluids with different projections of the Cooper-pair spins: $\mu=+1$ and $\mu=-1$, but with the same projection, $\nu=+1$, of the Cooper-pair orbital angular momentum.

In an analogous manner, the superfluid B phase, or the Balian-Werthamer state (see Balian and Werthamer, 1963), corresponds to the group H_B with the generator $\hat{\mathbf{J}}=\hat{\mathbf{L}}^{\rm int}+\hat{\mathbf{S}}$. Therefore the B-phase order parameter is obtained as the solution of the symmetry equation

$$\hat{\mathbf{J}}A_{\alpha i}=0 \ . \tag{2.13}$$

In other words, Cooper pairing in ^{3}He-B occurs in a state with the total angular momentum quantum number $J=0$. The corresponding solution yields

$$A_{\alpha i}\propto\delta_{\alpha i} \ . \tag{2.14a}$$

or three equal nonzero amplitudes

$$|a_{+-}|=|a_{-+}|=|a_{00}|=\tfrac{1}{3}|\,{\rm Tr}(A)\,| \ , \tag{2.14b}$$

i.e., the B phase is the solution—in equal proportion—of three interpenetrating superfluids with the following Cooper-pair quantum numbers: $(\mu=+1,\ \nu=-1)$, $(\mu=-1,\ \nu=+1)$, and $(\mu=0,\ \nu=0)$. Due to the symmetry of the B phase, no other components with $L^{\rm int}\neq 1$ appear, even far from T_c.

D. The Ginzburg-Landau functional

The relative stability of the most symmetric phases near T_c is found from a consideration of the Ginzburg-Landau free-energy functional, which must be invariant under the total symmetry group G in Eq. (2.1); this essentially restricts the number of fourth-order terms in the bulk energy as well as the number of gradient terms.

The bulk condensation-energy term in the Ginzburg-Landau free-energy functional, $F_B[A_{\alpha i}]$, in superfluid ^{3}He is given by

$$\begin{aligned}F_B=&-\alpha A^*_{\alpha i}A_{\alpha i}+\beta_1 A^*_{\alpha i}A^*_{\alpha i}A_{\beta j}A_{\beta j}+\beta_2 A^*_{\alpha i}A_{\alpha i}A^*_{\beta j}A_{\beta j}\\&+\beta_3 A^*_{\alpha i}A^*_{\beta i}A_{\alpha j}A_{\beta j}+\beta_4 A^*_{\alpha i}A_{\beta i}A^*_{\beta j}A_{\alpha j}\\&+\beta_5 A^*_{\alpha i}A_{\beta i}A_{\beta j}A^*_{\alpha j} \ ,\end{aligned} \tag{2.15}$$

where $\alpha=N(0)(1-T/T_c)/3$, with $N(0)=m^*k_F/2\pi^2\hbar^2$ abbreviating the density of the ^{3}He quasiparticle states (m^* denotes the effective ^{3}He mass) for one spin projection at the Fermi level; the coefficients β_i of the fourth-order invariants are in the weak-coupling approximation given by

$$-2\beta_1=\beta_2=\beta_3=\beta_4=-\beta_5 \ , \tag{2.16}$$

with

$$-\beta_1\equiv\beta_0=\frac{7N(0)\zeta(3)}{240(\pi T)^2} \ . \tag{2.17}$$

Several theories for the "strong coupling" corrections exist (e.g., Sauls and Serene, 1981; Bedell, 1982). In particular, the β's may be described simply in terms of the spin-fluctuation (paramagnon) parameter δ, which depends on pressure (Anderson and Brinkman, 1973, 1978):

$$\begin{aligned}&\beta_1=-(1+0.1\delta)\beta_0, \ \ \beta_2=(2+0.2\delta)\beta_0 \ ,\\&\beta_3=(2-0.05\delta)\beta_0, \ \ \beta_4=(2-0.55\delta)\beta_0 \ ,\\&\beta_5=-(2+0.7\delta)\beta_0 \ .\end{aligned} \tag{2.18}$$

(For a recent review and a comparison of different parametrizations for the β's, see Levin and Valls, 1983.)

The gradient energy in the Ginzburg-Landau functional is given by

$$F_G=\gamma_1\partial_i A_{\alpha j}\partial_i A^*_{\alpha j}+\gamma_2\partial_i A_{\alpha i}\partial_j A^*_{\alpha j}+\gamma_3\partial_i A_{\alpha j}\partial_j A^*_{\alpha i} \ , \tag{2.19}$$

where for weak coupling

$$\gamma_1=\gamma_2=\gamma_3=\gamma_0=7\zeta(3)N(0)\frac{v_F^2}{240(\pi T)^2}=\tfrac{1}{3}N(0)\xi_0^2 \ . \tag{2.20}$$

Here ξ_0 is of the order of several hundred Å and it defines the coherence length

$$\xi_{\rm GL}(T)=\left[\frac{\gamma}{\alpha}\right]^{1/2}=\frac{\xi_0}{[(1-T/T_c)]^{1/2}} \ , \tag{2.21}$$

which characterizes the spatial extent of an inhomogeneity, at which the gradient energy becomes comparable with the bulk energy in the liquid.

Provided that the size of the inhomogeneity region is larger than $\xi_{\rm GL}(T)$, the gradient terms may be neglected, and the superfluid phases are determined by the minimization of the bulk energy (2.15) alone.

Only two of the eight most symmetric inert phases in Table I exhibit an absolute minimum of the bulk free energy in practice. If the strong-coupling parameter $\delta<0.46$, the B phase corresponds to the absolute minimum

$$\begin{aligned}&A_{\alpha i}=\Delta_B(T)\delta_{\alpha i}, \ \ a_{+-}=a_{-+}=a_{00}=\Delta_B(T) \ ,\\&\Delta_B^2(T)=\frac{\alpha}{2(\beta_{345}+3\beta_{12})} \ ,\end{aligned} \tag{2.22}$$

where the symbol $\beta_{i\ldots j}$ denotes the sum $\beta_i+\cdots+\beta_j$ of the corresponding β's. For $\delta>0.46$, the A phase

$$\begin{aligned}&A_{\alpha i}=\Delta_A(T)\hat{z}_\alpha(\hat{x}_i+i\hat{y}_i), \ \ a_{0+}=\sqrt{2}\Delta_A(T) \ ,\\&\Delta_A^2(T)=\frac{\alpha}{4\beta_{245}}\end{aligned} \tag{2.23}$$

becomes stable.

The other phases [e.g., the β phase, the polar phase, and the noninert axiplanar phase (Mermin and Stare, 1974)] exist in the cores of quantized vortices of the size $\sim\xi_{GL}$, where the gradient energy is essential. Near T_c, the B phase becomes unstable in a magnetic field towards the formation of the A phase, and in the close vicinity of T_c, the A phase becomes unstable towards the formation of the A_1 phase (see Fig. 3). This is a result of the symmetry change due to the magnetic field.

E. Magnetic interactions in superfluid ^{3}He

There are two different magnetic interaction terms in the energy, one linear and the other quadratic in an applied magnetic field. The principal effect is due to the Pauli susceptibility of a Fermi liquid, which has no contribution from the pairs with zero spin projection on the magnetic field ($\mu=0$). Therefore a surplus in the magnetic energy appears due to the formation of Cooper pairs with $\mu=0$, in comparison with normal ^{3}He:

$$F_{2H}=g_{2H}H^2\sum_{\nu}|a_{0\nu}|^2=g_{2H}H_\alpha H_\beta A_{\alpha i}A^*_{\beta i}\ . \quad (2.24)$$

The magnetic coupling constant g_{2H} may be expressed in terms of the difference between the normal-phase susceptibility χ_N and the susceptibility χ_B of ^{3}He-B, which is reduced due to the a_{00} component in the B phase [Eq. (2.14)]:

$$g_{2H}=\frac{1}{2}\frac{\chi_N-\chi_B}{\Delta_B^2}\ , \quad (2.25)$$

thus g_{2H} is positive. The energy [Eq. (2.24)] makes the A phase advantageous near T_c because, by reorienting the spin axis, one may eliminate the components $a_{0\nu}$.

The linear term (Ambegaokar and Mermin, 1973) originates from the interaction of a magnetic field with the magnetic moment M of the Cooper pairs:

$$M=g_{1H}\sum_{\mu\nu}\mu|a_{\mu\nu}|^2\ . \quad (2.26)$$

This magnetic moment is nonzero only for a nonunitary order parameter and results from the small asymmetry between the ^{3}He quasiparticles and quasiholes on the Fermi surface.

Thus the linear magnetic energy is

$$F_{1H}=-\mathbf{M}\cdot\mathbf{H}=-g_{1H}H\sum_{\mu\nu}\mu|a_{\mu\nu}|^2$$
$$=-g_{1H}ie_{\alpha\beta\gamma}H_\alpha A_{\beta i}A^*_{\gamma i}\ . \quad (2.27)$$

Near T_c, this term causes nucleation of the nonunitary magnetically ordered A_1 phase, in which the Cooper pairs have a negative $\mu=-1$ (only a_{-+} is nonzero), and thus a positive magnetic moment $\hbar\gamma\mu$ ($\gamma=-2.0378\times10^4$ G^{-1}sec^{-1} is the gyromagnetic ratio for the ^{3}He nuclei; since γ is negative it produces a negative g_{1H}). The parameter g_{1H} may be extracted from recent experiments (Israelson, Crooker, Bozler, and Gould, 1984) on the A_1-phase boundary in an external magnetic field:

$$g_{1H}=\tfrac{1}{3}\gamma N(0)\frac{\eta}{T_c}\ , \quad (2.28)$$

where η changes from 4×10^{-3} (at zero pressure, $p=0$) to 2.2×10^{-2} (at $p=29$ bars).

Another important contribution to the free energy reflects the tiny magnetic dipole interaction between the ^{3}He nuclei, which couples the spin and orbital indices of the order parameter (Leggett, 1973, 1974),

$$F_d=g_d(A_{ii}A^*_{kk}+A_{ik}A^*_{ki})\ . \quad (2.29)$$

The characteristic dipole length

$$\xi_d=\left[\frac{\gamma_0}{g_d}\right]^{1/2}\ , \quad (2.30)$$

at which the gradient energy of distortion is comparable with the dipole energy (2.29), is of the order of 10^{-3} cm. For comparison, the characteristic magnetic length for the interaction (2.24) equals

$$\xi_{2H}=\xi_d\frac{H_d}{H}\ , \quad (2.31)$$

where the "dipole field" H_d is of the order of 25 G. For large fields $H\gg H_d$, the magnetic energy (2.24) dominates.

III. SUPERFLUIDITY OF ^{3}He-A

A. Degenerate states of ^{3}He-A

Cooper pairing in the superfluid A phase occurs in the state with the projection $S_z=0$ on the spin quantization axis, which is denoted by $\mathbf{d}$, and with internal orbital momentum projection $L_z^{\rm int}=1$ on the orbital quantization axis, denoted by $\boldsymbol{l}$ (see Table I). If one neglects the spin-orbital (dipole) interaction (2.29), these quantization axes may be chosen independently.

The energy does not depend on the orientation of $\mathbf{d}$ and $\boldsymbol{l}$, thus reflecting the degeneracy of the superfluid state as a result of the broken symmetry G. In order to express the order parameter $A_{\alpha i}$ (2.23) in the frame with arbitrary $\mathbf{d}$ and $\boldsymbol{l}$, one must introduce two further unit vectors in the orbital frame, $\mathbf{e}_1$ and $\mathbf{e}_2$, which are orthogonal to $\boldsymbol{l}$, such that the general A-phase order parameter is

$$A_{\alpha i}=\Delta_A(T)d_\alpha(e_{1i}+ie_{2i})e^{i\Phi}\ , \quad (3.1)$$

where we have also introduced the phase Φ of the Bose condensate.

The parameters $\mathbf{d}$, $\mathbf{e}_1+i\mathbf{e}_2$, and Φ define all the degenerate vacua of superfluid ^{3}He-A; hence they are called the degeneracy parameters of the ordered state (see Fig. 5).

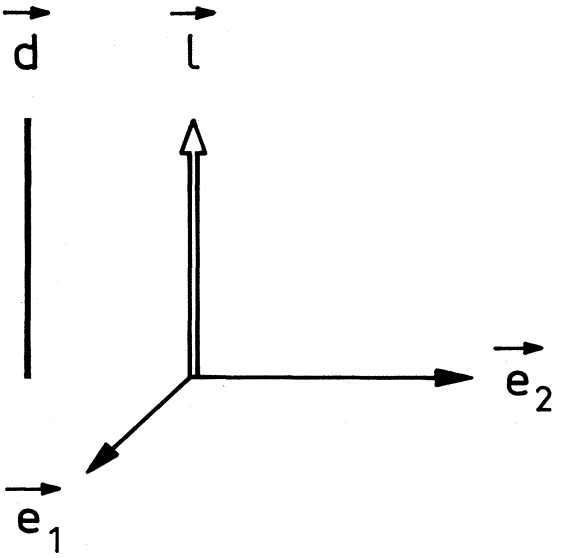

FIG. 5. The orthonormal order-parameter triad of the orbital degrees of freedom in ^{3}He-A. Together with the global phase Φ, the degeneracy parameters of the A phase are also $\mathbf{e}_1+i\mathbf{e}_2$ and $\mathbf{d}$. Owing to the nuclear dipole interaction, the vector $\mathbf{d}$ tends to orient parallel with $\boldsymbol{l}$—a behavior referred to as "dipole locking." When other interactions dominate over the nuclear dipole force, dipole unlocking occurs, whence $\mathbf{d}$ is no longer parallel with $\boldsymbol{l}$. This takes place in the cores of quantized vortices in ^{3}He-A.

B. Magnetic anisotropy

The vector $\mathbf{d}$, which appears due to the breaking of the $SO_3^{(S)}$ symmetry, specifies the direction of the spontaneous magnetic anisotropy axis. The magnetic susceptibility in the A phase is a uniaxial tensor,

$$\chi_{ij}=\chi_{\parallel}d_id_j+\chi_{\perp}(\delta_{ij}-d_id_j)\ , \tag{3.2}$$

and this is responsible for the orientational effect of the magnetic field on the $\mathbf{d}$ vector,

$$-\tfrac{1}{2}\chi_{ij}H_iH_j=-\tfrac{1}{2}\chi_{\perp}H^2+\tfrac{1}{2}(\chi_{\perp}-\chi_{\parallel})(\mathbf{d}\cdot\mathbf{H})^2\ . \tag{3.3}$$

The magnetic anisotropy is very large in the A phase (of order unity), especially at low temperatures, where $\chi_{\parallel}\to 0$ (Leggett, 1975). Near T_c, one has $\chi_{\perp}-\chi_{\parallel}=4\Delta_A^2 g_{2H}>0$ according to Eq. (2.24); therefore the spin axis $\mathbf{d}$ is orientated at equilibrium in the transverse plane—provided that there are no other orientating effects.

The $\mathbf{d}$ vector does not display the breaking of time-inversion symmetry, since $T\mathbf{d}=\mathbf{d}$. Therefore the nuclear spin subsystem has no features of ferromagnetic or antiferromagnetic order, as distinct from the orbital subsystem, with a tiny electronic ferromagnetism along the $\boldsymbol{l}$ vector (Leggett, 1977; Paulson and Wheatley, 1978).

Due to the spin-gauge symmetry (the A-phase state is invariant under $\mathbf{d}\to-\mathbf{d}$, $\Phi\to\Phi+\pi$), the $\mathbf{d}$ vector may be considered a bilateral vector, or director, in all cases in which the change of phase Φ is unimportant. Thus $\mathbf{d}$ resembles the director in nematic liquid crystals (de Gennes, 1975), and the A phase may as well be referred to as a spin nematic (Andreev and Grishchuk, 1984). The difference between $\mathbf{d}$ and a director vector becomes quite apparent, however, in connection with the half-quantum vortices (see Sec. IV.B.3 below).

C. Liquid-crystal-like properties of ^{3}He-A

The orbital vector $\boldsymbol{l}$, which appears due to the breaking of the $SO_3^{(L)}$ symmetry, indicates the direction of the orbital momentum of the Cooper pairs, and therefore changes sign under time inversion, $T\boldsymbol{l}=-\boldsymbol{l}$, thus producing the orbital ferromagnetism along $\boldsymbol{l}$. It also defines the spontaneous orbital liquid-crystal-like anisotropy in ^{3}He-A. All physical quantities connected with the orbital subsystem of ^{3}He-A have uniaxial anisotropy: viscosity, normal fluid and superfluid densities, heat conductance (Wölfle, 1973; Graham, 1974), dielectric constant (Swift, Eisenstein, and Packard, 1980), ion mobility (Salomaa, 1982; Salmelin and Salomaa, 1987a), etc.

The $\boldsymbol{l}$ vector also defines the nodes in the gaps of the ^{3}He quasiparticle excitation spectrum. According to Eqs. (2.4), (2.7), and (3.1), the ^{3}He quasiparticle energy in the superfluid A phase is

$$E_k=[\varepsilon_k^2+\Delta_A^2(\hat{k}\times\boldsymbol{l})^2]^{1/2},\quad \hat{k}\equiv\frac{\mathbf{k}}{k_F}\ . \tag{3.4}$$

These nodes in the directions $\hat{k}\parallel\boldsymbol{l}$ generate the unusual superfluid properties of the A phase at low temperatures, where the low-energy excitations near the nodes become essential.

In particular, in the presence of $\boldsymbol{l}$-vector textures, the nodes produce a nonzero density of states at the Fermi level, and therefore a nonzero density of the normal component at $T=0$ with nonanalytic behavior (Volovik and Mineev, 1981; Combescot and Dombre, 1983, 1986; Dombre and Combescot, 1984). Moreover, they produce an anomalous current and other effects which are quite analogous to the chiral anomalies in gauge theories (Volovik, 1985, 1986a, 1986b, 1986c, 1986d; Balatsky, Volovik, and Konyshev, 1986; Combescot and Dombre, 1986; see also Sec. VIII.D.2).

D. Combined gauge-orbital symmetry

More important than the density of states for our present purposes, is another feature of the liquid-crystal-like $\boldsymbol{l}$ texture: in the presence of $\boldsymbol{l}$ textures, the continuous superflow is nonpotential (Ambegaokar, de Gennes, and Rainer, 1974; Mermin and Ho, 1976). This is a result of the combined gauge-orbital symmetry of the A phase (with the generator $\hat{L}_z^{\rm int}-\hat{I}$), which intrinsically couples the liquid-crystal-like and superfluid properties.

This combined gauge-orbital symmetry means that a rotation of the orbital part $\mathbf{e}_1+i\mathbf{e}_2$ of the order parameter (3.1) by any angle α about the axis $\boldsymbol{l}$ does not change the

order parameter, provided this rotation is simultaneously accompanied with a gauge transformation U_α that changes the phase Φ of the Bose condensate: $\Phi \to \Phi + \alpha$. It is important that the angle α may depend on the coordinate. Even in this case the order parameter remains invariant. Thus ^{3}He-A possesses local gauge invariance, which previously was the sole privilege of quantum field theories [another local gauge invariance, as well as a general invariance, exists for low-energy fermionic excitations near gap nodes, producing a direct analogy between the ^{3}He excitations and chiral fermions within quantum electrodynamics (Volovik, 1986b)]. This results, in particular, in nonpotential ($\nabla \times \mathbf{v}_s \neq \mathbf{0}$) superflow in textures.

The existence of frictionless superflow $\mathbf{v}_s$ is in any superfluid a consequence of the breaking of the U(1) gauge symmetry. There appears an overall phase Φ of the Bose condensate, which in a homogeneous superflow with constant $\mathbf{v}_s$ is linear in the coordinate $\mathbf{r}$:

$$\Phi = \frac{M}{\hbar} \mathbf{v}_s \cdot \mathbf{r} \ . \tag{3.5}$$

Here $M = 2m_3$ is the boson mass in the Bose condensate, i.e., the Cooper-pair mass. In an inhomogeneous superflow, the superfluid velocity is usually generalized as

$$\mathbf{v}_s = \frac{\hbar}{M} \nabla \Phi \ , \tag{3.6}$$

thus resulting in potential (curl-free) superflow.

However, this generalization is not correct for the A phase, as the above expression is not invariant under local combined gauge-orbital symmetry, which transforms $\mathbf{v}_s \to \mathbf{v}_s + (\hbar/M)\nabla\alpha$. Since the superfluid velocity as a physical quantity should not change under this transformation, which does not change the state of the system, it should be generalized so as to include the liquid-crystal parameters $\mathbf{e}_1$ and $\mathbf{e}_2$ as well,

$$\mathbf{v}_s = \frac{\hbar}{M} (\nabla \Phi + e_{1i} \nabla e_{2i}) \ . \tag{3.7}$$

This expression is already invariant under the local combined symmetry: $\mathbf{v}_s \to \mathbf{v}_s$. However, the vorticity of superflow, $\nabla \times \mathbf{v}_s$, now depends on the $\boldsymbol{l}$ texture by means of the celebrated Mermin-Ho relation (Mermin and Ho, 1976), following from Eq. (3.7):

$$\nabla \times \mathbf{v}_s = \frac{\hbar}{2M} e_{ikl} l_i \nabla l_k \times \nabla l_l \ . \tag{3.8}$$

Therefore the A phase is irrotational only when the right-hand side of Eq. (3.8) is zero; a planar $\boldsymbol{l}$ field, for example, is such an $\boldsymbol{l}$ texture.

The nonpotential character of the superfluid velocity reflects the fact that the gauge group becomes coupled with the non-Abelian group of space rotations through the combined symmetry. Such conservation of combined symmetry with the violation of separate symmetries is also known as a broken relative symmetry (Liu, 1979, 1982). For a comprehensive discussion of the consequences of broken relative symmetry on the superfluid properties of the A phase, see the recent review of Volovik (1984b).

The same combined symmetry occurs in connection with the electroweak interaction in particle physics, only the orbital rotations are to be replaced by isotopic spin rotations. As a result, the properties of the A phase and the Higgs field in the Weinberg-Salam model (Weinberg, 1967; Salam, 1968) should share many common features—including continuous vorticity, in particular.

E. Energy, superflow, and orbital current in ^{3}He-A

In the London limit, in which the size of an inhomogeneity in a superfluid is larger than the coherence length $\xi_{\rm GL}$, so that the system is locally in the A phase, the energy depends only on the degeneracy parameters of the A-phase pairing state: $\mathbf{d}$, $\mathbf{e}_1 + i\mathbf{e}_2$, and Φ. Due to the local combined symmetry, $\mathbf{e}_1 + i\mathbf{e}_2$ and Φ cannot contribute to the energy explicitly, but must rather enter in invariant combinations, such as $\boldsymbol{l}$ and $\mathbf{v}_s$. Therefore the general expression for the A-phase energy, which is valid throughout the whole A-phase region, is as follows:

$$F = F_{\rm grad} + F_d + F_{2H} \ , \tag{3.9}$$

where the gradient energy is (Brinkman and Cross, 1978)

$$\begin{aligned} F_{\rm grad} = {} & [\tfrac{1}{2}\rho_s^{\parallel}(\boldsymbol{l}\cdot\mathbf{v}_s)^2 + \tfrac{1}{2}\rho_s^{\perp}(\boldsymbol{l}\times\mathbf{v}_s)^2] + \frac{1}{2}\left[\frac{\hbar}{M}\right]^2 [K_1(\nabla\cdot\boldsymbol{l})^2 + K_2(\boldsymbol{l}\cdot(\nabla\times\boldsymbol{l}))^2 + K_3(\boldsymbol{l}\times(\nabla\times\boldsymbol{l}))^2] \\ & + \frac{1}{2}\left[\frac{\hbar}{M}\right]^2 [\rho_{\rm sp}^{\parallel}((\boldsymbol{l}\cdot\nabla)\mathbf{d})^2 + \rho_{\rm sp}^{\perp}((\boldsymbol{l}\times\nabla)d_\alpha)^2] + \frac{\hbar}{M}[C\mathbf{v}_s\cdot(\nabla\times\boldsymbol{l}) - C_0(\boldsymbol{l}\cdot\mathbf{v}_s)(\boldsymbol{l}\cdot(\nabla\times\boldsymbol{l}))] \ . \end{aligned} \tag{3.10}$$

The quadratic magnetic-field energy in Eqs. (2.4) and (3.3) is

$$F_{2H} = \tfrac{1}{2}(\chi_\perp - \chi_{\parallel})(\mathbf{d}\cdot\mathbf{H})^2 \ , \tag{3.11}$$

and, finally, the dipole interaction equals, according to Eq. (2.29),

$$F_d = -2g_d \Delta_A^2 (\mathbf{d}\cdot\boldsymbol{l})^2 \ . \tag{3.12}$$

Near T_c, the coefficients in Eq. (3.10) may be obtained from Eq. (2.19):

$$\begin{aligned} \rho_s^{\parallel} = \rho_{\rm sp}^{\parallel} = \tfrac{1}{2}\rho_s^{\perp} = \tfrac{1}{2}\rho_{\rm sp}^{\perp} = 2K_1 = 2K_2 = \tfrac{2}{3}K_3 = C_0 = 2C \\ = \left[\frac{M}{\hbar}\right]^2 4\gamma_0 \Delta_A^2(T) \ . \end{aligned} \tag{3.13}$$

(For the values of these parameters far from T_c, see Williams, 1979; Williams and Fetter, 1979.)

The first term in Eq. (3.10) is the kinetic energy of anisotropic superfluids with the supercurrent

$$\mathbf{j}_s=\rho_s^{\parallel}\boldsymbol{l}(\boldsymbol{l}\cdot\mathbf{v}_s)+\rho_s^{\perp}(\mathbf{v}_s-\boldsymbol{l}(\boldsymbol{l}\cdot\mathbf{v}_s)) , \tag{3.14a}$$

where $\rho_s^{\parallel}$ and $\rho_s^{\perp}$ denote the longitudinal and transverse components of the superfluid density tensor.

The second term in (3.10) is the energy of the liquid-crystal field $\boldsymbol{l}$ distortion (de Gennes, 1973), where K_1, K_2, and K_3 are the twist, splay, and bend coefficients, as in liquid crystals. The third term, with $\rho_{\rm sp}^{\parallel}$ and $\rho_{\rm sp}^{\perp}$ referring to the longitudinal and transverse components of the spin rigidity tensor, together with the dipole energy (3.12), corresponds either to the energy of two-sublattice antiferromagnets with the antiferromagnetic axis $\mathbf{d}$, or to a spin nematic, both with an easy-axis anisotropy along the $\boldsymbol{l}$ vector.

Finally, the fourth term in (3.10) originates from the interaction of the $\mathbf{v}_s$ field with the orbital current,

$$\mathbf{j}_{\rm orb}=\frac{\hbar}{M}C\nabla\times\boldsymbol{l}-\frac{\hbar}{M}C_0\boldsymbol{l}(\boldsymbol{l}\cdot(\nabla\times\boldsymbol{l})) . \tag{3.14b}$$

This current is produced by internal rotation around $\boldsymbol{l}$ of Cooper pairs, which do not compensate each other if the $\boldsymbol{l}$ texture is inhomogeneous.

IV. TOPOLOGY OF VORTICES IN ^{3}He-A

A. The topological and symmetry classification schemes

The large number of the internal degrees of freedom—five in ^{3}He-A, with two for the unit vector $\hat{\boldsymbol{d}}$ and three for the order-parameter triad $\mathbf{e}_1$, $\mathbf{e}_2$, and $\boldsymbol{l}$—and the rich hierarchy of interactions with several length scales—$\xi_{\rm GL}$, ξ_d, and ξ_{2H}—produce a considerable variety of different stable textures in the superfluid phases of ^{3}He, such as vortices, helical textures, solitons, disgyrations, boojums, hedgehogs, domain walls, monopoles, and instantons.

The theoretical investigation of textures in ^{3}He, and in other ordered forms of condensed matter, proceeds through three consecutive stages. In the first stage, the textures are grouped into large classes defined by their distinct topological invariants, or topological "charges" (for reviews on topology in condensed-matter physics, see Mermin, 1979; Michel, 1980; Mineev, 1980; Trebin, 1982; Kléman, 1983).

Due to conservation of topological charge, textures from a given topological class cannot be continuously transformed into a texture in another class, while continuous deformation between textures within the given class is allowed by topology. The homogeneous state has zero topological charge; therefore textures with nonzero charge are topologically stable. They cannot dissolve into the uniform vacuum state in a continuous manner.

At the second stage, textures within a given topological class are subdivided into symmetry classes (Salomaa and Volovik, 1983b, 1985a, 1985b; Balinskiĭ, Volovik, and Kats, 1984)—essentially in the same manner as in the classification of the bulk superfluid phases. However, there occurs an interplay between symmetry and topology: some symmetry classes are strongly prohibited in given topological classes (see below). The textures with different internal symmetries display different physical properties, such as a spontaneous magnetic moment, an electric dipole moment, or a spontaneous supercurrent.

Finally, in the third stage, the numerical analysis of the textures is carried out. One then finds the texture inside each symmetry class with the minimal energy, and possible transitions between textures displaying different symmetries are investigated.

In this section, we consider the topological classification of the different vortex textures in superfluid ^{3}He-A. The degeneracy parameters in a texture depend on the coordinates, and these spatial variations serve to define a mapping of the coordinate space X into the space R of the degenerate states. In the case of vortices—and other linear defects—the topological classes are defined by the elements of the first homotopy group, $\pi_1(R)$, which describe the classes of continuous mappings of the closed contour around the defect line into the space R.

B. The small-distance topology of vortices

Due to the hierarchy of interactions, the order-parameter space R depends on the distance r from the linear defect. This makes the vortex textures quite complicated: the vortex may have two or more cores, one inside the other.

Let us first consider the small-distance topology of vortices. In the vicinity of the vortex axis, $\xi_{\rm GL}<r<(\xi_d,\xi_{2H})$, the dipole and magnetic anisotropy energies, Eqs. (3.11) and (3.12), may be neglected and the space R for the A phase is the five-dimensional manifold (Volovik and Mineev, 1976b, 1977a)

$$R_A=(S^2\times{\rm SO}_3)/Z_2 . \tag{4.1}$$

Here S^2 is the sphere of the spin vector $\mathbf{d}$, the $\rm SO_3$ is the space of the possible orientations of the orbital frame $\mathbf{e}_1$, $\mathbf{e}_2$, and $\boldsymbol{l}$. The factorization of these spaces by the discrete group Z_2 reflects the discrete combined spin-gauge symmetry of the A phase: this state (3.1) does not change if the spin rotation, which transforms $\mathbf{d}$ into $-\mathbf{d}$, is accompanied with the gauge transformation U_π: $\Phi\rightarrow\Phi+\pi$.

The first homotopy group of this space,

$$\pi_1(R_A)=Z_4 , \tag{4.2}$$

contains four elements. This means that there are four different topological classes of linear defects, which we shall identify with the numbers $N=0$, $\pm\frac{1}{2}$, and 1. These topological charges obey the following summation laws, corresponding to the cyclic group Z_4:

	0	$\frac{1}{2}$	$-\frac{1}{2}$	1
0	0	$\frac{1}{2}$	$-\frac{1}{2}$	1
$\frac{1}{2}$	$\frac{1}{2}$	1	0	$-\frac{1}{2}$
$-\frac{1}{2}$	$-\frac{1}{2}$	0	1	$\frac{1}{2}$
1	1	$-\frac{1}{2}$	$\frac{1}{2}$	0

(4.3)

The combination laws govern the fission and fusion processes of linear defects. For the sake of illustration, we shall next proceed to enlist several of the simplest representatives for each of these different topological classes.

1. Defects with topological charge $N=1$

Here we enumerate several symmetric representatives of the class with the topological charge $N=1$ in the region $\xi_{GL}<r<(\xi_d,\xi_{2H})$:

$$\mathbf{d}=\boldsymbol{l}=\hat{z},\quad \mathbf{e}_1+i\mathbf{e}_2=\hat{x}+i\hat{y},\quad \Phi=(2k-1)\phi\ , \tag{4.4a}$$

$$\mathbf{d}=\hat{z},\quad \boldsymbol{l}=\hat{r},\quad \mathbf{e}_1+i\mathbf{e}_2=\hat{z}-i\hat{\phi},\quad \Phi=2k\phi\ , \tag{4.4b}$$

$$\mathbf{d}=\hat{z},\quad \boldsymbol{l}=\hat{\phi},\quad \mathbf{e}_1+i\mathbf{e}_2=\hat{z}+i\hat{r},\quad \Phi=2k\phi\ , \tag{4.4c}$$

$$\mathbf{d}=\boldsymbol{l}=\hat{r},\quad \mathbf{e}_1+i\mathbf{e}_2=\hat{z}-i\hat{\phi},\quad \Phi=2k\phi\ , \tag{4.4d}$$

$$\mathbf{d}=\boldsymbol{l}=\hat{\phi},\quad \mathbf{e}_1+i\mathbf{e}_2=\hat{z}+i\hat{r},\quad \Phi=2k\phi\ . \tag{4.4e}$$

In the above, $\hat{z}$, $\hat{r}$, and $\hat{\phi}$ denote the unit vectors of a cylindrical coordinate frame, and k is an integer. Equation (4.4a) describes pure phase vortices with an odd number $[m=(2k-1)]$ of circulation quanta. According to Eq. (3.7), the superfluid velocity in these vortices and its circulation around the vortex axis obey

$$\mathbf{v}_s=\frac{\hbar}{M}\nabla\Phi=\frac{\hbar}{M}\frac{m}{r}\hat{\phi},\quad \oint \mathbf{v}_s\cdot d\mathbf{r}=m\frac{h}{M}\ . \tag{4.5}$$

The quantum of circulation is h/M, where $M=2m_3$ for the superfluid phases of ^{3}He ($h/2m_3=0.662\times10^{-3}$ cm^2/sec), and $M=m_4$ for He II ($h/m_4=0.997\times10^{-3}$ cm^2/sec).

Equations (4.4b) and (4.4c) describe defects in the $\boldsymbol{l}$ field: radial ($\boldsymbol{l}=\hat{r}$) and tangential ($\boldsymbol{l}=\hat{\phi}$) disgyrations (de Gennes, 1973), respectively, combined with vortices having an even number ($m=2k$) of circulation quanta. In Eqs. (4.4d) and (4.4e), these disgyrations are accompanied with radial and tangential disclinations in the $\mathbf{d}$ field. All these defects may transform into each other continuously, since they belong to the same topological class.

The defect with minimal energy in this class is essentially defined by the minimization of Eq. (3.10) in the London limit. With the Ginzburg-Landau parameters of Eq. (3.13), this minimization tends to favor the pure radial disgyration in Eq. (4.4b) with $k=0$ [see Sec. V.C, Eq. (5.26)]. That is, the pure phase vortex is unstable towards the formation of a radial disgyration at small distances (Volovik and Mineev, 1977a; Brinkman and Cross, 1978).

In all defects with $N=1$, the degeneracy parameters possess a singularity on the vortex axis. In the pure phase vortices the singularity is in the phase Φ which, according to Eq. (4.5), produces a divergent superfluid velocity, while in the case of the disgyration, the $\boldsymbol{l}$ field is singular and thus its gradients become unbounded. Therefore, in order to avoid divergent energy, the A-phase state should be destroyed in the core region of order ξ_{GL} near the vortex axis, where the density of the gradient energy (2.19) of the singularity becomes comparable with the condensation-energy density (2.15).

Hence defects with the topological charge $N=1$, as well as any other defects with nonzero topological charges, have a singular "hard" core with radius $\sim\xi_{GL}$. Outside the hard core of the pure phase vortex, superflow is potential; thus in this state all the vorticity, $\nabla\times\mathbf{v}_s$, is concentrated inside the hard core. During the transformation of this vortex into a radial disgyration, vorticity continuously "flares out" from the hard core of the singularity. The actual structure of the hard core depends on the symmetry and will be considered in Sec. V; it is determined by the competition between the gradient [Eq. (2.19)] and bulk [Eq. (2.15)] energies. For a pure phase vortex, the vorticity is concentrated in the origin or distributed continuously inside the hard core, depending on the core symmetry.

2. Continuous defects

Let us next write down some of the symmetric states in the trivial class with $N=0$, both singular and nonsingular, in the region $\xi_{GL}<r<(\xi_d,\xi_{2H})$:

$$\mathbf{d}=\boldsymbol{l}=\hat{z},\quad \mathbf{e}_1+i\mathbf{e}_2=\hat{x}+i\hat{y},\quad \Phi=0\ , \tag{4.6a}$$

$$\mathbf{d}=\boldsymbol{l}=\hat{z},\quad \mathbf{e}_1+i\mathbf{e}_2=\hat{x}+i\hat{y},\quad \Phi=2k\phi\ , \tag{4.6b}$$

$$\mathbf{d}=\boldsymbol{l}=\hat{r},\quad \mathbf{e}_1+i\mathbf{e}_2=\hat{z}-i\hat{\phi},\quad \Phi=(2k+1)\phi\ , \tag{4.6c}$$

$$\mathbf{d}=\hat{z},\quad \boldsymbol{l}=\hat{r},\quad \mathbf{e}_1+i\mathbf{e}_2=\hat{z}-i\hat{\phi},\quad \Phi=(2k+1)\phi\ . \tag{4.6d}$$

Besides the nonsingular homogeneous state in Eq. (4.6a), this class contains singular pure phase vortices with an even number ($m=2k$) of circulation quanta [Eq. (4.6b)], and the combination of a disgyration with singular pure phase vortices having an odd number ($m=2k+1$) of circulation quanta in Eqs. (4.6c) and (4.6d). These singular states are topologically unstable, i.e., they may be deformed into the state without any singularity in the degeneracy parameter fields. Consequently, the singular core of these vortices, with radius $\sim\xi_{GL}$, may be smoothly dissolved, producing continuously distributed vorticity.

For example, the vortex with $m=-2$ quanta of circulation [Eq. (4.6b), with $k=-1$] may be smoothly deformed into the continuous (without a singular core of size ξ_{GL}) Anderson-Toulouse-Chechetkin (ATC) vortex (Chechetkin, 1976; Anderson and Toulouse, 1977), having the same asymptotics. The degeneracy parameters and the superflow velocity in the ATC vortex are as follows:

$$\mathbf{d}=\mathbf{l}=\hat{z}\sin\eta(r)+\hat{r}\cos\eta(r)\ ,$$
$$(\mathbf{e}_1+i\mathbf{e}_2)e^{i\Phi}=[\hat{z}\cos\eta(r)-\hat{r}\sin\eta(r)-i\hat{\phi}]e^{-i\phi}\ , \quad (4.7)$$
$$\mathbf{v}_s=-\frac{\hbar}{Mr}[1+\sin\eta(r)]\hat{\phi}\ .$$

Here η changes from $\pi/2$ at $r\to\infty$ to $-\pi/2$ on the vortex axis ($r=0$) (see Fig. 6).

At infinity, this continuous vortex appears like a pure phase vortex with $m=-2$ quanta of circulation: $\mathbf{v}_s=-2(\hbar/Mr)\hat{\phi}$. However, $\mathbf{v}_s$ vanishes smoothly on the vortex axis, while both $\mathbf{d}$ and $\mathbf{l}$ become uniform near the axis, with $\mathbf{d}(0)=\mathbf{l}(0)=-\hat{z}$, but different from their asymptotic form $\mathbf{d}(\infty)=\mathbf{l}(\infty)=\hat{z}$. This vortex has continuously distributed vorticity:

$$\nabla\times\mathbf{v}_s=-\hat{z}\frac{\hbar}{M}\frac{\cos\eta}{r}\frac{\partial\eta}{\partial r}\ , \quad (4.8)$$

concentrated in the broad region where the $\mathbf{l}$ field is inhomogeneous. If there are no external fields, the extension of this region is only limited by the boundaries.

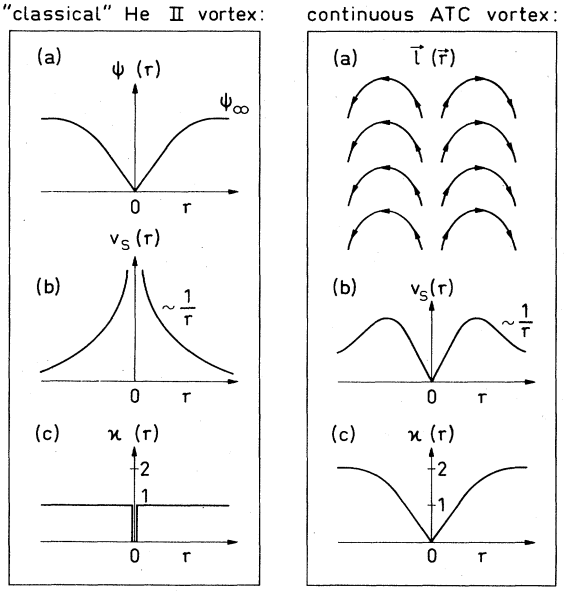

FIG. 6. Comparison of the "classical" singular pure phase vortex—like that in He II—and the continuous Anderson-Toulouse-Chechetkin (ATC) vortex texture. (a) The order parameter $\psi(\mathbf{r})$ in the classical vortex line displays a node where the phase becomes singular, while the order-parameter field $\mathbf{l}(\mathbf{r})$ in the ATC texture is everywhere continuously distributed. (b) The superflow velocity field $v_s(\mathbf{r})$ diverges for the classical vortex on its axis where the gradient of the phase Φ is singular, while the superflow velocity distribution in the ATC texture is everywhere finite; it exhibits a maximum beyond which the velocity profile tends to the asymptotic $1/r$ form. (c) The circulation of superflow, $\kappa(r)$, around the vortex line is quantized for the classical vortex for any distance from its axis, while the circulation in the ATC texture is only quantized asymptotically for large distances (two quanta of circulation).

Another important example of a nonsingular texture, the Mermin-Ho (MH) texture (Mermin and Ho, 1976), may be obtained by the deformation of one of the defects in Eq. (4.6c) with the elimination of the singularity at the origin. This texture is again given by Eq. (4.7), but now with the different boundary conditions $\eta(\infty)=0$ and

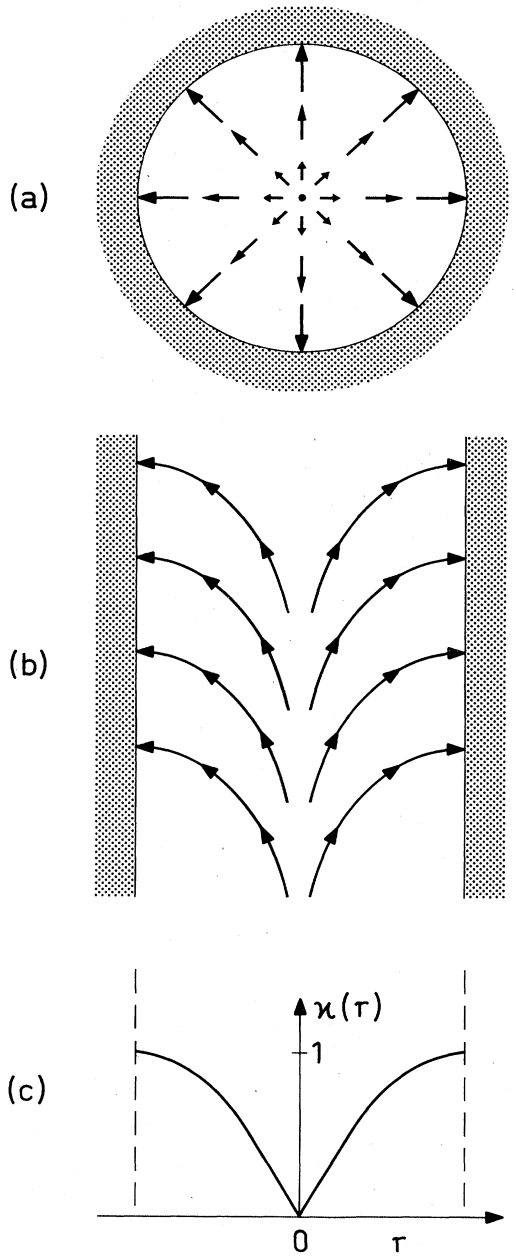

FIG. 7. The $\mathbf{l}$-vector distribution in the Mermin-Ho (MH) texture. (a) Projection of $\mathbf{l}_\perp$ on the cross-sectional plane of the cylindrical container. (b) Side view of the $\mathbf{l}$-vector texture illustrates the "escape into the third dimension." (c) The distribution of circulation in the Mermin-Ho texture is continuous, like that of the Anderson-Toulouse-Chechetkin texture in Fig. 6, but the total circulation in the MH vortex texture is unity, while it equals two in the ATC texture.

$\eta(0)=-\pi/2$. Asymptotically, it behaves like a vortex with a unit quantum of circulation $m=-1$, with $\mathbf{v}_s=-(\hbar/Mr)\hat{\phi}$, combined with a radial disgyration: $\boldsymbol{l}=\hat{r}$ [Eq. (4.6c) with $k=-1$]. This texture should exist in a cylindrical vessel where the boundary conditions ($\boldsymbol{l}$ parallel to the normal of the boundary) require $\boldsymbol{l}=\hat{r}$ on the wall (see Fig. 7).

If the asymptotics are not fixed, the ATC and MH textures, both having the topological charge $N=0$, may be continuously transformed into each other, as well as into the homogeneous state. However, the container walls—or any additional interactions at a large distance from the axis—partially fix the asymptotics, and this gives rise to the variety of topologically different textures (Mineev and Volovik, 1978), even inside the class $N=0$ (see Sec. IV.C). These textures are characterized by additional topological charges which distinguish them. Formally, these topological invariants specify the classes of mappings with boundary conditions taken into account; such classes form the so-called relative homotopy group.

3. Half-integer vortices

The most symmetric defects in the classes $N=\pm\frac{1}{2}$ for the region of distances $\xi_{\rm GL}<r<(\xi_d,\xi_{2H})$ are

$$\mathbf{d}=\hat{x}\cos p\phi+\hat{y}\sin p\phi,\quad \Phi=(2k\pm\tfrac{1}{2})\phi\ ,$$
$$\mathbf{e}_1+i\mathbf{e}_2=\hat{x}+i\hat{y}\ , \tag{4.9}$$

where p is a half-integer. These two classes of linear defects contain the singular vortices with a half-integer number of circulation quanta, $m=2k+N$; e.g., the superfluid velocity and the circulation of the superflow field for $k=0$ are given by

$$\mathbf{v}_s=\pm\frac{1}{2}\frac{\hbar}{Mr}\hat{\phi},\quad \oint \mathbf{v}_s\cdot d\mathbf{r}=\pm\frac{1}{2}\frac{h}{M}\ , \tag{4.10}$$

with the vorticity being concentrated in the hard cores. The possible existence of these vortices is a result of the discrete combined gauge-spin rotation symmetry of the A phase: $\mathbf{d}\rightarrow-\mathbf{d}$, $\Phi\rightarrow\Phi+\pi$ (Volovik and Mineev, 1976b; Cross and Brinkman, 1977).

Encircling the vortex line, the phase Φ only changes by π, thus changing the sign of the order parameter $A_{\alpha i}$. This change in sign is compensated by the reversal of $\mathbf{d}$, provided that the index p of this vector field is a half-integer (see Fig. 8). Therefore these vortices in the superflow field are simultaneously disclinations in the magnetic anisotropy $\mathbf{d}$ field with half-integer Frank index, analogous to the topologically stable disclinations in nematic liquid crystals (de Gennes, 1975).

The half-quantum vortex with the circulation quantum m and the disclination with the half-integer index p cannot exist separately, demonstrating one of the several topological mechanisms of confinement in superfluid ^{3}He. This is the principal difference between the $\mathbf{d}$ vector in the A phase and the director in nematic liquid crystals, where isolated half-integer disclinations exist.

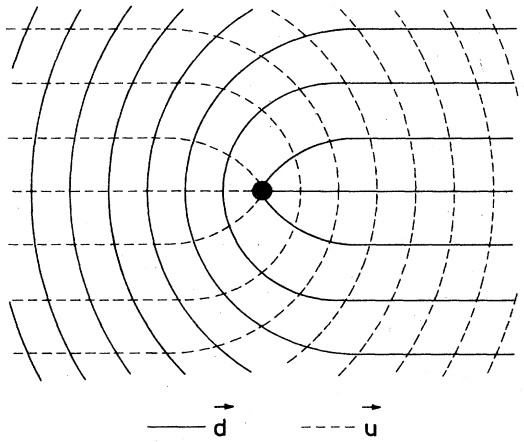

FIG. 8. A schematic illustration of an isolated half-quantum vortex in superfluid ^{3}He-A. Shown are both the spin anisotropy $\mathbf{d}$-vector field (solid lines) and the simultaneous phase field Φ (dashed lines), chosen to be represented here by the vector $\mathbf{u}\equiv\hat{x}\cos(\Phi+\phi_0)+\hat{y}\sin(\Phi+\phi_0)$, with $\phi_0=\pi/2=$const. The singularities for both of these fields occur on the same axis (confinement).

C. The large-distance topology of vortices

1. Zero-field vortices

At large distances from the vortex axis, the magnetic and dipole interactions (3.11) and (3.12) restrict the freedom of the order parameter. Let us first consider the situation in low fields, with $H\ll 25$ G. In this case, there is a region of distances $\xi_d<r<\xi_{2H}$, where the dipole energy is essential, while the magnetic field may be neglected. This region is relevant also for vortices in a vanishing magnetic field, where $\xi_{2H}=\infty$. The space of the degenerate A-phase states R is truncated in this region, since $\mathbf{d}$ is "dipole locked" with $\boldsymbol{l}$ (i.e., $\mathbf{d}\|\boldsymbol{l}$), and only the space of rotations of the orbital frame survives (Toulouse and Kléman, 1976):

$$R_A^d=\mathrm{SO}_3\ . \tag{4.11}$$

The first homotopy group of this space,

$$\pi_1(R_A^d)=Z_2\ , \tag{4.12}$$

contains only two elements, $N=0$ and $N=1$; the half-quantum vortices do not exist in this region owing to dipole locking.

It is crucial to note that, unlike the $\mathbf{d}$ vector, the vector $\boldsymbol{l}$ is single valued and cannot change sign after encircling the half-quantum vortex. Thus $\boldsymbol{l}$ cannot follow $\mathbf{d}$ in a half-quantum vortex, which violates the dipole-locking requirement. As a result, the half-quantum vortex gives rise to a soliton wall of width $\sim\xi_d$ (Volovik and Mineev, 1977a; Brinkman and Cross; 1978); this is illustrated in Fig. 9.

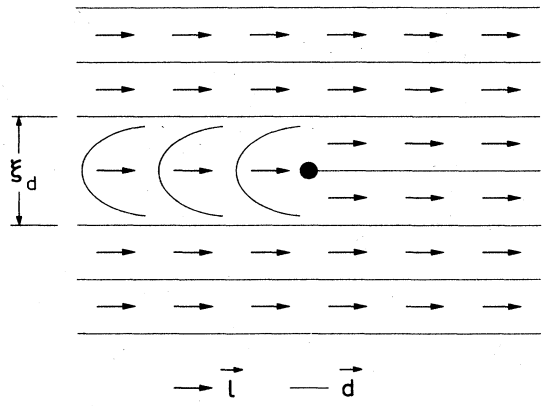

FIG. 9. Formation of soliton from a half-quantum vortex at distances larger than ξ_d: a disclination in the **d** field with half-integer Frank index cannot be accompanied with such a disclination in the l field. This discrepancy produces the soliton wall on the left-hand side of the disclination axis.

The simplest representatives of nonsingular vortices with $N=0$ are, as before, the ATC and MH textures with vorticity concentrated in a broad region. The most symmetric singular defects of the class with $N=1$ in the region $\xi_d < r < \xi_{2H}$ are the pure phase vortex [Eq. (4.4a)] and the dipole-locked disgyrations [Eqs. (4.4d) and (4.4e)]. The energetically stable defect of this class ($N=1$) is in this region defined by the minimization of Eq. (3.10), with dipole-locked $\mathbf{d}\|l$. With the parameters of Eq. (3.13), this defect has a rather complicated form: it is a one-quantum vortex with broken axisymmetry and with an inhomogeneous distribution of the l field (see Sec. V.C; Volovik and Mineev, 1977a; Volovik and Hakonen, 1981).

This vortex has two cores: the large "soft" core of the order of the dipole length ξ_d and the small "hard" core with radius $\sim\xi_{\rm GL}$. Outside the soft core, l and **d** are locked. In the soft-core region, where the gradient energy of the vortex texture becomes comparable with the dipole energy, dipole unlocking occurs. Inside this dipole-unlocked soft core, in the region $\xi_{\rm GL} < r < \xi_d$, this vortex continuously transforms into the linear defect with minimal energy, Eq. (3.10), without dipole locking, i.e., into the dipole-unlocked radial disgyration [Eq. (4.4b); see Sec. V.C], which has a "hard" core with radius of the order of $\xi_{\rm GL}$. Since the radial disgyration has no singular vorticity, all its vorticity is continuously distributed in the soft core. Therefore the singular vortex line in the class $N=1$ has, nevertheless, continuous vorticity.

2. Vortices in small magnetic fields

Let us now take into account a weak magnetic field (hence $\xi_{2H} > \xi_d$). There appears a new region of distances $r > \xi_{2H} > \xi_d$ from the vortex axis, where the magnetic anisotropy [Eq. (3.11)] further restricts the order-parameter space R, locking **d** into the plane perpendicular to **H**. This space consists of two circles:

$$R_A^{dH} = S^1 \times S^1 \ . \tag{4.13}$$

One circle is the space for the phase Φ, while the other circle is the space for both the **d**- and l-vector fields, which are dipole locked and confined in a plane. Superfluid velocity is potential in this region, since the l field has a planar structure, i.e., $\nabla \times \mathbf{v}_s = 0$ at distances $r > (\xi_{2H}, \xi_d)$ according to Eq. (3.8).

The first homotopy group of this space,

$$\pi_1(R_A^{dH}) = Z \times Z \ , \tag{4.14}$$

contains two different groups of integers, m and p, which are the winding numbers for the phase Φ and for the fields $\mathbf{d}\|l$, respectively. The topological class (m,p) contains disclinations with index p combined with vortices having m quanta of circulation. The simplest representation in this class is

$$\begin{aligned} &\mathbf{d} = l = \hat{x}\cos p(\phi-\phi_0) + \hat{y}\sin p(\phi-\phi_0) \ , \\ &\mathbf{e}_1 + i\mathbf{e}_2 = \hat{z} + i(l \times \hat{z}) \ , \\ &\Phi = m\phi, \quad \mathbf{v}_s = m\frac{\hbar}{Mr}\hat{\phi}, \quad \mathbf{H}\|\hat{z} \ . \end{aligned} \tag{4.15}$$

Thus, due to an additional magnetic interaction far from the vortex axis, defects of the two large topological classes with $N=0$ and $N=1$ acquire additional topological charges m and p. The distributions of these subclasses inside the large class is as follows: the defects with even $m+p$ belong to the class with $N=0$, while the defects with odd $m+p$ belong to the class with $N=1$. The defects in Eq. (4.15) have a soft core with radius $\sim\xi_{2H}$, with the core structures depending on the sum $m+p$ (see Secs. IV.C.3 and IV.C.4).

3. Topology of the soft core of continuous vortices in low fields

Defects with even $m+p$ belong in the trivial class $N=0$ in the region $r < \xi_{2H}$; therefore the order parameter can be made continuous inside this region. Thus these defects only have one core (a dipole-locked soft core) of the order of ξ_{2H} and no smaller core inside the region $r < \xi_{2H}$. Inside this soft core, the dipole-locked vectors l and **d** flare out from the $(\hat{x},\hat{y})$ plane, providing continuous unwinding of the quantum numbers p and m, and thus continuously distributed vorticity. These vectors have definite topological structure in the dipole-locked soft core.

Integrating the Mermin-Ho relation (3.8) along the surface σ crossing the soft core with the edge on the contour L outside the core, one obtains the relation between the circulation quantum number m and the quantum number

$$\tilde{m}_l = \frac{1}{4\pi}\int_\sigma dx\,dy \left[l \cdot \frac{\partial l}{\partial x} \times \frac{\partial l}{\partial y} \right] , \tag{4.16a}$$

describing the continuous mapping of the soft-core region onto the unit sphere, which is produced by the l field in the core:

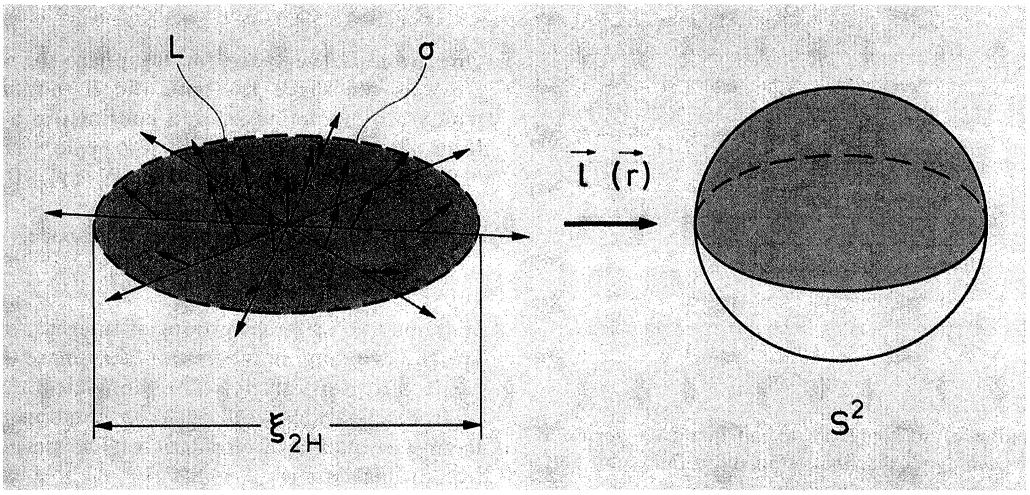

FIG. 10. Topology of the continuous Mermin-Ho (MH) vortex texture in the l-vector field (arrows) can be studied in the order-parameter space S^2 through the mapping $l(\mathbf{r})$ of the cross section of the MH texture onto the "northern" half of the unit sphere.

$$\tfrac{1}{2}m=\frac{1}{2}\frac{M}{h}\oint_L d\mathbf{r}\cdot\mathbf{v}_s=\frac{M}{2h}\int_\sigma d\mathbf{s}\cdot\nabla\times\mathbf{v}_s$$
$$=\frac{1}{4\pi}\int_\sigma dx\,dy\left[l\cdot\frac{\partial l}{\partial x}\times\frac{\partial l}{\partial y}\right]$$
$$=\tilde{m}_l\ . \qquad (4.16b)$$

In this mapping, the l vector (together with the $\mathbf{d}$ vector) covers the unit sphere $\tilde{m}_l$ times. The index $\tilde{m}_l$ is an integer for vortices with even circulation quantum numbers m [$\tilde{m}_l=1$ for the ATC texture, modified to restrict $l(\infty)$ to the plane, e.g., $l(\infty)=\hat{x}$], and a half-integer for odd m ($\tilde{m}_l=\frac{1}{2}$ for the MH texture). In the case of the MH texture, the l vector covers only the "northern" hemisphere (see Fig. 10). For both textures, superflow is potential outside the dipole-locked soft vortex core ξ_{2H}, ac-

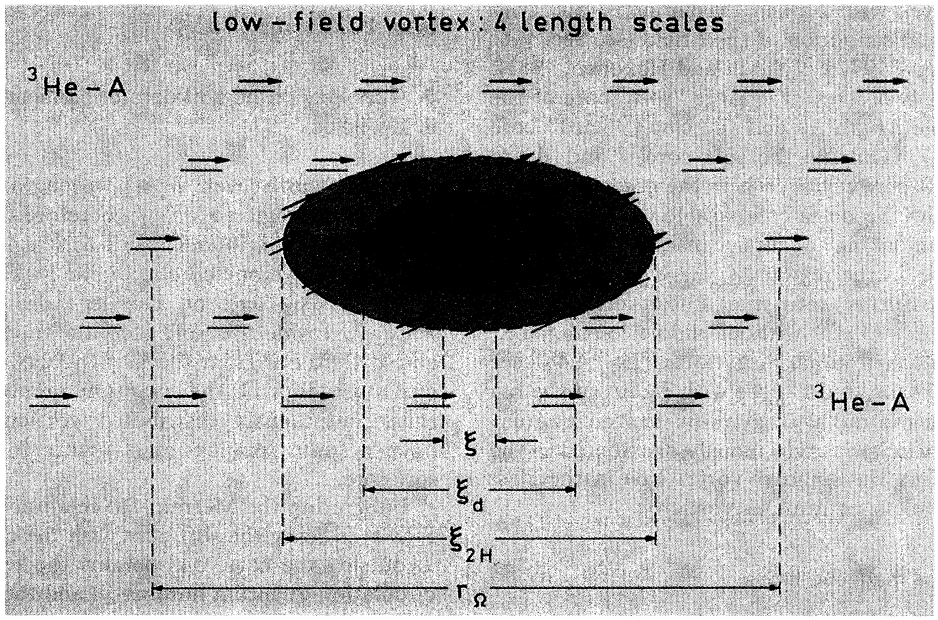

FIG. 11. Schematic illustration of the three cores of the singular ^{3}He-A vortex in a low magnetic field. Arrows indicate the l-vector distribution, while the $\mathbf{d}$-vector field is denoted by lines without arrowhead. In the outer soft-core region $\xi_d<r<\xi_{2H}$, the l and $\mathbf{d}$ vectors are dipole locked, but may deviate from the plane. For $\xi<r<\xi_d$, the $\mathbf{d}$ field remains constant, while the l field produces the unwinding of phase and forms a singularity at $r\sim\xi$ (hard core). Inside this hard vortex core, $r<\xi$, the superfluid A-phase pairing state is broken, and pairing into new superfluid phases results, thereby resolving the l-field singularity. The vortex-lattice constant is r_Ω. (Here ξ means ξ_{GL}.)

cording to the Mermin-Ho relation (3.8), since the $\boldsymbol{l}$-vector field is locked in a plane and the right-hand side of Eq. (3.8) is zero. Therefore all the vorticity is concentrated inside this core. Thus the application of a magnetic field results in the localization of vorticity in the soft cores of the ATC and MH textures.

4. Vortices with three cores

Defects with an odd sum $m+p$ belong to the nontrivial class $N=1$ in the region $\xi_d < r < \xi_{2H}$, and to the same class $N=1$ in the region $\xi_{GL} < r < \xi_d$; therefore all of them, including the one-quantum vortex ($p=0$, $m=1$), should have three concentric cores (ξ_{2H}, ξ_d, and ξ_{GL}) inside each other (Volovik and Hakonen, 1981; see Fig. 11). The outermost core is the dipole-locked core of size ξ_{2H}, inside which $\boldsymbol{l}$ and $\mathbf{d}$ are locked but may deviate from the plane: they are fixed in a plane by the magnetic field only outside this core. In the second (dipole unlocked) soft core, of size ξ_d, $\boldsymbol{l}$, and $\mathbf{d}$ are unlocked and the vortex with $m=1$ transforms into a disgyration in the $\boldsymbol{l}$ field with a uniform $\mathbf{d}$ field, which in turn has a singular hard core of size ξ_{GL} where the A-phase state is broken. Whether the vorticity is concentrated inside the soft dipole-unlocked or soft dipole-locked core depends on the details of the gradient energy [Eq. (3.10)]. In the third "hard" core, of size ξ_{GL}, the A-phase state is broken: the hard core is normal, or consists of new superfluid states.

5. Topology of vortices in high fields

The high-field situation is typical for NMR experiments on vortices (Hakonen, Ikkala, Islander, Lounasmaa, and Volovik, 1983), since they have been carried out in an external magnetic field $H \sim 300\ \text{G} \gg 25\ \text{G}$. In this case, there is a hierarchy of length scales for the vortices, different from that for the low-field vortices: ξ_{GL}, ξ_{2H}, and ξ_d.

At the largest distances, $r > \xi_d > \xi_{2H}$, where both the magnetic field and the dipole energies are essential, the linear defects are described by the same homotopy group (4.14) as before, with the indices m,p. However, their core structures are different, because the intermediate region is now $\xi_{2H} < r < \xi_d$. In this regime, there is no dipole locking, but $\mathbf{d}$ is locked in a plane by the magnetic field, and its sphere S^2 in Eq. (4.1) is restricted to the circle S^1. Thus the space of degenerate states in the region $\xi_{2H} < r < \xi_d$ is

$$R_A^H = (S^1 \times SO_3)/Z_2 \ , \tag{4.17}$$

with the homotopy group

$$\pi_1(R_A^H) = Z \times Z_4 \ . \tag{4.18}$$

In addition to the charge N of the group Z_4, the topological classes of the defects are also characterized by the integer charge p of the group Z, which denotes the index p of disclinations in the $\mathbf{d}$ field.

Topological stability of the disclinations in this intermediate region results in the fact that the nonsingular ATC and MH textures have quite different core structures and, therefore, very different energies. The ATC texture has only one (dipole-unlocked) soft core of size ξ_d, inside which unwinding of the phase Φ occurs due to the fountainlike $\boldsymbol{l}$ texture, while $\mathbf{d}$ remains nearly constant. The MH texture has a disclination in both the $\boldsymbol{l}$ and the $\mathbf{d}$ fields, with $p=1$ in the region $r > \xi_{2H}$. At a smaller distance, i.e., inside the dipole-locked core in the region $\xi_{2H} < r < \xi_d$, the $\boldsymbol{l}$-field disgyration is unwound (see Fig. 12). This disclination in the $\mathbf{d}$ field in turn has another smaller soft core of size $\xi_{2H} < \xi_d$, inside which $\mathbf{d}$ "escapes into the third dimension," i.e., comes out from the plane, destroying the singularity.

This double-core structure of the MH vortex, with large gradients in the region of the smaller core, makes it energetically unfavorable in comparison with the one-core ATC texture (see Sec. V.C.2). Thus the ATC vortices become the only nonsingular textures that are advantageous in a rotating vessel in the presence of a high magnetic field (Volovik and Hakonen, 1981; Zotos and Maki, 1984b; Fetter, 1985).

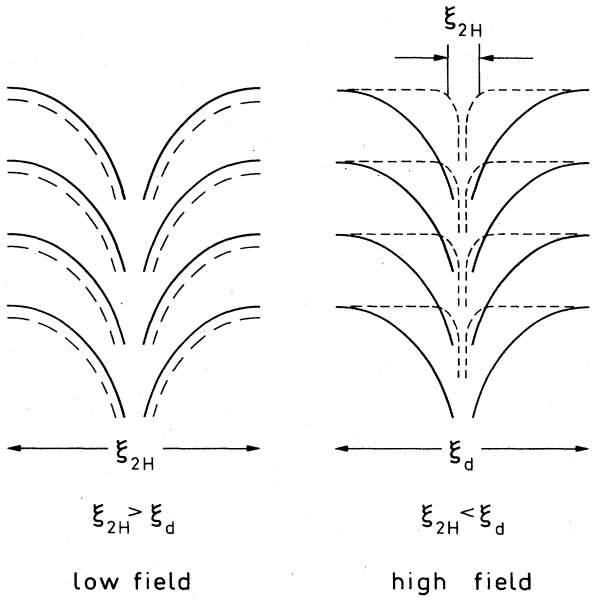

FIG. 12. The Mermin-Ho vortex textures in a low and in a high magnetic field. The solid curves denote the $\boldsymbol{l}$-vector distribution, while the dashed lines indicate the $\mathbf{d}$-vector field. In low magnetic fields, with $\xi_{2H} > \xi_d$, the $\boldsymbol{l}$ and $\mathbf{d}$ vectors are dipole locked, and both form a continuous vortex texture. In a high magnetic field, dipole unlocking occurs, and $\mathbf{d}$ does not follow $\boldsymbol{l}$. Here $\xi_{2H} < \xi_d$, and while $\boldsymbol{l}$ remains continuous, $\mathbf{d}$ becomes singular with the singularity being resolved in the inner core of size ξ_{2H}.

6. Structural core transition with a change of topological charge

It is important to recognize that the ATC core structure in high fields is topologically different from that in low fields. In the latter case, **d** follows $\boldsymbol{l}$ everywhere in the texture and therefore the index has the same value $\tilde{m}_d = 1$ as the index $\tilde{m}_l$ for the $\boldsymbol{l}$ field in Eqs. (4.16):

$$\tilde{m}_d = \frac{1}{4\pi} \int_\sigma dx\, dy \left[\mathbf{d} \cdot \frac{\partial \mathbf{d}}{\partial x} \times \frac{\partial \mathbf{d}}{\partial y} \right] . \tag{4.19}$$

Hence we find for the low-field ATC texture $\tilde{m}_d = \tilde{m}_l = 1$.

In the limit of large magnetic fields, the **d** vector in the ATC texture is locked into a plane inside the soft core $\sim \xi_d$, and cannot follow $\boldsymbol{l}$; therefore, while $\tilde{m}_l = 1$, the index $\tilde{m}_d = 0$ [see Fig. 13(a)]. Thus, on decreasing the magnetic field, one should expect to find a structural change from the high-field ATC vortex into a low-field ATC vortex, with a jump of the topological charge $\tilde{m}_d$ associated with the **d** field in the soft core of the vortex (Volovik and Hakonen, 1981; Zotos and Maki, 1984b).

The change in $\tilde{m}_d$ may occur, for example, through the creation of a point defect, or "hedgehog" [see Fig. 13(b)], in the **d** field with the topological charge $\tilde{m}_d = 1$. This hedgehog structure, created at the edge of a vortex line on the wall of the container, should move along the vortex axis to the other termination point of the vortex, thus producing the charge $\tilde{m}_d$ of the vortex [see Fig. 13(c)]. The finite time needed for the creation of the hedgehog would

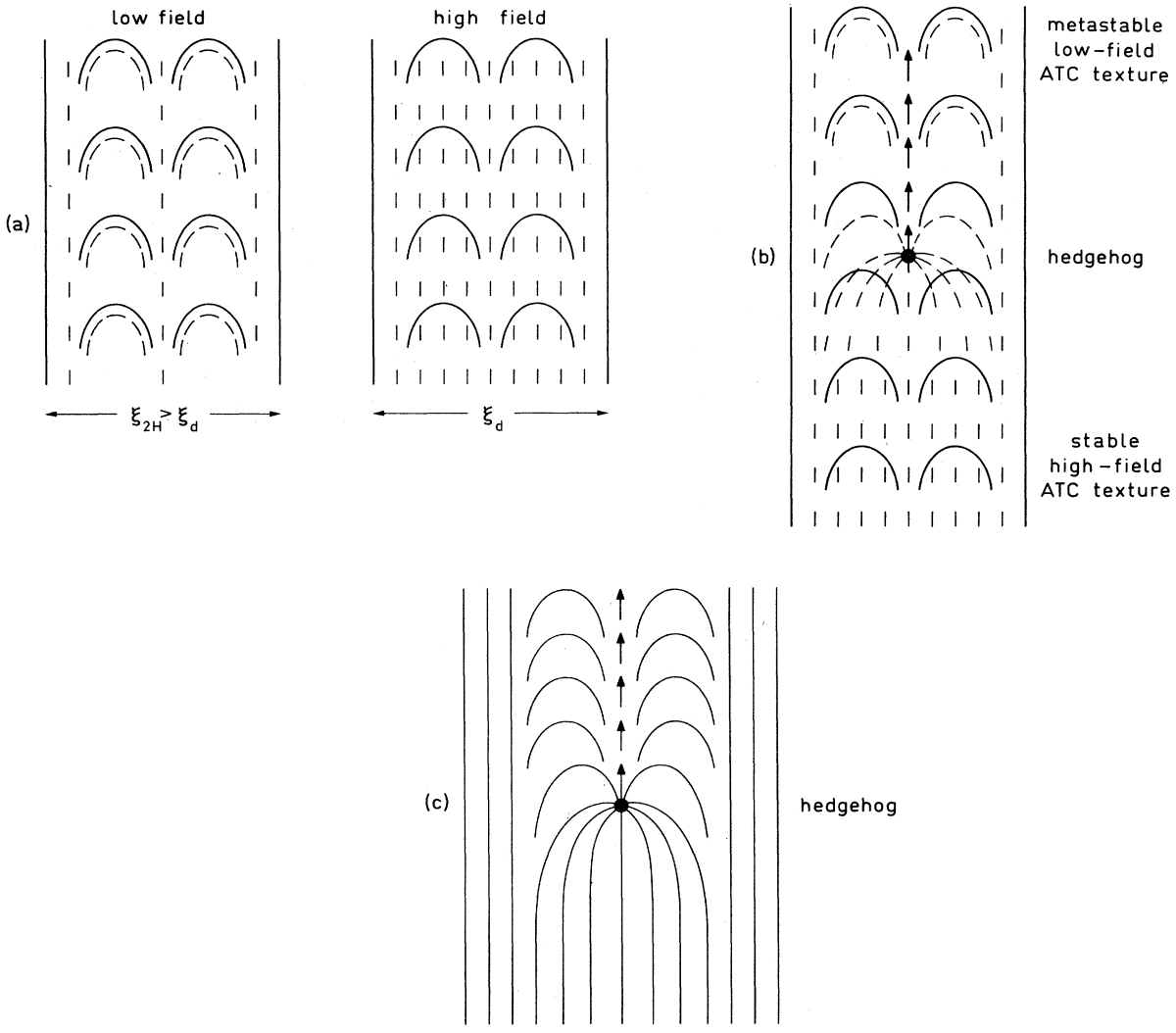

FIG. 13. (a) The Anderson-Toulouse-Chechetkin (ATC) textures in a low magnetic field (dipole locking) and in a high field (dipole unlocking). Solid curves, $\boldsymbol{l}$; dashed curves, **d**. (b) A "hedgehog," i.e., a point singularity, in the **d** field, while moving in the direction indicated by the arrows, annihilates the topological invariant of the metastable **d** field (ahead) and forms the stable high-field ATC texture (behind). (c) Only the **d**-vector field is shown here for the monopolelike hedgehog; the arrows illustrate the motion of the hedgehog.

mean a large metastability of the expected vortex-core transition. It is possible that the **d**-field hedgehog could be detected by NMR during such a transition. This structure has a specific NMR signature: the spectrum of spin-wave modes in the vicinity of a hedgehog is equivalent to the spectrum of an electron in the vicinity of a magnetic Dirac monopole.

7. Singular vortices in high fields

As in the case of low magnetic fields, the one-quantum vortex ($p=0$, $m=1$) in high fields also has three cores, in principle. In the dipole-unlocked soft core of size ξ_d, the $\boldsymbol{l}$ vector is unlocked from **d** and the vortex transforms into a disgyration in the $\boldsymbol{l}$ field with a hard core of size $\xi_{\rm GL}$. The **d** vector is locked in a plane inside ξ_d and has zero topological charge, $p=0$; this field may have an intermediate core of size $\xi_{2H}<\xi_d$, inside which **d** can escape from the plane. This deviation from the plane is usually negligibly small; therefore only two cores are relevant for the one-quantum vortex: a dipole-unlocked soft core ($\sim\xi_d$) and a hard core ($\sim\xi_{\rm GL}$) (Seppälä and Volovik, 1983; Vulovic, Stein, and Fetter, 1984; see Fig. 14).

The vorticity of this one-quantum high-field vortex, as well as the vorticity of the nonsingular ATC high-field vortex textures, is concentrated in the dipole-unlocked soft-core region, since outside the soft core the $\boldsymbol{l}$ texture is locked into a plane.

D. Topology of periodic vortex textures in a rotating container

1. Lattice of isolated vortices

If one neglects the centrifugal forces in the rotating container, which produce the density profile, the effect of rotation on superfluids is equivalent to the effect of an external magnetic field on a charged liquid. The gradient energy (2.19) must contain the covariant derivative **D** instead of the ordinary ∇; thus

$$\mathbf{D}A_{\alpha i}=(\nabla-i\mathbf{A})A_{\alpha i},\quad \mathbf{D}A^*_{\alpha i}=(\nabla+i\mathbf{A})A^*_{\alpha i}\ , \tag{4.20}$$

where the vector potential **A** is proportional to the normal-fluid velocity $\mathbf{v}_n=\mathbf{\Omega}\times\mathbf{r}$ in the rotating container:

$$\mathbf{A}=\frac{M}{\hbar}\mathbf{v}_n=\frac{M}{\hbar}\mathbf{\Omega}\times\mathbf{r}\ . \tag{4.21}$$

For the energy of the A phase in the London limit, this corresponds to the change $\mathbf{v}_s\rightarrow\mathbf{v}_s-\mathbf{\Omega}\times\mathbf{r}$ in Eq. (3.10). If the superfluid were at rest under rotation, i.e., if one had $\mathbf{v}_s=0$, then, due to the $\mathbf{\Omega}\times\mathbf{r}$ term, its energy would increase proportionally to R^4 with the radius R of the vessel, which is faster than the increase of volume. In order to avoid such a divergence of energy per unit volume, the condition of solid-body-like rotation must be fulfilled. On the average, the superfluid velocity $\mathbf{v}_s$ should increase as $\mathbf{\Omega}\times\mathbf{r}$, in order to compensate the vector-potential field:

$$\langle\mathbf{v}_s\rangle=\mathbf{\Omega}\times\mathbf{r},\quad\langle\nabla\times\mathbf{v}_s\rangle=2\mathbf{\Omega}\ . \tag{4.22}$$

In superfluids that exhibit potential superflow (such as He II, ^{3}He-B, and ^{3}He-A in a high magnetic field with potential superflow outside the soft core of the vortices), nonzero vorticity may exist only due to the presence of isolated quantized vortices. If each vortex line has m quanta of circulation, then Eq. (4.22) defines the density of vortices n_v per unit area of the vessel. Since the average vorticity in the vortex array is $n_v m\,(h/M)$, one finds

$$n_v=\frac{2M\Omega}{mh}\ . \tag{4.23}$$

The energy of a superfluid containing a vortex array with this density is now proportional to the volume of the container. However, this energy is different for the various types of vortices and distinct possible configurations of the vortex lattice. Different systems of vortices may be compared either in terms of their energy per unit volume or—equivalently—in terms of the energy per quantum of superflow.

2. Smooth vortex textures

This picture of isolated vortices is only valid if the cores, where the vorticity is concentrated, are nonoverlapping. For the ^{3}He-A vortices in a high magnetic field, this is valid even for the highest available rotational velocities $\Omega\sim2$ rad/sec: the distance between the vortices, $r_\Omega\sim n_v^{-1/2}\sim10^{-2}$ cm, is larger than the dipole-unlocked soft-core size, which is of the order of $\xi_d\sim10^{-3}$ cm, where the vorticity is concentrated. In low fields, the vorticity of nonsingular vortices (and possibly that of singular vortices as well) is concentrated in the dipole-locked soft core with size of the order of $\xi_{2H}>\xi_d$, and the overlapping of vorticity of the nearest vortices becomes important. Thus, instead of isolated vortices, one finds continuously distributed vorticity, which also should satisfy the solid-body rotation condition (4.22).

This texture has an equivalent to Eq. (4.23), provided that the vortex texture is periodic in the rotating equilibrium state (Volovik and Kopnin, 1977). In an external magnetic field a charged liquid may be periodic only provided that the quantization condition on the magnetic flux is fulfilled. The total magnetic flux $HS_{\rm cell}$ through an elementary cell $S_{\rm cell}$ of the periodic structure is quantized in units of the elementary flux quantum $\phi_0=h/e$ (see, for example, Brown, 1964; Zak, 1964a, 1964b):

$$HS_{\rm cell}=m\phi_0\ . \tag{4.24}$$

The transcription of this equation into the language of rotating superfluids yields the quantization rule

$$\Omega S_{\rm cell}=\frac{1}{2}m\frac{h}{M}\ . \tag{4.25}$$

Together with the solid-body-like rotation condition (4.22), this produces the quantization rule for the circulation of superfluid velocity along the boundary L of a

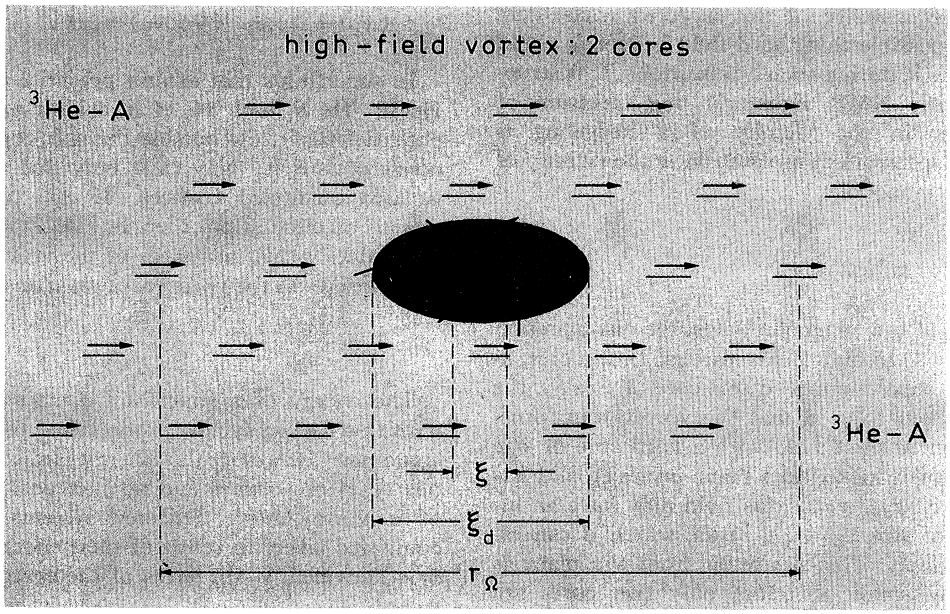

FIG. 14. The singular one-quantum vortex in ^{3}He-A in a high magnetic field. Compare with the three-core structure in Fig. 11 (notations are the same in both figures). The region between ξ_d and ξ_{2H} is absent in high fields: only the dipole-unlocked soft core remains.

primitive cell of the vortex lattice with area $S_{\rm cell}$:

$$\oint_L d\mathbf{r}\cdot\mathbf{v}_s = \int_{S_{\rm cell}} d\mathbf{S}\cdot\nabla\times\mathbf{v}_s = \mathbf{S}_{\rm cell}\cdot\langle\nabla\times\mathbf{v}_s\rangle = 2\Omega S_{\rm cell} = m\frac{h}{M} \ . \tag{4.26}$$

Thus each primitive cell behaves like a vortex with m quanta of circulation.

For the nonsingular vortex texture, one may apply Eq. (4.16b), which couples m with the index $\tilde{m}_l$ of the $\boldsymbol{l}$ field in the cell:

$$\tilde{m}_l = \tfrac{1}{2}m \ . \tag{4.27}$$

Here $\tilde{m}_l$ is the number of times the $\boldsymbol{l}$ vector in the primitive vortex-lattice cell covers the unit sphere, or—in other

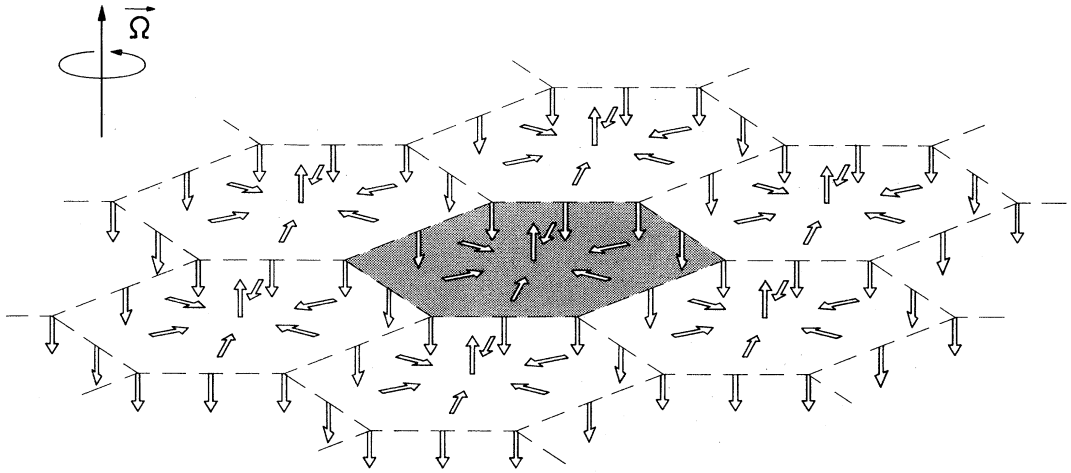

FIG. 15. Periodic hexagonal $\boldsymbol{l}$ texture (arrows) of continuous ATC vortices in rotating superfluid ^{3}He-A when $H=0$. Each elementary cell (one of which is darkened) of the lattice is a continuous vortex with two quanta of superfluid circulation $\oint \mathbf{v}_s\cdot d\mathbf{r}$ along and around the cell boundary (dashed).

words—$\tilde{m}_l$ is the degree of the mapping of the two-dimensional torus (the primitive lattice cell with periodic boundary conditions is equivalent to a torus) onto the sphere. This index should be an integer; therefore a nonsingular texture should possess an even number m of circulation quanta along the cell boundary.

The simplest example of a nonsingular low-field texture with $m=2$ is a hexagonal periodic structure of ATC vortices, displayed in Fig. 15 (Volovik and Kopnin, 1977). An example of a texture with $m=4$ is given in Fig. 16 (Fujita, Nakahara, Ohmi, and Tsuneto, 1978; Tsuneto, Ohmi, and Fujita, 1978; Nakahara, Ohmi, Tsuneto, and Fujita, 1979). The primitive cell contains four different nonsingular one-quantum MH vortices, producing four quanta of circulation per cell. According to Eq. (4.25), the area of the four-quantum unit cell is twice as large as that for the two-quantum unit cell. Different symmetry subclasses of textures are possible inside a given topological class with fixed $\tilde{m}_l$. The symmetry of vortex lattices in terms of magnetic classes is discussed by Sonin and Fomin (1985).

Note that even though $\boldsymbol{l}$ is periodic in the texture, the order parameter $A_{\alpha i}$ is not. In analogy with the charged system in a magnetic field, the texture should be periodic under "magnetic" translations (Peierls, 1933), i.e., the translation $\mathbf{r}\rightarrow\mathbf{r}+\mathbf{b}$ combined with a Galilean transformation

$$A_{\alpha i}(\mathbf{r})\rightarrow A_{\alpha i}(\mathbf{r}+\mathbf{b})e^{i(M/\hbar)(\boldsymbol{\Omega}\times\mathbf{b})\cdot\mathbf{r}} . \tag{4.28}$$

The only truly periodic quantities are those which are Galilean invariant, such as $\boldsymbol{l}$, $\mathbf{d}$, and $\mathbf{v}_s-\mathbf{v}_n$.

V. SYMMETRY OF VORTICES IN ^{3}He-A

A. Axial and discrete symmetries of vortices in superfluids

1. Symmetry of linear defects

In the preceding section we considered the topologically different classes of vortices and illustrated these classes by their simplest representatives. However, these examples are not necessarily solutions of the corresponding Ginzburg-Landau (or Gor'kov) equations for all length scales. A vortex solution may be rather complicated, requiring a minimization procedure that involves trial functions with a large number of amplitudes. This is different from the He II vortex, which is described by just one complex amplitude $\psi(\mathbf{r})=|\psi(r)|e^{im\phi}$, such that only a single radially varying function $|\psi(r)|$ is involved. However, a symmetry analysis is a powerful tool, providing essential restrictions on the number of the amplitudes. This analysis, moreover, allows one to describe the possible phase transitions, which should accompany the symmetry breaking, as well as to characterize the distinct physical properties of the broken-symmetry states.

The symmetry classification of defects in condensed matter is analogous to the classification of the ordered states of the system themselves. In order to find all the physically different, say, linear defects, it is sufficient to enumerate all the subgroups H of such a symmetry group G, which is relevant for the given type of defect. The existence of a line defect restricts the Euclidian group to $D_{\infty h}\times t^z$, where $D_{\infty h}$ includes rotations around the vortex axis $\hat{z}$, rotations by π around a perpendicular axis, and space inversion P; here t^z denotes translations along $\hat{z}$.

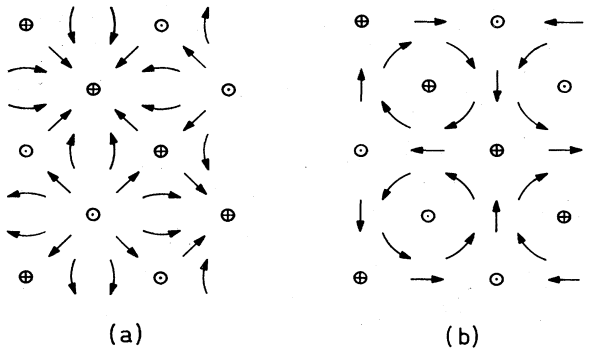

FIG. 16. (a) and (b): Two possible periodic lattices of continuous Mermin-Ho vortices with four quanta of circulation, $m=4$, per primitive cell. Every cell contains four Mermin-Ho vortices, each with unit quantum of circulation, $m=1$; $\oplus$, $\boldsymbol{l}$ down; $\odot$, $\boldsymbol{l}$ up.

The magnetic field and dipole interactions are important for vortices in ^{3}He-A; a magnetic field restricts the separate spin rotations, while the dipole energy completely destroys them. However, neither one violates the symmetry $D_{\infty h}$ if the field is along the vortex axis. Thus, in the presence of the line defect, the symmetry group G of physical laws is reduced to

$$G=(D_{\infty h}\times t^z)\times(T\times \mathrm{U}(1)) . \tag{5.1}$$

The most symmetric linear defects correspond to the maximal subgroups H of G, possible for a given topological class. The maximal symmetry groups H have two continuous subgroups, with the following generators (Salomaa and Volovik, 1983b, 1985a):

$$\hat{Q}=\hat{J}_z-n\hat{I} , \tag{5.2}$$

$$\hat{p}_z-q\hat{I},\quad \hat{p}_z=\frac{1}{i}\frac{\partial}{\partial z} . \tag{5.3}$$

Here n is an integer, which has the meaning of the total angular momentum eigenvalue of the vortex, while q is an arbitrary real number. For such physical quantities f which are gauge invariant ($\hat{I}f=0$), these two symmetries mean axisymmetry and translational invariance along the vortex axis, respectively.

2. Vortices in He II

Let us find the representatives of the symmetry class (n,q) of linear defects in He II, where the order parameter

is a complex scalar ψ, with the following action of the generator of gauge symmetry: $\hat{I}\psi=\psi$, $\hat{I}\psi^*=-\psi^*$. Superfluid He II has no internal structure; therefore $\hat{J}_z=(1/i)(\partial/\partial\phi)$.

The order parameter ψ, which is invariant under the continuous symmetries in Eqs. (5.2) and (5.3), must satisfy the symmetry equations

$$\hat{Q}\psi\equiv\left[\frac{1}{i}\frac{\partial}{\partial\phi}-n\right]\psi=0,\quad\left[\frac{1}{i}\frac{\partial}{\partial z}-q\right]\psi=0\ . \tag{5.4}$$

They have the solution

$$\psi(\mathbf{r})=C(r)e^{in\phi}e^{iqz}\ , \tag{5.5}$$

where $C(r)$ denotes an arbitrary complex amplitude that is a function only of the radial distance r from the axis of the line defect. This is a quantized vortex line with n quanta of circulation.

Since the bosons in He II have no internal structure, all the angular momentum originates from the superflow around the vortices, which is why the total angular momentum quantum number n coincides with the circulation quantum number m, i.e., $n=m$ for He II. This quantum number is simultaneously the topological charge for the He II vortex. For $q\neq0$, Eq. (5.5) also describes superflow along the z direction with the homogeneous velocity $v_s=(\hbar/M)q$. For $n\neq0$, the function $C(r)$ must vanish on the axis in order to avoid a divergent kinetic energy; therefore superfluidity is always broken on the axis of a He II vortex, where all the vorticity is concentrated.

In addition to the two continuous symmetries in Eqs. (5.2) and (5.3), the maximal symmetry group for vortices—with $n\neq0$—also has a discrete symmetry subgroup. This consists of discrete elements of G (time inversion T, space parity P, and rotations $O^{(J)}_{x,\pi}$ by π around the perpendicular axis x) in the following combinations, which are denoted by P_1, P_2, and P_3 (Salomaa and Volovik, 1983b, 1985b):

$$P_1\simeq P,\quad P_3\simeq TO^{(J)}_{x,\pi},\quad P_2=P_3P_1\ . \tag{5.6}$$

The pure symmetry T is not conserved in the vortex, since the time-inversion operation changes the direction of superflow circulation around the vortex axis ($Tm=-m$). Therefore T may enter into a symmetry operation only in combination with other symmetry elements: $O^{(J)}_{x,\pi}$ for vortices (and P for disgyrations; see Sec. V.E).

Above, in Eqs. (5.6), the symbol $\simeq$ means that these elements of the group may also include the gauge transformation U_π, i.e., multiplication by $e^{\pi i}$. For example, P_1, depending on the topological class, means either pure space parity P or space parity combined with U_π. Which parity is relevant will be seen below; however, irrespective of this, for any physical quantity f that is gauge invariant (i.e., $\hat{I}f=0$), P_1 coincides with P. It is important that if the gauge transformation is not taken into account, the classification of the vortices in superfluid ^{3}He may be expressed in terms of the magnetic classes (Landau and Lifshitz, 1984).

The most symmetric vortex should be invariant under the symmetries (5.6). [In terms of the magnetic classes, the most symmetric vortex belongs to the class $D_{\infty h}(C_{\infty h})$.] The symmetry P_2 requires that the function $C(r)$ in Eq. (5.5) for the He II vortex be real (apart from an arbitrary constant phase factor). The space parity operator P_1 for the n-quantum vortex in He II equals $PU_{\pi n}$, since only this combination is consistent with the solution (5.5) for the vortex in this topological class. The P_1 symmetry requires $q=0$; in what follows, we shall consider only the vortices with $q=0$. (However, see Secs. V.D.4 and VIII.C.6 for the w vortices, where the z dependence of the vortex texture is important.)

3. The most symmetric vortices in ^{3}He

In order to find the most symmetric vortices in superfluid ^{3}He, it is necessary first to solve the axisymmetry equation $\hat{Q}a_{\mu\nu}=0$, which in the case of ^{3}He yields [see Eqs. (5.2) and (2.8a)]

$$\hat{Q}a_{\mu\nu}\equiv\left[\frac{1}{i}\frac{\partial}{\partial\phi}+\hat{L}_z^{\rm int}+\hat{S}_z-n\right]a_{\mu\nu}=0\ . \tag{5.7}$$

The general solution of this equation is

$$a_{\mu\nu}(\mathbf{r})=C_{\mu\nu}(r)e^{i(n-\mu-\nu)\phi}\ . \tag{5.8}$$

Here, not all of the $C_{\mu\nu}$ need to vanish at the origin: if any $n-\mu-\nu=0$, then $C_{\mu\nu}$ at $r=0$ may be nonzero; this allows for the possibility of axisymmetric vortices that display no destruction of superfluidity in the hard core of the ^{3}He vortices.

The discrete symmetries in Eq. (5.6) restrict the number of possible parameters $C_{\mu\nu}(r)$. The P_1 symmetry operation, consistent with the solution (5.8), may be defined in two different ways: $P_1=P(U_\pi)^n$, as in He II, or with the opposite sign, $P_1=P(U_\pi)^{n+1}=-P(U_\pi)^n$. These functions $C_{\mu\nu}(r)$ transform under the symmetry P_1 in the following ways, depending on the form of P_1:

$$P_1C_{\mu\nu}=(-1)^{\mu+\nu}C_{\mu\nu}\ \text{ for } P_1=P(U_\pi)^{n+1}\ , \tag{5.9}$$

$$P_1C_{\mu\nu}=(-1)^{\mu+\nu+1}C_{\mu\nu}\ \text{ for } P_1=P(U_\pi)^{n}\ . \tag{5.10}$$

Thus, if the symmetry P_1 is given by Eq. (5.9), the most symmetric vortex, which obeys $P_1C_{\mu\nu}=C_{\mu\nu}$, has either five nonzero functions $C_{\mu\nu}$ for even $(\mu+\nu)$,

$$C_{++},\quad C_{+-},\quad C_{00},\quad C_{-+},\quad C_{--}\ , \tag{5.11}$$

or—if the symmetry P_1 is given by Eq. (5.10)—it has four nonzero functions $C_{\mu\nu}$ for odd $(\mu+\nu)$:

$$C_{+0},\quad C_{0+},\quad C_{0-},\quad C_{-0}\ . \tag{5.12}$$

Since there is no additional symmetry that couples the amplitudes $C_{\mu\nu}$, all the vortices in superfluid ^{3}He have nonunitary components and, therefore, have a net core magnetization. [See Salomaa and Volovik (1983b), and Sec. VIII for the B-phase vortices, and Passvogel,

Tewordt, and Schopohl (1984) for the magnetization of the continuous A-phase vortices.]

The number of amplitudes increases, however, if the conservation of P_1 symmetry is not compatible with topology. The topological constraints break the P_1 symmetry for the half-quantum vortices and for the continuous vortices (Sec. V.B). In these cases, the most symmetric vortices within a given topological class are not P_1 symmetric—and therefore have additional components.

Another restriction is imposed on the ^{3}He vortices by the symmetry P_2 in Eq. (5.6). Through an appropriate choice of common phase factor for the $C_{\mu\nu}$, this transformation may be reduced to complex conjugation:

$$P_2 C_{\mu\nu} = C^*_{\mu\nu} . \tag{5.13}$$

Therefore, in the most symmetric vortices, all the $C_{\mu\nu}$ are real (apart from the common constant phase factor). Thus, the most symmetric vortices in superfluid ^{3}He are described by an integer n, the total angular momentum quantum number, and have at least four (or five) real functions $C_{\mu\nu}(r)$—in contrast with the single real function $C(r)$ for the vortices in He II [cf. Eq. (5.5)].

In the ^{3}He-B vortices the nonzero $C_{\mu\nu}(r)$ in the asymptotics are $C_{+-}=C_{00}=C_{-+}$ according to Eq. (2.14b), and each of these has the same phase factor $e^{in\phi}$, as follows from Eq. (5.8). The symmetry P_1, compatible with these asymptotics, is given by Eq. (5.9). Thus the most symmetric vortices in ^{3}He-B have exactly five independent real functions $C_{\mu\nu}(r)$, and

$$m = n . \tag{5.14}$$

That is, in these vortices the angular momentum index n coincides with the circulation quantum number m, since—as is the case with He II—there is no internal angular momentum in the B phase. This vortex was first considered by Ohmi, Tsuneto, and Fujita (1983).

4. Vortex "isospin" in ^{3}He-A

Examples of axisymmetric vortices in ^{3}He-A, with the topological charges $N=0$ and $N=1$, are given by Eqs. (4.6) and (4.4), respectively. For the pure phase vortices [Eqs. (4.4a) and (4.6b)], the integer n is expressed through the circulation quantum number m: $n=m+1$. However, this is valid only for vortices with the asymptote $\boldsymbol{l}(\infty)=\hat{z}$; for the other axisymmetric asymptote, with $\boldsymbol{l}(\infty)=-\hat{z}$, the index n assumes the value $n=m-1$. Therefore, for the axisymmetric pure phase vortices, we find the following relation between the total angular-momentum quantum number n and the circulation quantum m (Fujita and Tsuneto, 1975):

$$n = m + \hat{z}\cdot\boldsymbol{l}(\infty) . \tag{5.15}$$

This equation is also valid for any other axisymmetric vortices in Eqs. (4.4) and (4.6), and even for the continuous ATC and MH textures given by Eq. (4.7). In the MH texture, one has $\hat{z}\cdot\boldsymbol{l}(\infty)=0$.

The quantum number n thus resembles the total angular momentum of a particle with the unitary "isospin" $\boldsymbol{l}(\infty)$, whose projection on the quantization axis $\hat{z}$ (vortex axis) assumes the values 0, or ± 1. This is the result of the internal angular momentum of the Cooper pairs in the A phase, which is directed along the $\boldsymbol{l}$ vector. Thus, the structure of the axisymmetric vortex in the A phase depends essentially on the orientation of the $\boldsymbol{l}$ field in the bulk liquid with respect to the vector $\hat{\Omega}$ of the angular velocity of rotation.

5. The most symmetric vortices in ^{3}He-A

From all the vortices in the examples of Eqs. (4.4) and (4.6), only the pure phase vortices are the most symmetric. The relevant P_1 transformation for them is given by Eq. (5.10). Therefore, in the general case, they are described by only four independent real functions [see Eq. (5.12)]. However, even this number may be reduced if the smallness of the dipole coupling is taken into account.

Let us first consider a situation in which the dipole energy may be neglected, e.g., well inside the soft core of singular vortex textures. In this case there are two separate continuous symmetries:

$$\hat{Q} = \hat{L}_z - n\hat{I}, \quad \hat{S}_z . \tag{5.16}$$

The symmetry $\hat{S}_z$ requires that $\mathbf{d}$ be parallel to $\hat{z}$. This completely rules out the consideration of half-integer vortices: their topology requirement that $\mathbf{d}$ be nonuniform is inconsistent with the symmetry $\hat{S}_z$. This is one of many examples of mutual incompatibility of the topology and symmetry requirements in superfluid ^{3}He (see also Sec. V.B). The topology of the half-quantum vortex is also incompatible with the symmetry P_1, which requires $\mathbf{d}(\mathbf{r})=\mathbf{d}(-\mathbf{r})$.

Thus, we consider the singular vortices of the topological class $N=1$. (We also consider the singular vortices within the class $N=0$. These vortices are, of course, unstable towards the elimination of the singularity; nevertheless, it is important to know their symmetry in order to understand what symmetry is broken when they transform into the nonsingular texture.) The most symmetric vortices with $N=1$ are given in the region $\xi_{GL}<r<\xi_d$ by Eqs. (4.4a)—(4.4c), with Eq. (5.15) for n [and with Eq. (4.6b) for $N=0$]. In the region $r\lesssim\xi_{GL}$, they are described by Eq. (5.12).

However, due to the additional continuous symmetry $\hat{S}_z$, the number of independent functions $C_{\mu\nu}$ in the most symmetric vortex is reduced to two: C_{0+} and C_{0-}. They correspond to the amplitudes of the Cooper-pair states with zero spin projection ($S_z=0$). Therefore the most symmetric vortices in ^{3}He-A with integer quanta of circulation m have the following general expression in the whole region $r<\xi_d$ (Salomaa and Volovik, 1985b):

$$A_{\alpha i} = \Delta_A \hat{z}_\alpha [C_{0+}(r)(\hat{x}_i + i\hat{y}_i)e^{i(n-1)\phi} + C_{0-}(r)(\hat{x}_i - i\hat{y}_i)e^{i(n+1)\phi}] . \tag{5.17}$$

Here $C_{0+}(\infty)=1$ and $C_{0-}(\infty)=0$ for the vortex with $m=n-1$ quanta of circulation and $\boldsymbol{l}(\infty)=\hat{z}$, while $C_{0+}(\infty)=0$ and $C_{0-}(\infty)=1$ for the vortex with $m=n+1$ circulation quanta and $\boldsymbol{l}(\infty)=-\hat{z}$. Note that the order parameter should be zero on the vortex axis for all these axisymmetric vortices, except for the doubly quantized vortices with $\boldsymbol{l}(\infty)=\hat{z}$, $m=-2$ [where $C_{0-}(0)\neq 0$], and with $\boldsymbol{l}(\infty)=-\hat{z}$, $m=2$ [in which $C_{0+}(0)\neq 0$].

Equation (5.17) for the most symmetric vortices is valid even at large distances $r>\xi_d$, where the dipole energy is essential: the contributions of the components C_{+0},C_{-0} in Eq. (5.12) are small in proportion to $(\xi_{\rm GL}/\xi_d)^2$, in comparison with C_{0+},C_{0-}.

Thus, the most symmetric singular vortices in ^{3}He-A, belonging to the topological classes $N=0$ and 1, are characterized by the integer index m of the number of circulation quanta and by the projection on the vortex axis of the asymptote of the $\boldsymbol{l}$ field [$\boldsymbol{l}(\infty)=\pm\hat{z}$, which resembles the spin of a particle] and are described by two real functions of the radial distance r from the vortex axis.

However, the most symmetric vortices are unstable in ^{3}He-A: their energies may be diminished by the spontaneous breaking of both axial and discrete symmetries. For example, it is energetically more advantageous for the singular doubly quantized $N=0$ vortex to transform into the continuous ATC texture, in which parity P is—inevitably—broken.

B. Broken space parity in continuous vortices: symmetry versus topology

The symmetry requirement is often incompatible with topological constraints. In particular, the space parity P should be broken for definite topological classes of continuous vortex textures. Let us consider this with the examples of the ATC and MH textures.

Since $\boldsymbol{l}(\mathbf{r})$ transforms under the P_1 transformation as

$$P_1\boldsymbol{l}(\mathbf{r})=\boldsymbol{l}(-\mathbf{r})\ , \tag{5.18}$$

the P_1 symmetry requires

$$\boldsymbol{l}(\mathbf{r})=\boldsymbol{l}(-\mathbf{r})\ . \tag{5.19}$$

This equation is incompatible with an axisymmetric distribution for the $\boldsymbol{l}$ field, which would require

$$\boldsymbol{l}_\perp(\mathbf{r})=-\boldsymbol{l}_\perp(-\mathbf{r})\ . \tag{5.20}$$

Equations (5.19) and (5.20) are only satisfied in the homogeneous case $\boldsymbol{l}\|\hat{z}$, with $\boldsymbol{l}_\perp=0$ (see Fig. 17).

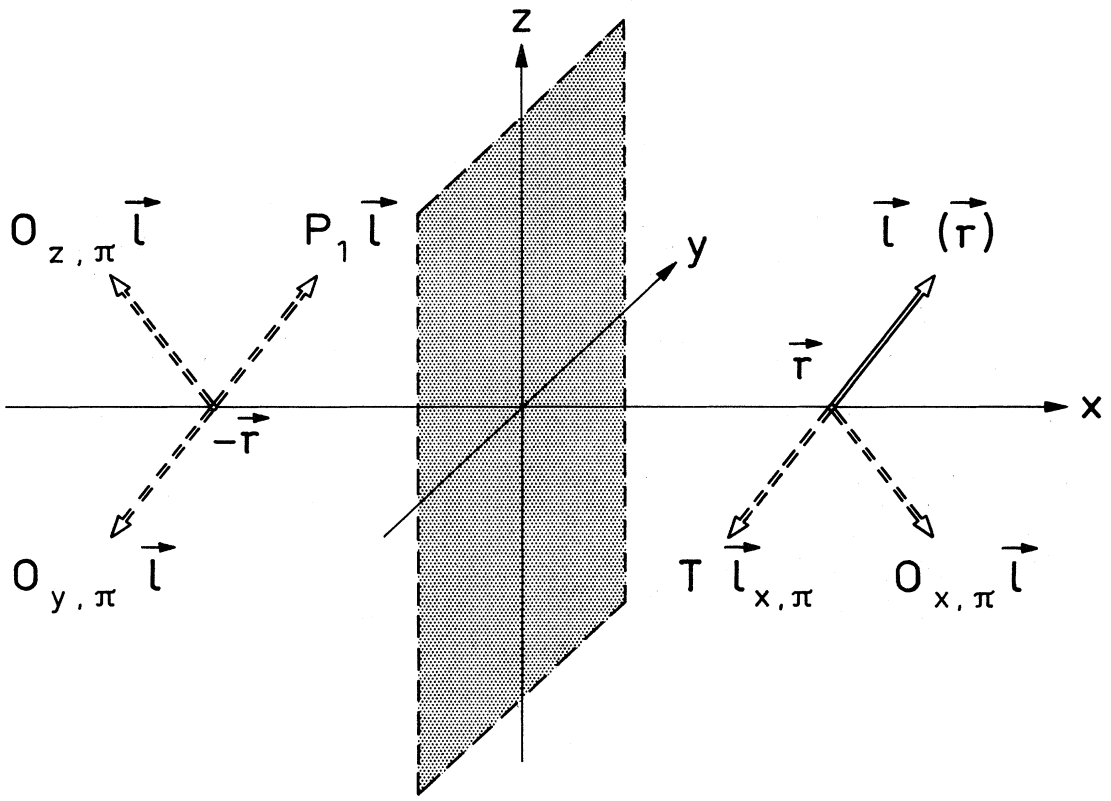

FIG. 17. Illustration of the transformation properties of $\boldsymbol{l}(\mathbf{r})$ under the different discrete parity changes discussed in the text. Both $\boldsymbol{l}$ and $\mathbf{r}$ may be changed under the symmetry operations (here the radius vector $\mathbf{r}$ is chosen along the x axis); for example, the rotation $O_{y\pi}$ (rotation by the angle π around the y axis) transforms $\mathbf{r}\rightarrow-\mathbf{r}$. [$\boldsymbol{l}$ is chosen here in the (x,z) plane.]

Therefore, in nonsingular axisymmetric vortices (ATC and MH) with inhomogeneous $\boldsymbol{l}$ fields, which are energetically favored over singular vortices in the same class $N=0$, space parity is spontaneously broken. There exists an even more general law, valid also for nonaxisymmetric continuous textures: in continuous vortices with odd topological charge $\tilde{m}_l$ in Eq. (4.16a), the space parity P_1 is broken. According to Eq. (5.18), the $\boldsymbol{l}$ vector in the P_1-symmetric texture assumes each value twice (or an even number of times): in the point $\mathbf{r}_0$ and in the diametrically opposite point $-\mathbf{r}_0$. This is in contradiction with the condition of odd topological charge $\tilde{m}_l$ [Eq. (4.16a)], which shows that the $\boldsymbol{l}$ vector covers the unit sphere $\tilde{m}_l$ times and therefore assumes each value an odd number of times for the ATC texture and covers a half-sphere for the MH texture. Thus parity in nonsingular textures is broken solely due to topological reasons.

As a consequence of the spontaneously broken symmetry P_1, the vortex texture is twofold degenerate. For example, there are two different states (see Fig. 18) with the same energy for the ATC vortex having $m=-2$ and with $\boldsymbol{l}(\infty)=\hat{z}$:

$$\begin{aligned} \boldsymbol{l} &= \hat{z}\sin\eta(r) \pm \hat{r}\cos\eta(r) , \\ \mathbf{v}_s &= -\frac{\hbar}{Mr}[1+\sin\eta(r)]\hat{\phi} , \end{aligned} \tag{5.21}$$

where $\eta(\infty)=\pi/2$ and $\eta(0)=-\pi/2$. These states are mapped onto each other through the P_1 transformation [see Eq. (5.18)].

It is important that the symmetry P_1 may be broken in two different ways, depending on which discrete symmetry in Eq. (5.6) is still retained, P_2 or P_3; the corresponding vortices are denoted by v and w (Salomaa and Volo-

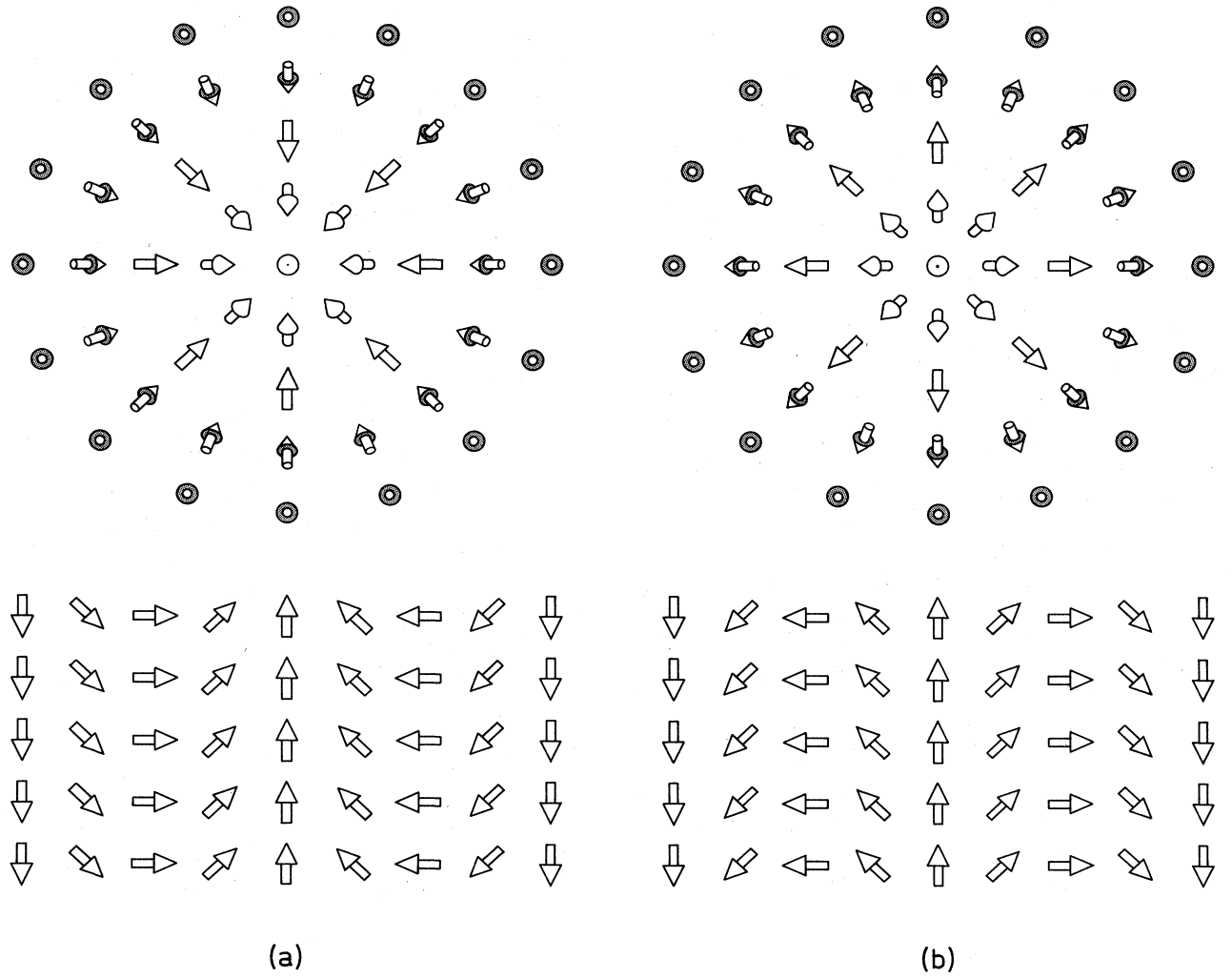

FIG. 18. Schematic illustration of the continuous ATC vortex in the two possible degenerate v states, v^+ and v^-, in (a) and (b), respectively. Arrows indicate the $\boldsymbol{l}$ vector. Above, view from the top; below, side view. These two degenerate states are mapped into each other through a parity transformation.

vik, 1983b; Seppälä, Hakonen, Krusius, Ohmi, Salomaa, Simola, and Volovik, 1984). The ATC vortex in Eq. (5.21) is the v vortex, since the combined symmetry P_2 is conserved in this case. The axisymmetric nonsingular w vortex, with $m=-2$ and with $\hat{l}(\infty)=\hat{z}$, displays a twisted l texture with the symmetry P_3 (see Fig. 19):

$$\hat{l}=\hat{z}\sin\eta(r)\pm\hat{\phi}\cos\eta(r)\ ,$$
$$\mathbf{v}_s=-\frac{\hbar}{Mr}[1+\sin\eta(r)]\hat{\phi}\ . \tag{5.22}$$

This vortex has twofold degeneracy as well; the two states also transform into each other through space inversion P_1.

Moreover, it is possible that all the discrete symmetries in Eq. (5.6) are simultaneously broken, due to energy considerations. The corresponding vortex is denoted as the uvw vortex (the u vortex, the P_1 symmetric vortex with broken symmetries P_2 and P_3, is impossible among the continuous vortices with $m=-2$ and therefore with odd $\tilde{m}_l=-1$). The corresponding axisymmetric ATC texture in the uvw vortex is

$$\hat{l}=\hat{z}\sin\eta(r)\pm\cos\eta(r)[\hat{\phi}\cos\alpha(r)\pm\hat{r}\sin\alpha(r)]\ ,$$
$$\mathbf{v}_s=-\frac{\hbar}{Mr}[1+\sin\eta(r)]\hat{\phi}\ . \tag{5.23}$$

This vortex has fourfold degeneracy. The four states are obtained from each other through the application of the elements P_1, P_2, and P_3, which form the group $Z_2\times Z_2$.

Due to different spontaneously broken symmetries, the v and w vortices also display distinct physical properties—to be discussed in Sec. V.D—while the uvw vortex shares properties of both the v and w vortices. In

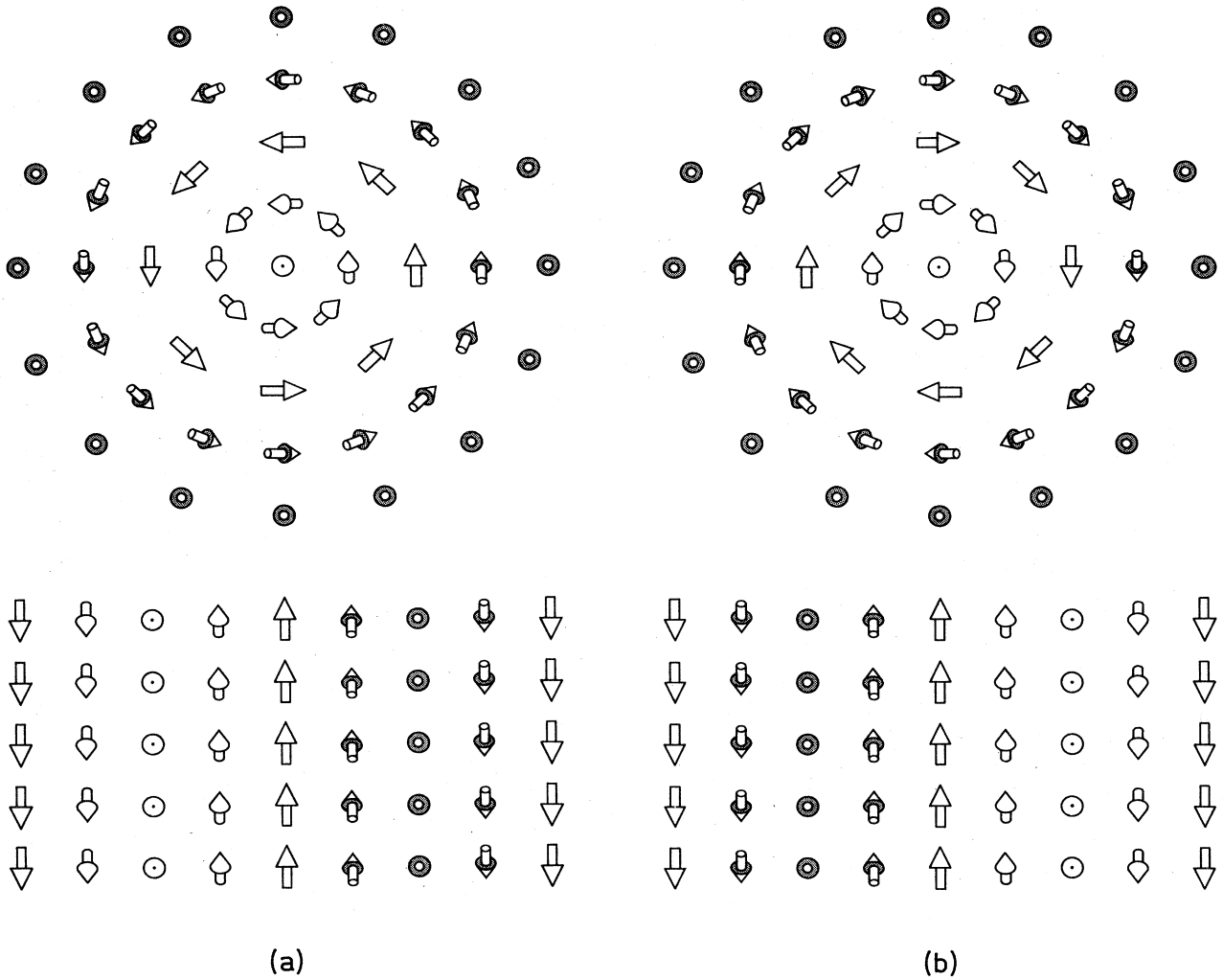

FIG. 19. The continuous ATC vortex in the two possible w states, w^+ and w^-, in (a) and (b), respectively, which are mutually degenerate.

terms of the magnetic classes, the axisymmetric v, w, and uvw vortices with broken parity belong to the classes $C_{\infty v}(C_\infty)$, $D_\infty(C_\infty)$, and C_∞, respectively. The axisymmetric u vortex corresponds to the class $C_{\infty h}$.

C. Broken axisymmetry in the ^{3}He-A vortices

As distinct from parity, which is broken due to topology, axisymmetry Q is spontaneously broken purely for reasons of energetics.

1. Singular vortices with broken axisymmetry

Let us first consider the energy of the singular vortices in the class $N=1$ in the absence of an applied magnetic field and outside the soft-core region, $r>\xi_d$, i.e., in the dipole-locked region. The best candidates for the vortex with minimal energy among vortices possessing axisymmetry are the pure-phase vortex [Eq. (4.4a)] ($p=0$, $m=1$) and the radial [Eq. (4.4d)] ($p=1$, $m=0$, $\mathbf{l}=\hat{r}$) and tangential [Eq. (4.4e)] ($p=1$, $m=0$, $\mathbf{l}=\hat{\phi}$) disgyrations. Let us also include a nonaxisymmetric pure phase vortex ($p=0$, $m=1$) with $\mathbf{l}=\mathbf{d}=\hat{x}$, for the sake of the following argument, and compare their respective energies [Eq. (3.9)] in the region $\xi_d<r<R$, where R is an external cutoff radius (the radius of the container or the intervortex distance), which naturally serves as the upper logarithmic cutoff for the divergent energy of the linear defects:

$$E(p=0,m,\mathbf{l}=\hat{z})=m^2\rho_s^{\perp}\kappa\ , \tag{5.24a}$$

$$E(p=1,m,\mathbf{l}=\hat{r})=(m^2\rho_s^{\perp}+K_1+\rho_{\rm sp}^{\perp})\kappa\ , \tag{5.24b}$$

$$E(p=1,m,\mathbf{l}=\hat{\phi})=(m^2\rho_s^{\parallel}+K_3+\rho_{\rm sp}^{\parallel})\kappa\ , \tag{5.24c}$$

$$E(p=0,m,\mathbf{l}=\hat{x})=\tfrac{1}{2}m^2(\rho_s^{\parallel}+\rho_{\rm sp}^{\perp})\kappa\ , \tag{5.24d}$$

where

$$\kappa=\frac{1}{2}\left[\frac{\hbar}{M}\right]^2\ln\frac{R}{\xi_d}\ . \tag{5.24e}$$

Near T_c, where the parameters involved in Eqs. (5.24) are given by Eq. (3.13), the ratios between these energies are

$$E(p=0,m=1,\mathbf{l}=\hat{z}):E(p=1,m=0,\mathbf{l}=\hat{r}):E(p=1,m=0,\mathbf{l}=\hat{\phi}):E(p=0,m=1,\mathbf{l}=\hat{x})=2:\tfrac{5}{2}:\tfrac{5}{2}:\tfrac{3}{2}\ . \tag{5.25}$$

Thus, although the pure phase vortex with $\mathbf{l}=\hat{z}$, $m=1$ has the lowest energy among the axisymmetric vortices in the topological class $N=1$, it is unstable towards the formation of a nonaxisymmetric vortex with $\mathbf{l}=\hat{x}$ (Volovik and Mineev, 1977a). This is the result of the anisotropy of the superfluid density tensor $\rho_s^{\perp}>\rho_s^{\parallel}$: superflow circulating around the vortex line tends to lock the $\mathbf{l}$ vector into the plane of flow. A more accurate estimation of the vortex with minimal energy in the class with topological charge $N=1$, which takes into account both that in the nonaxisymmetric vortex $\mathbf{l}$ may deviate from the $\hat{x}$ direction and that the phase Φ may deviate from ϕ, gives 1.4 instead of the $\frac{3}{2}$ in Eq. (5.25) (Volovik and Hakonen, 1981).

Another logarithmic contribution to the vortex energy comes from the soft-core region, where the ratio between the energies of vortices deviates from Eq. (5.25). Inside the soft core, where it is energetically more advantageous to make the $\mathbf{d}$ vector constant, the $\mathbf{d}$ field does not contribute to the energy of disgyrations, which makes them more profitable. The energies of the corresponding vortices in the soft-core region are given by Eqs. (5.24)—without $\rho_{\rm sp}$—and with the change $\ln(R/\xi_d)\to\ln(\xi_d/\xi)$. As a result, the ratios of the soft-core energies for the vortices near T_c are as follows:

$$E(p=0,m=1,\mathbf{l}=\hat{z}):E(p=1,m=0,\mathbf{l}=\hat{r}):E(p=1,m=0,\mathbf{l}=\hat{\phi}):E(p=0,m=1,\mathbf{l}=\hat{x})=2:\tfrac{1}{2}:\tfrac{3}{2}:1.4\ , \tag{5.26}$$

which gives preference to the radial disgyration.

Therefore the linear defect with minimal energy in the topological class $N=1$ has the form of a nonaxisymmetric vortex outside the soft core and that of the axisymmetric radial disgyration well inside the dipole-locked soft core. (The nonlogarithmic energy of the intermediate region, where the vortex continuously transforms into a disgyration, may be neglected in the logarithmic approximation.) The broken axisymmetry thus tends to be restored inside the soft core.

2. Continuous vortices with broken axisymmetry

An axial magnetic field strengthens the nonaxisymmetry of singular vortices, because it also locks the $\mathbf{d}$ and $\mathbf{l}$ vectors into the plane of flow in the region $r>\xi_d,\xi_{2H}$. In a magnetic field continuous vortices also become nonaxisymmetric outside their soft cores, of size $\max(\xi_d,\xi_H)$, which they acquire in a magnetic field. Let us compare the energies of vortices in the class $N=0$ with $\mathbf{l}\perp\mathbf{H}$ outside the core: the Mermin-Ho textures ($p=1,m=-1,\mathbf{l}=\hat{r}$), ($p=1,m=-1,\mathbf{l}=\hat{\phi}$) and the ATC texture with broken axisymmetry outside the soft core. The logarithmic energies outside the soft-core region are given by Eqs. (5.24) with $\xi_d\to\max(\xi_d,\xi_{2H})$. The ratios of the corresponding energies are

$$E(p=1,m=1,\mathbf{l}=\hat{r}):E(p=1,m=1,\mathbf{l}=\hat{\phi}):E(p=0,m=2,\mathbf{l}=\hat{x})=4.5:3.5:6\ . \tag{5.27}$$

Here the tangential MH texture is preferable. However, when the vortex array is in a rotating container, one should compare the vortex energies per quantum of circulation, i.e., $E(m)/m$. For these energies, the corresponding ratios are

$$4.5:3.5:3\ . \tag{5.28}$$

Moreover, the MH texture has an additional logarithmic energy inside the soft-core region, due to the stability of disgyrations in high fields (see Sec. IV.C.5).

Therefore, among the nonsingular vortex textures in rotating ^{3}He-A, under a large enough magnetic field ($\xi_{2H} \ll r_\Omega$, where $r_\Omega \sim n_v^{-1/2}$ is the intervortex distance), the nonsingular doubly quantized nonaxisymmetric vortices are the most advantageous (at least close to T_c, since far from T_c parameters in the gradient energy may change the ratio of the vortex energies; see Muzikar, 1979).

Thus there are two candidates for the vortex array in rotating superfluid ^{3}He-A in a large enough magnetic field: a system of doubly quantized nonsingular vortices, and a system of singly quantized vortices; both are nonaxisymmetric outside their soft cores. Vortices with a half-integer quantum of circulation would have a large bulk energy due to violation of the dipole constraint $\mathbf{d}\|\mathbf{l}$, and cannot therefore successfully compete with the others in an open geometry (see, however, Sec. V.F).

The doubly quantized vortices have an energy twice as large per unit quantum of circulation outside the soft core, but the singly quantized vortices have an additional logarithmic energy in the region outside the hard core. Therefore only detailed calculations of the structure and the energy of both textures may determine which one of these vortices is preferable. Preliminary numerical calculations have shown that the singly quantized vortex has slightly less energy per quantum of circulation than the doubly quantized vortex if the angular velocity of rotation, Ω, is less than ~ 3 rad/sec (Seppälä and Volovik, 1983; Vulovic, Stein, and Fetter, 1984).

Let us next write down the simplest representations of a nonaxisymmetric doubly quantized vortex in a large magnetic field ($\xi_{2H} \ll \xi_d$), a situation that occurs in the experiments on rotating ^{3}He (Seppälä, Hakonen, Krusius, Ohmi, Salomaa, Simola, and Volovik, 1984; see Fig. 20).

The P_3-symmetric w vortex (magnetic class D_1) is

$$\begin{aligned} &\mathbf{d}=\hat{y},\quad \mathbf{l}=\hat{y}\sin\eta(r)\pm\cos\eta(r)(\hat{x}\sin\phi-\hat{z}\cos\phi)\ , \\ &\mathbf{v}_s=\hat{\phi}\frac{\hbar}{Mr}[1+\sin\eta(r)]\ , \\ &(\mathbf{e}_1+i\mathbf{e}_2)e^{i\Phi}=e^{i\phi}[(-\hat{x}\sin\phi+\hat{z}\cos\phi)\sin\eta(r) \\ &\qquad\qquad \pm\hat{y}\cos\eta(r)+i(\hat{z}\sin\phi+\hat{x}\cos\phi)]\ , \end{aligned} \tag{5.29}$$

where $\eta(r \ll \xi_d)=-\pi/2$, $\eta(r \gg \xi_d)=\pi/2$, and $\mathbf{l}(\infty)=\hat{y}$.

The P_2-symmetric v vortex (magnetic class C_{1v}) is

$$\begin{aligned} &\mathbf{d}=\hat{y},\quad \mathbf{l}=\hat{y}\sin\eta(r)\pm\cos\eta(r)(\hat{z}\sin\phi-\hat{x}\cos\phi)\ , \\ &\mathbf{v}_s=\hat{\phi}\frac{\hbar}{Mr}[1+\sin\eta(r)]\ , \\ &(\mathbf{e}_1+i\mathbf{e}_2)e^{i\Phi}=e^{i\phi}[(-\hat{x}\cos\phi-\hat{z}\sin\phi)\sin\eta(r) \\ &\qquad\qquad \pm\hat{y}\cos\eta(r)+i(\hat{z}\cos\phi-\hat{x}\sin\phi)]\ , \end{aligned} \tag{5.30}$$

with the same asymptotics for $\eta(r)$ as those following Eq. (5.29) above.

The l-field projection in the transverse plane has interesting properties for both the v and the w vortices.

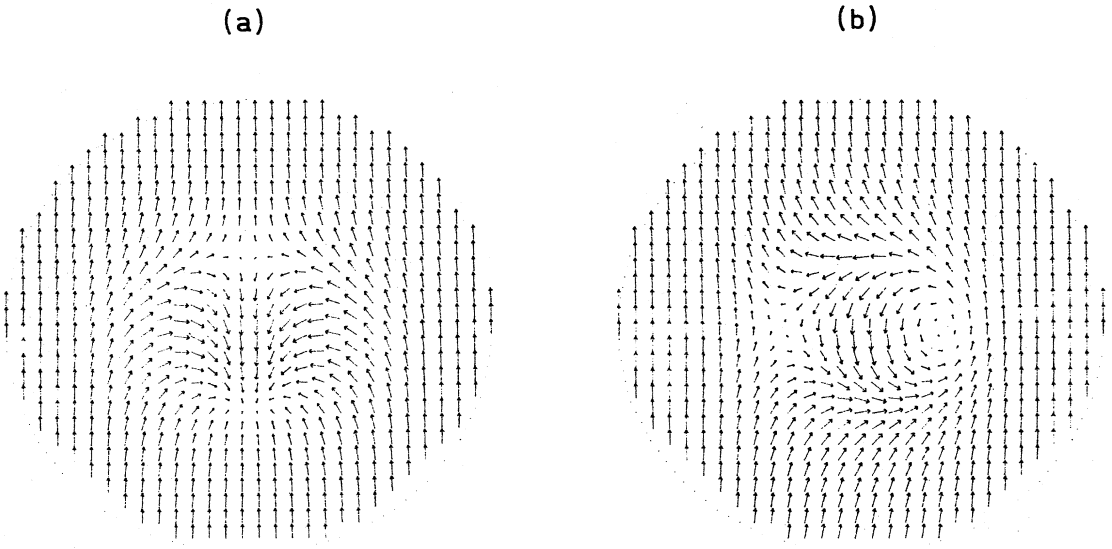

FIG. 20. The calculated (a) continuous doubly quantized v vortex with symmetry P_2 and (b) continuous doubly quantized w vortex with symmetry P_3. Both have similar NMR signature, but have different focusing properties for ions, which thus in principle may make it possible to distinguish between these structures (see Fig. 21). Arrows indicate the projection of the $\mathbf{l}$ vector into the (x,y) plane. The radii of the displayed areas are $\approx 5\xi_d$.

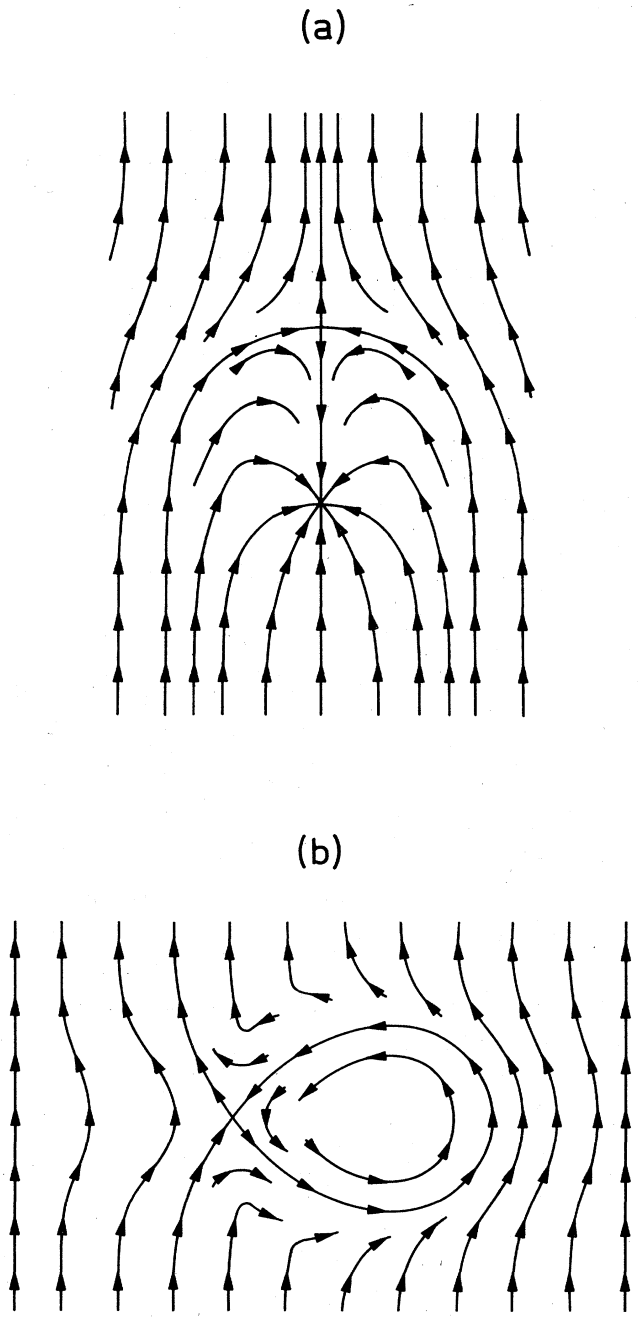

FIG. 21. The continuous representation of the same $\boldsymbol{l}_\perp$ field as in Fig. 20 associated with 4π-vortex configurations, according to Zotos and Maki (1984a). The arrows indicate the $\boldsymbol{l}_\perp$ direction. (a) The radial-hyperbolic pair (v vortex); (b) the circular-hyperbolic pair (w vortex). The lines of the $\boldsymbol{l}$ field coincide with the projection of ion trajectories into the cross-sectional plane of the vortex. In (a), the lower "quark" in the v^+ vortex is a focusing center for ions, while the $w^\pm$ vortices, as well as the v^- vortex (with opposite parity, or with opposite orientation of $\boldsymbol{l}_\perp$), have no focusing centers. Note that the topology of the ion trajectories is completely determined by the symmetry of the 4π vortices.

Since the $\boldsymbol{l}$-vector field covers all the unit sphere, there are two points in the vortex, $\mathbf{r}_1$ and $\mathbf{r}_2$, where $\boldsymbol{l}$ is strictly parallel to the vortex axis: $\boldsymbol{l}(\mathbf{r}_1)=\hat{z}$ and $\boldsymbol{l}(\mathbf{r}_2)=-\hat{z}$. At these points, the projection field $\boldsymbol{l}_\perp$ has singularities with the winding numbers $m=1$ and -1. This resembles the bound quark-antiquark pair in the instanton theory (Fateev, Frolov, and Schwarz, 1979). These quarks are of direct importance for NMR properties (see Sec. VI.B), as well as for the ion-vortex interaction (Maki and Zotos, 1984). The singularity with $m=-1$ has a hyperbolic distribution of the $\boldsymbol{l}_\perp$ field, while the singularity with $m=+1$ has a radial distribution for the v vortex and a circular distribution for the w vortex [see Fig. 21 (Zotos and Maki, 1984a)].

Numerical calculations of the energy (3.9) give preference to the w vortex [circular-hyperbolic pair of quarks; Eq. (5.29)] over the v vortex [radial-hyperbolic pair; Eq. (5.30)] (Seppälä, Hakonen, Krusius, Ohmi, Salomaa, Simola, and Volovik, 1984; Zotos and Maki, 1984a; Maki and Zotos, 1985a).

3. Distortion of the vortex lattice

Due to the spontaneously broken axisymmetry of the ^{3}He-A vortices, the vortex lattice becomes distorted (Ohmi, 1984). If $\hat{y}$ is the direction of the $\boldsymbol{l}$-vector field in the bulk liquid outside the soft cores of the vortices, then the hydrodynamic energy of the rotating liquid outside the core is anisotropic:

$$F=\tfrac{1}{2}\rho_s^{\parallel}(v_{sy}-\Omega x)^2+\tfrac{1}{2}\rho_s^{\perp}(v_{sx}+\Omega y)^2 . \tag{5.31}$$

However, a change in the length scale, different for the different directions

$$x=\tilde{x}p,\quad v_{sy}=\tilde{v}_{sy}p,\quad y=\tilde{y}p^{-1},\quad v_{sx}=\tilde{v}_{sx}p^{-1},\qquad p=\left[\frac{\rho_s^{\perp}}{\rho_s^{\parallel}}\right]^{1/4}, \tag{5.32}$$

restores the isotropy of the liquid in the distorted coordinate frame:

$$F=\tfrac{1}{2}(\rho_s^{\parallel}\rho_s^{\perp})^{1/2}(\tilde{\mathbf{v}}_s-\boldsymbol{\Omega}\times\tilde{\mathbf{r}})^2 . \tag{5.33}$$

The vortex lattice is symmetric in this frame, e.g., a square or hexagonal lattice. Therefore, in the laboratory frame, it is distorted, becoming a rectangular or rhombic lattice, correspondingly, with the same area of the primitive cell, but with the ratio of lengths obeying $r_\Omega^x/r_\Omega^y=p^2$ (see Fig. 22 for the hexagonal case).

D. Physical properties of vortices with broken parity

Spontaneous breaking of discrete symmetry in the soft core of the ^{3}He-A vortices results in the appearance of new physical properties for these vortices (Volovik, 1984a): there arise, depending on the type of vortex, v or w, a spontaneous electric polarization D_z along the vortex axis, an axial supercurrent j_z, and an axial spin current j_z^z

(the axial spin current with z projection on the vortex axis).

These three physical quantities have the following transformation properties under the symmetry operations P_1, P_2, and P_3 in Eq. (5.6):

$$P_1 j_z = -j_z, \quad P_2 j_z = -j_z, \quad P_3 j_z = j_z , \tag{5.34a}$$

$$P_1 D_z = -D_z, \quad P_2 D_z = D_z, \quad P_3 D_z = -D_z , \tag{5.34b}$$

$$P_1 j_z^z = -j_z^z, \quad P_2 j_z^z = j_z^z, \quad P_3 j_z^z = -j_z^z . \tag{5.34c}$$

1. Axial superflow in the w vortex

If there is P_1 or P_2 symmetry in the vortex, then, according to Eq. (5.34a), the net supercurrent j_z through the cross section of the vortex-core region is zero. Therefore a nonzero spontaneous axial superflow in the core of the vortex may arise only if the P_1 and P_2 symmetries are broken simultaneously. This is just the case for the w vortex. For example, the total supercurrent through the cross section of the dipole-unlocked soft core of the w vortex [Eq. (5.29)] is

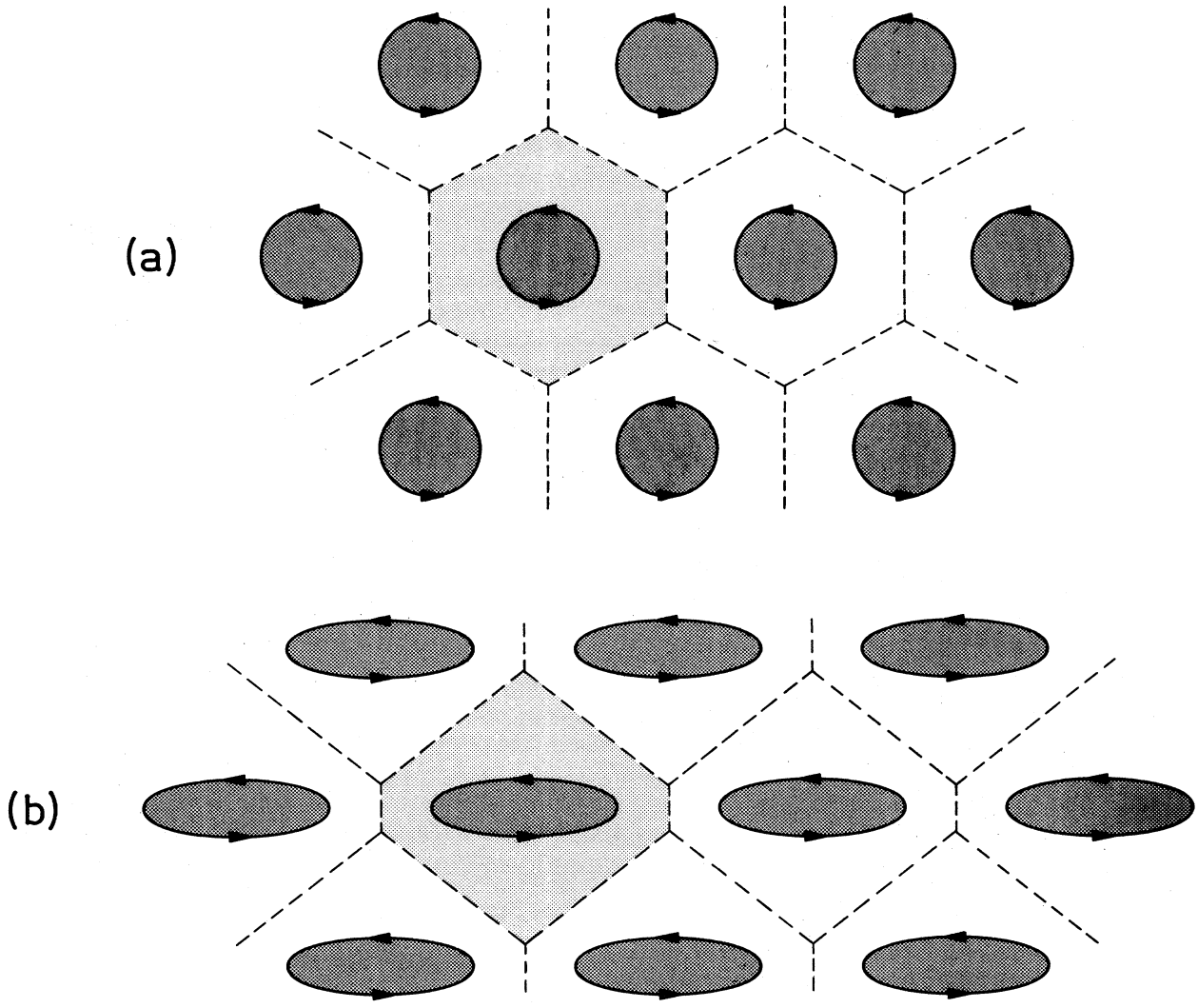

FIG. 22. (a) The periodic hexagonal lattice of axisymmetric vortices. (b) The rhombic lattice (distorted hexagonal lattice), which is energetically favored for a lattice of nonaxisymmetric vortices, such as those in Fig. 20. One vortex-lattice cell is shaded in each picture, and bordered by the dashed lines.

$$j_z = \int \mathbf{j}\cdot d\mathbf{s} = \pm\frac{h}{2M}\int_0^\infty [C_0\cos^3\eta + (\rho_s^\perp - \rho_s^{\parallel})\cos\eta\sin\eta(1+\sin\eta)]dr \ . \tag{5.35}$$

The sense ($\pm$) of the supercurrent is arbitrary, thus reflecting the twofold degeneracy due to the spontaneously broken discrete symmetry. Note that at $T=0$, where $\rho_s^{\parallel}=\rho_s^\perp=\rho$, only the orbital current [Eq. (3.14b)] contributes to the core supercurrent. Since the C_0 term in the orbital current at $T=0$ arises from the chiral anomaly (Volovik, 1985, 1986a; Balatsky, Volovik, and Konyshev, 1986; Combescot and Dombre, 1986), a measurement of the core supercurrent may experimentally prove the existence of the anomalous supercurrent in ^{3}He-A (see also Sec. VIII.D.2).

In an analogous way, the v vortex has both a spontaneous electric polarization and a spin supercurrent along the vortex axis. For the v vortex [Eq. (5.30)], the spin supercurrent is zero, because the spin vector $\mathbf{d}$ is kept constant in this trial function. However, there are no symmetry arguments that fix $\mathbf{d}$. Therefore, in the real v vortex, there occurs a net spin supercurrent through the cross section of the quantized vortex line:

$$j_z^z = \int \mathbf{j}_{\rm sp}^z\cdot d\mathbf{s} \sim \frac{h}{M}\rho_{\rm sp}\xi_d \ . \tag{5.36}$$

2. Spontaneous electric polarization in the v vortex

The electric polarization in superfluid ^{3}He arises because of the so-called flexoelectric effect, which is well known for ordinary (nonsuperfluid) liquid crystals (de Gennes, 1975). This polarization is caused by the bending of the anisotropy axis, which produces a small deformation of the atomic ^{3}He shells (Volovik, 1984a). By analogy with a nematic liquid crystal, the electric polarization $\mathbf{P}(\mathbf{r})$ may be written

$$\mathbf{P}(\mathbf{r}) = \beta_1\mathbf{l}(\nabla\cdot\mathbf{l}) + \beta_2(\mathbf{l}\cdot\nabla)\mathbf{l} \ , \tag{5.37}$$

where the flexoelectric parameters β_i are estimated to be

$$\begin{aligned}\beta_1-\beta_2 &\sim 10^{-10}-10^{-9}\left[1-\frac{T}{T_c}\right]^2 \text{ V} \ , \\ \beta_1+\beta_2 &\sim 10^{-7}\left[1-\frac{T}{T_c}\right] \text{ V} \ .\end{aligned} \tag{5.38}$$

Symmetry also allows for terms of the types $\mathbf{l}\times(\mathbf{v}_s-\mathbf{v}_n)$ and $\mathbf{l}\times\Delta\mathbf{v}_s$ in the polarization expression (5.37).

Integrating the electric polarization density $\mathbf{P}(\mathbf{r})$ in Eq. (5.37) over the cross section of the twofold-degenerate doubly quantized v vortex [Eq. (5.30)], we obtain the dipole moment D_z per unit length of the vortex line as

$$D_z = \pm\pi(\beta_1-\beta_2)\int_0^\infty r\frac{\partial\eta}{\partial r}\cos^2\eta\, dr \ . \tag{5.39}$$

This quantity is proportional to the soft-core radius of the vortex:

$$D_z \sim (\beta_1-\beta_2)r_{\rm core}, \quad r_{\rm core} = \max(\xi_d,\xi_{2H}) \ . \tag{5.40}$$

The twofold degeneracy of the v vortex makes possible topologically stable kinks, or point solitons, separating the two parts of the vortex line with opposite electric polarizations. Such a point on the vortex line is associated with an electric charge e^*, of the order of

$$e^* \sim D_z \sim 10^{-5}e \ . \tag{5.41}$$

In the above, e denotes the elementary charge of an electron, and $r_{\rm core}$ is chosen to be of the order of the dipole length $\xi_d \simeq 10^{-3}$ cm. One half of this amount of electric charge ought to be concentrated on the termination point of the vortex line at the surface of the container.

If one neglects intervortex interactions, the signs of these charges at the surface are random due to the disorder in the direction of the vortex polarization D_z. Thus the bulk liquid exhibits no features of the broken symmetry.

Note also that, besides the net electric polarization along the core in the v vortex, both v and w vortices have a radial polarization which decreases with distance from the vortex axis. This means that the soft core may also have a net electric charge with linear density $\sim(\beta_1+\beta_2)$. Therefore the processes of creation and annihilation of vortices on the sample boundaries are likely to be accompanied by electric currents.

3. Ordering of the "Ising" variables

The interactions of the vortices may produce a "ferromagnetic" ordering of the signs of D_z in the v vortices, and of the signs of j_z in the w vortices. Let us illustrate this with the example of w vortices. We show that a bulk superflow must spontaneously arise due to the interaction with currents in the vortex cores. The local axial supercurrents of the vortices, $j_{za} = \pm|j_z|$, where a counts the vortices in a vortex array of rotating ^{3}He-A, interact with the homogeneous external $\mathbf{v}_s$ field along the rotation axis. As a result, the energy density of homogeneous bulk superflow along the axis of the container is given by

$$\tfrac{1}{2}\rho_s^\perp v_{sz}^2 - v_{sz}\sum_a j_{za} \ . \tag{5.42}$$

Here we take into account that the $\mathbf{l}$ vector outside the soft cores of vortices is locked in the $(\hat{x},\hat{y})$ plane; therefore the transverse superfluid density $\rho_s^\perp$ is essential for an axial superflow. The sum over a in Eq. (5.42) is for vortices per unit area. If the unit area contains n_+ vortices with positive j_z and n_- vortices with negative j_z, their sum total being equal to $n_v = n_+ + n_-$, then the net energy of the superflow is

$$\tfrac{1}{2}\rho_s^\perp v_{sz}^2 - |j_z|\, v_{sz}(n_+ - n_-) \ . \tag{5.43}$$

The minimum of this energy corresponds either to

$$n_-=0,\quad n_+=n_v,\quad v_{sz}=n_v\,|\,j_z\,|\,/\rho_s^{\perp} \tag{5.44a}$$

or to

$$n_+=0,\quad n_-=n_v,\quad v_{sz}=-n_v\,|\,j_z\,|\,/\rho_s^{\perp}\ . \tag{5.44b}$$

Thus, it is more advantageous for the w vortices to be orientated uniformly. Due to this ordering, a bulk supercurrent $\rho_s^{\perp}v_{sz}$ appears, which on the average compensates the coherent axial supercurrents in the soft cores of the w vortices (see Fig. 23). The twofold degeneracy of the superflow [Eq. (5.44)] reflects the spontaneous broken symmetry in the bulk liquid.

An analogous indirect interaction of the v vortices through the bulk spin supercurrent is expected to result in the spontaneous uniform "ferromagnetic" ordering of the local spin supercurrents in the v vortices. Simultaneously, the v vortices become electrically polarized: there occurs a net surface density of electric charge e^*n_v, which results in a spontaneous electric field in the rotating bulk liquid ^{3}He, given by

$$4\pi e^* n_v \sim 10^{-2}-10^{-1}\ \mu\mathrm{V/cm}\ . \tag{5.45}$$

4. Helix in the *w*-vortex array

We have thus far discussed consequences of the breaking of discrete symmetry only. The simultaneous breaking of both discrete and axisymmetry should produce another interesting effect for the w vortices in ^{3}He-A. The $\boldsymbol{l}$ field in the bulk superfluid outside the soft vortex core is homogeneous and is oriented in an arbitrary direction in the $(\hat{x},\hat{y})$ plane. This continuous degeneracy in the plane reflects the spontaneously broken axisymmetry of the A-phase vortices.

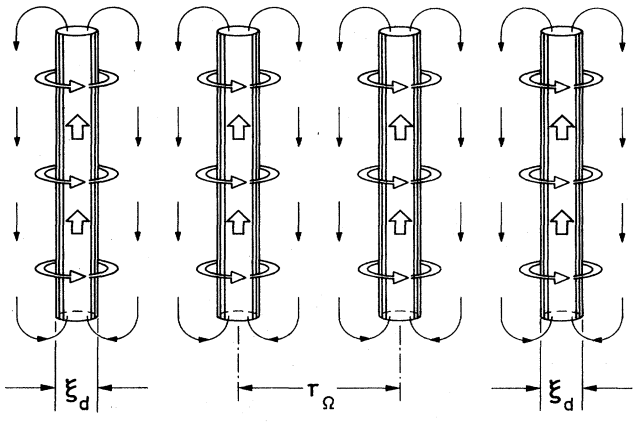

FIG. 23. Schematic illustration of superflow in w vortices. The interaction between the countersuperflow fields in the bulk liquid serve to orient ferromagnetically directions of superflow inside the cores of w vortices. These directions act like "Ising" variables. Such a ferromagnetic ordering of the Ising variables (with all the vortices of the same type, w^+ or w^-) may be energetically favored over the state with disordered supercurrents or with alternating w^+ and w^- vortices (antiferromagnetic ordering).

Due to the broken space parity in the vortices, this homogeneous $\boldsymbol{l}$ field may transform to an $\boldsymbol{l}$ texture, which resembles a cholesteric spiral (de Gennes, 1975),

$$\boldsymbol{l}_{\rm bulk}=\hat{x}\sin qz+\hat{y}\cos qz\ , \tag{5.46}$$

with $\boldsymbol{l}\cdot(\nabla\times\boldsymbol{l})\,|_{\rm bulk}=q$. A nonzero inverse period of the helix q appears due to the interaction of the bulk $\boldsymbol{l}\cdot(\nabla\times\boldsymbol{l})_{\rm bulk}$ field with the local $\boldsymbol{l}\cdot(\nabla\times\boldsymbol{l})_{\rm local}$ field in the cores of the w vortices:

$$F\sim\left[\frac{\hbar}{M}\right]^2 K_2(\boldsymbol{l}\cdot(\nabla\times\boldsymbol{l}))_{\rm bulk} \times\sum_a\int_{S_a}(\boldsymbol{l}\cdot(\nabla\times\boldsymbol{l}))_{\rm local}dS\ . \tag{5.47}$$

For the simplest w vortex [Eq. (5.29)], integration over the cross section S_a of the soft core of vortex a and a summation over the "positive" and "negative" vortices with number densities n_+ and n_-, respectively, yields for the pitch q

$$q=-\sum_a\int_{S_a}(\boldsymbol{l}\cdot(\nabla\times\boldsymbol{l}))_{\rm local}dS =-(n_+-n_-)\frac{\pi}{2}\int_0^{\infty}\sin 2\eta\,dr\ . \tag{5.48}$$

In parallel with the case of the interaction of vortices with an external superflow, the interaction (5.47) of the external $(\boldsymbol{l}\cdot(\nabla\times\boldsymbol{l}))_{\rm bulk}$ with the internal $(\boldsymbol{l}\cdot(\nabla\times\boldsymbol{l}))_{\rm local}$ of the vortex cores favors "ferromagnetic" ordering with $n_+=0$, $n_-=n_v$, or with $n_-=0$, $n_+=n_v$. Then the period, or "pitch," of the cholesteric spiral $2\pi q^{-1}$ is of the order of $(n_v r_{\rm core})^{-1}$.

The helix can only appear for the w vortex, which follows from the transformation properties of q under the symmetry operations in Eq. (5.6):

$$P_{1q}=-q,\quad P_2 q=-q,\quad P_3 q=q\ . \tag{5.49}$$

A nonzero q appears only if both the P_1 and P_2 symmetries are broken simultaneously, i.e., in the w vortex. (A bulk superflow along $\boldsymbol{l}$ may also arise, since $\boldsymbol{l}\cdot\mathbf{v}_s$ has the same symmetry properties as q.) This property of the w-vortex array may be used for experimental identification with ultrasonic techniques, since the ultrasound absorption is very sensitive to the direction of the $\boldsymbol{l}$ field. The physical properties of the A- and B-phase vortices with broken symmetry are summarized in Table II.

Superflow along the w-vortex axis could also be observed with ultrasound applied along the vortex axis: for a randomly disordered superflow array, there should occur a Doppler splitting of the ultrasound absorption, while in the case of fully aligned superflow, only a single Doppler-shifted ultrasound absorption spectrum would be observed.

The "ferromagnetic" ordering of the w vortices could also change the spectrum of the Kelvin waves in the vor-

TABLE II. Broken-symmetry properties displayed by vortices with discrete v and w symmetries in the superfluid A and B phases of ^{3}He.

	v vortex	w vortex
Results of broken parity	net electric polarization of the core and spin supercurrent along the vortex axis	Net superflow in the vortex core
Linear terms in gradient energy for polarized vortices with broken parity	$\hat{\Omega}\cdot\mathbf{n})(\nabla\cdot\mathbf{n})$ in ^{3}He-B	$(\mathbf{n}\cdot\nabla\times\mathbf{n})$ in ^{3}He-B $(\boldsymbol{l}\cdot\nabla\times\boldsymbol{l})$ and $(\boldsymbol{l}\cdot\mathbf{v}_s)$ in ^{3}He-A
	Anisotropy vector (or director) $\mathbf{b}$ in the transverse plane	
Results of the broken axisymmetry in the ^{3}He-B vortex core		Twist (spiral) of $\mathbf{b}$ along vortex axis with the pitch $q=\mathbf{b}\cdot\left[\hat{z}\times\frac{\partial\mathbf{b}}{\partial z}\right]$

tex array (Sonin and Fomin, 1985); these waves are oscillations in the vortex array with wave vector $\mathbf{p}$ along the vortex axis z. The broken P_3 symmetry of the w vortex array allows for a term linear in p in the spectrum:

$$\omega=2\Omega+v_s p^2+\alpha\frac{\hbar}{M}qp\ , \tag{5.50}$$

where v_s is the rigidity of the vortex line, q is given by Eq. (5.48), and α is a factor of order unity.

In the absence of an external magnetic field, when the core size of a nonsingular vortex coincides with the size of the primitive cell, $r_\Omega\sim n_v^{-1/2}$, the parameter $q\sim n_v r_\Omega\sim n_v^{1/2}$ is proportional to $\sqrt{\Omega}$. Thus, for small Ω, the frequency of the Kelvin wave increases at fixed p with Ω as $\sqrt{\Omega}$. An observation of such behavior would support the occurrence of the w vortices in rotating superfluid ^{3}He-A. However, dissipation effects [not included in Eq. (5.50)] may mask the phenomenon.

E. Symmetry classification of singular vortices with two cores

While the continuous vortices in ^{3}He-A may exist in two different states, v and w, the classification of singular vortices in the A phase is more complicated due to the two length scales (ξ and ξ_D) in the vortex-core structure. As a result, the discrete and axial symmetries of the maximally symmetric singular vortex in Eq. (5.17) may be broken in the hard core and in the soft core of the singular vortices independently, and in a different manner: this produces a rich spectrum of possible vortex structures (Salomaa and Volovik, 1985b).

The discrete symmetry classification of vortices does not depend on the continuous symmetry in an essential way. Therefore, for the sake of simplicity and clarity, we here confine ourselves to axisymmetric vortices. It is also likely that axisymmetry is indeed realized in the parallel-plate geometry, where the reorientation of the $\boldsymbol{l}$ vector by superflow is prevented by the boundary conditions, which lock $\boldsymbol{l}$ normal to the plates. In this geometry, with the plates normal to the axis of rotation $\hat{\Omega}$, the $\boldsymbol{l}$ vector may be orientated in two directions: $\boldsymbol{l}\cdot\hat{\Omega}=\pm1$. As we have discussed, the vortex structure essentially depends on this "isospin" quantum number (see Sec. V.A.4), which changes sign if the sense of rotation is reversed.

According to the general classification, the breaking of discrete symmetry in Eq. (5.6) may give rise to the u, v, or w vortices with the respective symmetries P_1, P_2, or P_3, and to the uvw vortex with no discrete symmetry. However, this classification is very rough for the A-phase vortices with two different cores and is only rigorous for the continuous vortex with just one core, the soft core, where the A-phase state is not disrupted.

1. Vortex substates

In order to facilitate a more refined classification of the vortices with two types of cores, one needs to specify the region where the symmetry breaking takes place. There are four important regions to consider: Region I of the dipole-locked asymptotics, $r\gg\xi_D$, which contributes a logarithmic term to the vortex energy; the texture in this region has the maximal discrete symmetry, Eq. (5.6), which we denote as the o symmetry; Region II of the soft core, $r\simeq\xi_D$; Region III of the intermediate dipole-unlocked asymptotics, $\xi_D\gg r\gg\xi_{GL}$, which also gives a logarithmic contribution to the vortex energy; and finally Region IV of the hard core, $r\simeq\xi_{GL}$.

The discrete symmetry o, which is broken in the soft core, may in principle be restored in Region III, since this

region has a large logarithmic contribution to the vortex energy and may form a vortex state independently of the other regions. (For example, in the case of the non-axisymmetric vortices, axisymmetry may tend to be restored in this region; see Sec. V.C.1.) Then the restored discrete symmetry may again be broken in Region IV, but in a different way.

Therefore there exists a large variety of distinct vortex substates, which we specify by a code of three letters, corresponding to the symmetries in the different Regions II, III, and IV, respectively. For example, the least symmetric uvw vortex state may be in the substate $v-o-w$ (which has the symmetry P_2 in the soft core, the total symmetry o in Region III, and symmetry P_3 in the hard core) or in the substates $w-o-v$, $v-v-uvw$, etc. The P_2-symmetric v-vortex state may thus contain four different substates: $v-v-v$, $v-o-o$, $v-o-v$, and $o-o-v$, and the P_3-symmetric state w also has four substates: $w-w-w$, $w-o-o$, $w-o-w$, and $o-o-w$.

2. Extended symmetry of the $m=1$ vortex

However, the most interesting classification is found for vortices with the quantum number $n=0$, i.e., the one-quantum vortex (with $m=-1$, if $\boldsymbol{l}\cdot\hat{\boldsymbol{\Omega}}=1$, and with $m=1$, if $\boldsymbol{l}\cdot\hat{\boldsymbol{\Omega}}=-1$). Since $S_z+L_z=0$ for this vortex class [see Eqs. (5.2) and (5.15)], new elements of discrete symmetry may emerge in the intermediate asymptotics of Region III. Besides the elements of o symmetry in Eq. (5.6), there may also occur new elements due to different combinations of the three basic transformations T, P, and U_2, where by U_2 we denote the element $O^{(J)}_{x,\pi}$ (here again we do not consider a gauge transformation U_π, which does not influence any of the observable variables: $\boldsymbol{l},\mathbf{v}_s$, electric polarization, etc.). Time-inversion symmetry is broken in the A phase because $T\boldsymbol{l}=-\boldsymbol{l}$. Therefore T may enter in a combined symmetry only.

Hence there exist three different sets of possible discrete symmetries for the asymptotics of linear defects in the A phase, which we denote the o_1, o_2, and o_3 symmetries:

$$P,\ TU_2,\ PTU_2\ , \tag{5.51a}$$

$$U_2,\ PT,\ PTU_2\ , \tag{5.51b}$$

$$PU_2,\ TU_2,\ PT\ . \tag{5.51c}$$

The o_1 symmetry in Eq. (5.51a) is just the o symmetry (5.6), which characterizes the vortices in the A and B phases, while the symmetries o_2 in Eq. (5.51b) and o_3 in Eq. (5.51c) characterize a radial disgyration ($\boldsymbol{l}=\hat{\boldsymbol{r}}$, $\mathbf{v}_s=0$) and a tangential disgyration ($\boldsymbol{l}=\hat{\boldsymbol{\phi}}$, $\mathbf{v}_s=0$), respectively. Both display continuous symmetry $S_z+L_z=0$ and may thus serve as the intermediate asymptotics in Region III of the vortex with $n=0$.

We denote the most symmetric defect with the asymptotics of a radial disgyration as the o_2 defect and that with the asymptotics of a tangential disgyration as the o_3 defect. Then, by x,y,z we denote the defect structures obtained by breaking the symmetries o_2 or o_3, i.e., the U_2 symmetric, the TP symmetric, and the PU_2 symmetric linear defects, respectively.

These new symmetries, Eqs. (5.51b) and (5.51c), give two additional substates for the v-vortex state with $m=1$ and $\boldsymbol{l}\cdot\hat{\boldsymbol{\Omega}}=-1$, $v-o_2-o_2$ and $v-o_2-v$; two substates for the w vortex, $w-o_3-o_3$ and $w-o_3-w$; and many additional uvw vortices, $v-o_2-x$, $w-o_3-z$, etc.

For example, the axisymmetric $m=1$ vortex with $\boldsymbol{l}\cdot\hat{\boldsymbol{\Omega}}=-1$ (Fetter, Sauls, and Stein, 1983) is a pure phase vortex in Region I, which transforms into a radial disgyration in Region III, and then to the polar phase (Muzikar, 1978) in Region IV. Within our classification, it is the substate $v-o_2-o_2$ of the v vortex. In Regions III and IV, the constraints imposed by the symmetry o_2 in Eq. (5.51) [$U_2C_{0\nu}=(-1)^\nu C_{0,-\nu}=C_{0\nu}$ and $TPU_2C_{0\nu}=C^*_{0\nu}=C_{0\nu}$] require the following form for this $v-o_2-o_2$ vortex:

$$A_{\alpha i}=\Delta_A\hat{z}_\alpha\sum_\nu\lambda_i^\nu C_{0\nu}e^{-i\nu\phi}=\Delta_A\hat{z}_\alpha(a\hat{z}_i+ib\hat{\phi}_i)\ , \tag{5.52}$$

where $a(r)$ and $b(r)$ are real functions, both tending to unity for $r\gg\xi_{\rm GL}$ in order to form a radial disgyration.

While the singularity in $\hat{\phi}$ at the vortex axis forces the prefactor $b(r)$ in Eq. (5.52) to tend to zero for $r=0$, the coefficient $a(r)$ need not vanish. Therefore the $v-o_2-o_2$ vortex always contains the polar phase on its axis (with nonzero a_{00}, see Table I). Other superfluid phases may appear if the continuous symmetries with generators $\hat{S}_z$ and $\hat{L}_z$ are broken in the hard core.

F. Half-quantum vortices in the parallel-plate geometry

1. Isolated half-quantum vortices

In an open geometry, the vortices with $m=\pm\frac{1}{2}$ in Eq. (4.9) always possess a large dipole energy (see Sec. V.C.1) and are, therefore, less advantageous than the vortices having $m=1,2$. This vortex with $m=\frac{1}{2}$ is the source of a planar soliton with its edge on the vortex (see Fig. 9); it expends a dipole energy proportional to the volume of the soliton. Hence, in order to facilitate the existence of vortices with $m=\frac{1}{2}$, the dipole energy must be neutralized.

There is an effective way of getting free of the dipole energy: to use a parallel-plate geometry with the distance $r_0<\xi_d$ between the plates and with a magnetic field $H\gg 25$ G, which is applied parallel with the normal $\boldsymbol{\nu}$ to the plates (Volovik and Salomaa, 1985a). In this case $\boldsymbol{l}$ is always parallel to $\boldsymbol{\nu}$ (axis $\hat{z}$), and $\mathbf{d}\perp\boldsymbol{\nu}$: $\mathbf{d}=\hat{x}\cos\alpha+\hat{y}\sin\alpha$ (see Fig. 24). Therefore, although the dipole energy possesses a maximum value, it is a constant independent of the type of the vortex. If $\boldsymbol{\Omega}\|\boldsymbol{\nu}$ and Φ and $\mathbf{d}$ depend only on the coordinates transverse to $\boldsymbol{l}$ and $\boldsymbol{\nu}$, the free-energy functional (3.9) for the rotating liquid reduces to the form

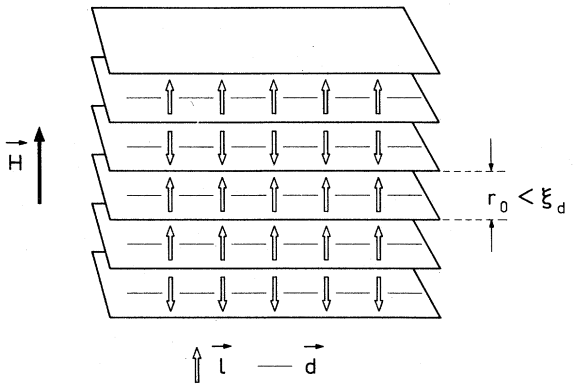

FIG. 24. A parallel-plate geometry, with spacing $r_0 < \xi_d$, serves to freeze the $\boldsymbol{l}$ vector (arrows) in the A phase perpendicular to the walls. In the presence of an external magnetic field $\mathbf{H}$, applied parallel to the normal of the plates, the $\mathbf{d}$ vector (lines without arrowhead) is in the plane of the plates. Singular vortices are expected to occur in rotating superfluid ^{3}He-A in this geometry; at a lower temperature, $T \sim 0.7T_c$, half-quantum vortices have been estimated to be energetically favored.

$$F=\frac{1}{2}\left[\frac{\hbar}{M}\right]^2\left[\rho_s^{\perp}\left[\nabla_{\perp}\Phi-\frac{M}{\hbar}\boldsymbol{\Omega}\times\mathbf{r}\right]^2+\rho_{\rm sp}^{\perp}(\nabla_{\perp}\alpha)^2\right] . \tag{5.53}$$

Let us compare the energies E per quantum of circulation for the different types of vortices, with $m=\frac{1}{2}$, 1, and 2, in the logarithmic approximation. The half-quantum vortex, accompanied with a half-quantum disclination, has the energy

$$E(m=\tfrac{1}{2})/\tfrac{1}{2}=\tfrac{1}{2}(\rho_s^{\perp}+\rho_{\rm sp}^{\perp})\frac{1}{2}\left[\frac{\hbar}{M}\right]^2\ln\frac{R}{\xi} , \tag{5.54}$$

where $R=r_{\Omega}\sim n_v^{-1/2}$ is the intervortex distance.

The axisymmetric singly quantized vortex in this geometry is the pure phase vortex with $m=1$ at distances $r>r_0$ from the vortex axis; at $r<r_0$ this is a radial disgyration. Thus its energy equals

$$E(m=1)=\frac{1}{2}\left[\frac{\hbar}{M}\right]^2\left[\rho_s^{\perp}\ln\frac{R}{r_0}+K_1\ln\frac{r_0}{\xi}\right] . \tag{5.55}$$

Finally, the doubly quantized vortex—the axisymmetric ATC texture which is a pure $m=2$ vortex outside the soft core of size r_0—has the following energy per unit quantum of circulation:

$$E(m=2)/2=2\rho_s^{\perp}\frac{1}{2}\left[\frac{\hbar}{M}\right]^2\ln\frac{R}{r_0} . \tag{5.56}$$

For temperatures near T_c, where $\rho_s^{\perp}=\rho_{\rm sp}^{\perp}=4K_1$, and choosing parameters $r_{\Omega}\simeq 10^{-2}$ cm, $r_0\simeq 10^{-4}$ cm, and $\xi_{\rm GL}\simeq 10^{-5}$ cm, we find in the logarithmic approximation

$$E(m=\tfrac{1}{2})/\tfrac{1}{2}:E(m=1):E(m=2)/2=1:\tfrac{3}{4}:\tfrac{4}{3} . \tag{5.57}$$

Therefore vortices with $m=\frac{1}{2}$ may compete with the $m=1$ vortices, although in this approximation the latter are energetically favored. However, the energy of the $m=\frac{1}{2}$ vortices can be lowered because (i) the nonlogarithmic corrections to the energies of the vortices with $m=1$ and 2, which result from the nonuniform distribution of $\boldsymbol{l}$, are essential; and (ii) at $T\simeq 0.7T_c$, the superfluid density anisotropy ratio $\rho_{\rm sp}^{\perp}/\rho_s^{\perp}$ decreases down to ~ 0.5, resulting in an essential decrease in the energy of the $m=\frac{1}{2}$ vortices with lowering temperature.

While the signs of the circulation quanta m for the vortices should be equal in the vortex array [the sign of m is defined by the sign of the "magnetic" field $\boldsymbol{\Omega}$ in Eq. (5.53)], the signs of the index $p=\pm\frac{1}{2}$ for the $\mathbf{d}$-vector field in a half-quantum vortex array are not fixed, since there is no corresponding "magnetic" field acting on the angle α as rotations act on Φ. Therefore, in order to avoid the divergence of the free energy (5.53) per unit volume, there should exist no surplus of vortices with a given "charge" p. Hence the system of disclinations resembles a two-dimensional plasma of electric charges $p=\pm\frac{1}{2}$, which interact logarithmically; the electroneutrality condition should be fulfilled.

2. Vortex molecule with soliton glue

An interesting situation occurs in a magnetic field that is slightly tilted, by the angle $\theta \ll 1$, with respect to the rotation axis $\hat{\Omega}\|\boldsymbol{\nu}\|\hat{z}$:

$$\mathbf{H}=H(\hat{z}\cos\theta+\hat{x}\sin\theta) . \tag{5.58}$$

The $\mathbf{d}$ vector is perpendicular to $\mathbf{H}$, and it therefore assumes the value

$$\mathbf{d}=(\hat{z}\sin\theta-\hat{x}\cos\theta)\cos\alpha+\hat{y}\sin\alpha . \tag{5.59}$$

The energy F (5.53) now equals

$$F=\frac{1}{2}\left[\frac{\hbar}{M}\right]^2\left[\rho_s^{\perp}\left[\nabla_{\perp}\Phi-\frac{M}{\hbar}\boldsymbol{\Omega}\times\mathbf{r}\right]^2+\rho_{\rm sp}^{\perp}[(\nabla_{\perp}\alpha)^2+\xi_{d\perp}^{-2}\sin^2\theta\sin^2\alpha]\right] \tag{5.60}$$

with

$$\xi_{d\perp}^2=\xi_d^2\frac{\rho_{\rm sp}^{\perp}}{\rho_{\rm sp}^{\|}} .$$

In comparison with Eq. (5.53), Eq. (5.60) has an additional dipole term, which tends to make the angle α equal to 0 or π. This new term is associated with the characteristic length $\tilde{\xi}_d\equiv\xi_{d\perp}/\sin\theta$. Provided that this length is larger than r_{Ω}, i.e., if $\theta\ll\xi_{d\perp}/r_{\Omega}$, we may neglect the dipole interaction, and the system of $m=\frac{1}{2}$ vortices with alternating p, which should exist at $T\simeq 0.7T_c$, is not distorted.

At larger values of θ, there appears a planar soliton between adjacent pairs of vortices with opposite p, i.e., a domain wall of width $\sim\tilde{\xi}_d$, where α changes from 0 to π (see Fig. 25). This produces another example of confine-

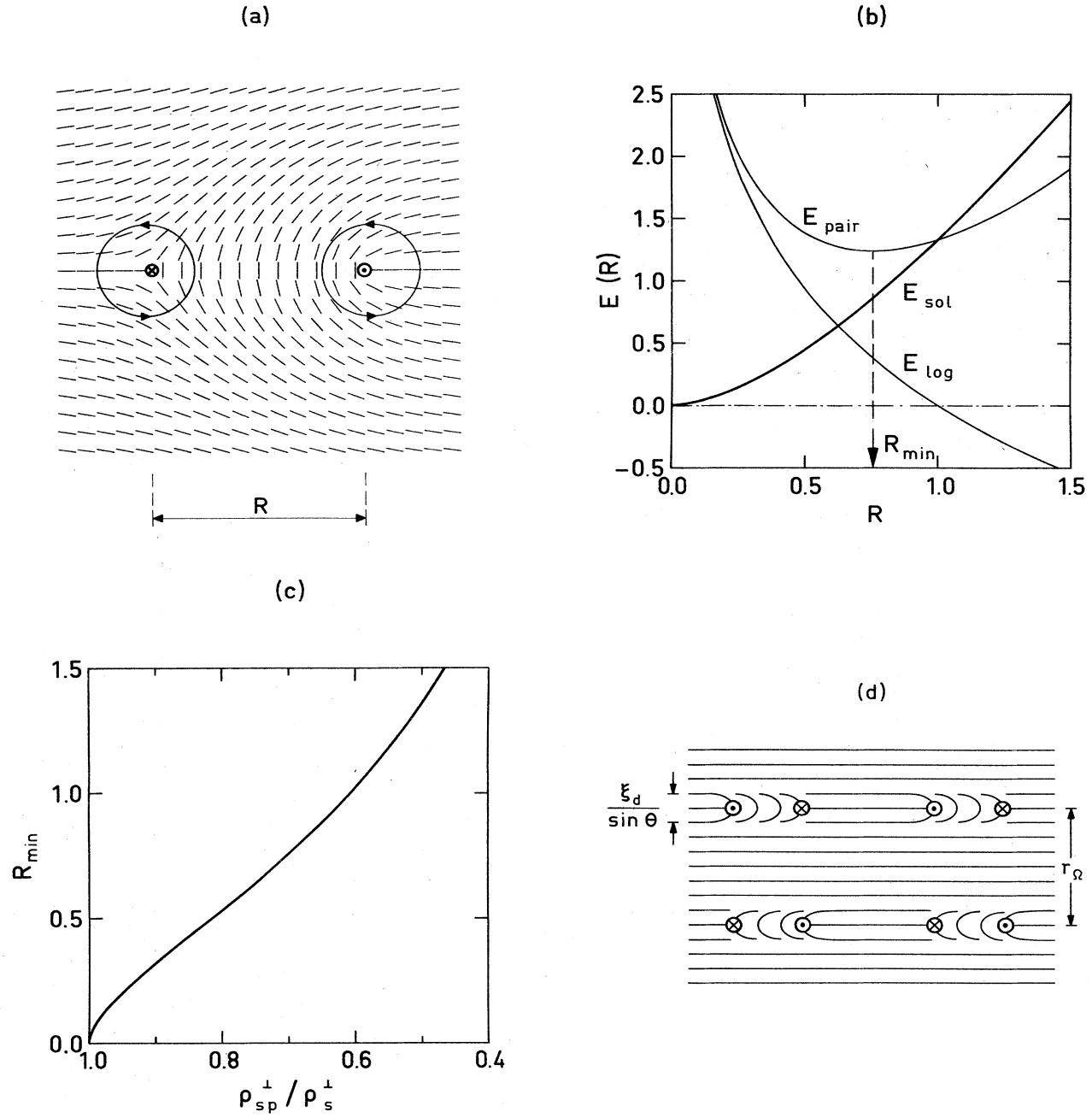

FIG. 25. (a) Calculated texture of the magnetic anisotropy vector **d** around a pair of vortices with one-half circulation quantum. This texture shows disclinations with half-integer Frank indices $p=\frac{1}{2}$ and $-\frac{1}{2}$ in ^{3}He-A confined between parallel plates (the plane of the figure is parallel with the plates). $\odot$ and $\otimes$ represent intersections of the vortex lines—each with $m=\frac{1}{2}$, but with p correspondingly $+\frac{1}{2}$ and $-\frac{1}{2}$—with the plane of the figure. The external magnetic field is slightly tilted by the angle θ with respect to the normal to the plates; as a result, there appears a topological soliton between neighboring vortices possessing the opposite signs $\pm\frac{1}{2}$. Outside the solitons, the **d** vector is directed along the projection of the magnetic field onto the plane. This yields the minimum of the spin-orbital (dipole) energy ($\alpha=0$ or $\alpha=\pi$). The half-quantum vortex separation $R=1.1\tilde{\xi}_D$ was used for this figure, where $\tilde{\xi}_D=\xi_D/\sin\theta$. Each of the half-quantum vortices has the same circulation quantum $m=\frac{1}{2}$, so that at a large distance an isolated half-quantum vortex molecule appears like a singly quantized vortex line, with $m=1$. (b) The computed energy $E_{\rm sol}$ of the topological **d** soliton in (a) as a function of R (in units of $\tilde{\xi}_D$). Here the hydrodynamical energy $E_{\rm log}$ and the total pair energy $E_{\rm pair}$ were calculated using $\rho_{\rm sp}^{\perp}/\rho_s^{\perp}=0.7$. (c) The calculated equilibrium half-quantum pair size $R_{\rm min}$ [in units of $\tilde{\xi}_d\equiv\xi_{d\perp}/\sin(\theta)$] as a function of the temperature-dependent ratio between the perpendicular components of the superfluid spin density and the superfluid density tensors. (d) The distribution of the magnetic anisotropy field **d** in the periodic structure which should arise under rotation (Salomaa and Volovik, 1985c).

ment in ^{3}He: the two defects cannot be separated, because of their energy of attraction. The energy of the soliton coupling them is proportional to the intervortex distance R.

This texture (two half-quantum vortices interconnected by a soliton) was calculated numerically (Salomaa and Volovik, 1985c). First the part of F depending on α in Eq. (5.60) was minimized for a given distance R between the vortices in the vortex molecule; a resulting texture is displayed in Fig. 25(a). The distance R is determined by the competition of the attraction between the vortices due to the soliton string—this energy is proportional to R—and of the repulsion of the vortex pair due to the positive logarithmic interaction of the vortices with equal circulation quanta m. The equilibrium vortex-molecule size is presented in Fig. 25(c) as a function of the temperature-dependent anisotropy parameter $\rho_{sp}^{\perp}/\rho_s^{\perp}$.

3. Nonconservation of quantum numbers with half-quantum vortices

The half-quantum vortices have an interesting effect on the collective modes in ^{3}He-A. These boson excitations of the ^{3}He-A vacuum are characterized by specific quantum numbers, among which there is the pair spin projection S_z on the spin quantization axis **d**. Since **d** reverses on circling the vortex axis, the same occurs with the quantum number S_z: When the boson adiabatically encircles the vortex line, its charge S_z changes to the opposite. This is analogous to the change of parity or electric charge in the grand unified theories when an elementary particle circles a hypothetical singular line (Schwarz, 1982).

In both of these cases, ^{3}He-A and grand unified theory (as well as in the case of nematic liquid crystals), the existence of these singular lines is a consequence of the spontaneous breaking of the continuous symmetry G, with the conservation of a discrete subgroup of this group. In ^{3}He-A, the continuous group $SO_3^{(S)}\times U(1)$ is broken, while the ^{3}He-A vacuum is invariant under a discrete combined symmetry transformation, which changes the sign of **d**. As a result, **d** may be continuously transformed into $-\mathbf{d}$ on moving along the non-singly-connected region (see Fig. 8).

Analogously, in the grand unified theory, some large continuous group, e.g., SO(20), may be broken, while the vacuum retains invariance under its discrete subgroup, which transforms left particles into right ones. In this case, one may continuously approach the world on the other side of a mirror without breaking the mirror; it is enough just to encircle the line.

The topological charge of a point singularity (hedgehog) in the **d** field in ^{3}He-A changes sign after encircling the half-quantum vortex (Volovik and Mineev, 1977a). Thus, in the presence of a half-quantum vortex one may obtain the net (e.g., positive) charge from the vacuum by the creation of pairs of hedgehogs (or bosons) with opposite charges and by moving the negative charges around the vortex line.

4. The Aharonov-Bohm effect

Another effect of these novel singular lines on the collective modes is an analog of the Aharonov-Bohm effect, which results from the half-integer circulation (Khazan, 1985). Let us consider this effect with an example of one of the different collective modes in ^{3}He-A, namely, the "clapping mode" (for a review of collective modes in superfluid ^{3}He, see Wölfle, 1977). In this mode, the $L_z^{\rm int}=-1$ component of the order parameter is oscillating on the background of the $L_z^{\rm int}=1$ vacuum in the A phase:

$$A_{\alpha i}=\Delta_A[\hat{z}_\alpha(\hat{x}_i+i\hat{y}_i)+\psi(\hat{x}_i-i\hat{y}_i)]\ . \tag{5.61}$$

Here ψ is a complex amplitude of the state with $L_z^{\rm int}=-1$, which is zero in equilibrium. In a parallel-plate geometry, in the presence of a vortex with m quanta of circulation, ψ obeys the wave equation (Khazan, 1985)

$$\frac{\partial^2\psi}{\partial t^2}=c^2\left[\frac{\nabla}{i}-\mathbf{A}\right]^2\psi+(\omega_0^2+U)\psi\ . \tag{5.62}$$

Here ω_0 and c are the energy gap and the velocity of this mode.

Besides the scalar potential U, the m-quantum vortex also produces a vector potential $\mathbf{A}$ in Eq. (5.62) for this mode, due to the superflow:

$$\mathbf{A}=\nabla\Phi=\frac{m}{r}\hat{\phi}\ . \tag{5.63}$$

This corresponds to the motion of a charged particle in a magnetic field, which is concentrated inside the vortex core,

$$\mathbf{H}=\nabla\times\mathbf{A}=2\pi m\hat{z}\delta_2(r)\ , \tag{5.64}$$

i.e., the situation is totally analogous to the Aharonov-Bohm effect (Aharonov and Bohm, 1959).

The particle (here the collective mode) with wave number q is scattered on this magnetic field tube (half-quantum vortex) with the differential cross section

$$d\sigma=\frac{\sin^2\pi m}{2\pi q}\frac{d\theta}{\sin^2(\theta/2)}\ . \tag{5.65}$$

This additional scattering is absent for the vortices with an integer number m of circulation quanta. Therefore an increased "Aharonov-Bohm" width of the clapping mode due to rotation would indicate the existence of the half-quantum vortices in a sample of superfluid ^{3}He-A, rotating in the parallel-plate geometry (the NMR properties of the half-quantum vortices are discussed in Sec. VI.C).

G. Possible phase transitions in rotating ^{3}He-A

Due to the large variety of different topological and symmetry classes of vortices and vortex textures in ^{3}He-A, a large number of phase transitions between these configurations are possible in a rotating container. They may be divided into several groups as follows.

(i) Transitions between vortices from different topological classes. Examples include the singular singly quantized vortex array↔continuous doubly quantized vortex array transition, with a change in the topological charge N; the low-field ATC vortex↔high-field ATC vortex transition, with a change of the topological charge $\tilde{m}_d$ [Eq. (4.19)], etc.

(ii) Transitions with a change in the symmetry of the isolated vortex. Examples include $v \leftrightarrow w$ transitions, axially symmetric↔nonaxisymmetric transitions, either in the inner or outer cores, or both, etc.

(iii) A change in the symmetry of the vortex array, which takes place at sufficiently high angular velocities of rotation. Examples include a change in the circulation quantum per primitive vortex-lattice cell, a transition into a helical texture, etc.

(iv) Successive transitions in the vortex texture in a slowly rotating vessel, when the continuous increase in angular velocity results in a step-by-step change of the total circulation number in the vessel (see, for example, Soda and Shiwa, 1978; Williams and Fetter, 1979).

VI. NMR ON VORTICES IN ^{3}He-A

A. Spin waves in ^{3}He-A

1. Leggett equations for spin dynamics

The NMR technique has as yet provided the most versatile tool for extracting information on vortex structures in the superfluid A and B phases of liquid ^{3}He. In the NMR experiments on these ordered liquid magnets, collective magnetic modes, or spin waves, are excited by an external rf magnetic field. The spectrum of spin waves depends on the orientation of the order parameter and its distribution in space in an essential manner; this makes possible the detection of different textures—including the vortex textures, in particular.

Propagating spin waves in ^{3}He-A are coupled oscillations of the spin density $\mathbf{S}$ with the spin part $\mathbf{d}$ of the order parameter. The dynamics of these variables are governed by the NMR equations derived by Leggett. These may also be obtained from the routine scheme of Poisson brackets for the spin-rotation group $SO_3^{(S)}$, relevant for the spin dynamics (the spin density $\mathbf{S}$ is the generator of this group):

$$\{S_\alpha(\mathbf{r}),S_\beta(\mathbf{r}')\}=e_{\alpha\beta\gamma}S_\gamma(\mathbf{r})\delta(\mathbf{r}-\mathbf{r}') , \tag{6.1a}$$

$$\{S_\alpha(\mathbf{r}),d_\beta(\mathbf{r}')\}=e_{\alpha\beta\gamma}d_\gamma(\mathbf{r})\delta(\mathbf{r}-\mathbf{r}') . \tag{6.1b}$$

The Leggett equations in ^{3}He-A (Leggett, 1974; Buchholtz, 1978) are the Liouville equations for $\mathbf{S}$ and $\mathbf{d}$:

$$\frac{\partial \mathbf{S}}{\partial t}=\{\mathbf{S},H\} , \tag{6.2a}$$

$$\frac{\partial \mathbf{d}}{\partial t}=\{\mathbf{d},H\} . \tag{6.2b}$$

The energy H includes contributions of the order-parameter field, Eqs. (3.10) and (3.12), and the magnetic energy (3.3) in terms of the spin density $\mathbf{S}$:

$$H=\tfrac{1}{2}\gamma^2 S_\alpha(\chi^{-1})_{\alpha\beta}S_\beta-\mathbf{H}\cdot\mathbf{S}+F_{\rm grad}+F_d , \tag{6.3}$$

where the anisotropic susceptibility is given by Eq. (3.2). Substituting Eq. (6.3) into Eqs. (6.2), and employing the Poisson brackets (6.1), one obtains the Leggett equations

$$\frac{\partial \mathbf{S}}{\partial t}=\gamma\mathbf{S}\times\mathbf{H}-\mathbf{d}\times\frac{\partial F_d}{\partial \mathbf{d}}+\mathbf{d}\times\nabla_i\frac{\partial F_{\rm grad}}{\partial\nabla_i\mathbf{d}} , \tag{6.4a}$$

$$\frac{\partial \mathbf{d}}{\partial t}=\gamma\mathbf{d}\times\left[\mathbf{H}-\frac{\gamma\mathbf{S}}{\chi_\perp}\right] . \tag{6.4b}$$

In NMR experiments on rotating ^{3}He, transverse continuous-wave NMR has been used (Ikkala, Volovik, Hakonen, Bun'kov, Islander, and Kharadze, 1982; Hakonen, Ikkala, Islander, Lounasmaa, and Volovik, 1983; Hakonen, Krusius, Salomaa, Simola, Bun'kov, Mineev, and Volovik, 1983; Hakonen, Krusius, and Seppälä, 1985). In this case the rf field $\mathbf{H}_{\rm rf}$ is transverse to the constant magnetic field $\mathbf{H}_0=H\hat{z}$, which is of the order of 300 G. In such a high field, the equilibrium $\mathbf{d}$ texture is locked in the $(\hat{x},\hat{y})$ plane:

$$\mathbf{d}_0(\mathbf{r})=\hat{x}\cos\alpha+\hat{y}\sin\alpha . \tag{6.5}$$

2. Schrödinger equation for the spin-wave modes

The spin modes excited in the transverse NMR are coupled oscillations of the transverse spin density $\mathbf{S}_\perp\perp\mathbf{H}_0$, and of the longitudinal deviation of $\mathbf{d}$ from its equilibrium value, $\mathbf{d}=\mathbf{d}_0(\mathbf{r})+\psi\hat{z}$.

Using Eq. (6.4b), one may express the $\hat{z}\times\mathbf{d}_0$ component of spin density $\mathbf{S}_\perp$ through ψ:

$$\hat{z}\times\mathbf{d}_0\cdot\mathbf{S}_\perp=-i\frac{\partial\psi}{\partial t}\frac{\chi_\perp}{\gamma^2} , \tag{6.6}$$

and from Eq. (6.4a), with scalar multiplication by $\mathbf{d}$, the other $\mathbf{d}_0$ component of $\mathbf{S}_\perp$ is obtained in terms of ψ:

$$\mathbf{d}_0\cdot\mathbf{S}_\perp=-\psi H\frac{\chi_\perp}{\gamma} . \tag{6.7}$$

After scalar multiplication of Eq. (6.4a) by $\hat{z}\times\mathbf{d}_0$, and expressing $\mathbf{S}_\perp$ through ψ by means of Eqs. (6.6) and (6.7), we obtain the wave equation obeyed by the transverse spin mode (see, for example, Maki and Kumar, 1977; Fetter, 1983; Vulovic, Stein, and Fetter, 1984):

$$-\frac{\partial^2\psi}{\partial t^2}=(\gamma^2H^2+\Omega_A^2)\psi+\Omega_A^2(U\psi+D\psi) , \tag{6.8}$$

where the spin-wave potential U for transverse spin modes is given by

$$U_T=-\left[(\boldsymbol{l}\times\mathbf{d}_0)^2+l_z^2+\xi_{d\perp}^2\left[(\boldsymbol{l}\times\nabla\alpha)^2+\frac{\rho_{\rm sp}^{\parallel}}{\rho_{\rm sp}^{\perp}}(\boldsymbol{l}\cdot\nabla\alpha)^2\right]\right] , \tag{6.9}$$

and D is the kinetic-energy operator

$$D\psi=-\xi_{d\perp}^2\left[\Delta\psi+\frac{\rho_{sp}^{||}-\rho_{sp}^{\perp}}{\rho_{sp}^{\perp}}\nabla\cdot(\boldsymbol{l}(\boldsymbol{l}\cdot\nabla)\psi)\right]. \tag{6.10}$$

In Eq. (6.8), we introduced the transverse NMR frequency shift Ω_A in the homogeneous bulk liquid (Leggett, 1973)

$$\Omega_A^2=\frac{\gamma^2 2\Delta_A^2 g_d}{\chi_\perp}. \tag{6.11}$$

The transverse NMR frequency in the homogeneous liquid, with $\boldsymbol{l}||\mathbf{d}\perp\mathbf{H}$, and when $U=0$, is the frequency of the spin wave excited by the homogeneous field, i.e., with infinite wavelength. Using Eq. (6.8), it is found to have the form

$$\omega_{T,\text{bulk}}^2=\gamma^2H^2+\Omega_A^2. \tag{6.12}$$

Textures produce the attractive potential Eq. (6.9), which is more effective if $\boldsymbol{l}$ deviates from $\mathbf{d}$. This takes place in solitons (Maki, 1978; Gould, Bartolac, and Bozler, 1980), and also occurs in the dipole-unlocked soft cores of vortices (Volovik and Hakonen, 1981); thus solitons and high-field vortices produce potential wells, which are one dimensional and two dimensional, respectively. In both cases, there always exists a bound state with negative energy E, which corresponds to the localized spin-wave frequency below the continuum part of the spectrum:

$$\omega_{\text{loc}}^2=\omega_{\text{bulk}}^2+E\Omega_A^2,\quad E<0; \tag{6.13}$$

here E is the eigenvalue of the "Schrödinger" equation

$$E\psi=(D+U)\psi. \tag{6.14}$$

The lowest bound state may also be found using the variational principle:

$$E=\min\left[\frac{\int dV\,\psi(U+D)\psi}{\int dV\,\psi^2}\right]. \tag{6.15}$$

The excitation of localized spin modes results in an additional (satellite) absorption peak in the NMR experiments at the frequency ω_{loc}, given by Eq. (6.13) (see Fig. 26). This was resolved for the high-field vortices in ^{3}He-A by Hakonen, Ikkala, and Islander (1982). The intensity of the satellite peak, I_{loc}, is given by the overlap of the spin-wave function with the rf magnetic field, which is uniform.

In the case of rotating ^{3}He-A in a high magnetic field, where identical well-separated singular or nonsingular vortices produce identical two-dimensional potential wells by their dipole-unlocked soft cores, the localized spin-wave modes with identical frequency are excited independently. The net intensity of the vortex satellite peak is thus proportional to the vortex density n_v, and its intensity (oscillator strength) relative to the intensity of the bulk absorption peak is

$$\frac{I_{\text{loc}}}{I_{\text{bulk}}}=n_v\frac{\left[\int dx\,dy\,\psi\right]^2}{\int dx\,dy\,\psi^2}, \tag{6.16}$$

which is thus proportional to the angular velocity of rotation; this was confirmed experimentally by Hakonen, Ikkala, and Islander (1982).

Equations (6.13)–(6.15) and (6.10) are also valid for longitudinal spin waves, excited in longitudinal NMR by $\mathbf{H}_{\text{rf}}||\mathbf{H}_0$. These spin modes are coupled oscillations of $S_{||}$ and $\mathbf{d}_\perp$. The corresponding bulk NMR frequency and spin-wave potential are

$$\omega_{L,\text{bulk}}^2=\Omega_A^2, \tag{6.17}$$

$$U_L=-[2(\boldsymbol{l}\times\mathbf{d}_0)^2-l_z^2]. \tag{6.18}$$

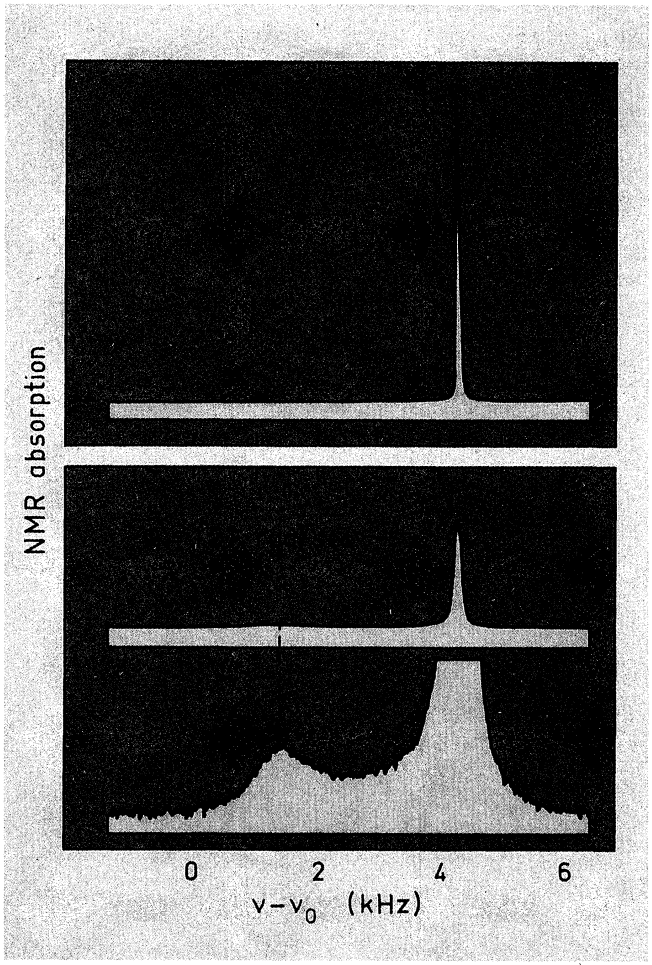

FIG. 26. Experimental NMR spectra of stationary and rotating ^{3}He-A (Hakonen, Ikkala, and Islander, 1982). The additional broadening of the main peak, due to rotation, is clearly apparent; the shift of this peak towards higher frequencies from the Larmor frequency is related to the spin-orbit coupling. The small satellite absorption peak, which appears in the NMR signal during rotation, is caused by the excitation of localized spin waves trapped by the continuous vortex textures.

B. NMR on continuous vortices in ^{3}He-A—singular versus continuous vortices

The bound-state spin-wave energies were calculated for the continuous w and v vortices, defined by Eqs. (5.29) and (5.30). In these trial functions, $\mathbf{d}$ was assumed uniform: $\mathbf{d}=\hat{y}$; this is the common asymptote for $\boldsymbol{l}$: $\boldsymbol{l}(\infty)=\hat{y}$. The spin-wave potential for this case, which, according to Eqs. (6.10) and (6.18), is

$$U_T=-(2l_z^2+l_x^2),\quad U_L=-(2l_x^2+l_z^2)\ , \tag{6.19}$$

has a minimum at the points where $\boldsymbol{l}||\hat{z}$ for transverse spin waves, and where $\boldsymbol{l}||\hat{x}$ for longitudinal spin waves. Due to the topological constraint expressed by Eq. (4.16a), the $\boldsymbol{l}$ vector passes through all the points on the unit sphere in the continuous doubly quantized vortices. Therefore, in both the v and the w vortices, there should be at least two points ("quarks"; see Sec. V.C.2) where U_T is minimal ($\boldsymbol{l}=\pm\hat{z}$), and two other points where U_L is minimal ($\boldsymbol{l}=\pm\hat{x}$); see Fig. 27.

Thus each vortex produces a double-well potential both for the longitudinal and transverse modes (Seppälä, Hakonen, Krusius, Ohmi, Salomaa, Simola, and Volovik, 1984; Zotos and Maki, 1984a; Maki and Zotos, 1985a, 1985b). However, the two wells are close to each other. Thus there exists only one state, the ground state, that is symmetric.

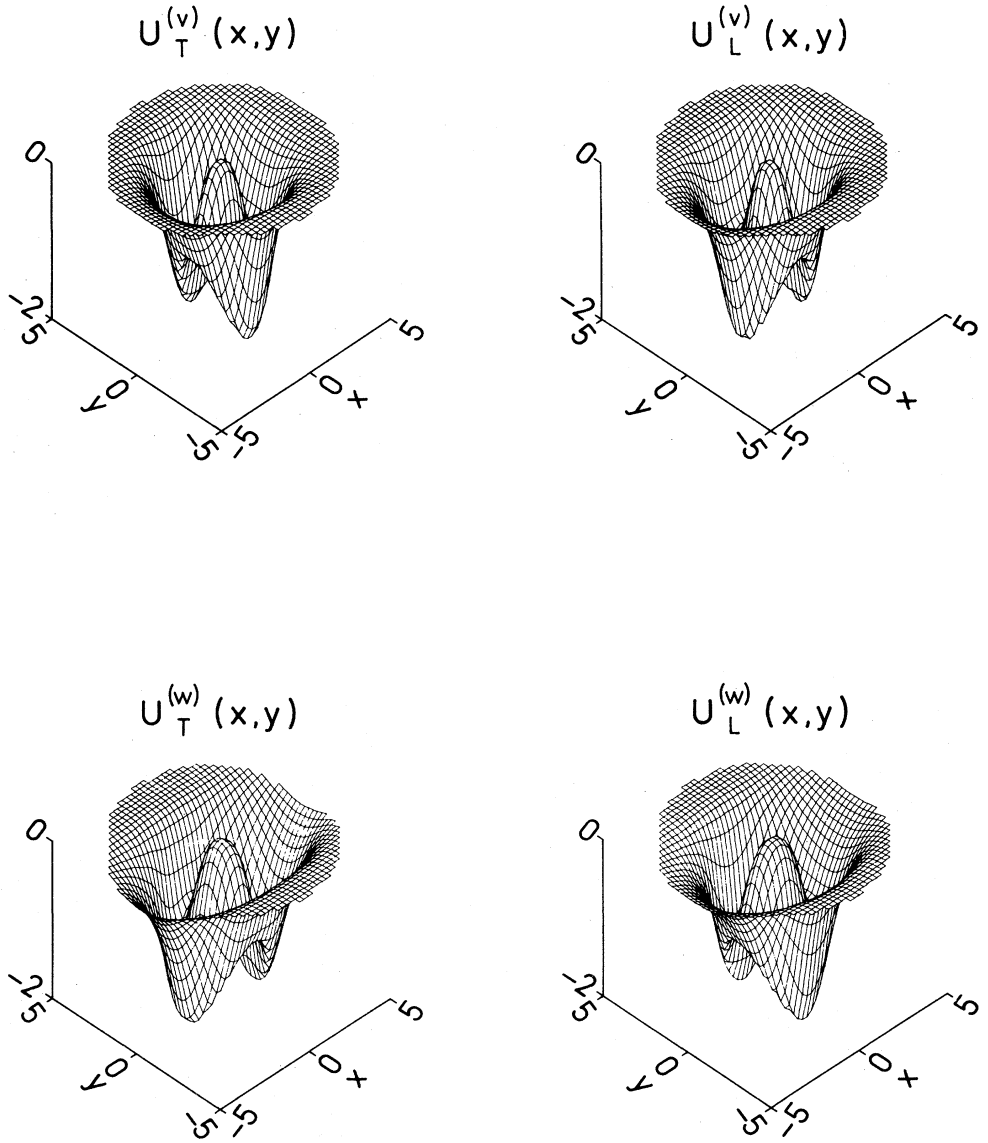

FIG. 27. The computed potential wells for transverse (T) and longitudinal (L) spin-wave modes for the continuous v and w vortices in ^{3}He-A displayed in Figs. 20 and 21. The potential well U_T^w (U_L^w) for the w vortex is obtained approximately from U_T^v (U_L^v) by a 90° rotation about $\boldsymbol{\Omega}$, and vice versa. Therefore these two vortex states, v and w, cannot be distinguished from each other by the use of NMR alone.

The soft core in the singly quantized vortex proves to be nearly half the size of the core of the continuous vortex, mostly because $\boldsymbol{l}$ traverses half the area on the unit sphere. This makes the potential well in singular vortices shallow, and results in a small value for the binding energy $E \ll 1$. On the other hand, the extent of the ground-state wave function increases, thus producing the large intensity $I_{\rm loc}$ in Eq. (6.16).

A comparison of the theoretical (Seppälä and Volovik, 1983; Vulovic, Stein, and Fetter, 1984) and experimental (Hakonen, Ikkala, and Islander, 1982; Hakonen, Ikkala, Islander, Lounasmaa, and Volovik, 1983; Hakonen, Krusius, and Seppälä, 1985) values in ^{3}He-A indicates that in high magnetic fields the doubly quantized continuous vortices seem to be created under rotation, although the energy of such a texture is slightly larger than that of the singular vortex array.

This circumstance may be attributed to the large metastability towards the creation of singular vortices with a hard core, in comparison with the continuous vortices. (See the discussion in Hakonen, Ikkala, Islander, Lounasmaa, and Volovik, 1983; on the creation mechanism of continuous vortices, see Anderson and Toulouse, 1977; Ho, 1978a, 1978b, 1978c; Hall and Hook, 1986.)

In ^{3}He-B, where only singular vortices are allowed by topology, the time needed for reaching the equilibrium vortex texture after rotation has been started is much longer in comparison with ^{3}He-A. This circumstance also favors continuous vortices in the A phase. Since continuous vortices are created first, they occupy the whole vortex lattice; thus there remains no space for singular vortices.

A direct transformation of a continuous vortex into two singular vortices, with formation of the hard core, seems highly improbable. Although this transformation is allowed by topology, since the summation laws for both N $(0=1+1)$ and m $(2=1+1)$ are fulfilled, the creation of singularities from a continuous texture requires that a large potential barrier be overcome. A simplified version of this fission process is shown in Fig. 28. The intermediate objects are monopoles, i.e., point singularities in the $\boldsymbol{l}$ field, accompanied by a singular vortex tail, which provides confinement in the monopole-antimonopole pair (Blaha, 1976; Volovik and Mineev, 1976a; Hu, Kumar, and Maki, 1977; Soni, 1978).

Monopoles carry away the topological charge $\tilde{m}_l$ of the continuous texture. The $\mathbf{v}_s$ field near a monopole resembles the vector potential (the field $\mathbf{A}$) near a magnetic Dirac monopole. These objects may possibly be detected in the process of phase transitions from continuous to singular vortex texture, or during the creation of continuous vortices.

C. NMR on the half-quantum vortex

The half-quantum vortex (HQV), which becomes stable in the parallel-plate geometry (see Sec. V.F), produces an analog of the Aharonov-Bohm effect (Salomaa and Volovik, 1986b) of the type considered in Sec. V.F.4 for transverse spin waves. This is another result of the double-valuedness (Maki, 1986) of the spin-wave function ψ in Eq. (6.8) in the presence of a HQV, which follows from its topology (Salomaa and Volovik, 1986b; Hu and Maki,

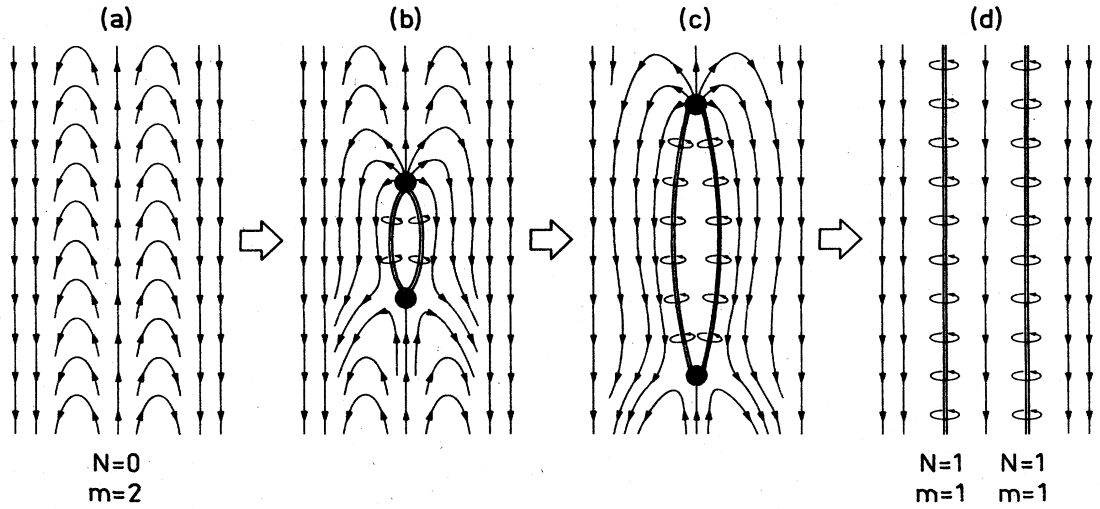

FIG. 28. The fissioning of a nonsingular ($N=0$) vortex with two quanta of circulation ($m=2$) in (a) into two singular ($N=1$) singly quantized ($m=1$) vortices in (d). This process involves two monopoles with opposite charges (radial and hyperbolic points, respectively) as the intermediate objects in (b) and (c). The monopoles are hedgehogs in the $\boldsymbol{l}$ field [see Fig. 13(c) for a hedgehog in the $\mathbf{d}$ field], and display the same distribution of the superflow $\mathbf{v}_s$ field near the poles as the gauge field $\mathbf{A}$ in the vicinity of a magnetic Dirac monopole.

1987): the function ψ, as well as the **d** field, changes sign after circling the HQV line. ψ may be regularized by introducing the phase λ, which changes by π upon circling the HQV:

$$\psi = e^{i\lambda}\tilde{\psi} . \tag{6.20}$$

Here $\tilde{\psi}$ is a regular, single-valued function. The Schrödinger-type equation for $\tilde{\psi}$ is obtained by substituting Eq. (6.20) into Eq. (6.8). For the parallel-plate geometry, with $\mathbf{l}=\hat{z}$ and with $\tilde{\psi}=\tilde{\psi}(x,y)$, this yields the equation

$$E\tilde{\psi} = \xi_{d\perp}^2 \left[\frac{\nabla}{i} - \mathbf{A} \right]^2 \tilde{\psi} + U_T \tilde{\psi} , \tag{6.21a}$$

$$\omega^2 = (\gamma H)^2 + E\Omega_A^2 - \Omega_A^2 \cos 2\theta , \tag{6.21b}$$

which corresponds to the "Schrödinger" equation (6.14) with scalar potential

$$U_T = -\xi_{d\perp}^2 (\nabla\alpha)^2 - \sin^2\theta \sin^2\alpha . \tag{6.22}$$

However, an inherent vector potential $\mathbf{A}=\nabla\lambda$ appears with the consequent "magnetic" field $\mathbf{B}=\nabla\times\mathbf{A}$, which is concentrated in the cores of the half-quantum vortices. For one HQV at the origin, one finds

$$\mathbf{B} = 2\pi m \hat{z} \delta(\mathbf{r}) . \tag{6.23}$$

This field corresponds to half a quantum of "magnetic" flux carried by the vortex core, since $m=\pm\frac{1}{2}$; thus, the vector potential cannot be eliminated through a gauge transformation.

Note that in the vicinity of the HQV, the scalar potential (6.22) diverges near the origin,

$$U_T \sim -\frac{1}{4}\frac{\xi_{d\perp}^2}{r^2} , \tag{6.24}$$

since $\alpha=\phi/2$ and $\nabla\alpha=(\frac{1}{2}r)\hat{\phi}$. However, this singularity is completely neutralized by the square of the vector potential $\mathbf{A}^2$, which has the same singularity—but with the opposite (positive) sign:

$$\xi_{d\perp}^2 \mathbf{A}^2 \sim \frac{1}{4}\frac{\xi_{d\perp}^2}{r^2} . \tag{6.25}$$

As a result, there is no "fall to the origin" in the HQV, which, nevertheless, should take place in a disclination with an integer index p.

The Aharonov-Bohm effect for the HQV's should produce additional spin-wave scattering, which is analogous to the scattering of the collective clapping mode (Sec. V.F.4). However, there is an important difference: while in an acoustic experiment the wave number q is large, in the NMR experiment $q\to 0$. This means that in an axial magnetic field **H**, where $\theta=0$, there is no Aharonov-Bohm scattering in the limit $q\to 0$; in this case there exists an exact solution of Eq. (6.2): $\tilde{\psi}=\text{const}, E=0$, which corresponds to the bulk NMR without any broadening.

The situation changes when the field is tilted, $\theta\neq 0$, and an effective q appears due to inhomogeneity. In this case, both the Aharonov-Bohm scattering and the ordinary spin-wave scattering on solitons should broaden the main NMR peak. This broadening should be essentially larger than that due to spin-wave scattering on vortices with integer quanta of circulation (for spin-wave scattering on integer-quantum vortices, see Fomin and Kamenski, 1982), since the cross section of the soliton, $\sim\xi_{d\perp}/\sin\theta$, is much larger than the cross section for the singly or doubly quantized vortices with cross section of the order of their soft core, which is also of the order of the distance between the plates. Therefore the HQV's may be identified by an abrupt increase in the NMR linewidth at the temperature $T\sim 0.7T_c$, where the transition from singly quantized vortices to HQV's is expected to occur.

VII. PROPERTIES OF SUPERFLUID ^{3}He-*B*

A. Degenerate states

The Cooper pairs in superfluid ^{3}He-*B* are in a pure state with the total angular-momentum quantum number $J=0$ [see Eqs. (2.13) and (2.14)]. This isotropic state is, however, manifestly different from the isotropic state in ordinary superconductors, where $J=0$, too. In addition, Cooper pairs in *s*-wave superconductors are invariant under separate spin and orbital rotations, $S=0$ and $L=0$.

There is no such invariance in ^{3}He-*B*, where the Cooper-pair wave function (2.14) is invariant only under simultaneous combined rotations around the same axis by the same angle. A separate rotation, e.g., of spin, described by the rotation matrix $R_{\alpha\beta}$, transforms the order parameter (2.14) into another order parameter, corresponding to a different state:

$$A_{\alpha i} \to R_{\alpha\beta} A_{\beta i} = \Delta_B R_{\alpha i} . \tag{7.1}$$

The degenerate states in ^{3}He-*B* are thus described by the matrix $R_{\alpha i}$, as well as by the phase Φ of the Bose condensate, and the general form for the order parameter is

$$A_{\alpha i} = \Delta_B(T) R_{\alpha i} e^{i\Phi} . \tag{7.2a}$$

It is convenient to express the orthogonal matrix $R_{\alpha i}$ by the angle θ and the axis $\hat{n}$ of the rotation, described by the following rotation matrix:

$$R_{\alpha\beta} = \delta_{\alpha\beta} - (1-\cos\theta)(\delta_{\alpha\beta} - n_\alpha n_\beta) - e_{\alpha\beta\gamma} n_\gamma \sin\theta . \tag{7.2b}$$

Note that the state described by Eq. (7.2a) is by no means an eigenstate of the operator $\hat{\mathbf{J}}=\hat{\mathbf{L}}^{\text{int}}+\hat{\mathbf{S}}$, but rather it is now the eigenstate of another operator, $\hat{\mathbf{J}}^{(R)}$:

$$\hat{\mathbf{J}}^{(R)} A_{\alpha i} = 0, \quad \hat{J}_i^{(R)} = \hat{L}_i^{\text{int}} + R_{\alpha i} \hat{S}_\alpha . \tag{7.3}$$

Above, $\hat{\mathbf{J}}^{(R)}$ denotes an operator of combined rotations, which is obtained from $\hat{\mathbf{J}}$ by rotation of the spin space.

B. Gyromagnetism of Cooper pairs in ^{3}He-B

The invariance of the B-phase state under the combined symmetry with the generator $\hat{\mathbf{J}}^{(R)}$ results in the unusual gyromagnetic properties of this superfluid (Leggett and Takagi, 1978; Liu and Cross, 1978; Combescot, 1980; Volovik and Mineev, 1984; Mineev, 1986). From Eq. (7.3) it follows that the average internal orbital moment $\langle \mathbf{L}^{\rm int} \rangle$ in the state of Cooper pairs with the wave function (7.2) may be expressed through the average spin moment:

$$\langle \hat{L}_i^{\rm int} \rangle = -R_{\alpha i} \langle S_\alpha \rangle \ . \tag{7.4}$$

This is trivial for ^{3}He-B at equilibrium since both $\langle \mathbf{L}^{\rm int} \rangle$ and $\langle \mathbf{S} \rangle$ are zero in this isotropic state; however, due to the rigidity of the Bose condensate, Eq. (7.4) remains valid even for the slightly perturbed B phase. As a result, an Einstein–de Haas effect arises in an external magnetic field, which induces an average spin density of Cooper pairs $\langle \mathbf{S} \rangle \sim \mathbf{H}$. Owing to the rigidity of the Cooper pairs, this in turn, according to Eq. (7.4), produces an average orbital momentum, given by

$$\langle L_i^{\rm int} \rangle \sim R_{\alpha i} H_\alpha \ . \tag{7.5}$$

Therefore the electrically neutral Cooper pairs start to rotate in a magnetic field. In the conjugate Barnett effect, the rotation of the liquid with angular velocity $\mathbf{\Omega}$, which gives rise to the average orbital momentum of the Cooper pairs, simultaneously produces a net spin density $\mathbf{S} \sim \overleftrightarrow{R}\mathbf{\Omega}$ and, therefore, the nuclear magnetic moment

$$M_\alpha \sim R_{\alpha i} \Omega_i \ . \tag{7.6}$$

C. Relative spin-orbital anisotropy in the isotropic liquid

Note the fundamental difference between gyromagnetism in ordinary substances and that in ^{3}He-B. In an isotropic condensed medium the magnetic moment is parallel to the orbital momentum, while in isotropic ^{3}He-B these moments are not parallel: they are coupled through a rotation represented by the matrix $R_{\alpha i}$ in the order parameter (7.2). Therefore ^{3}He-B presents a unique situation: while both the orbital and spin properties of this superfluid are isotropic, there occurs a kind of relative anisotropy represented by $R_{\alpha i}$.

This relative anisotropy of the magnetic and orbital properties in the isotropic liquid is manifested also through the following effect: if any anisotropy axis $\mathbf{n}^{(L)}$ of the orbital properties is induced by external conditions, there simultaneously appears an anisotropy axis $\mathbf{n}^{(S)} = \overleftrightarrow{R}\mathbf{n}^{(L)}$ for the magnetic properties. For example, the container wall produces an anisotropy in orbital space, with the anisotropy axis along the normal $\hat{\nu}$ to the wall. This automatically results in a magnetic axis $\mathbf{n}^{(S)} = \overleftrightarrow{R}\hat{\nu}$ near the wall and, therefore, in the surface term of the magnetic anisotropy energy (Brinkman and Cross, 1978):

$$F_{\rm surf} = -d(H_\alpha R_{\alpha i} \hat{\nu}_i)^2 \ , \tag{7.7}$$

with $d \sim \xi(\chi_N - \chi_B)$. This gives the boundary condition for the order parameter $R_{\alpha i}$ in the presence of an applied magnetic field: the vector $R_{\alpha i}\hat{\nu}_i$ should lie parallel to the external field $\mathbf{H}$.

An analogous bulk magnetic anisotropy is produced, for example, by superflow, which defines the anisotropy axis along $\mathbf{v}_s - \mathbf{v}_n$ in orbital space (Brinkman and Cross, 1978)

$$F_{H,\rm flow} = -\beta_{\rm flow}[H_\alpha R_{\alpha i}(v_{si} - v_{ni})]^2 \ , \tag{7.8}$$

where $\beta_{\rm flow} \sim (\chi_N - \chi_B)\xi_{\rm GL}^2 (M/\hbar)^2$. On the other hand, the interaction (7.8) means that the superfluid density, which is a scalar in zero field, becomes a tensor in an applied magnetic field, with

$$\begin{aligned} &\rho_{ij}^s = \rho_s^{\parallel} n_i^{(L)} n_j^{(L)} + \rho_s^{\perp}(\delta_{ij} - n_i^{(L)} n_j^{(L)}) \ , \\ &\rho_s^{\perp} - \rho_s^{\parallel} = 2\beta_{\rm flow} H^2 \sim \rho_s \left[\frac{\xi_{\rm GL}}{\xi_{2H}} \right]^2 , \end{aligned} \tag{7.9}$$

where the orbital anisotropy axis $\mathbf{n}^{(L)} \| \overleftrightarrow{R}\mathbf{H}$. (This effect is, however, absent at $T=0$, where $\rho_s^{\perp} = \rho_s^{\parallel} = \rho$.) Thus the anisotropy in spin properties, induced by an applied magnetic field, produces the orbital anisotropy axis $\mathbf{n}^{(L)}$.

Owing to the energies $F_{H,\rm flow}$ and $F_{\rm surf}$, the order-parameter matrix $R_{\alpha i}$ is orientated in the bulk B phase by the combined actions of magnetic field and superflow, or of magnetic field and boundary, respectively. In the absence of superflow and far from boundaries, the orientation of the order parameter by magnetic field occurs only due to the tiny dipole forces.

D. Small dipole anisotropy and textures

The dipole energy (2.29) partially lifts the degeneracy of the B phase: now only the rotation axis $\mathbf{n}$ in Eq. (7.2b) is arbitrary, while the rotation angle θ is fixed by the dipole energy (2.29)

$$\begin{aligned} F_d &= g_d \Delta_B^2(T)(R_{\alpha\alpha} R_{\beta\beta} + R_{\alpha\beta} R_{\beta\alpha}) \\ &= 4 g_d \Delta_B^2(T)(\cos\theta + 2\cos^2\theta) \ , \end{aligned} \tag{7.10}$$

which is minimal at the "magic" angle

$$\theta_0 = \arccos(-\tfrac{1}{4}) \simeq 104^\circ \ . \tag{7.11}$$

This angle is manifested in various NMR experiments (e.g., Corruccini and Osheroff, 1978; Borovik-Romanov, *et al.*, 1983; Golo, Leman, and Fomin, 1983).

The dipole forces also deform the Cooper-pair state, and thus produce a small anisotropy for both the orbital and magnetic properties, with the anisotropy axis along $\mathbf{n}$. Since $\overleftrightarrow{R}\mathbf{n} = \mathbf{n}$, this is a common axis for both the orbital and the magnetic subsystems. The magnetic anisotropy energy (see, for example, Osheroff, 1977),

$$F_{d,H} = -a(\mathbf{n}\cdot\mathbf{H})^2, \quad a \sim (\chi_N - \chi_B) \left[\frac{\xi_{\rm GL}}{\xi_d} \right]^2 , \tag{7.12}$$

is 5 orders of magnitude less than that in the A phase, since it is produced by tiny dipole forces. However, in the absence of superflow and far from the boundaries, this is the only orientating effect for the vector $\mathbf{n}$ in the bulk liquid. The characteristic length of this interaction

$$\xi_{d,H} \sim \frac{\xi_{2H}\xi_d}{\xi} \tag{7.13}$$

is of the order of 1 mm in fields of order 100 G, which is to be compared with the size of the container (the radius of the cylinder $R=2.5$ mm in the NMR experiment on rotating ^{3}He; see Hakonen, Ikkala, Islander, Markkula, Roubeau, Saloheimo, Garibashvili, and Tsakadze, 1981, 1983). Thus, textures produced within $\sim\xi_{dH}$ of the container walls by the combined action of magnetic anisotropy energy (7.12) and boundaries are practically always important in ^{3}He-B. The first traces of the quantized vortex lines in ^{3}He-B were found due to the influence of vortices on textures (Ikkala, Volovik, Hakonen, Bun'kov, Islander, and Kharadze, 1982). Therefore we are motivated to consider the order-parameter textures in some more detail.

The textures are obtained by minimization of the energy (7.12) and the gradient energy (2.19), which for ^{3}He-B near T_c has the form

$$F_{\rm grad}=\gamma_0\Delta_B^2(T)[(\nabla_i R_{\alpha j})(\nabla_i R_{\alpha j}) + 2(\nabla_i R_{\alpha i})^2+5(\nabla\Phi)^2] , \tag{7.14a}$$

or in terms of the $\mathbf{n}$-vector field

$$F_{\rm grad}\{\mathbf{n}\}=aH^2\xi_{d,H}^2[(\nabla_i\mathbf{n})^2-\tfrac{1}{16}(\sqrt{3}\nabla\cdot\mathbf{n}+\sqrt{5}\mathbf{n}\cdot\nabla\times\mathbf{n})^2] , \tag{7.14b}$$

where we have defined

$$\xi_{d,H}^2=\frac{10\Delta_B^2\gamma_0}{aH^2} . \tag{7.14c}$$

The boundary conditions for $\mathbf{n}$ follow from the minimization of the surface energy (7.7). The typical axisymmetric $\mathbf{n}$ texture, arising in the cylindrical experimental cell in an axial magnetic field $\mathbf{H}||\hat{z}$, is the flare-out texture, illustrated in Fig. 29 (Hakonen and Volovik, 1982; Spencer and Ihas, 1982; Maki and Nakahara, 1983):

$$\mathbf{n}=\hat{z}\cos\beta(r)+\sin\beta(r)[\hat{\phi}\sin\alpha(r)-\hat{r}\cos\alpha(r)] . \tag{7.15}$$

Here $\alpha(R)=60°$ and $\beta(R)=\arccos(1/\sqrt{5})=63.4°$ minimize the surface energy Eq. (7.7)] at the container wall ($r=R$) and $\beta\to 0$ in the bulk liquid in order to minimize the magnetic anisotropy energy $F_{d,H}=aH^2\sin^2\beta$ (apart from an additive constant). At small distances r from the container axis, the polar angle β varies linearly with r (Maki and Nakahara, 1983):

$$\beta=\beta_1 r,\quad \beta_1=1.38\left[\frac{R}{\xi_{d,H}^3}\right]^{1/2} e^{-(R/\xi_{d,H})} . \tag{7.16}$$

Here β_1 is the calculated value in the limit $\xi_{dH}\ll R$ (Hakonen and Volovik, 1982).

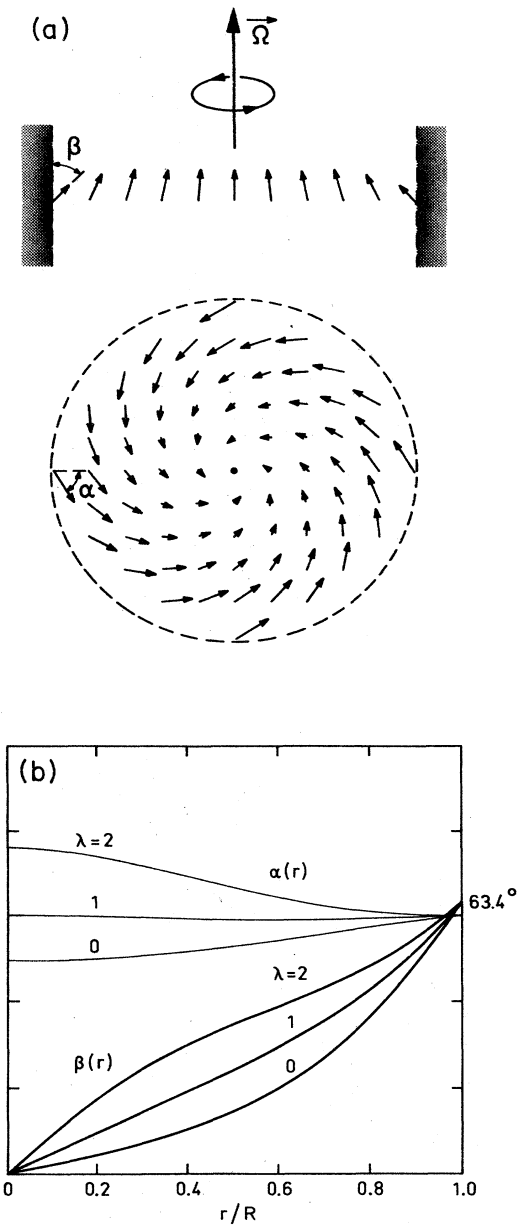

FIG. 29. (a) Side view (top) and a projection into the cross-sectional plane (bottom) of the axisymmetric "flare-out" $\mathbf{n}$-vector texture occurring in ^{3}He-B inside a cylindrical container of radius $R=4\xi_H$; boundary condition fixes the angles α and β of $\mathbf{n}$ in Eq. (7.15) to $\alpha=60°$ and $\beta=63.4°$ at the inner surface of the container, and $\mathbf{n}$ spirals towards the axis of the cylinder, parallel to Ω, where it is vertical. The spatial variation of the angle $\beta(\mathbf{r})$ near the cylinder axis provides the spin-wave potential, giving rise to the resonance peaks shown in Figs. 30. (b) Calculated distributions of the angles $\alpha(r)$ and $\beta(r)$ for different values of the parameter λ, which characterizes the orientational effect of vortices on the $\mathbf{n}$ vector [see Eq. (7.21)]. In the stationary case when there are no vortices, $\lambda=0$. Note how the slope of $\beta(r)$ at the cylinder axis ($r=0$) increases rapidly with λ, i.e., with Ω. For increasing λ, a plateau region appears [the plateau in $\beta(r)$ gives rise to the shifted NMR peak in Fig. 47], where β is approximately constant.

E. NMR on textures in superfluid ^{3}He-B

Superfluid ^{3}He-B does not exhibit any appreciable transverse NMR frequency shift in the bulk liquid where, according to Eq. (7.12), $\mathbf{n}||\mathbf{H}$ (i.e., $\beta=0$). However, textures with $\beta\neq 0$ cause the resonance peak to shift to higher frequencies. In magnetic fields $H \gg 25$ G, the frequency shift from the liquid with $\beta=$const is (see, for example, Osheroff, 1977)

$$\omega-\gamma H=\frac{\Omega_B^2}{2\gamma H}\sin^2\beta\ , \tag{7.17}$$

where Ω_B is the longitudinal resonance frequency in the bulk B phase.

As in the case of ^{3}He-A in the presence of textures, bound spin-wave modes are excited in NMR with frequencies corresponding to the eigenvalues of the Schrödinger equation, with the $\sin^2\beta$ term serving as the spin-wave potential:

$$\omega-\gamma H=\frac{\Omega_B^2}{2\gamma H}E\ , \tag{7.18a}$$

$$E\psi=(U+\hat{D})\psi\ , \tag{7.18b}$$

$$U=\sin^2\beta(\mathbf{r}),\quad \hat{D}=-(\tfrac{48}{65})^{1/2}\xi_d^2\nabla^2\ , \tag{7.18c}$$

where $\xi_d\sim 10^{-3}$ cm is the dipole length in ^{3}He-B.

The flare-out texture [Eq. (7.15)] produces a harmonic potential well $U(\mathbf{r})\approx\beta_1^2 r^2$ near the origin for bound spin-wave modes. This results in a series of satellite peaks with equal spacing (Hakonen and Volovik, 1982; Maki and Nakahara, 1983; see Fig. 30),

$$E=(n+1)(\tfrac{48}{65})^{1/2}\xi_d\beta_1\ . \tag{7.19}$$

Here, $n=0,2,4,\ldots$, because, due to Eq. (6.16), only the even harmonics are excited by a uniform rf magnetic field (see Fig. 31).

Note the difference between the bound spin waves of textures in ^{3}He-A and those in ^{3}He-B. The textures in ^{3}He-B are very shallow and extended; therefore there are many broad eigenstates with small energies. In ^{3}He-A, the spin-wave potential of textures is concentrated in small regions of the order of $\xi_d\sim 10^{-3}$ cm and, as a rule, allows only one very localized eigenstate with a large energy. Therefore, in order to have an appreciable satellite peak, one needs a large number of identical textures (solitons or vortices) in ^{3}He-A, while in ^{3}He-B one (bulk-liquid) texture gives rise to several observable satellite peaks.

F. NMR on vortices in ^{3}He-B

1. Orientational effects of vortices on the order parameter

Since the order parameter $R_{\alpha i}$ in ^{3}He-B is real, there is no continuous combined symmetry that would couple the superfluid and magnetic—or liquid-crystal-like—properties of ^{3}He-B. Therefore the quantized vortices in ^{3}He-B are pure phase vortices,

$$A_{\alpha i}=\Delta_B R_{\alpha i}e^{im\phi}\ , \tag{7.20}$$

which for any $m\neq 0$ have a singular hard core of a size of the order of $\xi_{\rm GL}$, where the B phase is distorted. The only difference from vortices in He II can be in the hard-core structure.

These vortices have been found in the NMR experiments through their orientational effect on the $\mathbf{n}$ texture, which changes the potential well for bound spin waves (Ikkala, Volovik, Hakonen, Bun'kov, Islander, and Kharadze, 1982; Hakonen, Ikkala, Islander, Lounasmaa, and Volovik, 1983). The rotation of the container has two additional effects on the $\mathbf{n}$ texture.

(i) First, there is an anisotropy axis along the vortex axis $\hat{\Omega}$ for orbital properties; this, according to the relative anisotropy of ^{3}He-B, simultaneously produces a magnetic anisotropy along the axis $\mathbf{n}^{(S)}=\overleftrightarrow{R}\hat{\Omega}$. Provided that the ^{3}He-B vortices are axisymmetric, the corresponding magnetic anisotropy energy is given by (Gongadze, Gurgenishvili, and Kharadze, 1981; Hakonen and Volovik, 1982; Maki and Nakahara, 1983; Salomaa and Volovik, 1985a)

$$F_{v,H}=\tfrac{2}{5}\lambda a(H_\alpha R_{\alpha i}\hat{\Omega}_i)^2\ . \tag{7.21}$$

This energy is produced by averaging of the orientational effects of isolated vortices over the vortices in a unit volume. In Eq. (7.21), the phenomenological vortex parameter λ has been introduced, which characterizes the orientational effect of axisymmetric vortices on the $\mathbf{n}$ field, as measured in units of the orientational effect of a magnetic field in Eq. (7.12). The vortex parameter λ is proportional to the number density of vortices, n_v [cf. Eqs. (8.27)].

(ii) Another orientational effect on the order parameter in the rotating B liquid is due to gyromagnetism. The gyromagnetic energy is expressed through another phenomenological parameter κ:

$$F_{\rm gm}=\tfrac{4}{5}\kappa a(H_\alpha R_{\alpha i}\hat{\Omega}_i)\ . \tag{7.22}$$

This effect was first thought to be of pure bulk nature (Volovik and Mineev, 1983), without any connection to quantized vortices, but immediately after the experimental observation of gyromagnetism (Hakonen, Krusius, Salomaa, Simola, Bun'kov, Mineev, and Volovik, 1983) it was identified with the magnetism of the vortex cores.

Therefore, in a rotating container, the combined orientational effect on the angle β in the presence of an axial field $\mathbf{H}=\pm H\hat{z}$, with

$$(H_\alpha R_{\alpha i}\hat{z}_i)=\pm H(1-\tfrac{5}{4}\sin^2\beta) \tag{7.23}$$

is, apart from an additive constant,

$$F_{d,H}+F_{v,H}+F_{\rm gm}=aH^2\sin^2\beta\left[1-\lambda\mp\frac{\kappa}{H}+\tfrac{5}{8}\lambda\sin^2\beta\right]\ . \tag{7.24}$$

For the effect of λ on the $\hat{n}$ texture, see Fig. 29(b). The effect of rotation on the texture becomes more transparent if the last term on the right-hand side of Eq. (7.24) may be neglected, i.e., if only small values of β are important; this is the situation in the center of the sample cell, where the spin waves are localized. Rotation simply renormalizes the magnetic anisotropy parameter a and, therefore, the characteristic length $\xi_{d,H}$ in Eq. (7.14c):

$$\xi_{d,H} \rightarrow \tilde{\xi}_{d,H}, \quad \tilde{\xi}_{d,H} = \xi_{d,H} \left[1 - \lambda \mp \frac{\kappa}{H} \right]^{-1/2} . \qquad (7.25)$$

As a result, the spectrum (7.19) and (7.16) of excited bound spin-waves modes is modified under rotation (Hakonen and Volovik, 1982; Jacobsen and Smith, 1983; Maki and Nakahara, 1983), and this was detected with use of the NMR technique (Ikkala, Volovik, Hakonen, Bun'kov, Islander, and Kharadze, 1982). Moreover, the spin-wave spectrum depends on the sense of the magnetic field **H** relative to $\boldsymbol{\Omega}$, which was also detected in the NMR experiments (see Fig. 32; Hakonen, Krusius, Salomaa, Simola, Bun'kov, Mineev, and Volovik, 1983).

A more pronounced effect of rotation was obtained in a magnetic field tilted with respect to the rotation axis $\hat{\Omega}$ (see Fig. 33; Bun'kov, Hakonen, and Krusius, 1983; Bun'kov, Krusius, and Hakonen, 1983; Bun'kov, Gurgenishvili, Krusius, and Kharadze, 1984). In this case the angle β between **n** and **H** is nonzero in the bulk liquid due to the combined orientational effect of the magnetic field and the vortices on the order parameter **n**; this produces a substantial frequency shift of the whole NMR absorption line according to Eq. (7.17).

2. The vortex-core transition and the core magnetization

The data on λ [Fig. 34(a); Bun'kov, Hakonen, and Krusius, 1983] and κ [Fig. 34(b); Hakonen, Krusius, Salomaa, Simola, Bun'kov, Mineev, and Volovik, 1983], extracted both from the bound spin-wave spectrum and the frequency shift, manifest the following important features: both λ and κ are proportional to the angular velocity of rotation Ω, i.e., to the density of vortices n_v; both λ and κ have a jump discontinuity at the tempera-

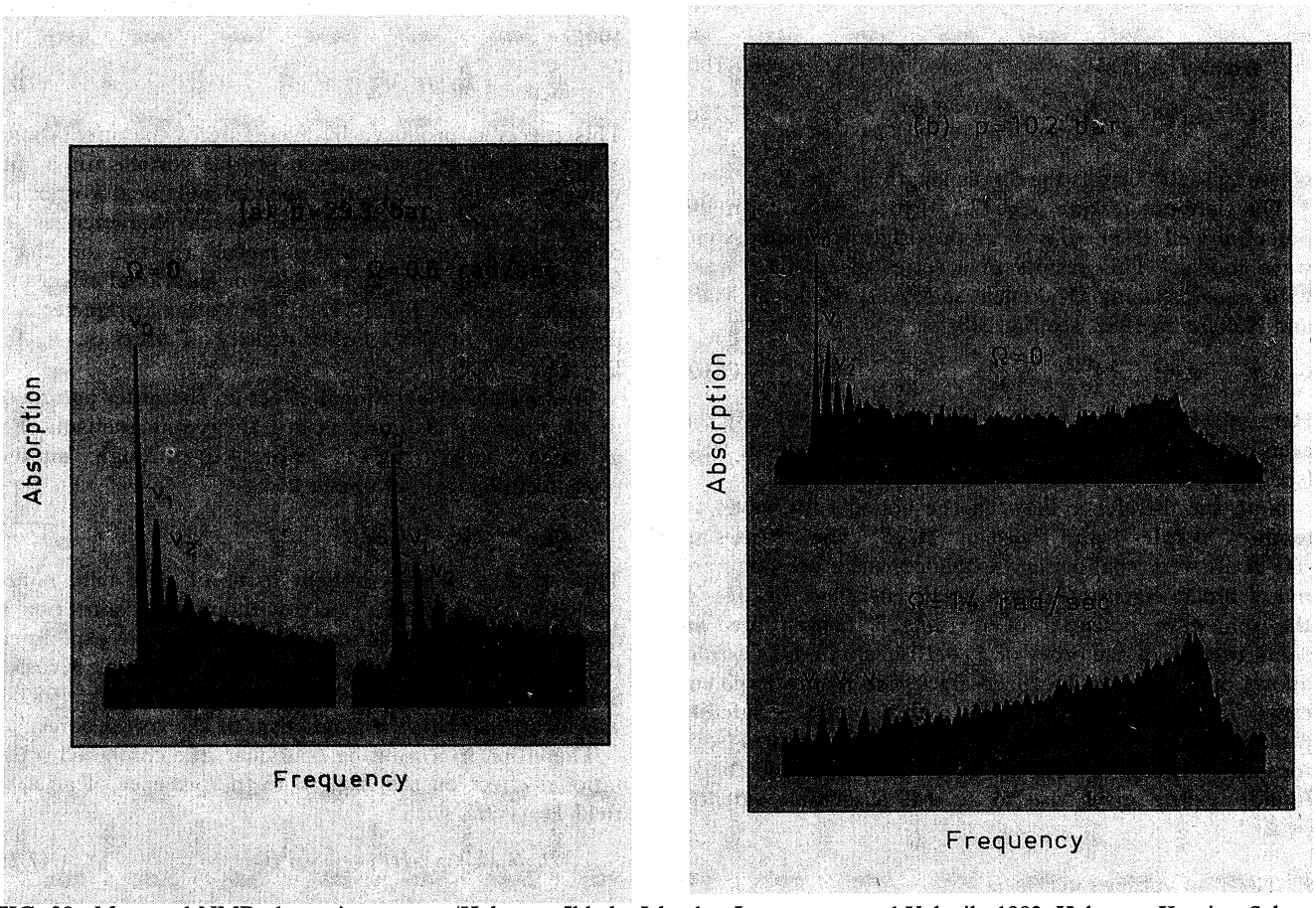

FIG. 30. Measured NMR absorption spectra (Hakonen, Ikkala, Islander, Lounasmaa, and Volovik, 1983; Hakonen, Krusius, Salmelin, Salomaa, Simola, Gongadze, Gurgenishvili, and Kharadze, 1987): (a) at $p = 29.3$ bars for $T = 0.45T_c$; (b) at $p = 10.2$ bars for $T = 0.50T_c$. Data are shown both in the stationary case and during rotation. The series of almost evenly spaced sharp spin-wave satellites results from the coherent nuclear motion of the Cooper-pair spins. The separation between the peaks at $\nu_0, \nu_1, \nu_2, \ldots$ is larger during rotation than in the stationary liquid. The envelope of the observed oscillatory curve corresponds to the flare-out textures in Fig. 29.

ture T_v, which does not depend on Ω or H, nor on the angle between them in the fields of $H=284$ and 568 G, depending only on pressure p. The linear dependence of λ on Ω supports the hypothesis that the orientating effect (7.21) is due to quantized vortex lines.

The independence of $T_v(p)$ from H means that the structural rearrangement occurs over distances much less than the characteristic length ξ_{2H} ($\sim 10^{-4}$ cm for these fields). This rules out any transition in the bulk B phase, as well as rearrangements in the type of the vortex lattice, since the intervortex distance is 10^{-2} cm. The observed discontinuities could be caused by a textural transition in the surface layer of thickness ξ_{GL} near the container walls, or in the cores of quantized vortex lines. The first possibility contradicts the results of measurements in tilted magnetic fields, where the shift of the main peak comes essentially from the bulk liquid independently of the boundary conditions, as well as from the fact that T_v does not depend on Ω.

The only hypothesis (Ikkala, Volovik, Hakonen, Bun'kov, Islander, and Kharadze, 1982) that fits all the data is that the transition occurs inside the hard singular core of size $\xi_{GL} \ll \xi_{2H}$; in this case T_v is a characteristic of an isolated vortex line and therefore does not depend on the vortex density n_v, nor on the magnetic field H. A dependence on **H** is expected in higher fields, where ξ_{2H} becomes comparable with ξ_{GL}. The jump in λ and the metastability phenomena (Bun'kov, Hakonen, and

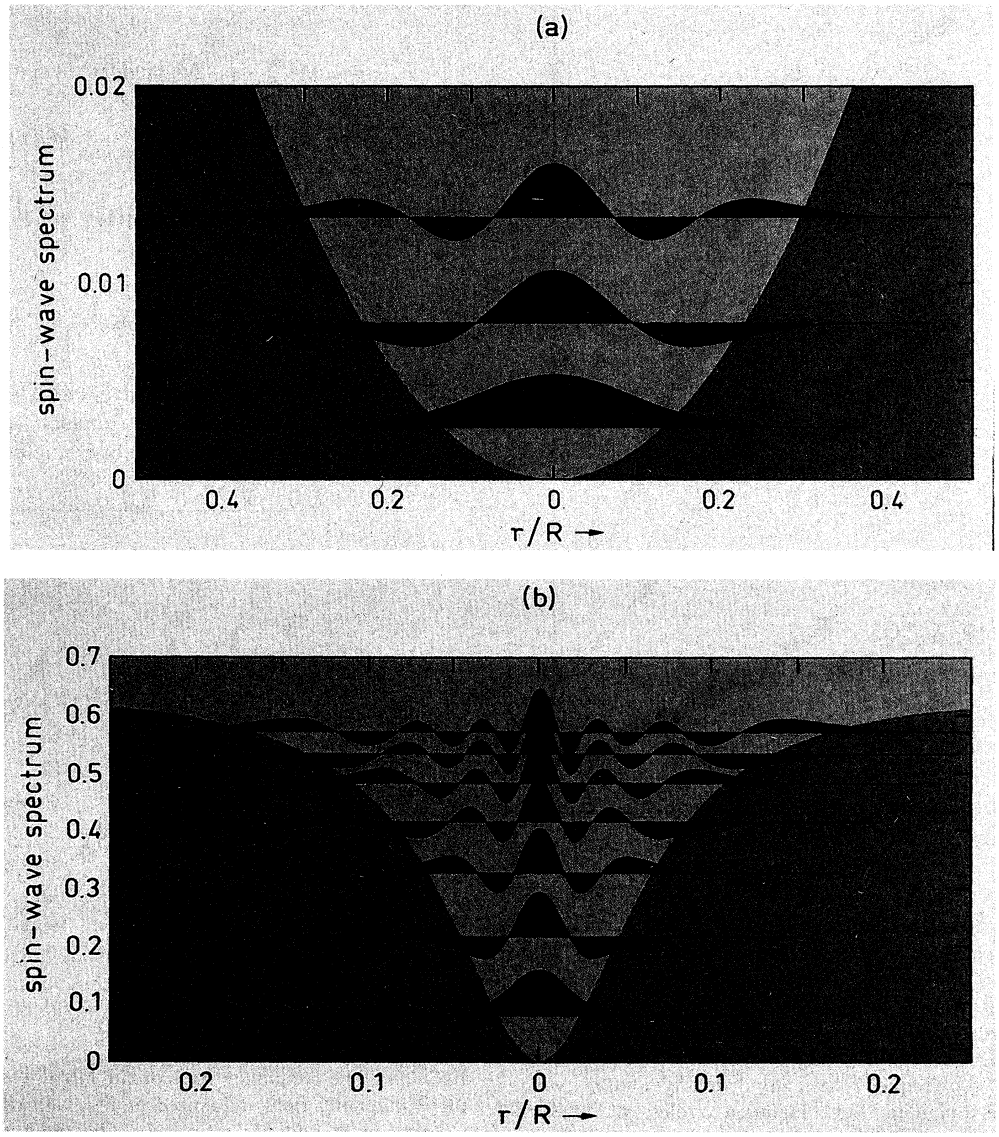

FIG. 31. The calculated spin-wave spectrum in the potential of the flare-out texture. (a) For $\lambda=0$ in the stationary state, the spectrum is very well approximated by that of a harmonic oscillator. (b) For large angular velocities of rotation (here $\lambda=10$), the $\beta(r)$ texture is strongly modified by rotation [see Fig. 29(b)], and the spectrum is no longer evenly spaced. [Dashed lines indicate $U(r)$, the spin-wave potential in Eq. (7.18c).]

Krusius, 1983) show that the transition in the core is of first order.

The jump in κ at T_v (Hakonen, Krusius, Salomaa, Simola, Bun'kov, Mineev, and Volovik, 1983) thus supports the hypothesis that at least a part of the gyromagnetic effect is related to the vortex core. Since there are nonunitary components in the core, it contains a frozen magnetic-moment density, directed along the spin axis of the vortex $\mathbf{n}^{(S)}=\overleftrightarrow{R}\hat{\Omega}$:

$$\mathbf{M}_v = M_v \overleftrightarrow{R}\hat{\Omega} \ . \tag{7.26}$$

The origin of the net magnetization in the vortex core is again the combined spin-orbital symmetry: the superflow, circulating around the core, produces an internal rotation of Cooper pairs with $\mathbf{L}^{\rm int}||\hat{\Omega}$, which is more pronounced in the core. This, according to Eq. (7.4) following from combined spin-orbital symmetry, produces the net spin density in the core. This, in turn, gives rise to the gyromagnetic energy of the vortices, which is linear in $\mathbf{H}$ and $\mathbf{\Omega}$, and obtained by averaging over identical vortices with density n_v:

$$F^v_{\rm gm} = -\mathbf{H}\cdot\sum_a \int_{S_a} \mathbf{M}_v(\mathbf{r})d^2r$$
$$= -H_\alpha R_{\alpha i}\Omega_i n_v \int_{\text{vortex core}} M_v(\mathbf{r})d^2r \ . \tag{7.27a}$$

Thus, the contribution of vortices in the parameter κ of Eq. (7.22) is

$$\kappa = -\frac{5}{4a} n_v \int_{\text{vortex core}} d^2r M_v(r) \ . \tag{7.27b}$$

The magnitude of $\mathbf{M}_v$, extracted from experimental data on the gyromagnetic parameter κ, corresponds to 10^{-11} nuclear magnetons per one nucleus of liquid ^{3}He

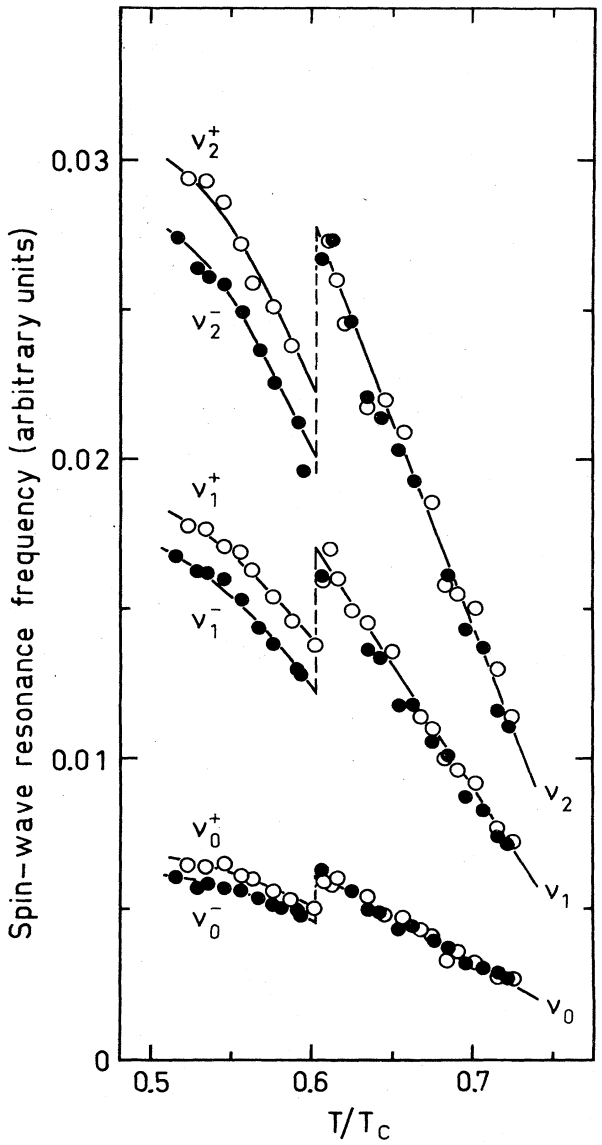

FIG. 32. The spin-wave resonance frequency as a function of the reduced temperature for the first three satellites ν_0, ν_1, and ν_2, of Fig. 30(a) at $\Omega=0.6$ rad/sec. The data (Hakonen, Krusius, Salomaa, Simola, Bun'kov, Mineev, and Volovik, 1983) illustrate the vortex-core transition at $T_v=0.6T_c$ and a gyromagnetic effect due to the magnetic moment of the vortex cores: the resonance frequency measured during rotation with $\mathbf{\Omega}$ parallel to the magnetic field $\mathbf{H}$ (open circles, ν^+) differs from that with $\mathbf{\Omega}$ antiparallel (solid circles, ν^-) in accordance with Eq. (7.22). The effect is large at $T<0.6T_c$, but hardly visible for $T>0.6T_c$; the vortices below and above the transition temperature have different core structures and, therefore, different intrinsic magnetic moments.

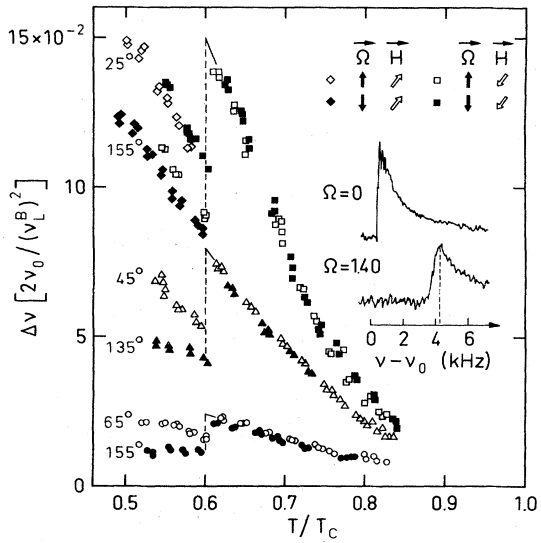

FIG. 33. The frequency shift of the NMR absorption peak in a tilted magnetic field, measured at $\Omega=1.40$ rad/sec. The angle μ between $\mathbf{\Omega}$ and $\mathbf{H}$ is quoted. The open and solid symbols represent forward and reverse rotation, respectively. For $\mu=25°$ and 155°, the directions of $\mathbf{\Omega}$ and $\mathbf{H}$ are shown by the arrows. The NMR signals in the inset were measured at $T=0.53T_c$ with $\mu=25°$ (Hakonen, Krusius, Salomaa, and Simola, 1987).

containing the equilibrium density of vortices at $\Omega \sim 1$ rad/sec, which is in reasonable agreement with the theoretical estimate of the core magnetization (see Sec. VIII.C.1). [The magnetic moment of quantized vortices was first predicted by Sauls, Stein, and Serene (1982) for a $^3P_2$ neutron superfluid. Independently from this work, the core magnetism was estimated by Hakonen, Krusius, Salomaa, Simola, Bun'kov, Mineev, and Volovik (1983), and by Ohmi, Tsuneto, and Fujita (1983).] On the other hand, the derivation of the bulk gyromagnetic effect (Mineev, 1985) shows that it is much smaller than the gyromagnetic effect due to vortices, thus the experimental κ essentially corresponds to the vortex-core magnetization (Salomaa and Volovik, 1983b, 1985a).

Therefore the experiments (Ikkala, Volovik, Hakonen, Bun'kov, Islander, and Kharadze, 1982; Hakonen, Krusius, Salomaa, Simola, Bun'kov, Mineev, and Volovik, 1983; Pekola, Simola, Hakonen, Krusius, Lounasmaa, Nummila, Mamniashvili, Packard, and Volovik, 1984) indicate the existence of two different vortex-core states in rotating superfluid ^{3}He-B, distinguished by different hard-core structures and associated with different magnitudes of their respective magnetic moments, which are concentrated in the core. Hence, the possible structures of the singular cores of quantized vortex lines in ^{3}He-B are to be investigated next.

VIII. CORE STRUCTURES OF VORTICES IN ^{3}He-B

A. The most symmetric o vortex

1. Axial and discrete symmetries of the o vortex

In investigating the hard core of the ^{3}He-B vortices, one may neglect the dipole interaction at low magnetic fields. Far from the hard core, the asymptotics of the order parameter of a vortex with m quanta of circulation is given by Eq. (7.20). This asymptotic form is axisymmetric, with the generator of symmetry

$$\hat{Q}=\hat{J}_z^{(R)}-m\hat{I},\quad \hat{J}_z^{(R)}=\hat{L}_z+R_{\alpha z}\hat{S}_\alpha\ , \tag{8.1}$$

corresponding to Eq. (5.2) with $n=m$. The general solution of the axisymmetry equation $\hat{Q}A_{\alpha i}=0$ gives the same nine complex amplitudes $a_{\mu\nu}(\mathbf{r})$ as in Eq. (5.8) of the states with spin projection μ and orbital momentum projection ν:

$$a_{\mu\nu}(\mathbf{r})=\Delta_B(T)C_{\mu\nu}(r)e^{i(m-\mu-\nu)\phi}\ . \tag{8.2}$$

However, the axes of the spin and the orbital coordinate frames are rotated with respect to each other through the matrix $R_{\alpha i}$, i.e., the order parameter $A_{\alpha i}$ is expressed in terms of $a_{\mu\nu}$ in Eq. (2.9), with the unit vectors of the two sets of coordinate frames (see Figs. 4) related by

$$\hat{z}_\alpha=R_{\alpha i}\hat{z}_i,\quad \hat{x}_\alpha=R_{\alpha i}\hat{x}_i,\quad \hat{y}_\alpha=R_{\alpha i}\hat{y}_i\ . \tag{8.3}$$

The discrete symmetry of the asymptotics is that of Eq. (5.6), with the elements

$$P_1=P(U_\pi)^{m+1},\quad P_2=P_1P_3,\quad P_3=TO^{(J)}_{x,\pi}\ . \tag{8.4}$$

Their action on $C_{\mu\nu}(r)$ is given by Eqs. (5.9) and (5.13). The most symmetric vortex, which retains the full symmetry of the asymptotics, and which we denote as the o vortex, obeys

$$P_1C_{\mu\nu}=P_2C_{\mu\nu}=P_3C_{\mu\nu}=C_{\mu\nu}\ , \tag{8.5}$$

and thus possesses five real $C_{\mu\nu}$, with even $\mu+\nu$ [Eq. (5.11)]. As distinct from the A-phase vortices, all five amplitudes are independent. In the A phase, there occurs an additional continuous symmetry at small distances,

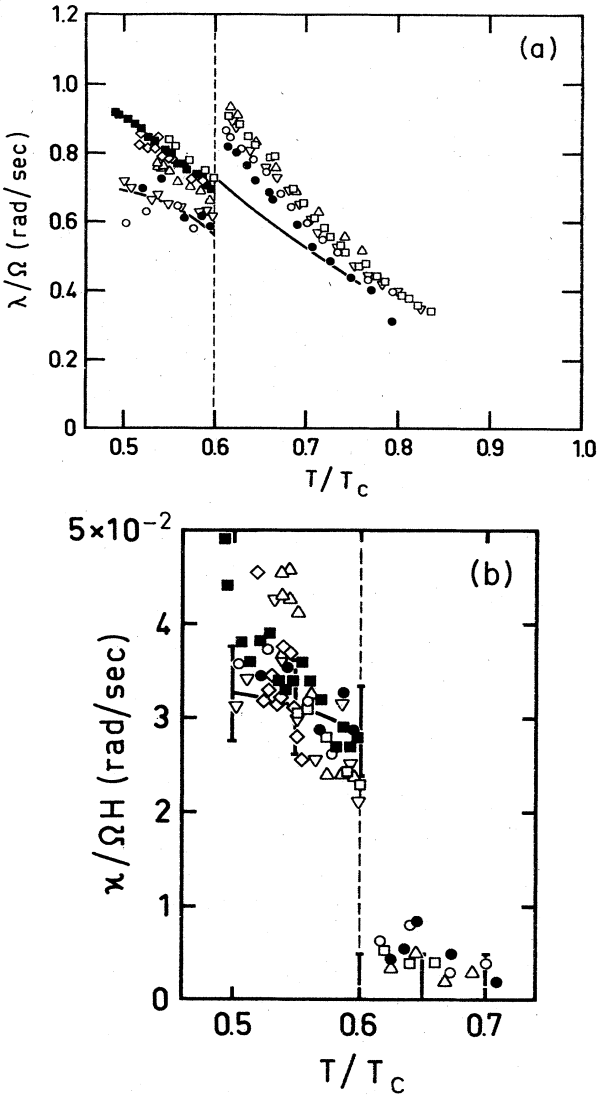

FIG. 34. The normalized (a) vortex and (b) gyromagnetic parameters, λ/Ω and $\kappa/\Omega H$, respectively, extracted from the tilted-field measurements (Fig. 33). The measurements and the analysis were done for $p=29.3$ bars. The different symbols refer to separate experiments. The solid lines are extracted from a comparison of the calculated spin-wave eigenfrequencies (see Fig. 31), with the measured NMR spectra in $\boldsymbol{\Omega}\|\mathbf{H}$ (see Fig. 30). Error bars are indicated for κ in Eq. (7.22). For $T>0.6T_c$, κ is so small that it cannot be resolved from the spin-wave analysis (Hakonen, Krusius, Salomaa, Simola, Bun'kov, Mineev, and Volovik, 1983).

TABLE III. The group-theoretical symmetry classification of axisymmetric quantized vortex lines in superfluid ^{3}He-B. For singly quantized vortices ($m=1$), the core fluid can be normal (N) or superfluid (consisting of the superfluid A phase and the ferromagnetic superfluid β phase). For doubly quantized vortices, the core is always of the superfluid A_1 phase, while for axisymmetric vortex lines with three or more quanta of circulation, the core matter is normal liquid ^{3}He.

Vortex	Discrete symmetry	$C_{\mu\nu}$ with $\mu+\nu$ even	$C_{\mu\nu}$ with $\mu+\nu$ odd	States of vortex-core matter $m=1$	$m=2$	$m\geq 3$
o	P_1,P_2,P_3	Real	Zero	N	A_1	N
u	P_1	Complex	Zero	N	A_1	N
v	P_2	Real	Real	A and β	A_1	N
w	P_3	Real	Imaginary	A and β	A_1	N
uvw	None	Complex	Complex	A and β	A_1	N

where the dipole forces may be neglected, which serves to reduce the number of the functions $C_{\mu\nu}$.

In ^{3}He-B, even after neglecting the dipole forces, there remains only one continuous symmetry, Eq. (8.1), since the B-phase state itself produces an effective intercoupling between the spin and orbital subsystems. Therefore the number of independent functions $C_{\mu\nu}$ in the most symmetric vortex cannot be further reduced.

For the singly quantized o vortex, all the amplitudes $a_{\mu\nu}$ tend to zero at the center of the vortex, since their phases,

$$\Phi_{\mu\nu}=(m-\mu-\nu)\phi \ , \tag{8.6}$$

display a discontinuity on the vortex axis. For $m=1$:

$$\Phi_{+-}=\Phi_{00}=\Phi_{-+}=-\Phi_{++}=\tfrac{1}{3}\Phi_{--}=\phi \ . \tag{8.7}$$

That is, the most symmetric vortex with $m=1$ possesses a normal core. [However, the doubly quantized o vortex (Salomaa and Volovik, 1984) has a nonzero component $a_{++}=\Delta_B C_{++}(r=0)\neq 0$, which corresponds to the A_1 phase on the vortex axis (see Table III).] Far from the hard core, the amplitudes a_{++} and a_{--} vanish, while the others should tend to unity, thus producing the bulk B-phase state, represented by

$$a_{+-}(\infty)=a_{00}(\infty)=a_{-+}(\infty)=\Delta_B(T)e^{im\phi} \ . \tag{8.8}$$

The o vortex possesses a magnetic moment [see Eq. (2.27)], given by (Ohmi, Tsuneto, and Fujita, 1983)

$$\begin{aligned} M_\alpha(\mathbf{r})&=R_{\alpha i}\hat{z}_i M(\mathbf{r}) \ , \\ M(\mathbf{r})&=g_{1H}\sum_{\mu\nu}\mu\,|\,a_{\mu\nu}\,|^2 \\ &=g_{1H}\Delta_B^2(T)\sum_\nu[\,|\,C_{+\nu}(r)\,|^2-|\,C_{-\nu}(r)\,|^2] \ . \end{aligned} \tag{8.9}$$

The integral over the cross section of the vortex core gives a nonzero value, since there is no additional symmetry. The time-inversion T symmetry

$$TC_{\mu\nu}=C^*_{-\mu,-\nu} \tag{8.10}$$

—which would make M equal to zero—is violated in all the ^{3}He-B vortices.

2. Core structure of the o vortex

The core structure of the o vortex was found by minimizing the Ginzburg-Landau free energy, Eqs. (2.15) and (2.19), expressed in terms of the $C_{\mu\nu}$. Scaling the distance in terms of the coherence length (2.21), $r=\xi_{\rm GL}\tilde{r}$, we obtain

$$F=\frac{\pi}{5}\left[\frac{\hbar}{M}\right]^2\rho_s\int_0^\infty d\tilde{r}\,\tilde{r}(f_b+f_{\rm grad}) \ , \tag{8.11a}$$

$$\begin{aligned} f_b=&-C_{\mu\nu}C^*_{\mu\nu}+\tilde{\beta}_1\,|\,C^*_{\mu\nu}C^*_{-\mu,-\nu}\,|^2+\tilde{\beta}_2(C_{\mu\nu}C^*_{\mu\nu})^2+\tilde{\beta}_3C_{\mu\nu}C^*_{\mu\kappa}C_{\rho,-\nu}C^*_{\rho,-\kappa} \\ &+\tilde{\beta}_4C^*_{\mu\kappa}C_{\nu\kappa}C^*_{\nu\rho}C_{\mu\rho}+\tilde{\beta}_5C_{\mu\nu}C_{-\mu\kappa}C^*_{\rho\nu}C^*_{-\rho\kappa} \ , \end{aligned} \tag{8.11b}$$

$$\begin{aligned} f_{\rm grad}=&\sum_{\mu\nu\nu'}\left[\,|\,\nu\,|\,\frac{\partial}{\partial\tilde{r}}C_{\mu\nu}-\nu\frac{(m-\mu-\nu)}{\tilde{r}}C_{\mu\nu}\right]\left[\,|\,\nu'\,|\,\frac{\partial}{\partial\tilde{r}}C^*_{\mu\nu'}-\nu'\frac{(m-\mu-\nu')}{\tilde{r}}C^*_{\mu\nu'}\right] \\ &+\sum_{\mu\nu}\left[\left|\frac{\partial}{\partial\tilde{r}}C_{\mu\nu}\right|^2+\left[\frac{m-\mu-\nu}{\tilde{r}}\right]^2|\,C_{\mu\nu}\,|^2\right] \ , \end{aligned} \tag{8.11c}$$

where ρ_s is the superfluid density in the bulk liquid,

$$\rho_s = 10 \left[\frac{M}{\hbar} \right]^2 \gamma_0 \Delta_B^2(T) \tag{8.12}$$

and

$$\tilde{\beta}_i = \frac{\beta_i}{2(\beta_{345}+3\beta_{12})} . \tag{8.13}$$

The result of minimizing Eq. (8.11) within the symmetry class of the o vortex with $m=1$ is shown in Fig. 35 (Ohmi, Tsuneto, and Fujita, 1983; Salomaa and Volovik, 1983b; the simpler version of the o vortex, with $C_{++}=C_{--}=0$, was investigated by Passvogel, Schopohl, and Tewordt, 1983).

Figure 36 displays the bulk and gradient energy densities as functions of the radial distance from the o-vortex axis. While f_B tends to zero on the vortex axis, which consists of normal liquid ^{3}He, $f_{\rm grad}$ obtains its maximum value at $r=0$. This behavior is just like that in the "classical" quantized vortices in He II.

The axial component of the superfluid density tensor in the vortex

$$\rho_s^{\parallel}(r) = \rho_s \frac{1}{5} \left[2 \sum_{\mu} |C_{\mu 0}|^2 + \sum_{\mu\nu} |C_{\mu\nu}|^2 \right] , \tag{8.14}$$

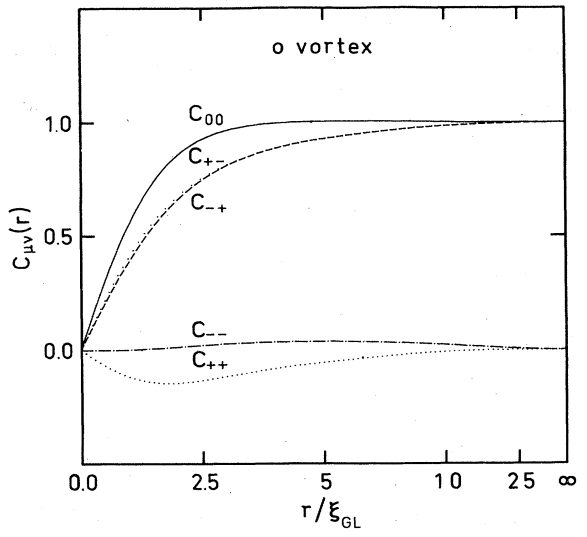

FIG. 35. The structure of the most symmetric singly quantized vortex, the o vortex (Ohmi, Tsuneto, and Fujita, 1983), in superfluid ^{3}He-B at the weak-coupling limit. Here the real pairing amplitudes $C_{\mu\nu}(r)$ (with $C_{\mu\nu}\equiv 0$ for $\mu+\nu$ odd) are scaled so that the bulk ^{3}He-B order parameter at $r=\infty$ is described by $C_{+-}(\infty)=C_{00}(\infty)=C_{-+}(\infty)=1$. Radial distances r from the vortex axis are measured in units of the Ginzburg-Landau coherence length $\xi_{\rm GL}(T)$ [in Eq. (2.21)]. The scale is linear in r for $r<5\xi_{\rm GL}$, and varies as $1/r$ for $r>5\xi_{\rm GL}$, so that the structure of an isolated vortex line can be represented for $0\le r\le\infty$. This normal-core vortex structure has a weak pressure dependence.

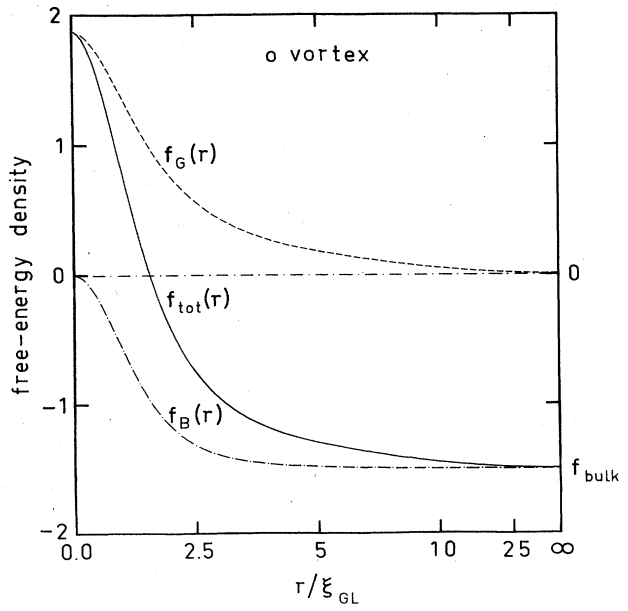

FIG. 36. The radial distribution of the normalized free-energy density for the singly quantized o vortex in the weak-coupling limit. Note that, because of the normal vortex-core structure, the bulk condensation energy f_B tends to zero for $r\to 0$ and there remains only a finite gradient energy f_G on the vortex axis. The total free-energy density $f_{\rm tot}$ is a monotonically decreasing function of r.

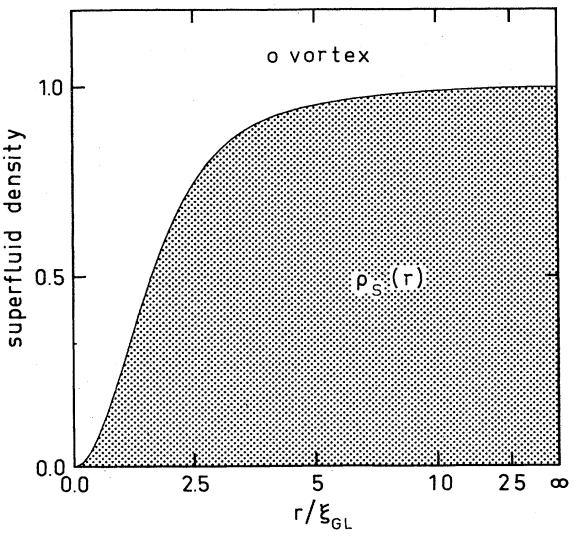

FIG. 37. The calculated normalized superfluid density ρ_s of the o vortex presented in Fig. 35. This figure shows $\rho_{s\parallel}$, the component of the superfluid density tensor parallel with the vortex axis. The o-vortex core is normal, with $\rho_s(r=0)=0$, as for the "classical" ^{4}He vortex illustrated in Fig. 6.

displayed in Fig. 37 for the o vortex, also behaves as in He II: $\rho_s(r=0)=0$. The magnetic moment of the o vortex and its contribution to the magnetic anisotropy of the core will be discussed later.

B. The v vortices with broken parity

1. Spontaneous breaking of space parity

The free-energy minimum corresponding to a vortex solution in a given symmetry class is always an extremum of the free-energy functional in the whole function space (see Table III). However, this extremum may not be a true minimum, but rather a saddle point. As in ^{3}He-A, the most symmetric o vortex may be unstable towards the breaking of space parity and/or axisymmetry.

Let us first relax the conditions (8.5) of the discrete symmetry, but retain the axisymmetry Q. Numerical calculations near T_c show that in the whole region of the strong-coupling parameter $0<\delta<0.46$, where the B phase is stable, the minimum of the Ginzburg-Landau free-

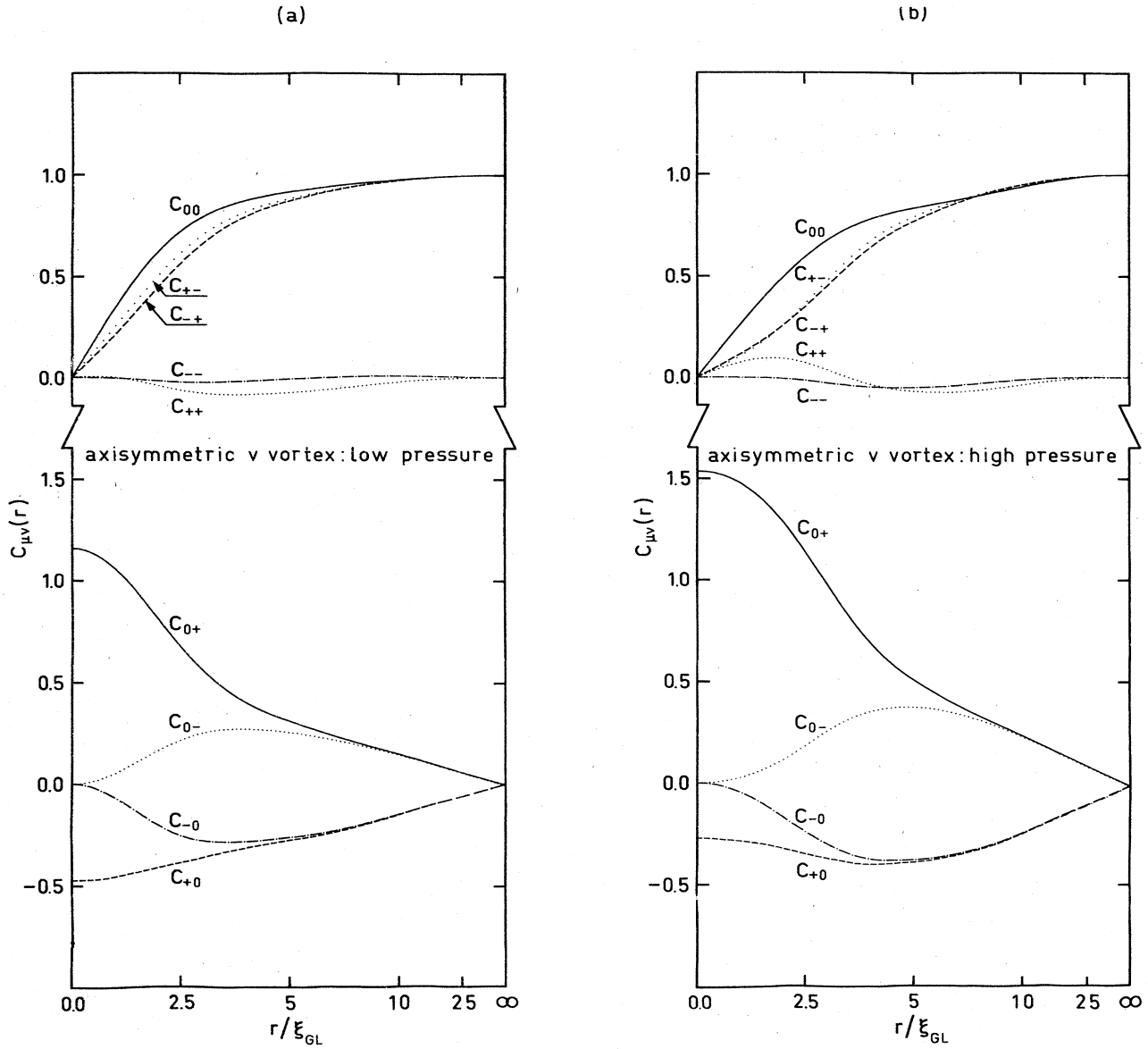

FIG. 38. The calculated structure of the axisymmetric v vortex (with broken parity) as a function of pressure in the Ginzburg-Landau regime (Salomaa and Volovik, 1983b, 1985a). It is possible that this superfluid core-vortex structure is the one observed in the NMR experiments on rotating bulk superfluid ^{3}He-B in zero magnetic field at high pressures. The upper curves represent the same five pairing amplitudes $C_{\mu\nu}(r)$ (for $\mu+\nu$ even) that also occur in the maximally symmetric o vortex; the lower curves display the four additional pairing amplitudes $C_{\mu\nu}(r)$ (with $\mu+\nu$ odd; A phase and the spontaneously ferromagnetic β phase and their dual phases) that exist in this P_2-symmetric vortex structure. The scales are as in Fig. 35. (a) The weak coupling (zero-pressure) limit $\delta=0.0$. (b) Polycritical point $\delta=0.46$. Note that in contrast to the o vortex displayed in Fig. 35, the structure of this v vortex is a strong function of pressure; in particular, the superfluid core depends sensitively on pressure.

energy functional (8.11) in the class of axisymmetric vortices with $m=1$ corresponds to the P_2-symmetric v vortex, with broken symmetry P_1, while the o vortex is unstable towards the formation of the v vortex and corresponds to a saddle point of the Ginzburg-Landau functional (Salomaa and Volovik, 1983b, 1985a; Passvogel, Tewordt, and Schopohl, 1984).

The v vortex has all nine real functions $C_{\mu\nu}(r)$ (see Fig. 38). The temperature corrections to the Ginzburg-Landau structure of the v vortex have been obtained (Passvogel, Tewordt, and Schopohl, 1984). Two of the amplitudes, $a_{0+}=\Delta_B C_{0+}$ and $a_{+0}=\Delta_B C_{+0}$, remain finite on the vortex axis. They correspond to the A phase and the β phase (see Table I) in the vortex core. This nonunitary β phase is principally responsible for the large magnetic moment of the v vortex, as compared with that of the o vortex.

2. The A-phase core of the axisymmetric v vortex

Figure 38 shows the change in the structure of the v vortex with increasing strong-coupling parameter δ, which changes with pressure from $\delta\simeq 0$ at $P=0$ to $\delta=0.46$ at the polycritical pressure (see Fig. 1). A most interesting behavior is exhibited by the superfluid core at $\delta=0.46$, in the immediate vicinity of the polycritical point, where the B phase is about to become metastable in the bulk liquid and the A phase becomes stable. With further increase of δ, the amplitude C_{0+} of the A-phase component in the core begins to increase towards its value in the bulk A phase,

$$C_{0+}\mid_{r=0}\rightarrow C_{0+}^{\rm bulk}(A)=\sqrt{2}\frac{\Delta_A}{\Delta_B}=\left[\frac{3\beta_{12}+\beta_{345}}{\beta_{245}}\right]^{1/2}=\left[\frac{5-0.4\delta}{2-1.05\delta}\right]^{1/2}, \quad (8.15)$$

while the β-phase amplitude decreases for increasing values of δ right on the vortex axis (the extension of the β phase increases dramatically, however, in the outer core region, resulting in roughly the same integrated value for the normalized vortex magnetization; see Sec. VIII.C). That is, the vortex core becomes the bulk A phase. The extension of this A-phase nucleation center increases with δ.

The free-energy density for the v vortex is shown in Fig. 39. The bulk condensation energy $f_B(r)$ remains finite everywhere, and the gradient energy $f_G(r)$ is appreciably reduced on the vortex axis from its value in the o vortex, Fig. 36, because of the escape of the superfluid into new pairing states. The total energy density $f_{\rm tot}(r)$ displays an extremal value at a finite distance from the vortex axis. This can be interpreted as the result of a

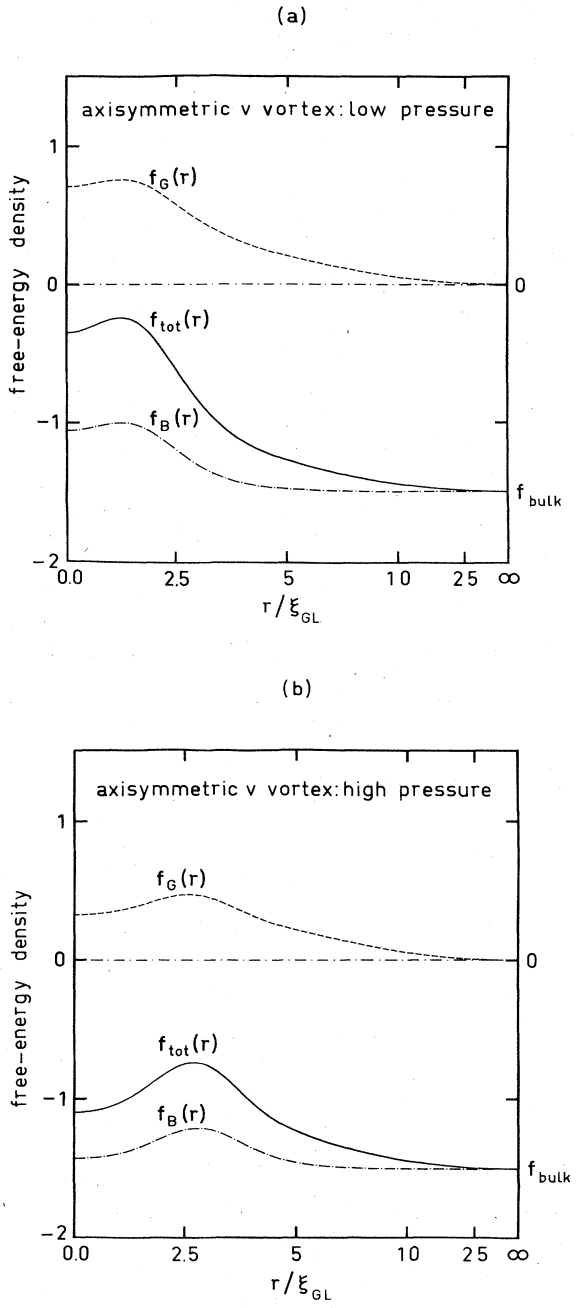

FIG. 39. Components of the free-energy density in the axisymmetric v vortex with superfluid core. Note that the bulk condensation energy f_B remains finite everywhere. (a) For $\delta=0$, the condensation-energy density is diminished by 29% from its bulk equilibrium value; (b) for $\delta=0.46$, the condensation-energy loss on the vortex axis from its bulk value is only 6%, since for this value of δ the transition to the A phase in bulk superfluid ^{3}He is in close proximity. The gradient energy f_G is greatly diminished at $r=0$ from that of the o vortex in Fig. 36 because of the escape of the superfluid to other pairing states. Note that the total energy density $f_{\rm tot}$, as well as the bulk condensation-energy density f_B, exhibits extremal values at a finite distance from the vortex axis. This may be visualized as resulting from a domain wall that separates the bulk B phase from the A phase in the vortex core.

domain wall separating the bulk B phase from the A phase, nucleated at the vortex core. For $\delta=0$ [Fig. 39(a)], the domain wall is close to the vortex axis, and the A phase in the core produces a condensation-energy density appreciably higher than in the bulk B phase. At $\delta=0.46$ [Fig. 39(b)], the A phase in the core results in almost the same low condensation-energy minimum as in the B phase. The vortex-core radius is much increased, and the A-B boundary separating the superfluids in the bulk and in the vortex-core regions is more pronounced. This suggests that the axisymmetric v vortex is more advantageous in the vicinity of the transition to the A phase, due to a proximity effect. Therefore it is a good candidate for the high-pressure vortex.

The normalized superfluid density for the axisymmetric v vortex is shown in Fig. 40. Unlike the o vortex, or the "classical" vortex line in He II, this axisymmetric v vortex possesses a finite superfluid density everywhere, including, in particular, the vortex axis. Figure 41 illustrates the axisymmetric distribution of supercurrent in the v vortex.

In the vortex core, the nucleation of the superfluid A phase leads to the appearance of nodes in the ^{3}He quasiparticle energy gap (local l-vector field with its associated superfluid flow properties). This results in vortices in the $\hat{k}$ space, which are discussed in Sec. VIII.D.

Owing to its A-phase core, the axisymmetric B-phase v vortex may act as a nucleation center for the superfluid A phase in the metastable superfluid B phase. As a result, in the presence of vortices, there should exist a catastrophe line in the (p,T) plane, at which the metastable B phase becomes unstable towards the spontaneous growth of the A-phase core region. According to the calculated structure of the high-pressure v vortex, its energy per unit length may be qualitatively expressed in terms of the vortex-core radius $r_{\rm core}$:

$$E=\pi r_{\rm core}^2(F_A-F_B)+2\pi r_{\rm core}\sigma_s+\pi\rho_s\left[\frac{\hbar}{M}\right]^2\ln\frac{R}{r_{\rm core}}\ . \tag{8.16a}$$

The first term is the condensation energy of the A-phase core region, in comparison with the bulk B-phase energy, the second term is the energy of the domain wall, with σ_s denoting the surface energy of the interface between the A and B phases, while the last term is the hydrodynamical energy of the vortex outside the core.

Minimizing Eq. (8.16a), it follows that a finite core size exists only provided that the difference between the bulk B-phase energy and that of the A phase does not exceed the critical value

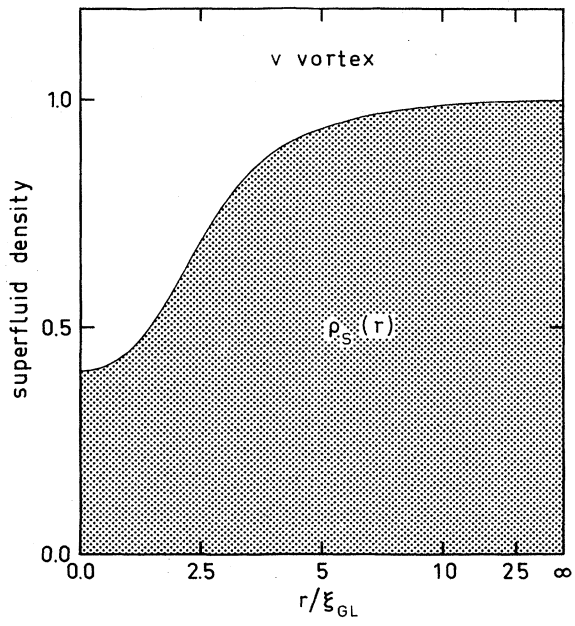

FIG. 40. The component of the normalized superfluid density along the vortex axis, calculated for the axisymmetric v vortex in Fig. 38(a). Note that unlike the case for the o vortex (Fig. 37), here the superfluid density remains finite everywhere, including the vortex axis. This is because of the superfluid core structure of this quantized vortex line.

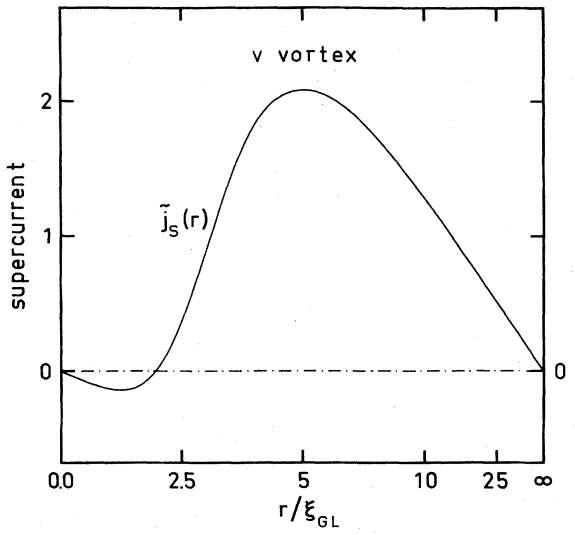

FIG. 41. The tangential supercurrent in the superfluid-core axisymmetric v vortex at a high pressure [$\delta=0.46$, Fig. 38(b)]. Here the superflow tends to the potential flow regime only for radial distances $r>r_{\rm core}$ from the axis, where the vortex-core radii are shown in Fig. 51. For $r<r_{\rm core}$, the superflow distribution is governed by the nodes of the energy gap on the Fermi sphere. In particular, note that, close to the vortex axis, there is a region where the superflow is counterrotating. Since $\rho_s(r=0)$ remains finite (Fig. 40), while $\tilde{j}_s$ tends to zero at $r\to 0$, this may be visualized as a solid-body rotation of the superfluid near the vortex axis.

$$(F_B-F_A)_{\rm cr}=\frac{\sigma_s^2}{2\rho_s\left[\frac{\hbar}{M}\right]^2}\ . \tag{8.16b}$$

At the critical threshold value [Eq. (8.16b)], the vortex becomes unstable towards spontaneous increase of the core radius to infinity, thus producing the transition to the A phase without overcoming any energy barrier, as in the wetting transition. (On the metastability effects at the $A\leftrightarrow B$ phase transition, see Leggett, 1984; Salomaa, 1987b). From numerical calculations of the core structure in the Ginzburg-Landau region, it follows that the instability of the axisymmetric B-phase v vortex takes place at the value $\delta\approx 0.5$.

3. Asymptotics in the axisymmetric v and w vortices

The superfluid-core v vortex has one more property that distinguishes it from the o vortex and the classical quantized vortex line in He II. The order parameter falls off as $1/r$, distinctly from the $1/r^2$ behavior in the o vortex and the He II vortex (Passvogel, Tewordt, and Schopohl, 1984; Hasegawa, 1985). This is a result of the fact that the degeneracy of states in ^{3}He-B is larger than that in He II (Hasegawa, 1985), where the only degeneracy parameter is the phase Φ. The degeneracy parameters in the ordered systems constitute additional slow hydrodynamical variables; therefore they fall slowly, if at all. The phase, for example, does not decrease outside the vortices, since $\Phi=m\phi$.

The degeneracy parameters in ^{3}He-B also contain the components of the matrix $R_{\alpha i}$. If there were a linear coupling between $R_{\alpha i}$ and Φ, like that in ^{3}He-A between $\boldsymbol{l}$ and Φ, the matrix would not tend to a constant value at infinity. However, such an interaction is absent due to the different time-inversion properties of $R_{\alpha i}$ and Φ ($TR_{\alpha i}=R_{\alpha i}$, while $T\Phi=-\Phi$); therefore $R_{\alpha i}$ has the definite constant asymptotic form $R_{\alpha i}(\infty)$, with a power-law falloff for the deviation $\delta R_{\alpha i}$ of $R_{\alpha i}$ from this value. This power law is defined by the solution of the Ginzburg-Landau equation for $R_{\alpha i}$ outside the vortex core, which follows from the minimization of Eq. (7.14a).

Let us introduce the small three-dimensional angle θ, which describes the deviation $\delta R_{\alpha i}$ from its value $R_{\alpha i}(\infty)$ at infinity. Then the general expression for the energy of the θ field, which follows from Eq. (7.14a), is given by

$$a(\nabla\theta)^2+b(\nabla_i\theta)^2\ . \tag{8.17a}$$

In the most symmetric o vortex, the symmetries P_2 and P_3—as well as axisymmetry—require that $\theta=0$. In the axisymmetric v vortex, the symmetry allows a nonzero θ of the form $\theta(\mathbf{r})=\theta(r)\hat{\phi}$, while in the axisymmetric w vortex one has $\theta(\mathbf{r})=\theta(r)\hat{r}$. In both cases the equation for θ, obtained by variation of Eq. (8.17a), is

$$\frac{d^2\theta}{dr^2}+\frac{1}{r}\frac{d\theta}{dr}-\frac{\theta}{r^2}=0\ , \tag{8.17b}$$

and yields $\theta\sim 1/r$. This asymptote is also valid at distances larger than the dipole length ξ_d, where the dipole energy partially lifts the degeneracy. In this case, $\theta(\mathbf{r})$ corresponds to the small deviation of the degeneracy parameter, the $\mathbf{n}$ vector, from its asymptotic value $\mathbf{n}(\infty)=\hat{z}$: $\delta\mathbf{n}=\boldsymbol{\theta}\times\mathbf{n}(\infty)$.

4. Spontaneous breaking of axisymmetry in the v vortex

The v vortex displays at low pressure a further breaking of symmetry: in addition to the parity P, the axial symmetry Q is broken (Thuneberg, 1986b; Volovik and Salomaa, 1985b; Salomaa and Volovik, 1986a).

Nonaxisymmetric B-phase vortices were first considered by Theodorakis and Fetter (1983); they used trial functions of the type $A_{\alpha i}=\Delta(r)R_{\alpha k}[\delta_{ik}-f(r)\hat{s}_i\hat{s}_k]e^{i\phi}$ and found that the nonaxisymmetric vortex with $\hat{s}=\hat{x}\perp\hat{z}$ has the minimum energy among the vortices within this class. Their vortex is a simple version of the o vortex, with director-type nonaxisymmetry. The energy of their vortex was, however, larger than that of the axisymmetric v vortex; therefore further analysis was motivated. In particular, Salomaa and Volovik (1983a) suggested that the mechanism of the vortex-core transition in ^{3}He-B could be the breaking of axisymmetry.

Thuneberg was the first to perform a full two-dimensional energy minimization by solving numerically the Ginzburg-Landau differential equations (Thuneberg ingeniously employed the method of functional fixed-point iteration in 2D x-y space, similar to that employed by Thuneberg for the problem of the ^{3}He-B state near the surface (Thuneberg, 1986a); his results are illustrated in Fig. 42. At all pressures the energy of the axisymmetric o vortex is clearly higher than the energies of the axisymmetric v vortex or the nonaxisymmetric "double core" new vortex with two points of local minima in the energy density. At low pressures the "new" vortex has the lowest energy. With an increase of pressure, the energy difference between the new vortex and the axisymmetric v vortex decreases and their energies are equal at about 3 bars below the tricritical pressure; in agreement with the experimental data of Fig. 1, Thuneberg's calculations show that the axisymmetric v vortex becomes stable at higher pressures and that the transition between the two vortex cores may be of first order.

As distinct from Thuneberg's calculations, we use the symmetry approach (Volovik and Salomaa, 1985b; Salomaa and Volovik, 1986a), which allows one to distinguish the possible ways of breaking axisymmetry and the physical consequences of the different types of broken symmetries.

Let us relax the condition of axisymmetry, $\hat{Q}A_{\alpha i}=0$, and investigate the stability of the axisymmetric v-vortex state towards perturbations that break axisymmetry. The nonaxial perturbations $\delta A_{\alpha i}$ on the background of the "vacuum," which in this case is the axisymmetric v-vortex core state, are characterized by the quantum number Q, which is conserved in this vacuum (Salomaa and

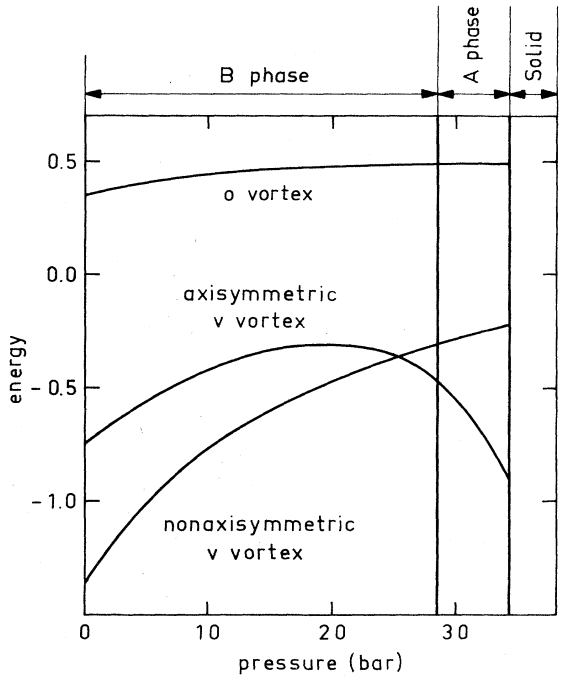

FIG. 42. Energies of the axisymmetric o and v vortices, and the nonaxisymmetric v vortex, as functions of pressure according to the numerical calculations of Thuneberg (1986b). The axisymmetric v vortex is the energy minimum only at a few bars below polycritical pressure.

Volovik, 1985a). Therefore perturbations $\delta A_{\alpha i}^{(Q)}$ are specified by the integer Q according to the following equation:

$$\hat{Q}\delta A_{\alpha i}^{(Q)} = Q\delta A_{\alpha i}^{(Q)} , \tag{8.18}$$

which has the solutions

$$\delta a_{\mu\nu}^{(Q)} = C_{\mu\nu}^{(Q)}(r)e^{i(Q+1-\mu-\nu)\phi} . \tag{8.19a}$$

Thus, the general expression for $a_{\mu\nu}$ in an m-quantum vortex is

$$a_{\mu\nu}(r,\phi) = e^{i(m-\mu-\nu)\phi}\sum_{Q} C_{\mu\nu}^{(Q)}(r)e^{iQ\phi} . \tag{8.19b}$$

The perturbations $C_{\mu\nu}^{(Q)}$ with different Q are not coupled with each other in the linear approximation (however, due to discrete symmetry, the perturbations with the same $|Q|$ are mixed). Therefore one may look for the instability at each nonzero $|Q|$ independently.

The most important perturbations are those with $|Q|=1$ and 2 (see Fig. 43). An instability towards the harmonics with $|Q|=1$ generates through the nonlinearity of the Ginzburg-Landau equations, the occurrence of all the other harmonics, i.e., the symmetry under rotations about the vortex axis is completely destroyed. In the plane transverse to the vortex axis, there appears in this case a preferred direction denoted by a unit vector $\hat{b}\perp\hat{z}$. This "vector"-type instability is analogous to the broken axial symmetry in the A phase, where

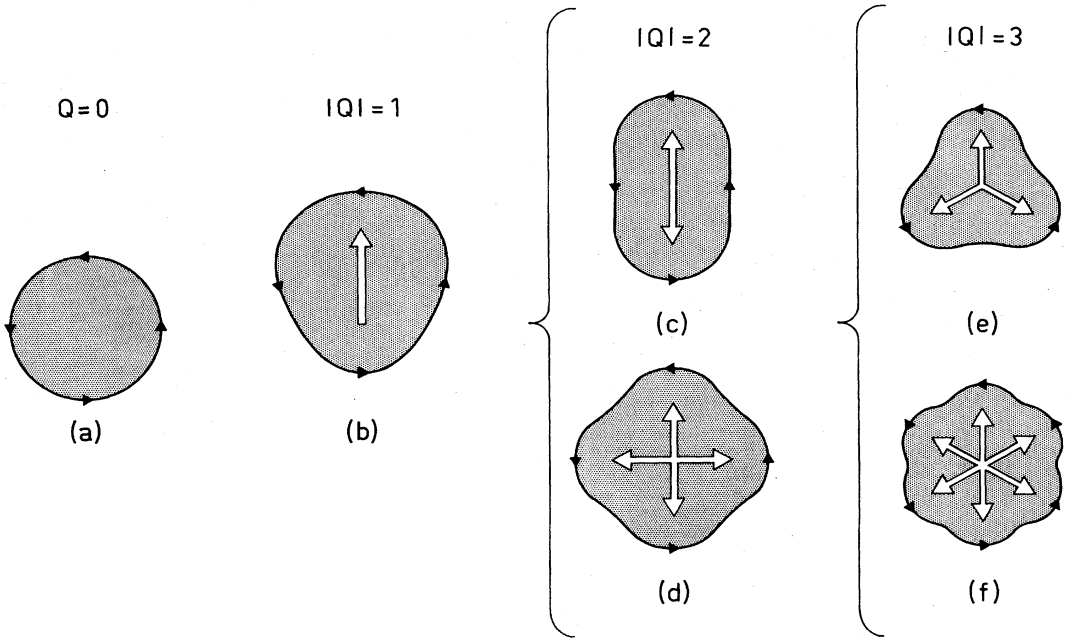

FIG. 43. A schematic illustration of the possible nonaxisymmetric sectors of the vortex-core matter in superfluid ^{3}He-B. (a) The axisymmetric "vacuum" state, specified by the quantum number $Q=0$. (b) The possible "vector" instability, having $|Q|=1$. (c) The "director" instability with $|Q|=2$. (d) Due to the complicated order-parameter structure, the sector with $|Q|=2$ also admits the investigation of the quadrupole instability with a fourfold symmetry axis. The sector with $|Q|=3$ allows us to investigate instabilities towards (e) the formation of threefold symmetry axis core vortices and (f) vortices with sixfold axis core. Sectors with $|Q|\geq 4$ are responsible for nonaxisymmetric vortices with normal core only.

in the transverse plane there appears the preferred direction, specified by the $\boldsymbol{l}$ vector: $\boldsymbol{l}(\infty)$ [see Sec. V.C, Eqs. (5.29) and (5.30)]. This analogy is strong, since the v-vortex core in ^{3}He-B contains the superfluid A phase, with the $\boldsymbol{l}$ vector directed along the vortex axis, and the vector-type instability means that $\boldsymbol{l}(0)$ tilts from the vortex axis towards the direction of $\mathbf{b}$. Therefore $\mathbf{b}$ has the same time-inversion property as $\hat{\boldsymbol{l}}$: $T\mathbf{b}=-\mathbf{b}$.

The $|Q|=2$ instability generates only even harmonics. In this case, the symmetry C_2 with respect to a rotation by the angle π about the vortex axis is retained, and $\mathbf{b}$ becomes a bilateral vector, or director, which indicates only the direction of the anisotropy axis in the transverse plane, but not a physical vector (thus, here $T\mathbf{b}=\mathbf{b}$). However, for special discrete symmetry, the $|Q|=2$ instability may generate a vortex with fourfold symmetry in the core (see Sec. VIII.E).

We found that the axisymmetric v vortex, as well as the o vortex, is stable towards small nonaxial perturbations with the nonaxisymmetry quantum numbers $|Q|=1,2,\ldots$ (see Fig. 43), thus proving, in particular, that this v-vortex state is a local free-energy minimum.

However, at low pressures the axisymmetric v-vortex state proves to be unstable towards large perturbations with $|Q|=2$, but not with $|Q|=1$. This means that there exists another local free-energy minimum corresponding to the nonaxisymmetric v vortex with a "director"-type core anisotropy in the transverse plane. The structure of this C_2-symmetric v-vortex state [magnetic class $C_{2v}(C_2)$] was computed with trial functions containing harmonics with $Q=0,+2$, and -2. The result is shown in Fig. 44. In spite of such a truncation, the result practically coincided with the exact numerical calculations by Thuneberg (1986b); this is because the remaining even harmonics may be neglected, since they vanish both in the origin and at infinity. Thus, the vortex described numerically by Thuneberg (see Thuneberg, 1986b) is nothing but the C_2-symmetric v vortex, also obtained by the present authors (Volovik and Salomaa, 1985b; Salomaa and Volovik, 1986a) using a different method.

In this C_2-symmetric v-vortex state, four amplitudes are nonzero on the vortex axis: besides the amplitudes C_{0+} and C_{+0} in the axisymmetric v vortex, there appear the two additional components C_{0-} and C_{-0}. The approximate relation $C_{+0}\simeq C_{-0}$ on the vortex axis indicates the existence of the so-called axi-planar phase in the vortex core:

$$A_{\alpha i}(0)\simeq\frac{1}{\sqrt{2}}[(C_{+0}+C_{-0})\hat{x}_\alpha\hat{z}_i+(C_{0+}+C_{0-})\hat{z}_\alpha\hat{x}_i +i(C_{0+}-C_{0-})\hat{z}_\alpha\hat{y}_i]\ . \tag{8.20}$$

This noninert biaxial phase was first predicted by Mermin and Stare (1974, 1977). The physical properties of a vortex, related to the breaking of axisymmetry, was discussed in Sec. VIII.C.6, while the internal topology of this vortex is presented in Sec. VIII.D.4.

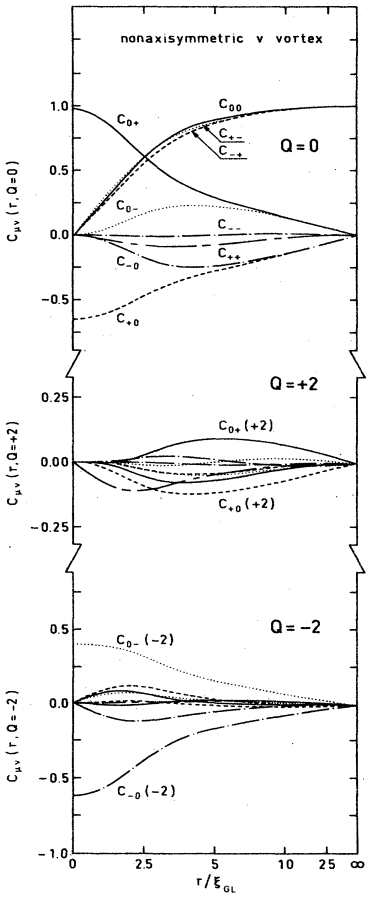

FIG. 44. The structure of the singly quantized nonaxisymmetric v vortex (Thuneberg, 1986b; Volovik and Salomaa, 1985b). In the representation of Salomaa and Volovik (1986a), the order-parameter components are conveniently truncated into the three sectors $Q=0$ and ±2. The radial axis is as in the o vortex, Fig. 35; the five order-parameter components also occurring in the most symmetric o vortex are displayed by the following fine curves: C_{00}, solid; C_{+-}, dotted; C_{-+}, dashed; C_{++}, short-long-dashed; C_{--}, dot-dashed. The four additional Cooper-pairing amplitudes occurring in the axisymmetric v vortex are displayed with heavy curves: C_{0+}, solid; C_{+0}, dashed; C_{0-}, dotted; and C_{-0}, dot-dashed. The $Q=0$ sector, ensures that at $r=\infty$ the vortex state is a pure-phase vortex with unit quantum of circulation $m=1$. The v-symmetric sector of $Q=-2$ introduces large superfluid components C_{0-} and C_{-0} in the core, which are responsible for the restructuring of the $Q=0$ sector. In particular, the additional amplitudes appearing in the vortex wave function by this sector resemble those of an axisymmetric vortex line with the *opposite* quantum of circulation: $m=-1$, i.e., *a counterrotating vortex*. The v-symmetric sector of $Q=+2$ possesses only small components for $0\le r\le\infty$.

C. The physical properties of vortices in ^{3}He-B

Here we begin by considering the axisymmetric v vortex, and then discuss the nonaxisymmetric v vortex.

1. The magnetic moment in the vortex core

The reduced magnetic moment $\tilde{m}=\sum_\nu(|C_{+\nu}|^2-|C_{-\nu}|^2)$ is displayed in Fig. 45 for both the o and v vortices (for the integrated values, see Salomaa and Volovik, 1985a). It is important that the integrated value $\int d\tilde{r}\,\tilde{r}\,\tilde{m}(\tilde{r})$ is positive. This produces a positive contribution to the gyromagnetic parameter κ. According to Eqs. (7.27b), (8.9), and (2.28),

$$\kappa_v=-\frac{5}{4a}\frac{1}{3}\gamma N(0)\eta\frac{\Delta^2}{T_c}2\pi\xi^2 n_v\int_0^\infty d\tilde{r}\,\tilde{r}\sum_\nu(|C_{+\nu}(\tilde{r})|^2-|C_{-\nu}(\tilde{r})|^2)\,. \tag{8.21}$$

This κ is positive, since the gyromagnetic ratio γ for the ^{3}He nucleus is negative: $\gamma=-2.04\times10^4$ G^{-1}sec^{-1}. This is in accordance with the NMR experiments (Hakonen, Krusius, Salomaa, Simola, Bun'kov, Mineev, and Volovik, 1983), which also gave a positive κ. On the other hand, a calculation of the bulk value of κ for ^{3}He-B without vortices, $\kappa_{\rm bulk}$, shows that it is negative and much smaller than κ_v (Mineev, 1986). Therefore one may conclude that the experiment measures the magnetic moment of the vortices.

For a rough estimate of the order of magnitudue for κ_v, let us choose the following values for the parameters involved [all the parameters are taken at the pressure $p=18$ bars (Theodorakis and Fetter, 1983; Israelsson, Crooker, Bozler, and Gould, 1984) and are in cgs units]:

$$\begin{aligned}&\eta=0.016,\quad n_v=0.3\times10^4\ (\text{at }\Omega=1\text{ rad/sec})\,,\\&\Delta^2=10^{-36}\left[1-\frac{T}{T_c}\right],\quad N(0)=10^{38}\,,\\&\xi^2=1.6\times10^{-12}\left[1-\frac{T}{T_c}\right],\quad a=10^{-12}\,,\\&T_c=3.2\times10^{-19}\,.\end{aligned} \tag{8.22}$$

Then we find

$$\kappa\sim1\text{ G}\times\int_0^\infty d\tilde{r}\,\tilde{r}(|C_{+\nu}|^2-|C_{-\nu}|^2)\,. \tag{8.23}$$

A detailed comparison with experiments is rendered difficult because the most reliable data for κ are obtainable only far from T_c. The experimental value of κ at $p=18$ bar and at temperatures $0.5<T/T_c<0.7$ may be written as

$$\kappa(\Omega=1\text{ rad/sec})\sim50\text{ G}\times\left[0.8-\frac{T}{T_c}\right]. \tag{8.24}$$

Near T_c, κ is essentially smaller, which is in reasonable agreement with the calculated magnitude of the vortex magnetization, Eq. (8.23), near T_c.

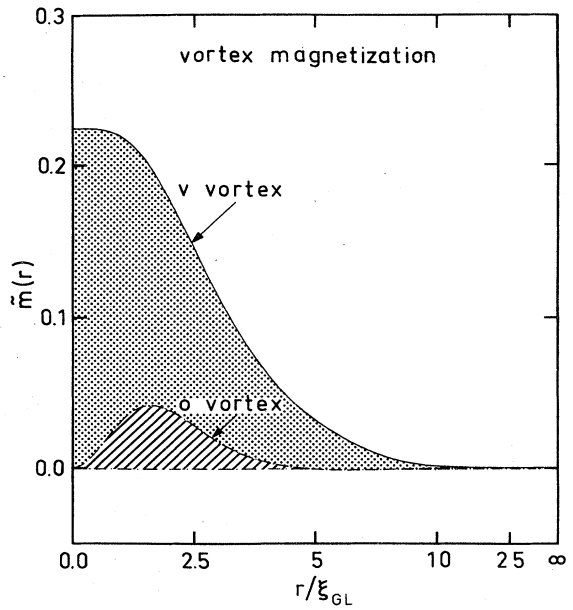

FIG. 45. The normalized magnetization density $\tilde{m}(r)=\sum_\nu(C_{+\nu}^2-C_{-\nu}^2)$ for the axisymmetric o and v vortices in ^{3}He-B in the weak-coupling limit. The large value of the v-vortex magnetization is essentially due to the distribution of the spontaneously ferromagnetic β phase in the core. The vanishing of the o-vortex magnetization on the vortex axis is due to the normal core.

2. The magnetic anisotropy of the axisymmetric vortices

The isotropic bulk superfluid ^{3}He-B becomes anisotropic near the vortex axis, where new anisotropic superfluid phases appear. Due to the magnetic anisotropy energy F_{2H} in Eq. (2.24), which is concentrated in the vicinity of the core, the vortex cores influence the orientation $R_{\alpha i}$ of the vortex asymptotics [Eq. (7.20)]. Substituting $A_{\alpha k}=R_{\alpha j}A^0_{jk}$, where A^0_{jk} is the vortex-core order parameter with the asymptotics $A^0_{jk}(\infty)=\Delta_B\delta_{jk}e^{i\phi}$, into Eq. (2.24), and averaging over the vortex cores with density n_v, one obtains the magnetic anisotropy energy

$$F_{2H}=\chi_{ij}(R_{\alpha i}H_\alpha)(R_{\beta j}H_\beta)\,, \tag{8.25a}$$

with the magnetic anisotropy tensor χ_{ij} depending only on the vortex-core structure,

$$\chi_{ij}=g_{2H}n_v\int d^2r A^0_{ik}(A^0_{jk})^*\,, \tag{8.25b}$$

where the integral is over the cross section of the vortex.

The tensor structure χ_{ij} depends on the symmetry of

the vortex core. If the core is axisymmetric, the tensor χ_{ij} is uniaxial with the anisotropy axis $\hat{z}$ (or $\hat{\Omega}$) along the vortex axis:

$$\chi_{ij}=\chi_0\delta_{ij}+\chi_a\hat{\Omega}_i\hat{\Omega}_j \ . \tag{8.26}$$

The second term in Eq. (8.26) produces the combined orientational effect $F_{v,H}$ in Eq. (7.21) of vortices and the magnetic field on the bulk order parameter $R_{\alpha i}$. Thus, the vortex parameter λ in Eq. (7.21) is expressed in terms of the vortex-core order parameter

$$\lambda=\frac{5}{2a}\chi_a=\frac{5}{2a}(\chi_{zz}-\tfrac{1}{2}\chi_{xx}-\tfrac{1}{2}\chi_{yy}) \tag{8.27a}$$

with

$$\chi_a=\tfrac{1}{2}g_{2H}n_v\int d^2r[-A^0_{ik}(A^0_{ik})^*+3A^0_{zk}(A^0_{zk})^*]$$
$$=\tfrac{1}{2}(\chi_N-\chi_B)2\pi n_v\xi^2\int_0^{r_\Omega/\xi}d\tilde{r}\,\tilde{r}\,\tilde{\lambda}(\tilde{r}) \ , \tag{8.27b}$$

where

$$\tilde{\lambda}(\tilde{r})=\sum_\nu[\,|\,C_{0\nu}(\tilde{r})\,|^2-\tfrac{1}{2}\,|\,C_{+\nu}(\tilde{r})\,|^2-\tfrac{1}{2}\,|\,C_{-\nu}(\tilde{r})\,|^2] \ . \tag{8.27c}$$

Above, the intervortex spacing is denoted as $r_\Omega\sim n_v^{-1/2}$; it serves as the cutoff for the logarithmically divergent integral, because the asymptotics of $\tilde{\lambda}$ in Eq. (8.27c), calculated analytically from the free energy in Eq. (8.11), fall off as $1/r^2$:

$$\tilde{\lambda}(\tilde{r}\to\infty)=\left[1+\frac{3\beta_{12}}{\beta_{345}}\right]\frac{m^2}{\tilde{r}^2} \ , \tag{8.28}$$

where $m=1$ for the singly quantized vortices.

There are roughly two principal contributions to the vortex parameter λ: the orientational effects coming from the core anisotropy and those from the asymptotic region. The asymptotic part, Eq. (8.28), is due to the superflow around the vortex line; it is described by Eq. (7.8), which is valid not only in the Ginzburg-Landau region but in the whole regime of ^{3}He-B (Gongadze, Gurgenishvili, and Kharadze, 1981). The integral of this contribution is logarithmically divergent due to the $(1/r)$ behavior of the superfluid velocity. This flow contribution to $\tilde{\lambda}$ must vanish for $T\to 0$, where the anisotropy of superflow disappears: at $T=0$ the superfluid density ρ_s must coincide with the total density ρ in ^{3}He-B. Therefore the phenomenological parameter $\beta_{\rm flow}$ in Eqs. (7.9) and (7.8) is zero at $T=0$. Since the flow contribution does not depend on the vortex-core structure, the jump in λ at the vortex-core transition temperature T_v and the finite value of λ for $T\to 0$ (see Fig. 46; Hakonen, Krusius, Salmelin, Salomaa, Simola, Gongadze, Gurgenishvili, and Kharadze, 1987) show that a substantial part of λ comes from the magnetic anisotropy inside the core. The theoretical estimates for λ (Salomaa and Volovik, 1985a) are in reasonably good agreement with experimental values.

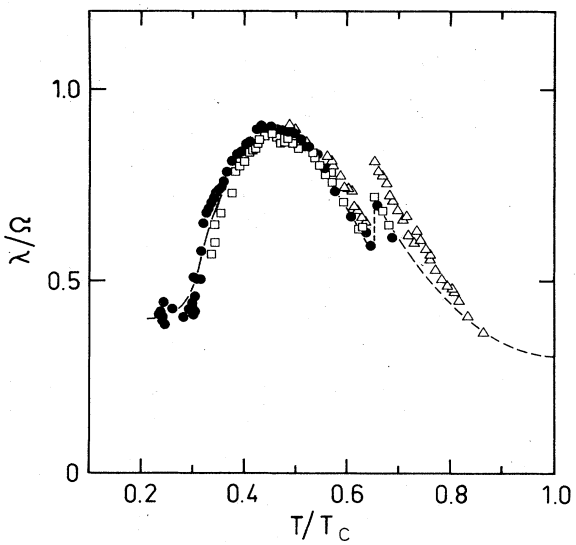

FIG. 46. The experimental vortex parameter $\lambda(T)$, extracted from the measured data: □, in an axial field, 570 G; ●, in a magnetic field tilted by the angle 25°, 570 G; △, in a magnetic field tilted by the angle 25°, 284 G. λ proved to be proportional to Ω, thus providing the vortex origin of the magnetic anisotropy of the rotating liquid. At low temperatures $\lambda(T)$ tends to a constant value (Hakonen, Krusius, Salmelin, Salomaa, Simola, Gongadze, Gurgenishvili, and Kharadze, 1986) arising from the vortex-core contribution alone.

3. Consequences of broken parity in the vortex core

As in the A phase (see Sec. V.D.2), also in the v vortices in superfluid ^{3}He-B, the broken P_1 and P_3 symmetries produce a spontaneous electric polarization. The quantity $\mathbf{D}$ is here proportional to the core radius of these vortices, which is of the order of $\xi_{\rm GL}$. The estimation of $\mathbf{D}$ may be performed readily on recalling that the cores of these vortices consist predominantly of the A phase, so that the same flexoelectric parameters β_i as in Eqs. (5.37) to (5.40) are involved:

$$\mathbf{D}\sim\pm\hat{\Omega}(\beta_1-\beta_2)\xi_{\rm GL} \ . \tag{8.29}$$

As in the A phase, the twofold degeneracy of the v vortex gives rise to the possibility of having topologically stable kinks, or point solitons, separating the two parts of the vortex line with different electric polarizations. Such a point on the vortex line has an electric charge e^* associated with it; the charge is of the order of

$$e^*\sim(\beta_1-\beta_2)\xi\sim 10^{-7}e \ . \tag{8.30}$$

An equal amount of electric charge should be concentrated on the surface of the container at the point of termination of the vortex line.

However, the interaction between the vortices is very small, compared with that in the A phase, so that these electric charges of the vortices are randomly disordered in

^{3}He-B. Thus, the bulk liquid displays no features of the broken symmetry. The situation will be different if a strong orientating electric field is applied for some period of time along the axis of rotation. In this case, there will result a surplus of vortices with their polarizations $\mathbf{D}$ along the electric field, and the rotating bulk superfluid B phase will acquire features of the broken symmetry. As a result, linear terms in the gradient energy will appear, which are compatible with the P_2 symmetry of the v vortex,

$$F_{\rm lin}^{(v)} = \tfrac{1}{2}K^{(v)}\hat{\Omega}_j(R_{\alpha j}\nabla_i R_{\alpha i} - R_{\alpha i}\nabla_i R_{\alpha j}) = K^{(v)}2(1-\cos\theta)(\hat{\Omega}\cdot\mathbf{n})(\nabla\cdot\mathbf{n}) , \quad (8.31)$$

where the estimate for $K^{(v)}$ of the v-vortex array, with the densities n_+ and n_- of vortices with given charge, is

$$K^{(v)} \sim \rho_s(n_+ - n_-)\xi_{\rm GL}\left[\frac{\hbar}{M}\right]^2 . \quad (8.32)$$

Equation (8.31) produces an additional orientating effect on the order-parameter texture in the rotating B phase, which is due to the presence of polarized vortices, i.e., vortices with coherently orientated Ising variables. This effect should be more pronounced in a weak magnetic field, where the bulk orientational effects are small. Thus, if in the rotating B phase v (or uvw) vortices are present, the NMR eigenfrequency will change after the strong electric field is turned on for a time sufficient to polarize the vortex cores coherently.

In the case of the P_3-symmetric w vortex, as well as that of the uvw vortex, with spontaneous superflow along the vortex axis, the corresponding linear term in the gradient energy, compatible with the P_3 symmetry, is given by

$$F_{\rm lin}^{(w)} = K^{(w)}e_{imn}R_{\alpha i}\nabla_m R_{\alpha n} = K^{(w)}2(1-\cos\theta)(\mathbf{n}\cdot(\nabla\times\mathbf{n})) , \quad (8.33)$$

with the same estimate for $K^{(w)}$ as in Eq. (8.32). This term will produce a cholesteric spiral for the $\mathbf{n}$ vector in the case of coherently orientated w vortices if the $\mathbf{n}$ vector in the bulk liquid is not fixed by the magnetic field. This occurs when the vortex parameter λ exceeds unity, in which case the axial symmetry of the $\mathbf{n}$ texture is spontaneously broken in an axial field (see the next section), even if the vortex-core structure retains its axisymmetry. The vortex in the magnetic class $D_{2d}(S_4)$ displays neither spontaneous axial superflow, nor spontaneous electric polarization.

4. Breaking of axisymmetry in the vortex texture outside the cores

The axisymmetry of the whole $\mathbf{n}$ texture is broken in the vortex array at some critical value of the angular velocity of rotation, at which the vortex parameter λ is unity [Gongadze, Gurgenishvili, and Kharadze (GGK), 1981]. According to Eq. (7.24), where we may neglect the small gyromagnetic parameter κ/H, the equilibrium angle β between $\mathbf{n}$ and $\mathbf{H}||\mathbf{\Omega}$ becomes nonzero in the bulk if $\lambda > 1$:

$$\sin^2\beta = \frac{4}{5}\frac{\lambda-1}{\lambda} . \quad (8.34)$$

The deviation of the $\mathbf{n}$ vector from the axis of the cylindrical container is axisymmetric in small fields, since boundaries are important. However, in a large magnetic field ($\xi_{d,H} \ll R$), where the influence of the boundaries may be neglected, the $\mathbf{n}$ vector should deviate uniformly from the container axis: $\mathbf{n} = \hat{z}\cos\beta + \hat{x}\sin\beta$, with β from Eq. (8.34). Therefore axisymmetry of the texture becomes broken at $\lambda > 1$: an anisotropy axis in the transverse direction $\hat{x}$ appears, and the vortex texture becomes degenerate.

For the w vortices, the broken axial symmetry of the texture will produce the effect discussed in the previous subsection: if the vortices are of the w type and polarized, then due to the linear term in Eq. (8.33), a cholesteric spiral will appear, $\mathbf{n} = \hat{z}\cos\beta + \sin\beta(\hat{x}\cos qz + \hat{y}\sin qz)$. The same spiral should appear for the vortices of class $D_{2d}(S_4)$, since, due to the breaking of rotational symmetry of the texture, they acquire the features of the w vortices.

The GGK textural transition with breaking of axisymmetry has been seen experimentally due to the shift of the main peak in NMR in an axial field (Hakonen, Krusius, Salmelin, Salomaa, Simola, Gongadze, Gurgenishvili, and Kharadze, 1987). This shift is proportional to $\sin^2\beta$ [Eq. (7.17)] and exists only at $\lambda > 1$ [Eq. (8.34)]; it is shown in Fig. 47.

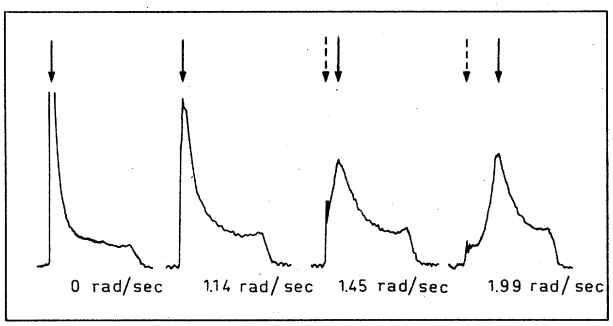

FIG. 47. The textural Gongadze, Gurgenishvili, and Kharadze (GGK) transition observed with NMR in an axial field, according to the experiments of Hakonen, Krusius, Salmelin, Salomaa, Simola, Gongadze, Gurgenishvili, and Kharadze (1987). For $\Omega = 0$ and $\Omega = 1.14$, the peak position is unshifted (one arrow), while at $\Omega = 1.45$ and 1.99, the shift of the peak is pronounced (pair of arrows, with the unshifted position indicated by a dashed arrow). The shift appears at some Ω below 1.45, where λ crosses the threshold value $\lambda_{\rm cr} = 1$. For a finite geometry, this phenomenon may be understood in terms of the textural changes induced by rotation in Fig. 29(b).

5. Broken rigidity of the vortex asymptote

Another transition with breaking of axisymmetry is predicted in high magnetic fields (Sonin, 1983, 1984). It takes place in the asymptotics of the isolated vortex. In considering the orientating effect of the vortices, we took for granted that the asymptotics of the vortex, Eq. (7.20), is the same everywhere outside the hard core. However, this rigidity of asymptote is violated in high fields. Let us consider the orientating effect, Eqs. (7.21) and (8.27), of vortices on the **n** texture prior to averaging over the vortices. This effect is concentrated in the vortex core and in the vicinity of the core on the $(1/r)$ tail of the superflow. Since the core size is much less than the intervortex distance, $r_\Omega \sim 10^{-2}$ cm, at the typical angular velocities of rotation, $\Omega \sim 1$–2 rad/sec, the core effect may be approximated by two-dimensional δ-function potentials, counted by the index a of the vortex:

$$F_{v,H} = \frac{2}{5}\frac{\lambda a}{n_v}(H_\alpha R_{\alpha i}\hat{\Omega}_i)^2 \sum_a \delta_2(\mathbf{r}-\mathbf{r}_a) \ . \tag{8.35}$$

The normalization of the prefactor of the δ functions is chosen in such a way that integration over the vortices reproduces Eq. (7.21).

The rigidity of the asymptote $R_{\alpha i}$ is provided by the gradient energy. If this energy (7.14) is neglected, the **n** texture, obtained by the minimization of Eq. (8.35) and the bulk anisotropy energy (7.12), is nonuniform—being different far from and close to the core. Near the core, the **n** vector is directed in such a way that the spin anisotropy axis of the vortex $\hat{n}_\alpha^{(S)} = R_{\alpha i}\hat{\Omega}_i$ is perpendicular to **H**: this minimizes Eq. (8.35) in the core, while far from the core, in the bulk liquid, **n** is parallel to **H**, and $\hat{n}^{(S)} \| \mathbf{H}$ as well. Thus, besides the hard core, the vortex has a soft core, where the $\hat{n}^{(S)}$ field changes from parallel to perpendicular direction. However, this nonuniform double-core state is disadvantageous at small enough fields due to the gradient energy, which in this case exceeds the orientational energies of vortices. Therefore, at small fields, the **n**-vector distribution should be uniform: $\mathbf{n} \| \hat{n}^{(S)} \| \mathbf{H}$, i.e., the asymptote of the vortex is rigid and the vortex has only one core: the hard core.

The uniformity is broken in high enough magnetic fields, $H > H_v$, when the orientational effect of the vortex core dominates the gradient energy. At the critical magnetic fields H_v, the uniform **n** texture becomes unstable towards perturbations which cause $\hat{n}^{(S)}$ near the core to deviate from the direction of the magnetic field:

$$\hat{n}^{(S)} = \hat{z}\cos\alpha(\mathbf{r}) + \hat{x}\sin\alpha(\mathbf{r}) \ . \tag{8.36}$$

Thus, the translational symmetry of the **n** texture is also broken at this transition. In terms of the angle α, the total energy of the **n** texture is

$$F_{\rm grad} + F_{v,H} + F_{d,H} = \tfrac{2}{5}aH^2 \left[\tfrac{3}{4}\xi_{d,H}^2 (\nabla\alpha)^2 + \frac{\lambda}{n_v}\cos^2\alpha \sum_a \delta(\mathbf{r}-\mathbf{r}_a) + 2(1-\cos\alpha) \right] . \tag{8.37}$$

The instability of the uniform state ($\alpha = 0$) towards the axially nonsymmetric nonuniform perturbations [$\alpha(\mathbf{r}) \neq 0$] occurs when the linearized equation for $\alpha(\mathbf{r})$, obtained from Eq. (8.37), first acquires a negative eigenvalue; this takes place at the following critical value of $\xi_{d,H}$ (Sonin, 1983, 1984):

$$\xi_{d,H}^2 = \frac{2\lambda \ln(r_\Omega/\xi)}{3\pi n_v} \ . \tag{8.38}$$

The corresponding critical field H_v, obtained from Eq. (7.14c), which expresses $\xi_{d,H}$ in terms of H, does not essentially depend on the angular velocity, since $\lambda \sim n_v$, and is of the order of 1 kG.

Note the difference between the GGK and Sonin transitions: The first is a collective effect of the vortex array on the **n** texture, which becomes nonaxisymmetric at $\lambda > 1$, i.e., when the density of vortices is high enough. In contrast, the Sonin transition is the property of an individual vortex line (the breaking of rigidity), and the critical field does not essentially depend on the vortex density. However, the interplay of these transitions is possible.

The Sonin transition can be detected experimentally. For $H > H_v$, the rigidity of the vortex asymptotics is broken, and this will result in the weakening of the orientational effect of the vortices on the order-parameter texture in the bulk superfluid outside the cores. Thus, the effective value of λ, as measured by NMR, should decrease at $H > H_v$. An abrupt drop in λ is also possible, if this transition is of first order.

6. Properties of vortices with broken axisymmetry

The breaking of axisymmetry in the core of the v vortex, which conserves all the properties of the v vortex connected with the broken parity, produces new properties related to the appearance of the preferred direction **b** of the vortex-core anisotropy in the transverse plane. First, there appears an additional Goldstone mode for the vortex, besides the usual oscillations of the vortex line: oscillations of the **b** vector can propagate along the vortex axis.

For the w vortex with broken axisymmetry, the **b** vector forms a spiral texture along the axis, since the expression $\hat{\Omega}\cdot\mathbf{b}\times(\hat{\Omega}\cdot\nabla)\mathbf{b}$ has the symmetry of the w vortex. The pitch of the spiral is of the order of the vortex-core

size. As distinct from the collective twist of the l and $\mathbf{n}$ textures in the A-phase w-vortex array (see Sec. V.D.4) and the axially symmetric polarized B-phase w-vortex array (see Sec. VIII.C.3), the twist of the $\mathbf{b}$ field is the property of an individual nonaxisymmetric w vortex, since $\mathbf{b}$ is only defined in the vortex core.

Second, the interaction of vortices with the order parameter $\mathbf{n}$ in the bulk superfluid is modified: the total orientational effect of vortices on the order parameter now has a more complicated structure. For the nonaxisymmetric vortex, the magnetic anisotropy tensor χ_{ij} contains additional components. In the most general case of the completely asymmetric uvw vortex, with all the discrete symmetries broken, the symmetric tensor χ_{ij} contains five components. Four of them, excluding $\mathrm{Tr}(\chi)$, produce the orientation effect. The number of components is reduced if symmetry elements are present.

For the v vortex, with completely broken axisymmetry (magnetic class C_{1v}), i.e., with vector-type asymmetry, the tensor χ_{ij} contains four components:

$$\chi_{ij}=\begin{bmatrix}\chi_{xx} & 0 & \chi_{xz}\\ 0 & \chi_{yy} & 0\\ \chi_{zx} & 0 & \chi_{zz}\end{bmatrix} . \tag{8.39}$$

Here $\chi_{yz}=\chi_{zy}$ and the axis of the U_2 transformation in the $PTU_2\chi_{xy}=-\chi_{xy}$ symmetry is directed along y, which corresponds to real $C^{(Q)}_{\mu\nu}$ in Eq. (8.19). The components χ_{xy} and χ_{yz} are zero due to the PTU_2 symmetry:

$$PTU_2\chi_{xy}=-\chi_{xy},\quad PTU_2\chi_{yz}=-\chi_{yz} . \tag{8.40}$$

For the v vortex with C_2 symmetry [magnetic class $C_{2v}(C_2)$] i.e., with director-type asymmetry, χ_{xz} also equals 0:

$$\chi_{ij}=\begin{bmatrix}\chi_{xx} & 0 & 0\\ 0 & \chi_{yy} & 0\\ 0 & 0 & \chi_{zz}\end{bmatrix} . \tag{8.41}$$

Introducing the unit vector $\mathbf{b}$ along the x axis, we may write the orientational part of the vortex magnetic anisotropy energy [Eqs. (7.21) and (8.27)] for the case of Eq. (8.39) in the following form:

$$F_{v,H}=\tfrac{2}{5}a\big(\lambda_{11}(H_\alpha R_{\alpha i}\hat{\Omega}_i)^2+\lambda_{12}(H_\alpha R_{\alpha i}\hat{\Omega}_i)(H_\alpha R_{\alpha i}\hat{b}_i) +\tfrac{1}{2}\lambda_{22}\{(H_\alpha R_{\alpha i}\hat{b}_i)^2-[H_\alpha R_{\alpha i}(\hat{\Omega}\times\hat{b})_i]^2\}\big) , \tag{8.42a}$$

where

$$\tfrac{2}{5}a\lambda_{11}=(\chi_{zz}-\tfrac{1}{2}\chi_{yy}-\tfrac{1}{2}\chi_{xx}) , \tag{8.42b}$$

$$\tfrac{2}{5}a\lambda_{12}=2\chi_{xz} , \tag{8.42c}$$

$$\tfrac{2}{4}a\lambda_{22}=(\chi_{xx}-\chi_{yy}) . \tag{8.42d}$$

In the case of an axisymmetric vortex, as well as that of a nonaxisymmetric vortex of the magnetic class $D_{2d}(S_4)$, where $\chi_{xz}=0$ and $\chi_{xx}=\chi_{yy}$, Eq. (8.42a) transforms into Eqs. (7.21) and (8.27) with $\lambda=\lambda_{11}$.

In the nonaxisymmetric v vortex, two additional parameters λ_{12} and λ_{22} appear, while $\lambda_{12}=0$ if the C_2 symmetry is conserved. [The parameter λ_{22} for the C_2-symmetric vortex was introduced by Theodorakis and Fetter (1983) and by Salomaa and Volovik (1983a).] All these parameters may be extracted from NMR experiments, which will permit the identification of the vortex symmetries. For example, the type of nonaxial instability may be probed in an axial-field NMR experiment. In this case, the angle β between $\mathbf{n}$ and $\mathbf{H}$ is nonzero in bulk liquid only if $\lambda_{12}\neq 0$, i.e., for vortices with vector-type instability:

$$\sin^2\beta=\frac{\lambda_{12}^2}{10(1-\lambda_{11})^2} . \tag{8.43}$$

This estimate is obtained by minimization of Eq. (8.42) for $|\lambda_{12}|\ll 1$, and with $\lambda_{22}\ll\lambda_{11}<1$.

An interesting possibility of orientational transitions and metastable vortex states may be related to the orientation of the $\mathbf{b}$ vectors of isolated vortices. This orientation may be coherent or chaotic, depending on the details of the vortex structure and the interaction of vortices with the external field. This influences the effective λ values

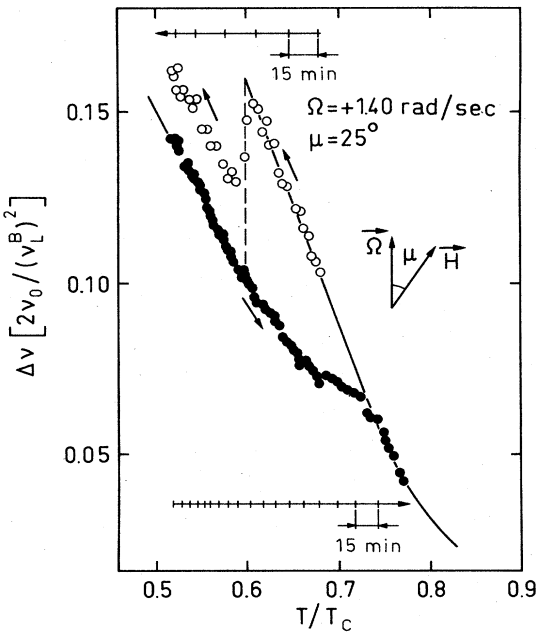

FIG. 48. The hysteresis effect associated with the vortex-core transition: the NMR frequency change $\Delta\nu$ (normalized by the maximum frequency shift in ^{3}He-B) as a function of the reduced temperature. In this measurement, at $p=29.3$ bars, $H=284$ G, and with the tilting angle μ of $\mathbf{H}$ from $\mathbf{\Omega}$ equal to 25°, the cryostat was continuously rotated at $\Omega=1.4$ rad/sec during cooldown (open circles) and warmup (closed circles). Thermal hysteresis near $T_v=0.6T_c$ is evident on comparing the data points with the solid curve, showing the measured equilibrium behavior.

found in experiments. For example, the measured λ_{11} is different for uniform and random distributions of the **b**'s:

$$\lambda_{\text{uniform}}=\lambda_{\text{random}}+\tfrac{1}{2}\,|\,\lambda_{22}\,|\ . \tag{8.44}$$

This may explain the curious hysteresis behavior observed during cooling under continuous rotation (Pekola, Simola, Hakonen, Krusius, Lounasmaa, Nummila, Mamniashvili, Packard, and Volovik, 1984), in which a new metastable state with larger λ seems to exist (see Fig. 48). Note that below the $T=0.6T_c$ transition, the NMR shift under continuous rotation (open circles) is larger than the NMR shift for the stable vortex state (solid circles, for $T<0.6T_c$).

The gyromagnetic energy [Eq. (8.21)] is also modified if the v vortex has a vector-type instability. In this case, the magnetic moment of vortices has a component along the **b** vector,

$$M_\alpha=-\tfrac{4}{5}a\kappa_1(R_{\alpha i}\hat{\Omega}_i+\kappa_2 R_{\alpha i}\hat{b}_i)\ , \tag{8.45}$$

and the corresponding gyromagnetic energy is

$$F_{\text{gm}}=\tfrac{4}{5}a\,[\kappa_1(H_\alpha R_{\alpha i}\hat{\Omega}_i)+\kappa_2(H_\alpha R_{\alpha i}\hat{b}_i)]\ . \tag{8.46}$$

For the C_2-symmetric v vortex, and for the vortex in the class $D_{2d}(S_4)$, one has $\kappa_2=0$, identically.

D. Topology and boojums on the Fermi surface in the core

1. Nodes in the energy gap

The nonunitary structure of the vortex core in the B phase is intimately related to the properties of the ^{3}He quasiparticle spectrum inside the core, in particular, to the topology of the nodes in the energy gap. In triplet pairing, there are in general two branches of the quasiparticle excitation spectrum, according to the two eigenvalues of Eq. (2.4),

$$E_\uparrow=[\,|\,\Delta_\uparrow(\hat{k})\,|^2+v_F^2(k-k_F)^2]^{1/2}\ , \tag{8.47a}$$

$$E_\downarrow=[\,|\,\Delta_\downarrow(\hat{k})\,|^2+v_F^2(k-k_F)^2]^{1/2}\ , \tag{8.47b}$$

which correspond to the two possible opposite spin projections for the ^{3}He quasiparticles. For a unitary state, these energies coincide. The direction of the quasiparticle spin quantization axis, which in the general nonunitary case depends on $\hat{k}$, and the magnitudes of the gaps $\Delta_\uparrow(\hat{k})$ and $\Delta_\downarrow(\hat{k})$ are obtained upon diagonalization of the 2×2 gap matrix $\hat{\Delta}(\hat{k})$ [Eq. (2.7)],

$$\hat{U}(\hat{k})\hat{\Delta}(\hat{k})\hat{U}(\hat{k})^T=\begin{bmatrix}\Delta_\uparrow(\hat{k}) & 0\\ 0 & \Delta_\downarrow(\hat{k})\end{bmatrix}\ , \tag{8.48}$$

where $\hat{U}(\hat{k})$ is a unitary transformation (spin rotation matrix).

For an arbitrary order parameter $A_{\alpha i}$, the nodes of the energy gaps may be found from a consideration of the determinant for the gap matrix $\hat{\Delta}(\hat{k})$:

$$\det[\hat{\Delta}(\hat{k})]=-A_{\alpha i}\hat{k}_i A_{\alpha j}\hat{k}_j=\Delta_\uparrow(\hat{k})\Delta_\downarrow(\hat{k})\ . \tag{8.49}$$

If one finds that $\det[\hat{\Delta}(\hat{k})]=0$ for a given $\hat{k}$, then at least one of the gaps, $\Delta_\uparrow$ or $\Delta_\downarrow$, is zero.

For the bulk unitary B phase, with the superfluid order parameter given by Eqs. (2.7) and (2.14), one finds

$$\det(\hat{\Delta})=-\Delta_B^2(T)\ , \tag{8.50}$$

so that there exists no nodes in the energy gap [see Fig. (49a)].

For the bulk unitary superfluid A phase, with the order parameter (2.23), both of the two species of ^{3}He quasiparticles, with spin projections $\pm\frac{1}{2}$ on the spin quantization axis **d**, display a node for **k** parallel to the orbital quantization axis $\hat{l}=\mathbf{e}_1\times\mathbf{e}_2$ [see Fig. (49b)]. The corresponding determinant is [cf. Eq. (3.4)]

$$\det[\hat{\Delta}(\hat{k})]=\Delta_A^2(T)[\,(\mathbf{e}_2\cdot\hat{k})^2-(\mathbf{e}_1\cdot\hat{k})^2 -2i(\mathbf{e}_1\cdot\hat{k})(\mathbf{e}_2\cdot\hat{k})]\ , \tag{8.51a}$$

$$|\det[\hat{\Delta}(\hat{k})]|=\Delta_A^2(T)(\hat{k}\times\hat{l})^2\ . \tag{8.51b}$$

2. Real-space versus k-space vortices

The nodes in the energy gap define almost all the superfluid properties of ^{3}He, including the peculiar continuous vorticity of superflow, which appears in textures where the positions of the nodes (in the A phase, the $\hat{l}$ vector) are distributed continuously in space. This results from the vortex nature of the nodes. The gap determinant $\det\Delta(\mathbf{k})$ is a complex scalar and may be represented in terms of its modulus and phase:

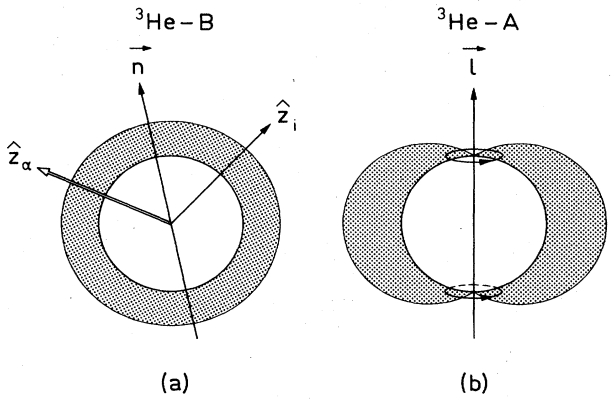

FIG. 49. The energy gap for ^{3}He quasiparticles in the quasi-isotropic superfluid ^{3}He-B and in the anisotropic superfluid ^{3}He-A. The gap in ^{3}He-A goes to zero at two points (boojums) on the poles of the Fermi sphere.

$$\det\Delta(\mathbf{k}) = |\det\Delta(\mathbf{k})| e^{i\Phi(\mathbf{k})} . \quad (8.52)$$

In the presence of the texture, the phase Φ depends both on the real-space coordinates $\mathbf{r}$ and on the pair momentum $\mathbf{k}$: $\Phi=\Phi(\mathbf{k},\mathbf{r})$. This generalizes the ordinary $\mathbf{r}$-dependent phase of the Bose condensate to more subtle structures of the gap, including the $\mathbf{k}$ dependence, in particular, which is specific for Cooper pairing with nonzero orbital angular momentum. The phase $\Phi(\mathbf{k},\mathbf{r})$ may display a vortex singularity in the five-dimensional $(\mathbf{k},\mathbf{r})$ space (three coordinates of $\mathbf{r}$ and two for $\mathbf{k}$ on the Fermi sphere), which generalizes the concept of an ordinary quantized vortex singularity in the $\mathbf{r}$ space: the phase Φ changes by $2\pi N$ (with N an integer) upon encircling the vortex axis. On the vortex axis, the phase is not well defined and therefore the modulus of $\det\Delta(\mathbf{k},\mathbf{r})$ becomes zero. The dimension of the vortex axis in $(\mathbf{k},\mathbf{r})$ space, i.e., the dimension of the manifold where $\det\Delta(\mathbf{k},\mathbf{r})=0$ is three, as may be seen from the example of an o vortex in ^{3}He-B.

Let us consider the simplest (nonrealistic) ansatz for an m-quantum o vortex in the B phase,

$$\Delta_{ab}(\mathbf{k},\mathbf{r})=\Delta_B(r)(g\sigma^i)_{ab}\hat{k}_i e^{im\phi} , \quad (8.53)$$

where there would be a B phase everywhere within the core, except for the origin $r=0$, where $\Delta_B(0)=0$. The determinant, $\det\Delta(\mathbf{k},\mathbf{r})$, for this ansatz [see Eq. (8.50)],

$$\det\Delta(\mathbf{k},\mathbf{r}) = -\Delta_B^2(r)e^{2im\phi} , \quad (8.54)$$

is independent of $\mathbf{k}$, and thus vanishes at $r=0$ for all $\mathbf{k}$ on the Fermi sphere. Therefore the dimension of the vortex axis in $(\mathbf{k},\mathbf{r})$ space is $3=1+2$ (dimension 1 for the vortex line in $\mathbf{r}$ space plus the dimension 2 of the Fermi sphere). Note also that the topological invariant N for this vortex is $N=2m$.

Another realization of the vortex singularity in the phase $\Phi(\mathbf{k},\mathbf{r})$ is the node in the energy gap of the uniform A-phase state. According to Eq. (8.51a), the phase $\Phi(\mathbf{k})$ changes by 4π when circling the axis k_z in $\mathbf{k}$ space. Thus, the uniform A-phase state has the vortex singularity in $\mathbf{k}$ space with $N=2$, while the singly quantized o vortex in the B phase has the vortex singularity in $\mathbf{r}$ space with the same $N=2$. Since these objects are described by the same phase winding number N, they are different realizations of the same vortex in $(\mathbf{k},\mathbf{r})$ space and may transform into each other through a continuous change of $\Delta_{ab}(\mathbf{k},\mathbf{r})$. The transformation process is simply the reorientation of the three-dimensional vortex axis in $(\mathbf{k},\mathbf{r})$ space: the axis is parallel to the $\mathbf{r}$ space in the uniform A phase, but occupies $1+2$ dimensional subspace of $(\mathbf{k},\mathbf{r})$ space in the B-phase o vortex. Because of these transformations, singular vorticity of the quantized vortex in $\mathbf{r}$ space may be smoothened by "flaring out" of the vortex into $\hat{k}$ space. This occurs, for example, when the singular doubly quantized vortex in ^{3}He-A transforms into the nonsingular ATC vortex. The same mechanism takes place in the singular ^{3}He-B vortex, where the normal hard core in the o vortex becomes superfluid due to "flaring out" of singularity, when the o vortex transforms into the v vortex. This also gives rise to the continuous phase slip in superfluid ^{3}He, as distinct from He II, where only singular vortices produce phase slips.

The mechanism for the "flaring out" of singular vorticity in the fifth dimension couples the real-space topology with the topology of the Fermi surface, which is a spherical surface for superfluid ^{3}He—a topologically nontrivial object (for heavy-fermion superconductors, the Fermi surface may have different topology). The important notion in this theory is the motion of the "boojum on the Fermi surface" (Volovik and Mineev, 1982; Salomaa and Volovik, 1985a; Salomaa and Volovik, 1986c), the intersection of the vortex line in $\mathbf{k}$ space with the Fermi surface. They resemble the point vortices that may occur on the surface of a container in real space; such objects were first introduced by Mermin (1977) and called "boojums." In the $\mathbf{k}$ space, the "vessel" that contains the Fermi sea of ^{3}He atoms is the Fermi surface.

The topological charge N for a boojum on the Fermi surface is equal to the phase Φ winding number of the intersecting vortex line if the vortex line leaves the Fermi sphere and $-N$ if the line enters the Fermi sphere. For example, the north-pole boojum in the A phase has a topological charge $N=2$, while the south-pole boojum has $N=-2$.

The singly quantized o vortex has no nodes in the gap and therefore no boojums anywhere across the core, for $\det[\hat{\Delta}(\hat{k})]$ never goes to zero. Only at the origin where the normal state occurs does $\det[\hat{\Delta}(\hat{k})]$ vanish together with the order parameter over all of the Fermi surface. The vanishing of the gap at the origin and the absence of vortices in $\mathbf{k}$ space are related. Since there is no escape of an $\mathbf{r}$ vortex into $\mathbf{k}$ space, the vorticity in the singly quantized o vortex is strictly singular: the circulation of superflow along any path embracing the vortex axis is 2π, irrespective of the path chosen, and the superfluid velocity has a singularity on the vortex axis, thus making the order parameter vanish, $\hat{\Delta}(\hat{k},\mathbf{r}=0)=0$.

The singularity in the order parameter may be dissolved, provided that the singular vorticity in $\mathbf{r}$ space transforms into a $\mathbf{k}$-space vortex line, i.e., pairs of boojums associated with opposite topological charges appear at the Fermi surface for some finite distance from the vortex axis. Here we choose to denote this distance where the nodes in the ^{3}He quasiparticle excitation spectrum first appear as the vortex-core radius ($r_{\rm core}$), since everywhere in the core region inside this radius superflow is nonpotential.

For decreasing distances $r<r_{\rm core}$ from the vortex axis, these boojums move continuously in $\mathbf{k}$ space, covering on their way certain parts of the Fermi surface. There is a powerful topological rule, which serves to couple the real-space topology with the topology of the Fermi sphere: in order to completely resolve the m-quantum vortex singularity in real space, the total area of the Fermi sphere covered by all the boojums with positive charge $N=+1$ should equal m times the area of the Fermi

sphere, $4\pi k_F^2$, provided that one takes into account the sign of surface orientation (Volovik and Mineev, 1982). This is easy to check in the example of the continuous ATC vortex in the A phase. This ATC vortex is obtained by dissolving the doubly quantized ($m=2$) vortex singularity due to formation of l texture with l covering the unit sphere once [see Eq. (4.16)]. Since l indicates the position of the boojum with $N=2$ on the Fermi sphere (or, what here is equivalent, two boojums—each with $N=1$), the total area covered by two boojums with $N=1$ is twice the area $4\pi k_F^2$ of the Fermi sphere.

This relation between the real-space and k-space topology may be expressed in terms of the generalized Mermin-Ho relation in Eq. (3.8). Let us introduce the vectors $\boldsymbol{l}_a$ in the directions of the boojums with $N=+1$ (in the A phase, there are two such boojums, with $\boldsymbol{l}_1=\boldsymbol{l}_2=\boldsymbol{l}$; in the most general case of p-wave pairing, four boojums are possible); then the number of superflow circulation quanta m around the vortex with dissolved vortex singularity is expressible in terms of the gradients of the $\boldsymbol{l}_a$ fields:

$$m=\frac{M}{h}\oint_{\text{around core}} d\mathbf{r}\cdot\mathbf{v}_s=\frac{M}{h}\int_{\text{over core}} d\mathbf{r}\cdot(\nabla\times\mathbf{v}_s)$$
$$=\sum_a \int_{\text{over core}} \frac{dx\,dy}{4\pi}\left[\boldsymbol{l}_a\cdot\frac{\partial \boldsymbol{l}_a}{\partial x}\times\frac{\partial \boldsymbol{l}_a}{\partial y}\right]. \tag{8.55}$$

Hence, for dissolving one quantum of vorticity in the ^{3}He-B o-vortex core, the boojums should cover the Fermi surface once. However, this topological requirement is incompatible with the symmetry of the o vortex (see Sec. V.B). Thus, for smoothing the singularity, the parity P should be broken and the o vortex should transform into the v vortex.

3. Topology of k-space vortices in the axisymmetric v-vortex core

Let us next consider the topology of boojums in the singly quantized axisymmetric v-vortex structure in some detail. Specifically, let us find how the positions of the boojums on the Fermi surface in the v vortex depend on the coordinate $\mathbf{r}=(r,\phi)$ in real space. Due to axisymmetry, the positions $\hat{k}(\mathbf{r})$ of the boojums are determined by two parameters, $\alpha(r)$ and $\beta(r)$:

$$\hat{k}(\mathbf{r})=\hat{z}\cos\beta(r)+\sin\beta(r)[\hat{r}\cos\alpha(r)+\hat{\phi}\sin\alpha(r)]\,. \tag{8.56}$$

Here β and α denote the polar and azimuthal angles on the Fermi sphere, where $\beta(r)$ is measured with respect to the axis ($\hat{z}$) of the vortex, while $\alpha(r)$ is measured from the direction $\hat{r}$ of the radial vector in real space; for an illustration, see Fig. 50.

These parameters $\alpha(r)$ and $\beta(r)$ obey the following equation at the directions in which the nodes of the gap occur:

$$\det[\hat{\Delta}(\hat{k})]=0\,. \tag{8.57}$$

This equation has four solutions in the v vortex for $r\le r_{\text{core}}$, where the core radius is indicated in Fig. 51 for different values of δ. These solutions represent two pairs of boojums on the Fermi sphere, defined by the vectors $\boldsymbol{l}_1$ and $\boldsymbol{l}_2$. One pair contains the boojum 1^+ with the topological charge $N=+1$ and with angles $\beta_1^+(r)$ and $\alpha_1^+(r)$ of vector $\boldsymbol{l}_1$, illustrated in Fig. 51, and the diametrically opposite boojum 1^- with the topological charge $N=-1$ and with the corresponding angles $\beta_1^-(r)=\pi-\beta_1^+(r)$ and $\alpha_1^-(r)=\pi+\alpha_1^+(r)$. The respective positions of the second pair of boojums, $2^+(\boldsymbol{l}_2)$ and 2^-, are given by

$$\beta_2^+(r)=\beta_1^+(r),\quad \alpha_2^+(r)=-\alpha_1^+(r) \tag{8.58a}$$

and

$$\beta_2^-(r)=\pi-\beta_1^+(r),\quad \alpha_2^-(r)=\pi-\alpha_1^+(r)\,. \tag{8.58b}$$

The angles $\beta_2^-(r)$ and $\alpha_2^-(r)$ of the boojum 2^- are also shown in Fig. 51. At the core radius, boojums 1^+ and 2^-

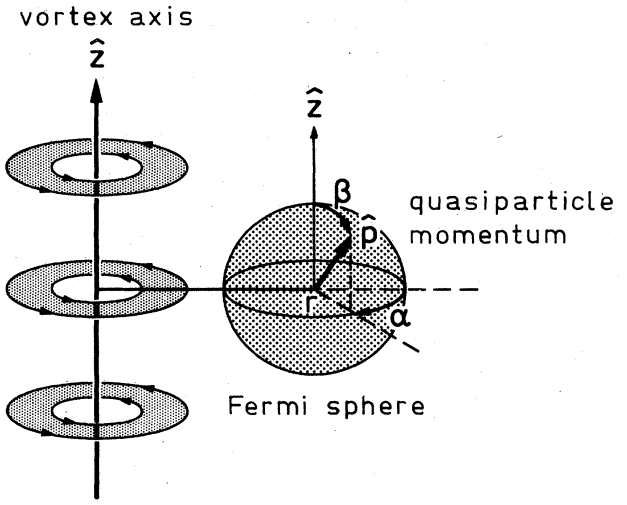

FIG. 50. Schematic illustration of the direction of ^{3}He quasiparticle momentum on the Fermi sphere in terms of the angles α and β, defined in Eq. (8.56), for a quasiparticle located at distance r from the vortex axis.

mutually annihilate each other; boojums 2^+ and 1^- also coalesce together, so that no boojums remain for distances $r > r_{\rm core}$.

Figure 52 illustrates the computed cross sections of the Fermi surface for the axisymmetric v vortex, shown in Fig. 38. Here $|\det[\hat{\Delta}(\hat{k})]|$ is drawn in the plane that contains all four nodes. These cross sections are given for several different chosen distances r from the vortex axis. Note that for $r > r_{\rm core}$, the magnitude $|\det(\hat{\Delta})|$ is represented in the equatorial plane ($\beta = \pi/2$), where boojums first appear at $r = r_{\rm core}$. On the vortex axis, two boojums with $N = \pm 2$ exist on the poles of the Fermi surface, which corresponds to the A phase with its $\boldsymbol{l}$ vector directed along the axis $\boldsymbol{l}_1 = \boldsymbol{l}_2 = \boldsymbol{l} = \hat{z}$. They split at $r \neq 0$ into two pairs of boojums, each with $N = \pm 1$ at $r > 0$. For r tending to $r_{\rm core}$, the boojums move towards the equator, where the opposite topological charges annihilate each other at $r = r_{\rm core}$. Nodes then disappear for $r > r_{\rm core}$. It is quite easy to verify that the boojums with a positive topological charge do cover all the Fermi surface once: actually the area on the Fermi surface covered by the boojum $\boldsymbol{l}_1$ with charge $N = +1$ is

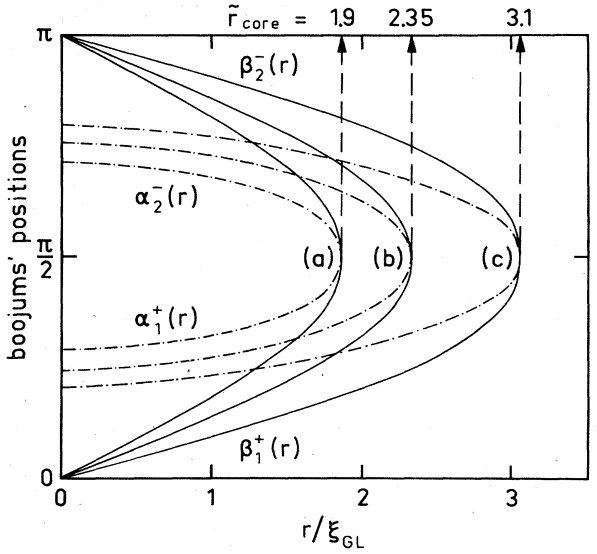

FIG. 51. The angles $\alpha(r)$ and $\beta(r)$, obtained as solutions of Eq. (8.57), which determine the positions of boojums (nodes) in the ^{3}He quasiparticle energy gap on the Fermi sphere for the singly quantized axisymmetric v vortex. The three sets of curves [(a),(b),(c)] correspond to three different values: (a) $\delta = 0.0$; (b) $\delta = 0.3$; (c) $\delta = 0.46$. Also shown in this figure is the vortex-core radius $r_{\rm core}$, which in this paper is defined as the distance at which nodes in the ^{3}He quasiparticle energy gap first appear. The core radius is measured in units of the Ginzburg-Landau coherence length: $\tilde{r} = r/\xi_{\rm GL}$. Angles α_1^+ and β_1^+ refer to the position of the $\boldsymbol{l}_1$ vector of boojum 1^+ with unit positive topological charge, while α_2^- and β_2^- refer to boojum 2^- with unit negative topological charge (or the position of $-\boldsymbol{l}_2$ vector). At $r = r_{\rm core}$, these two boojums with opposite charges annihilate each other.

$$k_F^2 \int_0^\infty dr \int_0^{2\pi} d\phi\, \boldsymbol{l}_1 \cdot \frac{\partial \boldsymbol{l}_1}{\partial r} \times \frac{\partial \boldsymbol{l}_1}{\partial \phi} = 2\pi k_F^2 \int_0^\infty dr \sin\beta \frac{\partial \beta}{\partial r} = 2\pi k_F^2 , \quad (8.59)$$

which comprises one-half the Fermi sphere. Therefore, in the axisymmetric v vortex with $m = 1$, each $\boldsymbol{l}_a$ covers one-half of the Fermi sphere, thus providing the unwinding of the circulation quantum, $m = 1 = \frac{1}{2} + \frac{1}{2}$ in accordance with Eq. (8.55). (Note that the scenario of the topological flaring out of the singularity is different in the nonaxisymmetric v vortex—see Sec. VIII.D.4—and it is just this difference that may explain the first-order nature of the phase transition in the core.)

The features described above serve to render the problem of scattering of superfluid ^{3}He quasiparticle excitations off the quantized vortex line in superfluid ^{3}He-B an interesting one. The calculation of the coefficient of mutal friction of the vortex lines with the liquid ^{3}He (Hall, Gammel, and Reppy, 1984) must include a solution of the continuum part of the scattering problem. Unlike the solutions for vortices in ordinary s-wave superconductors, the solutions of the Bogoliubov—de Gennes equations here yield a spectrum of bound fermion quasiparticle states (Combescot and Dombre, 1983, 1986; Maki and Combescot, 1985) even for finite distances $r \leq r_{\rm core}$, not only on the vortex axis. This equation is identical to the Dirac equation (more accurately, the Weyl equation) for charged massless chiral fermions moving in electromagnetic and gravitational fields (Volovik, 1986b, 1986d). The part of the vector potential $\mathbf{A}$ of the electromagnetic field in ^{3}He-A is played by the vector $\boldsymbol{l}$ for the boojum position: $\mathbf{A}(\mathbf{r},t) = k_F \boldsymbol{l}(\mathbf{r},t)$ (Combescot and Dombre, 1986). If the doubly quantized boojum is split into two boojums, an additional field acting on the fermion appears, which corresponds to the weak interaction (Volovik, 1986b). Any $\boldsymbol{l}$ texture with nonzero curl $\boldsymbol{l}$ produces the "magnetic" field $\mathbf{B} = \mathrm{rot}\mathbf{A}$, as a result of which the discrete bound states of quasiparticles near the boojums are generated, corresponding to the Landau levels for electrons in a magnetic field.

Many interesting physical phenomena are connected with the boojums. They give rise to the anomalous mass current [the second term in Eq. (3.14b)], nonanalytical gradient expansion, nonconservation of the linear momentum of superflow at $T = 0$, the paradox of the orbital angular momentum, the nonzero density of the normal component at $T = 0$, etc. Since the interaction of fermions with some of the collective variables of the order parameter $A_{\alpha i}$ is identical with the interaction of the chiral fermions with photons, W bosons, and gravitational field, these phenomena are of the same origin as the chiral anomaly and vacuum polarization effects in quantum field theory (Balatsky, Volovik, and Konyshev, 1986; Volovik, 1986a, 1986b, 1986c, 1986d).

In particular, the creation of the quasiparticle current in a space- and time-dependent $\boldsymbol{l}$ texture, which takes place due to the vanishing of the gap at the boojum, is

completely equivalent to the creation of a chiral current from the vacuum in the presence of electric and magnetic fields. These creation processes are even described by the very same equation. The source of the chiral current in quantum electrodynamics with massless fermions is given by the Schwinger equation

$$\frac{e^2}{16\pi^2}F_{\mu\nu}F_{\alpha\beta}\varepsilon^{\mu\nu\alpha\beta}\equiv\frac{e^2}{2\pi^2}\mathbf{E}\cdot\mathbf{B}\ . \tag{8.60a}$$

while the source of the quasiparticle momentum in the l texture of ^{3}He-A is obtained after multiplying Eq. (8.60a) by the quasiparticle momentum $k_F\hat{l}$ near the boojum:

$$\frac{k_F\hat{l}}{2\pi^2}(\mathbf{E}\cdot\mathbf{B})=\frac{k_F^3\hat{l}}{2\pi^2}(\dot{\hat{l}}\cdot\nabla\times\hat{l})\ . \tag{8.60b}$$

Here we used $\mathbf{E}=k_F\dot{\hat{l}}$ and $\mathbf{B}=k_F\nabla\times\hat{l}$ for the analog "electric" and "magnetic" fields in ^{3}He-A, imitated by the time- and space-dependent l texture.

The moving v vortex, with a time- and space-dependent l texture (boojums), also serves as a source for the quasiparticle current even at $T=0$. Thus, the moving quantized vortex line experiences an additional force during motion. However, the dynamics of the vortices is beyond the scope of our present review.

4. The nonaxisymmetric v vortex is a half-quantum pair

The scenario for the flaring out of the vortex singularity in momentum space for the nonaxisymmetric v vortex is topologically different from that in the axisymmetric vortex: the core of the singly quantized nonaxisymmetric v vortex in rotating ^{3}He-B has been found to display novel topological structure—it is *a bound pair of vortices with half-integer circulation* (Salomaa and Volovik, 1986c). Such vortices have been considered in Sec. V.F for the case of the rotating superfluid A phase, where they are an

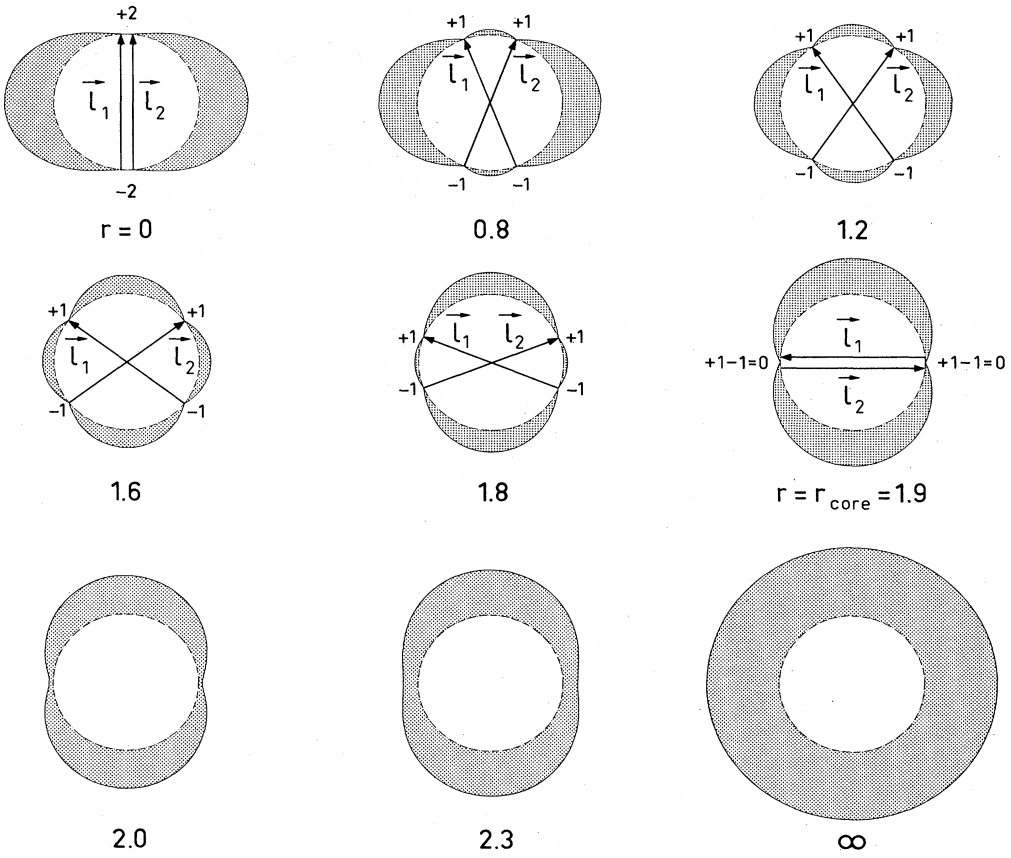

FIG. 52. The computed magnitude of the ^{3}He quasiparticle energy gap $|\det[\hat{\Delta}(\hat{k})]|=\Delta_\uparrow(\hat{k})\Delta_\downarrow(\hat{k})$ as a function of the quasiparticle momentum and the reduced radial distance $\tilde{r}=r/\xi_{GL}$ from the vortex axis. For $r<r_{core}$, we choose the cross-sectional plane of the Fermi surface such that it contains all four different nodes; this plane can be readily visualized with the help of Figs. 50 and 51. For $r=0$, there is a pair of boojums on the antipodal points with double topological charges, $N=\pm2$ ($l_1=l_2$). For $r>0$, these divide into two pairs of boojums, each carrying unit topological charges $N=\pm1$. For increasing r, the boojums move continuously towards the equatorial plane, where they annihilate each other ($+1-1=0$) at $r=r_{core}$, as shown in Fig. 51. For $r>r_{core}$, the energy gap is strongly anisotropic, but no more nodes exist. For $r\to\infty$, one obtains the isotropic B-phase energy gap.

admixture of a vortex and a disclination in the magnetic anisotropy vector **d**. These objects were predicted to occur for $T<0.7T_c$; however, no evidence has yet been found for half-quantum vortices in the NMR experiments on rotating ^{3}He-A. Nevertheless, an identification of the vortex-core transition observed in rotating ^{3}He-B as a topological phase transition involving half-quantum vortices has been suggested.

In the axisymmetric v vortex, whose core topology is summarized in Fig. 53, the singularity in the vortex core is resolved through the formation of point vortices in momentum space, such that superfluidity is not broken on the vortex axis.

Let us now consider the topology of boojums in the case of the singly quantized v-vortex structure with broken axisymmetry, specified by the nonaxisymmetry quantum number $|Q|$. This vortex may be represented as [cf. Eq. (8.19b)]

$$a_{\mu\nu}^{(Q)}(\mathbf{r})=a_{\mu\nu}(Q=0)+e^{iQ\phi}a_{\mu\nu}(+Q)+e^{-iQ\phi}a_{\mu\nu}(-Q) \tag{8.61}$$

with $Q=2$, and with $a_{\mu\nu}(Q)$ as in Eq. (8.2). Specifically, let us find the boojums on the Fermi surface in this vortex and investigate how they depend on the coordinate **r** in space. Since this v vortex is axially nonsymmetric, the positions of the boojums determined by two angles α and β depend not only on r, but also—distinctly from Eq. (8.56)—on the cylindrical coordinate ϕ:

$$\hat{k}(r,\phi)=\hat{z}\cos\beta(r,\phi) +\sin\beta(r,\phi)[\hat{r}\cos\alpha(r,\phi)+\hat{\phi}\sin\alpha(r,\phi)] . \tag{8.62}$$

These angles may be determined by obtaining solutions of the complex-valued equation (8.57): $\det[\hat{\Delta}(\hat{k})]=A_{\alpha i}\hat{k}_i A_{\alpha j}\hat{k}_j=0$ for the directions where the gap nodes occur. This yields

$$\sum_\mu (f_\mu f_{-\mu}-g_\mu g_{-\mu})=0 , \tag{8.63a}$$

$$\sum_\mu (f_\mu g_{-\mu}+g_\mu f_{-\mu})=0 , \tag{8.63b}$$

where

$$f_\mu=\{C_{\mu 0}+[C_{\mu 0}(+)+C_{\mu 0}(-)]\cos Q\phi\}\cos\beta +\frac{\sin\beta}{\sqrt{2}}\{C_{\mu +}+C_{\mu -}+\cos Q\phi[C_{\mu +}(+)+C_{\mu +}(-)+C_{\mu -}(+)+C_{\mu -}(-)]\cos\alpha -\sin Q\phi[C_{\mu +}(+)-C_{\mu -}(-)-C_{\mu -}(+)+C_{\mu -}(-)]\sin\alpha\} \tag{8.64a}$$

and

$$g_\mu=[C_{\mu 0}(+)-C_{\mu 0}(-)]\sin Q\phi\cos\beta +\frac{\sin\beta}{\sqrt{2}}\{C_{\mu +}-C_{\mu -}+\cos Q\phi[C_{\mu +}(+)+C_{\mu +}(-)-C_{\mu -}(+)-C_{\mu -}(-)]\sin\alpha +\sin Q\phi[C_{\mu +}(+)-C_{\mu +}(-)+C_{\mu -}(+)-C_{\mu -}(-)]\cos\alpha\} . \tag{8.64b}$$

Above, $C_{\mu\nu}(\pm)$ refer to the nonaxisymmetric sectors in the Cooper-pair amplitudes of Eq. (8.61) with $Q=\pm 2$, respectively, while $C_{\mu\nu}$ denotes the sector with $Q=0$. We shall exploit the amplitudes $C_{\mu\nu}(Q)$ of Fig. 44.

Figure 53(b) illustrates a summary of our analysis. The core region of the singly quantized nonaxisymmetric vortex, where vorticity escapes from real space to momentum space, may be conceived of as a composite object—a v-vortex "molecule." In the core, where the boojums l_1 and l_2 appear, there occur two centers, separated by the distance $R_{\rm pair}$, which can be identified as *half-quantum vortices*. These HQV's have further inner core regimes of radius $r_{\rm HQV}$, which are attached to a soliton "string," topologically confining the HQV's—or "quarks"—in the v-vortex molecule, as in the A phase (cf. Sec. V.F.2).

Outside the cores of the HQV's, in the "planarlike" phase, the nodes in the energy gaps $\Delta_1(\hat{k})$ and $\Delta_2(\hat{k})$, and hence l_1 and l_2, lie predominantly in the cross-sectional plane of the vortex,

$$l_{1,2}=\hat{z}\cos\eta\pm\sin\eta\left[\hat{x}\cos\frac{\zeta}{2}+\hat{y}\sin\frac{\zeta}{2}\right] , \tag{8.65}$$

with ζ changing by 2π around each HQV and with $\eta=\pi/2$. The planar distribution of l_1 and l_2 means that there is no vorticity outside the HQV cores, according to the Mermin-Ho relations. Therefore all the vorticity is concentrated in the axi-planar cores of the HQV's, where $\eta\neq\pi/2$, and the vectors l_1 and l_2 deviate from the plane and become mutually nonparallel.

Note that the directions of the l vectors interchange upon encircling either HQV: $l_1\rightleftarrows l_2$. Hence disclinations occur simultaneously in both l_1 and l_2; this resembles the **d**-field disclination for the HQV in the A phase [see Fig.

25(a)]. In order to prove that the two "quarks" really represent objects with fractional topological charge, one may verify that each point vortex covers one-fourth of the Fermi surface. Thus, according to Eq. (8.55), the circulation number m around the HQV is one-half:

$$m=\frac{M}{h}\oint_{\text{around HQV}}\mathbf{v}_s\cdot d\mathbf{r}$$
$$=\int_{\text{over HQV core}}\frac{dx\,dy}{4\pi}\left[\boldsymbol{l}_1\cdot\frac{\partial\boldsymbol{l}_1}{\partial x}\times\frac{\partial\boldsymbol{l}_1}{\partial y}+\boldsymbol{l}_2\cdot\frac{\partial\boldsymbol{l}_2}{\partial x}\times\frac{\partial\boldsymbol{l}_2}{\partial y}\right]$$
$$=\tfrac{1}{4}+\tfrac{1}{4}=\tfrac{1}{2}\ . \tag{8.66}$$

The smooth winding $\boldsymbol{l}_1\rightleftarrows\boldsymbol{l}_2$ around the HQV reverses orbital quantum numbers of excitations, such as fermion quasiparticles. This is analogous to the properties of the singular lines postulated to occur according to the grand unified theories (Schwarz, 1982). Moreover, due to topological constraints, the HQV's cannot exist separately, a condition demonstrating a possible topological mechanism of confinement. This makes the identification of such objects of great interest in a general context of physics.

E. Discussion of the possible nature of the vortex-core transition

Since the C_2-symmetric v vortex presently seems to be the most stable one near T_c, at least at low pressures, it may tentatively be identified with the vortex in Region I of the phase diagram in Fig. 1 (see Fig. 54). It remains to identify the vortex-core structure at high pressures. It is important that the "director"-type breaking of axisymmetry proves to be of first order. Therefore the high-pressure vortex could be the axisymmetric v vortex, which has a lower free energy close to the polycritical pressure. This is supported by numerical work of Thuneberg (1986b) and by Salomaa and Volovik (1986a) near T_c, which shows that at high pressures this vortex has less energy than the C_2-symmetric one.

However, recalling the variety of possible transitions in rotating ^{3}He-A (see Sec. V.G.), one may expect that the symmetry change is not the only possible reason for the phase transition in the vortex core. Volovik and Mineev (1982) were the first to propose that the observed vortex-core transition in ^{3}He-B could be due to a change in the topology of boojums in the vortex-core matter. The phase transition proved to be different—but more interesting—than that put forward by them: the dimerization of a one-quantum vortex (the high-pressure vortex) into a pair of half-quantum vortices (the low-pressure vortex), producing a new topological feature—the transformation of boojums into one another after circling either half-quantum vortex. Figure 54 presents the tentative topological identification of the vortices involved in the core transition in rotating ^{3}He-B. The first-order nature of the core transition may follow from the change in the topology at the bifurcation process of the vortex core.

Other possibilities cannot be excluded, since the computations are sensitive to the actual numerical values of the five β parameters as functions of pressure, which are not known with good precision. In particular, it is possible that a third—metastable—vortex state occurs in ^{3}He-B during continuous rotation (see Fig. 48). This could be due to the spiral vortex textures, with pitch of the order of the coherence length; alternatively, it might be identified with another nonaxisymmetric vortex (Volovik and Salomaa, 1987), also possessing $|Q|=2$ (see Fig. 55), but with similar topology to that of the axisymmetric v-vortex. No *topological* barrier would occur for a transition into this metastable state. This new nonaxisymmetric vortex state belongs to the magnetic class $D_{2d}(S_4)$ (see Table IV).

The symmetry group $D_{2d}(S_4)$ is formed from the combined symmetry elements PC_4 and TU_2. The quantity $\sum_{\mu\nu}a_{\mu\nu}a^*_{\mu\nu}$ possesses a fourfold symmetry axis; therefore the vortex-core cross section displays the symmetry of a square ("vortex with square core"; see Fig. 56), as distinct from the axisymmetric v vortex with a "round core" and the nonaxisymmetric v vortex with a "double core." The properties of this vortex state, which follow from the symmetry and may be used for its identification, are as follows: as in the o vortex, there occur no spontaneous axial mass and spin flows, nor any spontaneous electric polarization; only a single component λ_{11} of the vortex magnetic anisotropy tensor survives, since the anisotropy vector $\mathbf{b}$ in the cross-sectional plane is absent due to the fourfold symmetry. However, as distinct from the o vortex, superfluidity is not broken in the core; this is due to the formation of boojums on the Fermi surface. The topology of the boojums in this new "square" vortex state is the same as in the "round" core of the axisymmetric v vortex, and, therefore, it is distinct from that of the nonaxisymmetric v vortex, which is the bound pair of half-quantum vortices. Therefore it is possible that far below T_c there exists a topological barrier between the $D_{2d}(S_4)$ and the $C_{2v}(C_2)$ vortices, and hence $D_{2d}(S_4)$ may become locally—or even absolutely—stable far away from T_c.

Clearly, the present tentative identification of the vortex-core structures in ^{3}He-B need not be final. Further work is in progress, especially on the spiral vortex textures. Moreover, the "vector"-type vortex instability may become important. An analogy may be made, again, with the situation in the A phase, where competition occurs between the v and w vortices, both with a "vector"-type asymmetry [see Eqs. (5.29) and (5.30)]. Note that the nonaxisymmetric w vortex, which necessarily has a twist (spiral) in the vector (or director) anisotropy axis $\mathbf{b}$ (see Sec. VIII.C.6), with pitch of the order of the vortex-core size, has not yet been reported near T_c. This $v\leftrightarrow w$ transition is necessarily of first order—since the symmetry groups for the v and w vortices are not subgroups of each other. (See the symmetry subordination scheme in Table IV, which includes the four vortices in ^{3}He-B that have been found numerically, as well as the nonaxisymmetric

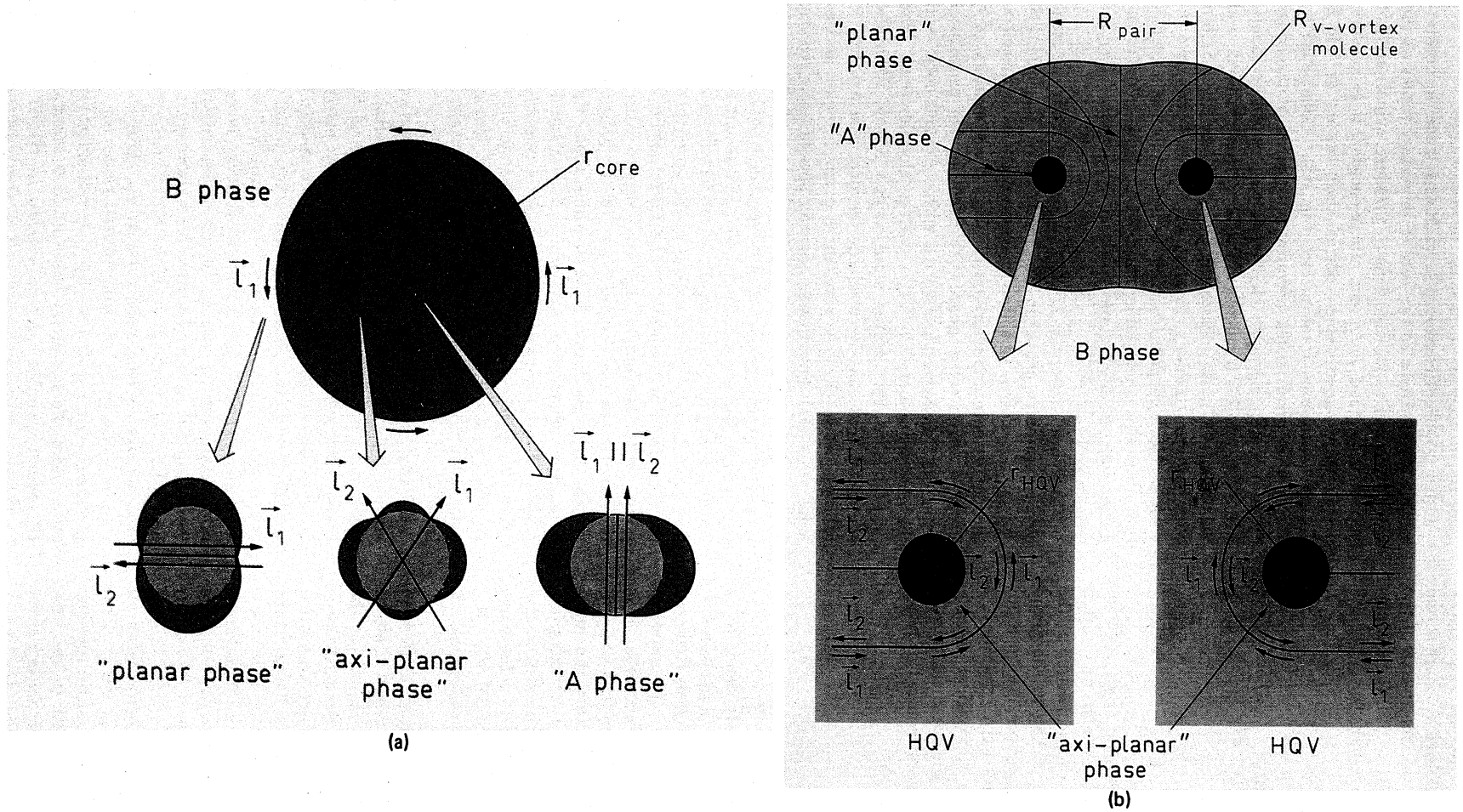

FIG. 53. Topological structure of the two vortices found to be stable in ^{3}He-B. (a) Topological structure of the energy gap in the cross-sectional plane of the axisymmetric v-vortex core (Salomaa and Volovik, 1985a), proposed to occur in rotating superfluid ^{3}He-B at high pressures. Point vortices, or boojums, on the Fermi sphere first appear in the "planarlike" phase at the distance $r_{\rm core}$, signalling the radius at which the flaring out of vorticity from real space into momentum space first starts. Vorticity is supported in the core by the continuous winding—in the "axi-planar-like" phase—of the $\boldsymbol{l}$ vectors for the quasiparticles with spin projection up ($\boldsymbol{l}_1$) and for those with spin projection down ($\boldsymbol{l}_2$). As the $\boldsymbol{l}$ vectors "escape into the third dimension" (cf. Fig. 7 for an analogous situation in the MH texture), the vortex singularity "escapes into the fourth and fifth dimensions" in the $(\mathbf{r},\mathbf{k})$ space. They change from antiparallel at $r=r_{\rm core}$ to parallel at $r=0$ on the vortex axis, where the "A-phase-like" core occurs. This summarizes the inner structure of the core for vortex II in Fig. 2(b). The topological model for the core structure of the nonaxisymmetric v-vortex molecule (Salomaa and Volovik, 1986c), suggested to occur in rotating ^{3}He-B at low pressures (Thuneberg, 1986b; Volovik and Salomaa, 1985b). On the basis of their topological properties the two centers, separated by the distance $R_{\rm pair}$, have been identified each as a half-quantum vortex (HQV) confined in the v-vortex molecule. Each HQV is accompanied by a disclination in the $\boldsymbol{l}$-vector field with half-integer winding number—or topological charge—which reverses $\boldsymbol{l}_1$ into $\boldsymbol{l}_2$ (and vice versa) on circling once around either HQV. The $\boldsymbol{l}$ vectors lie predominantly in the cross-sectional plane of the v-vortex molecule ("planarlike" phase). However, inside the inner cores of radius $r_{\rm HQV}$, these vectors flare out of the plane, deviate from each other (in the "axi-planar-like" phase), and each covers one-quarter of the Fermi sphere. The spatial variation in the directions of the point vortices on the Fermi surface may be regarded as forming a string which topologically confines the HQV pair (vortex I in Fig. 2). This "bag" model of the v-vortex core "molecule" resembles the structure of hadrons with the half-quantum vortices corresponding to quarks.

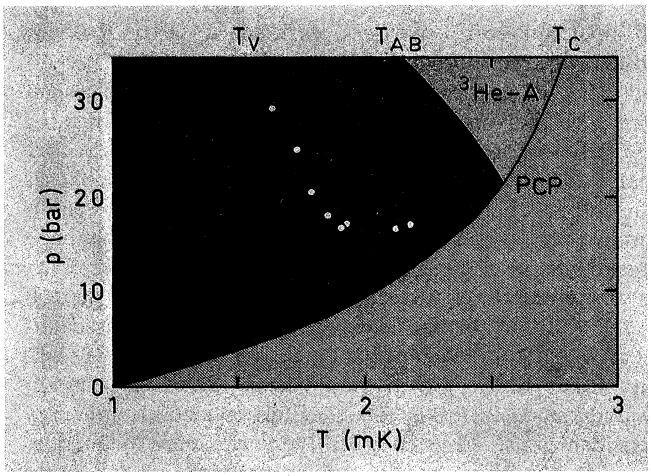

FIG. 54. Phase diagram of ^{3}He; compare with Fig. 1. According to our present understanding (Salomaa and Volovik, 1986c), we tend to identify the change in the vortex-core structure in ^{3}He-B as the *topological transition between two inequivalent ways in which vorticity can flare out* (Volovik and Mineev, 1982), illustrated in Figs. 53(a) and 53(b) for the axisymmetric and nonaxisymmetric vortices, both with v symmetry. The vortex-core transition signals this topological bifurcation in the escape of vorticity into the momentum space.

w and uvw vortices, which have not been reported thus far. Arrows indicate the direction of the symmetry breaking.) It is important that the first-order vortex-core transition is observed far from T_c (although there is some indication that the low-pressure end of the T_v line may approach T_c), while the axisymmetric and nonaxisymmetric v vortices were found near T_c.

It is possible that, away from T_c, there exist additional T_v lines of second-order vortex-core transitions, which have not yet been observed with NMR, due to the continuous nature of second-order phase transitions. Therefore the vortices observed far from T_c may in principle differ from those near T_c. Thus whether the observed transition is indeed connected with the breaking of axisymmetry may be determined only by experiments. This seems to be possible, since the additional vortex-core anisotropy in the transverse plane changes the interaction of the vortices with the order parameter in different ways, depending on the type of anisotropy (see Sec. VIII.C).

Since there are so many different possibilities for vortex-core transitions (see also Sec. V.G), one may only be surprised that nature so far has chosen only one of them in rotating superfluid ^{3}He-B.

IX. DISCUSSION

Prior to experiments on the rotating A and B phases of superfluid ^{3}He, it was anticipated that new continuous "coreless" vortices would be found in rotating ^{3}He-A. Vortices in rotating ^{3}He-B had not been considered theoretically in any detail, and it was, in fact, quite commonly believed that the B-phase vortices would be dull in comparison with those in the A phase—simple phase vortices, like those occurring in superfluid ^{4}He, with no particular internal structure and with a normal core.

However, even the first NMR measurements on the rotating B phase revealed a discontinuity in the NMR spectrum, which are attributed to a phase transition in the vortex-core structure (Ikkala, Volovik, Hakonen, Bun'kov, Islander, and Kharadze, 1982). Subsequent measurements indicated that there is a clear discontinuity in the

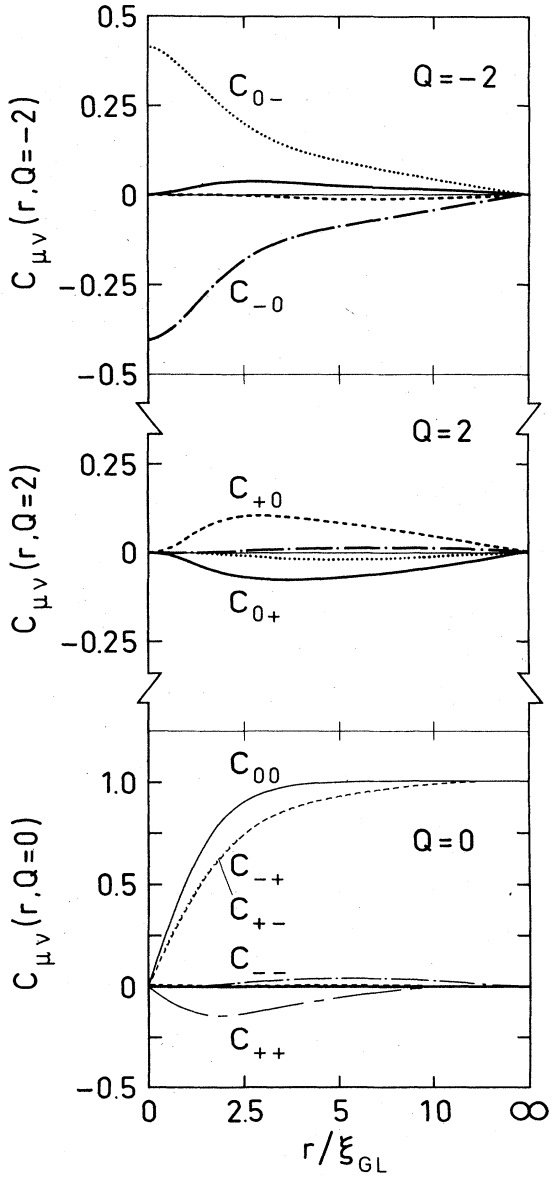

FIG. 55. The metastable nonaxisymmetric vortex in ^{3}He-B. It possesses $|Q|=2$ components with odd $\mu+\nu$ only, in addition to the o-vortex sector with $|Q|=0$. This vortex is *metastable* (i.e., a saddle point or a local minimum) in the whole Ginzburg-Landau regime towards the nonaxisymmetric v vortex, but may become stable far from T_c. It has symmetries PC_4 and TU_2 (Volovik and Salomaa, 1987).

TABLE IV. The vortex symmetry subordination scheme in superfluid ^{3}He-B. Arrows indicate symmetry breaking; P is space parity, TU_2 is time inversion combined with rotation π about a transverse axis, while C_2, C_4, and C_∞ are groups of rotations about the vortex axis by $\pi, \pi/2$, and by an arbitrary angle (axial symmetry).

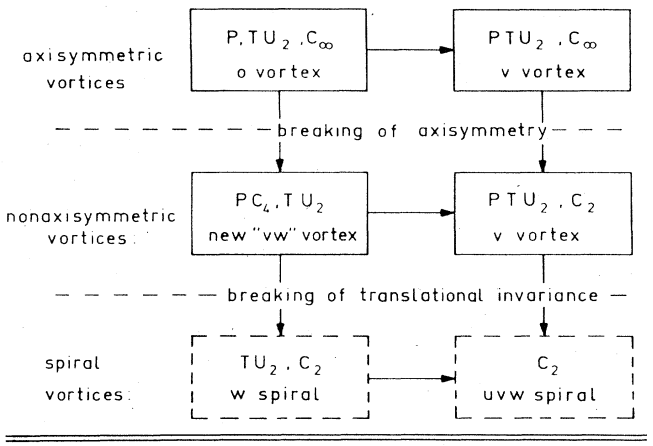

gyromagnetic effect, observed under rotation, that was associated with the vortex-core transition as well. The vortex-core transition was also seen in the gyroscope experiments on persistent currents in ^{3}He-B (Pekola, Simola, Hakonen, Krusius, Lounasmaa, Nummila, Mamniashvili, Packard, and Volovik, 1984; Pekola and Simola, 1985). These observations launched an intensive theoretical effort to explain the experimental discoveries. Indeed, a close collaboration between experiment and theory has been instrumental in identifying the nature of the physical phenomena involved.

From the symmetry analysis, it was realized that it is possible to have five different types of axisymmetric quantized vortex lines in rotating ^{3}He-B, with different internal symmetries. This led to the theoretical discovery of superfluid-core v vortices, with space parity P as the broken discrete vortex symmetry. The gyromagnetic effect detected in the experiment is now known to be associated with the vortex magnetization, which is concentrated in the hard-core vortex matter. It is important to realize that new spontaneously ferromagnetic superfluid phases nucleate in the vortex core, explaining the large magnitude of the vortex-core magnetization and the magnetic anisotropy in the rotating B phase. Though there are several possibilities for different axisymmetric vortices, it was found that the vortex-core transition may be associated with the topological change accompanying the breaking of axisymmetry Q of the v vortex. This can be readily understood in terms of superfluid condensation-energy considerations. The change in the vortex-core magnetization follows from the different superfluid core structures on either side of the phase-transition line.

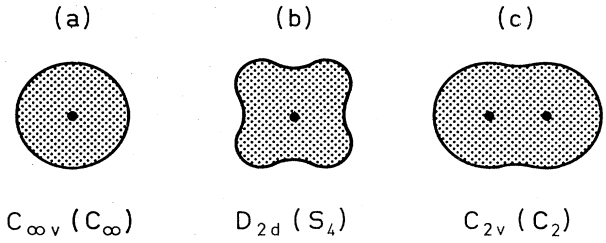

FIG. 56. The form of the cross section for the different vortex cores in ^{3}He-B. Inside the core, boojums on the Fermi surface (zeros of the energy gap for the fermion excitations) appear. At the points indicated, the l vectors of the boojums are parallel to the vortex axis. (a) The axisymmetric v vortex with "round" core. (b) The metastable nonaxisymmetric vortex with "square" core. (c) Nonaxisymmetric "double"-core v vortex: a half-quantum pair.

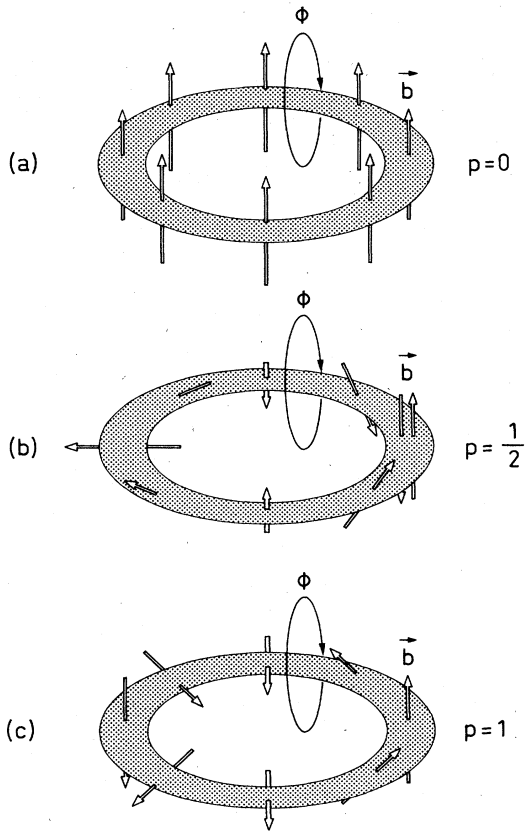

FIG. 57. The vortex ring in ^{3}He-B acquires at low pressures a new topological charge due to breaking of axisymmetry Q in the hard core. The phase Φ winds transverse to the vortex axis. In addition, the winding of the anisotropy axis $\mathbf{b}$ in the cross-sectional plane through the angle $\theta = 2\pi p$ along the vortex ring leads, for example, to rings with charges $p = 0, \frac{1}{2}$, and 1, illustrated here for a vortex ring with hard core possessing C_2 symmetry. In the absence of this symmetry, vortex rings with half-integer spiral index p—like those in (b)—are forbidden, for topological reasons.

For vortex rings ^{3}He-B (see Fig. 57), the broken axisymmetry Q of the v vortices with superfluid core results in a total of three topological invariants: (i) The usual winding of the phase Φ of the order parameter around a path encircling the curved vortex closing on itself to form the ring. (ii) The winding of the vortex-core anisotropy vector $\mathbf{b}$ around a path along the vortex ring through the angle $\theta=2\pi p$, where p denotes an integer index for $|Q|=1$, while p may also assume half-integer values in the case of $|Q|=2$, with the vortex core possessing C_2 symmetry. (iii) A topological charge, not illustrated in Fig. 57, that is analogous to the π_3 homotopy of the A-phase vortex ring (Volovik and Mineev, 1977b; Ho, 1978c); for both the axisymmetric and the nonaxisymmetric v vortices in ^{3}He-B with superfluid core, this charge originates from boojums on the Fermi surface.

The symmetry classification of vortices is useful in a broad context, e.g., for the superfluid A-B-phase boundary, which may exist in six different states and has recently been found to undergo a phase transition during motion (Salomaa, 1987b). Symmetry is even useful in connection with the Abrikosov vortices (Abrikosov, 1957) in ordinary s-wave superconductors—not to mention the vortices in the heavy-fermion systems, where unconventional superconductivity appears to be possible (Stewart, 1984). While the s-wave order parameter tends to zero on the vortex axis, due to a singularity in the phase Φ, the p-wave pairing amplitude necessarily appears in the vortex core if the spin-orbit interaction is taken into account, since there is a linear coupling between these components. Moreover, just as for the new superfluid components of v vortices in ^{3}He-B, this amplitude has no phase winding around the origin, due to the symmetry requirement, and this means that the p-wave pairing amplitude, unlike the conventional s-wave amplitude, is nonzero on the axis of the Abrikosov vortex (see Fig. 58).

In rotating ^{3}He-A, a satellite NMR absorption line was detected during rotation (Hakonen, Ikkala, and Islander, 1982). The finding that the satellite intensity was proportional to the angular velocity of rotation, Ω, and, consequently, to the number density of the quantized vortices, made the identification of the satellite as a vortex effect quite plausible. The intensity and the frequency shift of this "vortex satellite" is only consistent with theoretical calculations made for bound spin-wave modes localized on continuous, doubly quantized "coreless" vortices in the A phase. However, here it is again possible to have several different vortex types, and the observed vortex satellite peak is, in fact, found to be consistent with either of two different continuous vortex textures, with internal symmetries of the v and w types; NMR alone cannot distinguish between these two possibilities, and further experimental work is required in order to identify nonequivocally the continuous vortex textures in the rotating A phase.

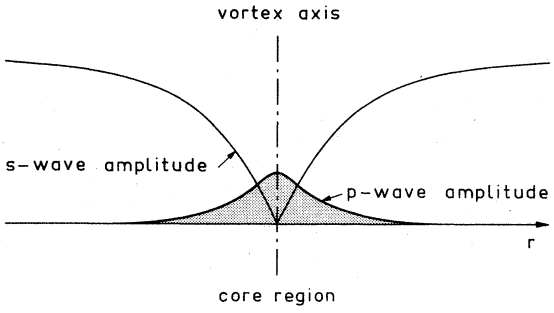

FIG. 58. Schematic illustration of the Abrikosov vortex in an s-wave superconductor in the presence of spin-orbit interaction. The vortex acquires new superconducting p-wave pairing components concentrated in the vortex-core region. These could be observable, in principle, through the modification of the low-temperature specific heat.

Many interesting experiments have yet to be performed on the rotating superfluid A and B phases of ^{3}He, with several different techniques. It would be of great fundamental interest to measure the intrinsic angular momentum in the A phase, and that induced by an external magnetic field in the B phase (see Mineev, 1986, and references therein).

With further applications of the NMR method, one can investigate whether in the A-phase singular vortices will indeed occur in the parallel-plate geometry, as expected. In addition, with NMR one may find the expected transition at a lower temperature from such singular vortices into a lattice of half-quantum vortices. Further NMR experiments on vortices in the rotating B phase should be performed in order to check the suggested nature of the vortex-core transition, i.e., the bifurcation of vorticity associated with the appearance of half-quantum vortices, and to study it at high magnetic fields. In particular, as discussed in Sec. VIII.C.5, the broken rotational symmetry of the vortex line is expected to generate new and experimentally verifiable NMR properties.

An ultrasonic study of vortex textures in the rotating A and B phases is expected to be potentially comparable in its versatility with the NMR method. In the rotating A phase, ultrasound could probe the $\mathbf{l}$ field in the vortex texture (Nakahara, Ohmi, Tsuneto, and Fujita, 1979), in particular, to distinguish between the continuous v and w vortices (Maki and Zotos, 1984). It could also be used to discover the helix predicted in Sec. V.D.4 of the present paper. Provided that one could perform ultrasonic investigations on the half-quantum vortices in the A phase, one might possibly detect the analog of the Aharonov-Bohm effect on the collective modes, mentioned in Sec. V.F.4. Ultrasound spectroscopy of the rotating B-phase textures would be quite interesting as well; one could probe the ^{3}He quasiparticle bound states in the superfluid core vortices. This could yield information about the topology of the superfluid energy gap around the Fermi surface inside the vortex-core region, as well as information on the change in topology of the $\mathbf{n}$ texture due to vortices (Mineev and Volovik, 1984).

First experiments on the mutual friction of vortex lines with the normal excitations of superfluid ^{3}He have been performed at Cornell University (Hall, Gammel, and Rep-

py, 1984). Such measurements are clearly of fundamental interest in both the superfluid A and B phases; the details of the supporting theory of mutual friction in superfluid ^{3}He should be worked out (see Hall and Hook, 1986). An investigation of the friction force due to the creation of the ^{3}He excitations during the vortex motion is also important. The excitations should be created even by moving B-phase vortices because of the gap nodes in the fermionic spectrum in the vortex core. This effect is analogous to the chiral anomaly in quantum field theory, where the chiral current arises under the external fields (see Sec. VIII.D.2). The effect of this chiral anomaly on the vortex dynamics is expected to be pronounced at low enough temperatures, $T \ll T_c$, where this mechanism predominates over the ordinary mutual friction force.

Ion motion also provides a unique microscopic probe for the investigation of vortex textures. While ion trapping by the superfluid core vortices in both phases is expected to be extremely weak (Mineev, 1984; Mineev and Salomaa, 1984), the focusing of ions by the anisotropy of the vortex-core region (Salomaa, 1982; Maki and Zotos, 1984; Salmelin and Salomaa, 1987b) can be employed to study the continuous vortex textures in the A phase (Simola, Nummila, Hirai, Korhonen, Schoepe, and Skrbek, 1986; the anisotropy of the A-phase ion mobility was recently evaluated by Salmelin and Salomaa, 1987a). This may help one to distinguish between vortices with different internal symmetries, since the symmetry determines the focusing properties of the A-phase vortices. Moreover, first experiments suggesting the presence of a new vortex state have been reported (Simola, Skrbek, Nummila, and Korhonen, 1987). This new state is characterized by a high ion mobility along the core. Salmelin and Salomaa (1987b) explain how this high core-phase mobility may be understood, provided the vortices in rotating ^{3}He-A in the new vortex state are singular, and with a superfluid polar-phase core.

Vortex oscillations in rotating superfluid ^{3}He are expected to display a much wider variety than those in superfluid ^{4}He. For example, it would be interesting to observe the Kelvin waves of the w-vortex array in the A phase (Sonin and Fomin, 1985). This would be one of the manifestations of broken parity. The other consequences of broken parity should be investigated as well: spontaneous superflow and electric polarization. In particular, a measurement of the spontaneous superflow in the vortex core at $T \ll T_c$ would confirm the existence of the anomalous current in ^{3}He-A, originating from the chiral anomaly due to the gap nodes (see Sec. V.D.1). Further, the predicted Goldstone oscillation of the "director"-type anisotropy axis of the nonaxisymmetric v vortex in ^{3}He-B could verify the tentative identification of the vortex-core transition discussed in Sec. VIII.B.5. The coherent and random distribution of the vortex anisotropy axis $\mathbf{b}$ may be investigated in transient effects. The half-quantum vortex lattice could exhibit both optical and acoustic modes of vortex oscillations because of the internal structure of the vortex pair, a half-quantum "vortex molecule," which serves as a nontrivial primitive lattice cell.

In addition to the vortex transition observed in the rotating B phase and attributed to a change in the hard-core structure of the quantized vortex lines, one may find several new transitions in both rotating superfluid A and B phases. In ^{3}He-A, it would be interesting to obtain evidence for the occurrence of singular vortices, which can possess three different core regimes, as discussed in Sec. IV.C.4; transitions may occur in each of these different regimes independently of each other. This leads to several new possibilities for vortex-core transitions.

Singular half-quantum vortices may also occur at a lower temperature. Again, the core structures of the half-quantum vortices may undergo phase transitions. For the B-phase vortices, new vortex-core transitions may occur in different regimes of the phase space. In particular, in high magnetic fields there should be a transition in the soft-core structure of the vortex line with the breaking of the rigidity of the vortex asymptotics. New transitions are also possible in the hard-core structure, as is the formation of hedgehogs and monopoles as the intermediate objects in the process of vortex formation and during vortex transitions in ^{3}He-A. Moreover, stable monopoles, which have many features in common with the Dirac and 't Hooft-Polyakov magnetic monopoles, may be observed under rotation at the A-B interface (Salomaa, 1987a).

The novel physical properties of quantized vortex lines in rotating superfluid A and B phases serve to make these structures some of the most interesting objects in condensed-matter physics. In the investigation of the quantized vortices in superfluid ^{3}He, the close interrelationship between experimental efforts and theoretical investigations has been crucially important. While several novel features of the quantized vortex lines in superfluid ^{3}He have already been found—and identified—and interesting new effects have also been predicted, it is to be expected that surprises await us in this system, which displays an unprecedented richness of physical phenomena.

ACKNOWLEDGMENTS

This work has resulted from the project ROTA, which is a joint research effort between the Academy of Finland and the Soviet Academy of Sciences. We are grateful to E. L. Andronikashvili, O. Avenel, P. Berglund, A. S. Borovik-Romanov, D. F. Brewer, Yu. M. Bun'kov, P. L. Gammel, P. J. Hakonen, A. Hirai, O. T. Ikkala, S. T. Islander, J. S. Korhonen, M. Krusius, J. Kyynäräinen, K. K. Nummila, R. E. Packard, J. P. Pekola, J. D. Reppy, P. Roubeau, W. Schoepe, H. Seppälä, J. T. Simola, L. Skrbek, the late J. S. Tsakadze, E. Varoquaux, and the late J. C. Wheatley for useful discussions and their contributions in the experiments and to V. Ambegaokar, P. W. Anderson, G. A. Baym, R. Combescot, A. L. Fetter, I. A. Fomin, A. D. Gongadze, H. E. Hall, J. R. Hook, C.-R. Hu, G. A. Kharadze, I. M. Khalatnikov, N. B. Kopnin, A. J. Leggett, M. Liu, K. Maki, N. D. Mermin, V. P. Mineev, P. Muzikar, S. P. Novikov, T. Ohmi, C. J. Pethick, D. Pines, L. P. Pitaevskii, D. Rainer, R. H. Salmelin,

J. A. Sauls, N. Schopohl, J. W. Serene, H. Smith, É. B. Sonin, D. L. Stein, T. Tsuneto, A. Veselov, D. Vollhardt, G. A. Williams, P. Wölfle, and X. Zotos for theoretical conversations, preprints, and information on their work. In particular, we thank O. V. Lounasmaa for stimulating interest in our work. One of us (M.M.S.) is grateful to the Finnish Academy of Science and Letters for a grant. This research was supported by the Soviet Academy of Sciences, the Commission for Scientific and Technical Collaboration between Finland and the Soviet Union, and by the Academy of Finland.

REFERENCES

Abrikosov, A. A., 1957, "On the magnetic properties of superconductors of the second group," Zh. Eksp. Teor. Fiz. **32**, 1442 [Sov. Phys.—JETP **5**, 1174 (1957)].

Aharonov, Y., and D. Bohm, 1959, "Significance of electromagnetic potentials in the quantum theory," Phys. Rev. **115**, 485.

Ahonen, A. I., M. T. Haikala, M. Krusius, and O. V. Lounasmaa, 1974, "Phase diagram of ^{3}He between 0.7 and 2.5 mK," Phys. Rev. Lett. **33**, 628.

Ambegaokar, V., P. G. de Gennes, and D. Rainer, 1974, "Landau-Ginsburg equations for an anisotropic superfluid," Phys. Rev. A **9**, 2676; **12**, 345(E) (1975).

Ambegaokar, V., and N. D. Mermin, 1973, "Thermal anomalies of He^3: pairing in a magnetic field," Phys. Rev. Lett. **30**, 81.

Anderson, P. W., and W. F. Brinkman, 1973, "Anisotropic superfluidity in ^{3}He-B: a possible interpretation of its stability as a spin-fluctuation effect," Phys. Rev. Lett. **30**, 1108.

Anderson, P. W., and W. F. Brinkman, 1978, "Theory of anisotropic superfluidity in ^{3}He-B," in *The Physics of Liquid and Solid Helium, Part II,* edited by K. H. Bennemann and J. B. Ketterson (Wiley, New York), Chap. 3.

Anderson, P. W., and P. Morel, 1961, "Generalized Bardeen-Cooper-Schrieffer states and the proposed low-temperature phase of liquid He^3," Phys. Rev. **123**, 1911.

Anderson, P. W., and G. Toulouse, 1977, "Phase slippage without vortex cores: vortex textures in superfluid ^{3}He," Phys. Rev. Lett. **38**, 508.

Andreev, A. F., and I. A. Grishchuk, 1984, "Spin nematics," Zh. Eksp. Teor. Fiz. **87**, 467 [Sov. Phys.—JETP **60**, 267 (1984)].

Andronikashvili, E. L., and Yu. G. Mamaladze, 1966, "Quantization of macroscopic motions and hydrodynamics of rotating helium II," Rev. Mod. Phys. **38**, 567.

Balinskiĭ, A. A., G. E. Volovik, and E. I. Kats, 1984, "Disclination symmetry in uniaxial and biaxial nematic liquid crystals," Zh. Eksp. Teor. Fiz. **87**, 1305 [Sov. Phys.—JETP **60**, 748 (1984)].

Balatsky, A. V., G. E. Volovik, and V. Konyshev, 1986, "On the chiral anomaly in superfluid ^{3}He-A," Zh. Eksp. Teor. Fiz. **90**, 2038 [Sov. Phys.—JETP **63**, 1194 (1986)].

Balian, R., and N. R. Werthamer, 1963, "Superconductivity with pairs in a relative p wave," Phys. Rev. **131**, 1553.

Barton, G., and M. A. Moore, 1974a, "Superfluids with $l\neq 0$ Cooper pairs: parametrization of the Landau free energy," J. Phys. C **7**, 2989.

Barton, G., and M. A. Moore, 1974b, "Some p-wave phases of superfluid helium-3 in strong-coupling theory," J. Phys. C **7**, 4220.

Bedell, K., 1982, "Strong-coupling corrections and polarization potentials in superfluid ^{3}He," Phys. Rev. B **26**, 3747.

Blaha, S., 1976, "Quantization rules for point singularities in superfluid ^{3}He and liquid crystals," Phys. Rev. Lett. **36**, 874.

Borovik-Romanov, A. S., Yu. M. Bun'kov, V. V. Dmitriev, and Yu. M. Mukharskiĭ, 1983, "Threshold effects in pulsed NMR in superfluid ^{3}He-B," Pis'ma Zh. Eksp. Teor. Fiz. **37**, 600 [JETP Lett. **37**, 716 (1983)].

Brinkman, W. F., and M. C. Cross, 1978, "Spin and orbital dynamics of superfluid ^{3}He," in *Progress in Low Temperature Physics,* edited by D. F. Brewer (North-Holland, Amsterdam), Vol. VIIA, p. 106.

Brown, E., 1964, "Bloch electrons in a uniform magnetic field," Phys. Rev. **133**, 1038A.

Bruder, C., and D. Vollhardt, 1986, "Symmetry and stationary points of a free energy: the case of superfluid ^{3}He," Phys. Rev. B **34**, 131.

Buchholtz, L. J., 1978, "Dynamic spin behavior of superfluid ^{3}He in the presence of textures," Phys. Rev. B **18**, 1107.

Bun'kov, Yu. M., G. E. Gurgenishvili, M. Krusius, and G. E. Kharadze, 1984, "NMR spectroscopy of rotating superfluid ^{3}He," Usp. Fiz. Nauk. **144**, 141 [Sov. Phys. Usp. **27**, 731 (1984)].

Bun'kov, Yu. M., P. J. Hakonen, and M. Krusius, 1983, in *Quantum Fluids and Solids—1983,* AIP Conference Proceedings No. 103, edited by E. D. Adams and G. G. Ihas (AIP, New York), p. 194.

Bun'kov, Yu. M., M. Krusius, and P. J. Hakonen, 1983, "Texture of superfluid ^{3}He-B rotating in an inclined magnetic field," Pis'ma Zh. Eksp. Teor. Fiz. **37**, 395 [JETP Lett. **37**, 468 (1983)].

Chechetkin, V. R., 1976, "Types of vortex solutions in superfluid He^3," Zh. Eksp. Teor. Fiz. **71**, 1463 [Sov. Phys.—JETP **44**, 766 (1976)].

Combescot, R., 1980, "The Barnett effect in superfluid ^{3}He," Phys. Lett. A **78**, 85.

Combescot, R., and T. Dombre, 1983, "Superfluid current in ^{3}He-A at $T=0$," Phys. Rev. B **28**, 5140.

Combescot, R., and T. Dombre, 1986, "Twisting in superfluid ^{3}He-A and consequences for hydrodynamics at $T=0$," Phys. Rev. B **33**, 79.

Corruccini, L. P., and D. D. Osheroff, 1978, "Pulsed NMR experiments in superfluid ^{3}He," Phys. Rev. B **17**, 126.

Crooker, B. C., B. Hebral, and J. D. Reppy, 1981, "Critical velocity effects in superfluid ^{3}He-B," Physica **108B**, 795.

Cross, M. C., and W. F. Brinkman, 1977, "Textural singularities in the superfluid A phase of ^{3}He," J. Low Temp. Phys. **27**, 683.

de Gennes, P. G., 1973, "Long range distortions in an anisotropic superfluid," Phys. Lett. A **44**, 271.

de Gennes, P. G., 1975, *The Physics of Liquid Crystals* (Clarendon, Oxford).

Dirac, P. A., 1931, "Quantized singularities in the electromagnetic field," Proc. R. Soc. London Ser. A **133**, 60.

Dombre, T., and R. Combescot, 1984, "Excitation spectrum and superfluid density of ^{3}He-A at $T=0$," Phys. Rev. B **30**, 3765.

Fateev, V. A., I. V. Frolov, and A. S. Schwarz, 1979, "Quantum fluctuations of instantons in the nonlinear σ model," Nucl. Phys. B **154**, 1.

Fetter, A. L., 1983, in *Quantum Fluids and Solids—1983,* AIP Conference Proceedings No. 103, edited by E. D. Adams and G. G. Ihas (AIP, New York), p. 229.

Fetter, A. L., 1985, "Magnetic textural deformation in rotating ^{3}He-A," J. Low Temp. Phys. **58**, 545.

Fetter, A. L., 1986, "Vortices in rotating superfluid ^{3}He," in *Progress in Low Temperature Physics,* edited by D. F. Brewer

(North-Holland, Amsterdam), Vol. X, p. 1.
Fetter, A. L., J. A. Sauls, and D. L. Stein, 1983, "Vortices in rotating superfluid ^{3}He-A," Phys. Rev. B **28**, 5061.
Feynman, R. P., 1964, "Application of quantum mechanics to liquid helium," in *Progress in Low Temperature Physics,* edited by C. J. Gorter (North-Holland, Amsterdam), Vol. I, Chap. II.
Fomin, I. A., and V. G. Kamenski, 1982, "Effect of rotation on the NMR signal in the helium-3 A phase," Pis'ma Zh. Eksp. Teor. Fiz. **35**, 241 [JETP Lett. **35**, 302 (1982)].
Fujita, T., M. Nakahara, T. Ohmi, and T. Tsuneto, 1978, "Textures in rotating superfluid ^{3}He-A," Prog. Theor. Phys. **60**, 671.
Fujita, T., and T. Tsuneto, 1975, "Vortex states of superfluid ^{3}He," Prog. Theor. Phys. **53**, 289.
Gammel, P. L., H. E. Hall, and J. D. Reppy, 1984, "Persistent currents in superfluid ^{3}He-B," Phys. Rev. Lett. **52**, 121.
Gammel, P. L., T.-L. Ho, and J. D. Reppy, 1985, "Persistent currents and dissipation in the A and B phases of liquid ^{3}He," Phys. Rev. Lett. **55**, 2708.
Golo, V. L., A. A. Leman, and I. A. Fomin, 1983, "Pulsed NMR in ^{3}He-B for a non-Leggett configuration," Pis'ma Zh. Eksp. Teor. Fiz. **38**, 123 [JETP Lett. **38**, 146 (1983)].
Gongadze, A. D., G. E. Gurgenishvili, and G. A. Kharadze, 1981, "Orienting effect of vortices on the directrix of rotating ^{3}He-B," Fiz. Nizk. Temp. **7**, 821 [Sov. J. Low Temp. Phys. **7**, 397 (1981)].
Gould, C. M., T. J. Bartolac, and H. M. Bozler, 1980, "Experimental studies of solitons in superfluid ^{3}He-A," J. Low Temp. Phys. **39**, 291.
Graham, R., 1974, "Hydrodynamics of ^{3}He in anisotropic A phase," Phys. Rev. Lett. **33**, 1431.
Hakonen, P. J., O. T. Ikkala, and S. T. Islander, 1982, "Experiments on vortices in rotating superfluid ^{3}He-A," Phys. Rev. Lett. **49**, 1258.
Hakonen, P. J., O. T. Ikkala, S. T. Islander, O. V. Lounasmaa, T. K. Markkula, P. Roubeau, K. M. Saloheimo, G. E. Volovik, E. L. Andronikashvili, D. I. Garibashvili, and J. S. Tsakadze, 1982, "NMR experiments on rotating superfluid ^{3}He-A: evidence for vorticity," Phys. Rev. Lett. **48**, 1838.
Hakonen, P. J., O. T. Ikkala, S. T. Islander, O. V. Lounasmaa, and G. E. Volovik, 1983, "NMR experiments on rotating superfluid ^{3}He-A and ^{3}He-B and their theoretical interpretation," J. Low. Temp. Phys. **53**, 425.
Hakonen, P. J., O. T. Ikkala, S. T. Islander, T. K. Markkula, P. Roubeau, K. M. Saloheimo, D. I. Garibashvili, and J. S. Tsakadze, 1981, "ROTAting MINILAB—DESIGN AND PERFORMANCE," Physica B **107**, 567.
Hakonen, P. J., O. T. Ikkala, S. T. Islander, T. K. Markkula, P. M. Roubeau, K. M. Saloheimo, D. I. Garibashvili, and J. S. Tsakadze, 1983, "Rotating nuclear demagnetization refrigerator for experiments on superfluid ^{3}He," Cryogenics **23**, 243.
Hakonen, P. J., M. Krusius, R. H. Salmelin, M. M. Salomaa, J. T. Simola, A. D. Gongadze, G. E. Gurgenishvili, and G. A. Kharadze, 1987, "NMR and textures in rotating superfluid ^{3}He-B. I. Axial field," J. Low Temp. Phys. (in press).
Hakonen, P. J., M. Krusius, M. M. Salomaa, and J. T. Simola, 1987, "NMR and textures in rotating superfluid ^{3}He-B. II. Tilted field," J. Low. Temp. Phys. (in press).
Hakonen, P. J., M. Krusius, M. M. Salomaa, J. T. Simola, Yu. M. Bun'kov, V. P. Mineev, and G. E. Volovik, 1983, "Magnetic vortices in rotating superfluid ^{3}He-B," Phys. Rev. Lett. **51**, 1362.
Hakonen, P. J., M. Krusius, and H. K. Seppälä, 1985, "NMR studies on vortices in rotating ^{3}He-A," J. Low Temp. Phys. **60**, 187.
Hakonen, P. J., and G. E. Volovik, 1982, "On textures and spin waves in rotating superfluid ^{3}He-B at high magnetic fields," J. Phys. C **15**, L1277.
Hall, H. E., P. L. Gammel, and J. D. Reppy, 1984, "Superfluid dissipation in rotating ^{3}He-B," Phys. Rev. Lett. **52**, 1701.
Hall, H. E., and J. R. Hook, 1986, "The hydrodynamics of superfluid ^{3}He," in *Progress in Low Temperature Physics,* edited by D. F. Brewer (North-Holland, Amsterdam), Vol. IX, p. 143.
Hasegawa, Y., 1985, "On vortex in superfluid ^{3}He-B," Prog. Theor. Phys. **73**, 1258.
Ho, T.-L., 1978a, "Continuous creation and annihilation of coreless vortices in ^{3}He-A in the presence of a heat flow," Phys. Rev. Lett. **41**, 1473.
Ho, T.-L., 1978b, "The screening effect and nucleation of coreless vortices in superfluid ^{3}He-A in stationary and rotating containers," J. Phys. (Paris) **39**, C6-21.
Ho, T.-L., 1978c, "Coreless vortices in superfluid ^{3}He-A: topological structure, nucleation, and the screening effect," Phys. Rev. B **18**, 1144.
Hu, C.-R., P. Kumar, and K. Maki, 1977, USC Physics preprint.
Hu, C.-R., and K. Maki, 1987, "Satellite magnetic resonances of a bound pair of half-quantum vortices in rotating superfluid ^{3}He-A," USC Physics preprint.
Ikkala, O. T., G. E. Volovik, P. J. Hakonen, Yu. M. Bun'kov, S. T. Islander, and G. A. Kharadze, 1982, "NMR in rotating superfluid ^{3}He-B," Pis'ma Zh. Eksp. Teor. Fiz. **35**, 338 [JETP Lett. **35**, 416 (1982)].
Israelsson, U. E., B. C. Crooker, H. M. Bozler, and C. M. Gould, 1984, "Phase diagram of superfluid ^{3}He-A_1," Phys. Rev. Lett. **53**, 1943; **54**, 254(E) (1985).
Jacobsen, K. W., and H. Smith, 1983, "Textures and spin waves in rotating superfluid ^{3}He-B," J. Low Temp. Phys. **52**, 527.
Khazan, M. V., 1985, "The analog of Aharonov-Bohm's effect in superfluid ^{3}He-A," Pis'ma Zh. Eksp. Teor. Fiz. **41**, 396 [JETP Lett. **41**, 486 (1985)].
Khlopov, M. Yu., and S. Obukhov, 1982, private communication.
Kléman, M., 1983, *Points, Lines and Walls in Liquid Crystals, Magnetic Systems and Various Ordered Media* (Wiley, New York).
Landau, L. D., and E. M. Lifshitz, 1980, *Statistical Physics, Part 1* (Pergamon, Oxford).
Landau, L. D., and E. M. Lifshitz, 1984, *Electrodynamics of Continuous Media,* 2nd ed. (Pergamon, Oxford).
Lee, D. M., and R. C. Richardson, 1978, "Superfluid ^{3}He," in *The Physics of Liquid and Solid Helium, Part II,* edited by K. H. Bennemann and J. B. Ketterson (Wiley, New York), Chap. 4.
Leggett, A. J., 1973, "NMR lineshifts and spontaneously broken spin-orbit symmetry: I. General concepts," J. Phys. C **6**, 3187.
Leggett, A. J., 1974, "The spin dynamics of an anisotropic Fermi superfluid (^{3}He?)," Ann. Phys. (N.Y.) **85**, 11.
Leggett, A. J., 1975, "A theoretical description of the new phases of liquid ^{3}He," Rev. Mod. Phys. **47**, 331; **48**, 357(E) (1976).
Leggett, A. J., 1977, "Superfluid ^{3}He-A is a liquid ferromagnet," Nature **270**, 585.
Leggett, A. J., 1984, "Nucleation of ^{3}He-B from the A phase: A cosmic-ray effect," Phys. Rev. Lett. **53**, 1096.
Leggett, A. J., and S. Takagi, 1978, "Orientational dynamics of superfluid ^{3}He: a 'Two-fluid' model. II. Orbital dynamics,"

Ann. Phys. (N.Y.) **110**, 353.
Levin, K., and O. T. Valls, 1983, "Phenomenological theories of liquid ^{3}He," Phys. Rep. **98**, 1.
Liu, M., 1979, "Broken relative symmetry and the dynamics of the A_1 phase of ^{3}He," Phys. Rev. Lett. **43**, 1740.
Liu, M., 1982, "Broken relative symmetry and the hydrodynamics of superfluid ^{3}He," Physica B **109+110**, 1615.
Liu, M., and M. C. Cross, 1978, "Broken spin-orbit symmetry in superfluid ^{3}He and *B*-phase dynamics," Phys. Rev. Lett. **41**, 250.
Lounasmaa, O. V., 1974a, "The superfluid phases of liquid ^{3}He," Contemp. Phys. **15**, 353.
Lounasmaa, O. V., 1974b, "^{3}He-two superfluid phases," Europhys. News **5**, No. 10, p. 1.
Lounasmaa, 1974c, *Experimental Principles and Methods Below 1 K* (Academic, London).
Maki, K., 1978, "Planar textures in superfluid ^{3}He-*A*," J. Low. Temp. Phys. **32**, 1.
Maki, K., 1986, "Comment on half-quantum vortices in superfluid ^{3}He-*A*," Phys. Rev. Lett. **56**, 1312.
Maki, K., and R. Combescot, 1985, "^{3}He-*A* textures and the ultrasonic attenuation," Phys. Rev. Lett. **54**, 2257.
Maki, K., and P. Kumar, 1977, "Composite solitons and magnetic resonances in superfluid ^{3}He-*A*," Phys. Rev. B **16**, 182.
Maki, K., and M. Nakahara, 1983, "Spin waves in superfluid ^{3}He-*B* in a rotating cylinder," Phys. Rev. B **27**, 4181.
Maki, K., and X. Zotos, 1984, "Sound attenuation of vortex state in rotating superfluid ^{3}He-*A*," USC Physics preprint.
Maki, K., and X. Zotos, 1985a, "Vortex-pair state in rotating superfluid ^{3}He-*A* at low temperatures," Phys. Rev. B **31**, 177.
Maki, K., and X. Zotos, 1985b, "Vortex pairs in rotating ^{3}He-*A* in a tilted magnetic field," Phys. Rev. B **31**, 3116.
Mermin, N. D., 1977, "Surface singularities and superflow in ^{3}He-*A*," in *Quantum Fluids and Solids,* edited by S. B. Trickey, E. D. Adams, and J. W. Dufty (Plenum, New York), p. 3.
Mermin, N. D., 1979, "The topological theory of defects in ordered media," Rev. Mod. Phys. **51**, 591.
Mermin, N. D., and T.-L. Ho, 1976, "Circulation and angular momentum in the *A* phase of superfluid helium-3," Phys. Rev. Lett. **36**, 594; **36**, 832(E).
Mermin, N. D., and D. M. Lee, 1976, "Superfluid helium 3," Sci. Am. **235** (No. 6), 56.
Mermin, N. D., and G. Stare, 1974, "*p*-wave models for the *A* phase of superfluid helium-3," Materials Science Center, Cornell University, Report No. 2186.
Mermin, N. D., and G. Stare, 1977, "*p*-wave models for the *A* phase of superfluid helium-3," in *Sverkhtekuchest' Geliya-3,* edited by I. M. Khalatnikov (Mir, Moscow), p. 121.
Michel, L., 1980, "Symmetry defects and broken symmetry. Configurations. Hidden symmetry," Rev. Mod. Phys. **52**, 617.
Mineev, V. P., 1980, "Topologically stable defects and solitons in ordered media," in *Soviet Scientific Reviews,* Section A: Physics Reviews, Volume 2, edited by I. M. Khalatnikov (Harwood Academic, Chur, Switzerland), p. 173.
Mineev, V. P., 1983, "Superfluid ^{3}He: introduction to the subject," Usp. Fiz. Nauk. **139**, 303 [Sov. Phys. Usp. **26**, 160 (1983)].
Mineev, V. P., 1984, "Exchange interaction of positive ions with vortices in ^{3}He-*B*," Pis'ma Zh. Eksp. Teor. Fiz. **39**, 301 [JETP Lett. **39**, 361 (1984)].
Mineev, V. P., 1986, "Angular momentum in superfluid ^{3}He-*B* under a magnetic field," Zh. Eksp. Teor. Fiz. **90**, 1236 [Sov. Phys.—JETP **63**, 721 (1986)].
Mineev, V. P., and M. M. Salomaa, 1984, "Interaction of negative ions with vortices in superfluid ^{3}He-*B*," J. Phys. C **17**, L181.
Mineev, V. P., M. M. Salomaa, and O. V. Lounasmaa, 1986, "Superfluid ^{3}He in rotation," Nature **324**, 333.
Mineev, V. P., and G. E. Volovik, 1978, "Planar and linear solitons in superfluid ^{3}He," Phys. Rev. B **18**, 3197.
Mineev, V. P., and G. E. Volovik, 1984, "Texture induced splitting of the collective modes in ^{3}He-*B*," Physica B **126**, 453.
Muzikar, P., 1978, "The internal structure of a de Gennes disgyration in ^{3}He-*A*," J. Phys. (Paris) **39**, C6-53.
Muzikar, P., 1979, "Energies of line singularities in ^{3}He-*A*," J. Low Temp. Phys. **36**, 225.
Nakahara, M., T. Ohmi, T. Tsuneto, and T. Fujita, 1979, "Detectability of vortex lattice in rotating superfluid ^{3}He-*A*," Prog. Theor. Phys. **62**, 874.
Ohmi, T., 1984, "Vortex lattice structure of superfluid ^{3}He-*A* in a magnetic field," J. Low Temp. Phys. **56**, 183.
Ohmi, T., T. Tsuneto, and T. Fujita, 1983, "Core structure of vortex line in ^{3}He-*B*," Prog. Theor. Phys. **70**, 647.
Osheroff, D. D., 1977, "Textural spin waves in ^{3}He-*B*," Physica B **90**, 20.
Osheroff, D. D., R. C. Richardson, and D. M. Lee, 1972, "Evidence for a new phase of solid ^{3}He," Phys. Rev. Lett. **28**, 885.
Paalanen, M. A., and D. D. Osheroff, 1980, "Dissipation of flow in superfluid ^{3}He-*A*," Phys. Rev. Lett. **45**, 362.
Packard, R. E., 1982, "Vortex photography in liquid helium," Physica B **109+110**, 1474.
Passvogel, T., N. Schopohl, and L. Tewordt, 1983, "Structure of isolated vortex lines in rotating ^{3}He-*A* and ^{3}He-*B*," J. Low Temp. Phys. **50**, 509.
Passvogel, T., L. Tewordt, and N. Schopohl, 1984, "Stability, orientational effects, and temperature dependence of nonunitary vortex structures in superfluid ^{3}He," J. Low Temp. Phys. **56**, 383.
Paulson, D. N., and J. C. Wheatley, 1978, "Evidence for electronic ferromagnetism in superfluid ^{3}He-*A*," Phys. Rev. Lett. **40**, 557.
Peierls, R. L., 1933, "Zur theorie des diamagnetismus von leitungselektronen," Z. Phys. **80**, 763.
Pekola, J. P., and J. T. Simola, 1985, "Persistent currents in superfluid ^{3}He," J. Low Temp. Phys. **58**, 555.
Pekola, J. P., J. T. Simola, P. J. Hakonen, M. Krusius, O. V. Lounasmaa, K. K. Nummila, G. Mamniashvili, R. E. Packard, and G. E. Volovik, 1984, "Phase diagram of the first-order vortex-core transition in superfluid ^{3}He-*B*," Phys. Rev. Lett. **53**, 584.
Pekola, J. P., J. T. Simola, K. K. Nummila, O. V. Lounasmaa, and R. E. Packard, 1984, "Persistent-current experiments on superfluid ^{3}He-*B* and ^{3}He-*A*," Phys. Rev. Lett. **53**, 70.
Salam, A., 1968, "Weak and electromagnetic interactions," in *Elementary Particle Theory,* edited by N. Svartholm (Almquist and Wiksell, Stockholm), p. 367.
Salmelin, R. H., and M. M. Salomaa, 1987a, "Anisotropy of ion mobility and the superfluid energy gap in ^{3}He-*A*," J. Phys. C Lett. (in press).
Salmelin, R. H., and M. M. Salomaa, 1987b, "Ion mobility along superfluid vortices with polar core in ^{3}He-*A*," J. Phys. C Lett. (in press).
Salomaa, M. M., 1982, "The mobility of negative ions in superfluid ^{3}He," Contemp. Phys. **23**, 169.
Salomaa, M. M., 1987a, "Monopoles in the rotating superfluid helium-3 *A-B* interface," Nature **326**, 367.
Salomaa, M. M., 1987b, "A phase transition of the moving superfluid ^{3}He *A-B* interface," Helsinki University of Tech-

nology Report TKK-F-A606.
Salomaa, M. M., and G. E. Volovik, 1983a, in *Quantum Fluids and Solids—1983,* AIP Conference Proceedings No. 103, edited by E. D. Adams and G. G. Ihas (AIP, New York), p. 210.
Salomaa, M. M., and G. E. Volovik, 1983b, "Vortices with ferromagnetic superfluid core in ^{3}He-*B*," Phys. Rev. Lett. **51**, 2040.
Salomaa, M. M., and G. E. Volovik, 1984, "Response to comment on vortices with ferromagnetic superfluid core in ^{3}He-*B*," Phys. Rev. Lett. **52**, 2008.
Salomaa, M. M., and G. E. Volovik, 1985a, "Symmetry and structure of quantized vortices in superfluid ^{3}He-*B*," Phys. Rev. B **31**, 203.
Salomaa, M. M., and G. E. Volovik, 1985b, "Classification of axisymmetric vortices in ^{3}He-*A*," Phys. Rev. Lett. **54**, 2127.
Salomaa, M. M., and G. E. Volovik, 1985c, "Half-quantum vortices in superfluid ^{3}He-*A*," Phys. Rev. Lett. **55**, 1184.
Salomaa, M. M., and G. E. Volovik, 1986a, "Vortices with spontaneously broken axisymmetry in ^{3}He-*B*," Phys. Rev. Lett. **56**, 363.
Salomaa, M. M., and G. E. Volovik, 1986b, "Reply to comment on half-quantum vortices in superfluid ^{3}He-*A*," Phys. Rev. Lett. **56**, 1313.
Salomaa, M. M., and G. E. Volovik, 1986c, "Topological transition of v-vortex core matter in superfluid ^{3}He-*B*," Europhys. Lett. **2**, 781.
Sauls, J. A., and J. W. Serene, 1981, "Potential-scattering models for the quasiparticle interactions in liquid ^{3}He," Phys. Rev. B **24**, 183.
Sauls, J. A., D. L. Stein, and J. W. Serene, 1982, "Magnetic vortices in a rotating $^3P_2$ neutron superfluid," Phys. Rev. D **25**, 967.
Schwarz, A. S., 1982, "Field theories with no local conservation of the electric charge," Nucl. Phys. B **208**, 141.
Seppälä, H. K., P. J. Hakonen, M. Krusius, T. Ohmi, M. M. Salomaa, J. T. Simola, and G. E. Volovik, 1984, "Continuous vortices with broken symmetry in rotating superfluid ^{3}He-*A*," Phys. Rev. Lett. **52**, 1802.
Seppälä, H. K., and G. E. Volovik, 1983, "Evidence for nonsingular vorticity in the Helsinki experiments on rotating ^{3}He-*A*," J. Low Temp. Phys. **51**, 279.
Simola, J. T., K. K. Nummila, A. Hirai, J. S. Korhonen, W. Schoepe, and L. Skrbek, 1986, "Focusing of negative ions by continuous vortices in rotating ^{3}He-*A*," Phys. Rev. Lett. **57**, 1923.
Simola, J. T., L. Skrbek, K. K. Nummila, and J. S. Korhonen, 1987, "Two different vortex states in rotating ^{3}He-*A* observed by use of negative ions," Phys. Rev. Lett. **58**, 904.
Soda, T., and Y. Shiwa, 1978, in *Physics at Ultralow Temperatures,* proceedings of the International Symposium at Hakone, Japan, 1977, edited by T. Sugawara, S. Nakajima, T. Ohtsuka, and T. Usui (Physical Society of Japan, Tokyo), p. 150.
Soni, V., 1978, "Monopole-antimonopole pairs of fixed angular momentum in superfluid ^{3}He-*A*," Phys. Rev. B **18**, 6076.
Sonin, É. B., 1983, "Orientational phase transition near a vortex in ^{3}He-*B*," Pis'ma Zh. Eksp. Teor. Fiz. **38**, 11 [JETP Lett. **38**, 11 (1983)].
Sonin, É. B., 1984, "The orientational phase transition at a vortex in ^{3}He-*B*," J. Low Temp. Phys. **55**, 533.
Sonin, É, B., 1987, "Vortex oscillations and hydrodynamics of rotating superfluids," Rev. Mod. Phys. **59**, 87.
Sonin, É. B., and N. V. Fomin, 1985, "Symmetry of vortex structures, axial currents, and Kelvin waves in superfluid ^{3}He," Pis'ma Zh. Eksp. Teor. Fiz. **42**, 185 [JETP Lett. **42**, 229 (1985)].
Spencer, G. F., and G. G. Ihas, 1982, "Texture of superfluid ^{3}He-*B* in a large cylindrical geometry near T_c," Phys. Rev. Lett. **48**, 1118.
Stewart, G. R., 1984, "Heavy-fermion systems," Rev. Mod. Phys. **56**, 755.
Swift, J. W., J. P. Eisenstein, and R. E. Packard, 1980, "Measurement of the anisotropy in the dielectric constant of ^{3}He-*A*," Phys. Rev. Lett. **45**, 1955.
Theodorakis, S., and A. L. Fetter, 1983, "Vortices and NMR in rotating ^{3}He-*B*," J. Low Temp. Phys. **52**, 559.
Thuneberg, E. V., 1986a, "Surfaces of superfluid ^{3}He-*B*," Phys. Rev. B **33**, 5124.
Thuneberg, E. V., 1986b, "Identification of vortices in superfluid ^{3}He-*B*," Phys. Rev. Lett. **56**, 359.
Toulouse, G., and M. Kléman, 1976, "Principles of a classification of defects in ordered media," J. Phys. (Paris) Lett. **37**, L-149.
Trebin, H.-R., 1982, "The topology of non-uniform media in condensed matter physics," Adv. Phys. **31**, 195.
Tsuneto, T., T. Ohmi, and T. Fujita, 1978, in *Physics at Ultralow Temperatures,* proceedings of the International Symposium at Hakone, Japan, 1977, edited by T. Sugawara, S. Nakajima, T. Ohtsuka, and T. Usui (Physical Society of Japan, Tokyo), p. 153.
Vilenkin, A., 1985, "Cosmic strings and domain walls," Phys. Rep. **121**, 263.
Vinen, W. F., 1961, "Vortex lines in liquid helium II," in *Progress in Low Temperature Physics,* edited by C. J. Gorter (North-Holland, Amsterdam), Vol. III, Chap. I.
Volovik, G. E., 1984a, "Spontaneous electrical polarization of vortices in superfluid ^{3}He," Pis'ma Zh. Eksp. Teor. Fiz. **39**, 169 [JETP Lett. **39**, 200 (1984)].
Volovik, G. E., 1984b, "Superfluid properties of ^{3}He-*A*," Usp. Fiz. Nauk **143**, 73 [Sov. Phys. Usp. **27**, 363 (1984)].
Volovik, G. E., 1985, "Normal Fermi liquid in a superfluid ^{3}He-*A* at $T=0$ and the anomalous current," Pis'ma Zh. Eksp. Teor. Fiz. **42**, 294 [JETP Lett. **42**, 363 (1985)].
Volovik, G. E., 1986a, "Chiral anomaly and momentum conservation law in ^{3}He-*A*," Pis'ma Zh. Eksp. Teor. Fiz. **43**, 428 [JETP Lett. **43**, 551 (1986)].
Volovik, G. E., 1986b, "Superfluid ^{3}He-*A* and the electroweak interaction," Pis'ma Zh. Eksp. Teor. Fiz. **43**, 535 [JETP Lett. **43**, 693 (1986)].
Volovik, G. E., 1986c, "The Wess-Zumino action for orbital dynamics of ^{3}He-*A*," Pis'ma Zh. Eksp. Teor. Fiz. **44**, 144 [JETP Lett. **44**, 185 (1986)].
Volovik, G. E., 1986d, "Analog of gravity in superfluid ^{3}He-*A*," Pis'ma Zh. Eksp. Teor. Fiz. **44**, 388 [JETP Lett. **44**, 498 (1986)].
Volovik, G. E., and P. J. Hakonen, 1981, "Vortices in ^{3}He-*A* in a weak magnetic field," J. Low Temp. Phys. **42**, 503.
Volovik, G. E., and N. B. Kopnin, 1977, "Rotating ^{3}He-*A*," Pis'ma Zh. Eksp. Teor. Fiz. **25**, 26 [JETP Lett. **25**, 22 (1977)].
Volovik, G. E., and V. P. Mineev, 1976a, "Vortices with free ends in superfluid He^3-*A*," Pis'ma Zh. Eksp. Teor. Fiz. **23**, 647 [JETP Lett. **23**, 593 (1976)].
Volovik, G. E., and V. P. Mineev, 1976b, "Line and point singularities in superfluid ^{3}He," Pis'ma Zh. Eksp. Teor. Fiz. **24**, 605 [JETP Lett. **24**, 561 (1976)].
Volovik, G. E., and V. P. Mineev, 1977a, "Investigation of singularities in superfluid He^3 and in liquid crystals by the homotopic topology methods," Zh. Eksp. Teor. Fiz. **72**, 2256 [Sov. Phys.—JETP **45**, 1186 (1977)].

Volovik, G. E., and V. P. Mineev, 1977b, "Particle-like solitons in superfluid ^{3}He phases," Zh. Eksp. Teor. Fiz. **73**, 767 [Sov. Phys.—JETP **46**, 401 (1977)].

Volovik, G. E., and V. P. Mineev, 1981, "Orbital angular momentum and orbital dynamics: ^{3}He-A and the Bose liquid," Zh. Eksp. Teor. Fiz. **81**, 989 [Sov. Phys.—JETP **54**, 524 (1981)].

Volovik, G. E., and V. P. Mineev, 1982, "Current in superfluid Fermi liquids and the structure of vortex cores," Zh. Eksp. Teor. Fiz. **83**, 1025 [Sov. Phys.—JETP **56**, 579 (1982)].

Volovik, G. E., and V. P. Mineev, 1983, "Orbital angular momentum in B phase of ^{3}He and its effect on the texture in a rotating vessel," Pis'ma Zh. Eksp. Teor. Fiz. **37**, 103 [JETP Lett. **37**, 127 (1983)].

Volovik, G. E., and V. P. Mineev, 1984, "Gyromagnetism of Cooper pairs in superfluid ^{3}He-B," Zh. Eksp. Teor. Fiz. **86**, 1667 [Sov. Phys.—JETP **59**, 972 (1984)].

Volovik, G. E., and M. M. Salomaa, 1985a, "Vortices with half-integer number of circulation quanta in superfluid ^{3}He-A," Zh. Eksp. Teor. Fiz. **88**, 1656 [Sov. Phys.—JETP **61**, 986 (1985)].

Volovik, G. E., and M. M. Salomaa, 1985b, "Spontaneous breaking of axial symmetry in the v vortices in superfluid ^{3}He-B," Pis'ma Zh. Eksp. Teor. Fiz. **42**, 421 [JETP Lett. **42**, 521 (1985)].

Volovik, G. E., and M. M. Salomaa, 1987, "On the metastable vortex in superfluid ^{3}He-B," Pis'ma Zh. Eksp. Teor. Fiz. **45**, 44 [JETP Lett. **45**, 56 (1987)].

Vulovic, V. Z., D. L. Stein, and A. L. Fetter, 1984, "NMR of textures in rotating ^{3}He-A," Phys. Rev. B **29**, 6090.

Weinberg, S., 1967, "A model of leptons," Phys. Rev. Lett. **19**, 1264.

Wheatley, J. C., 1975, "Experimental properties of superfluid ^{3}He," Rev. Mod. Phys. **47**, 415.

Williams, M. R., 1979, "The unusual hydrodynamics of the A-phase of helium three," Ph. D. thesis (Stanford University).

Williams, M. R., and A. L. Fetter, 1979, "Textures in slowly rotating ^{3}He-A," Phys. Rev. B **20**, 169.

Wölfe, P., 1973, "Soundlike collective excitations in superfluid ^{3}He," Phys. Rev. Lett. **31**, 1437.

Wölfe, P., 1977, "Collisionless collective modes in superfluid ^{3}He," Physica B **90**, 96.

Wölfe, P., 1979, "Low-temperature properties of liquid ^{3}He," Rep. Prog. Phys. **42**, 269.

Wölfe, P., and D. Vollhardt, 1987, *The Superfluid Phases of ^{3}He* (Taylor and Francis, London), in press.

Zak, J., 1964a, "Magnetic translation group," Phys. Rev. **134**, 1602A.

Zak, J., 1964b, "Magnetic translation group. II. Irreducible representations," Phys. Rev. **134**, 1607A.

Zel'dovich, Ya. B., I. Yu. Kobzarev, and L. B. Okun, 1974, "Cosmological consequences of a spontaneous breakdown of a discrete symmetry," Zh. Eksp. Teor. Fiz. **67**, 3 [Sov. Phys.—JETP **40**, 1 (1974)].

Zotos, X., and K. Maki, 1984a, "Analytic vortices and magnetic resonances in rotating superfluid ^{3}He-A. III," Phys. Rev. B **30**, 145.

Zotos, X., and K. Maki, 1984b, "Vortex states in rotating ^{3}He-A in a weak magnetic field," USC Physics preprint No. 84/034.

Zurek, W. H., 1985, "Cosmological experiments in superfluid helium?" Nature **317**, 505.

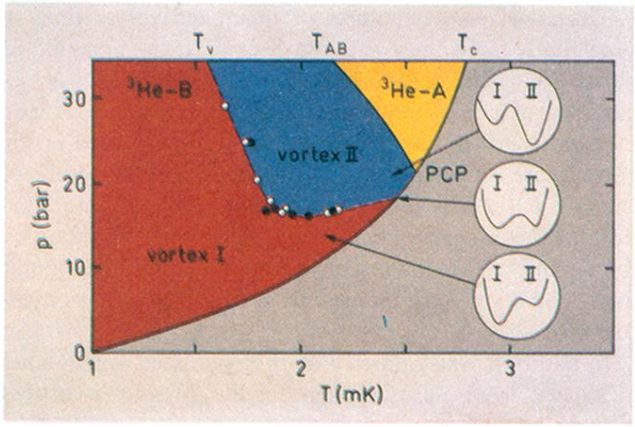

FIG. 1. Phase diagram of ^{3}He (Ahonen, Haikala, Krusius, and Lounasmaa, 1974). The intersection of the T_{AB} curve, separating the A and B phases, and the T_c curve is called the polycritical point (PCP). When superfluid ^{3}He-B was rotated in an open-volume NMR cell, a first-order vortex-core transition was observed (Ikkala, Volovik, Hakonen, Bun'kov, Islander, and Kharadze, 1982) upon crossing the dashed T_v line in the (p,T) plane. ○, $H=284$ G; ●, $H=568$ G. Note that at high pressures the core-transition temperature is roughly parallel to the A-B transition, but curves towards T_c below the polycritical pressure (Pekola, Simola, Hakonen, Krusius, Lounasmaa, Nummila, Mamniashvili, Packard, and Volovik, 1984). The first-order vortex-core transition can possibly be associated with two distinct vortex free-energy minima, illustrated schematically in the insets and identified tentatively in Fig. 54.

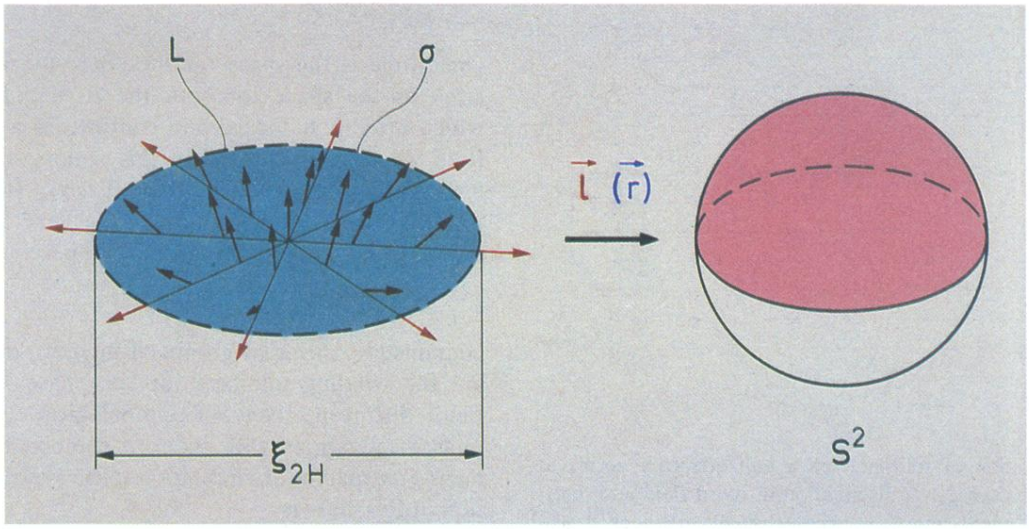

FIG. 10. Topology of the continuous Mermin-Ho (MH) vortex texture in the l-vector field (arrows) can be studied in the order-parameter space S^2 through the mapping $l(\mathbf{r})$ of the cross section of the MH texture onto the "northern" half of the unit sphere.

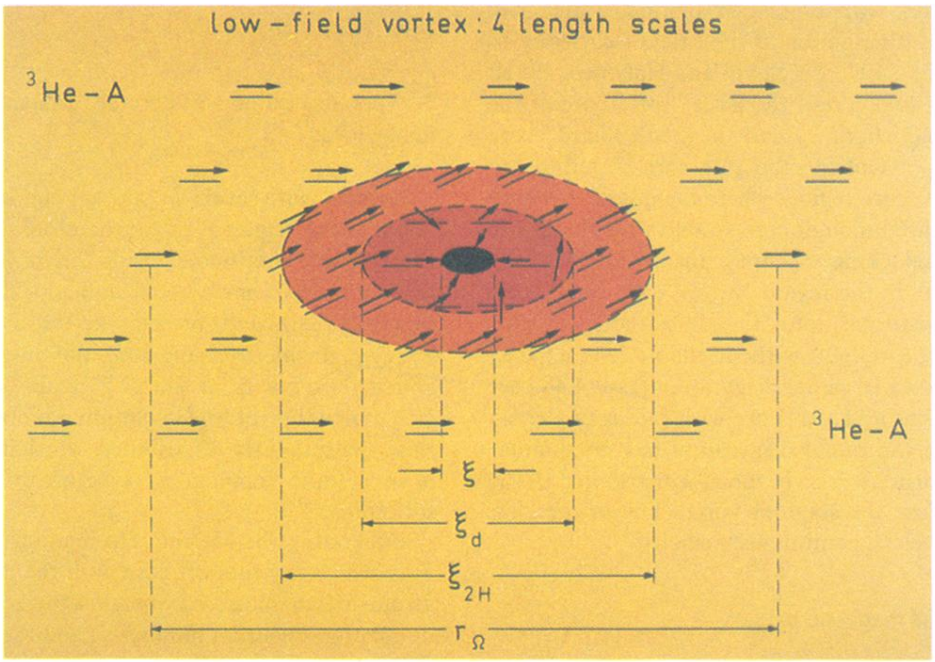

FIG. 11. Schematic illustration of the three cores of the singular ^{3}He-A vortex in a low magnetic field. Arrows indicate the $\boldsymbol{l}$-vector distribution, while the **d**-vector field is denoted by lines without arrowhead. In the outer soft-core region $\xi_d < r < \xi_{2H}$, the $\boldsymbol{l}$ and **d** vectors are dipole locked, but may deviate from the plane. For $\xi < r < \xi_d$, the **d** field remains constant, while the $\boldsymbol{l}$ field produces the unwinding of phase and forms a singularity at $r \sim \xi$ (hard core). Inside this hard vortex core, $r < \xi$, the superfluid A-phase pairing state is broken, and pairing into new superfluid phases results, thereby resolving the $\boldsymbol{l}$-field singularity. The vortex-lattice constant is r_Ω. (Here ξ means ξ_{GL}.)

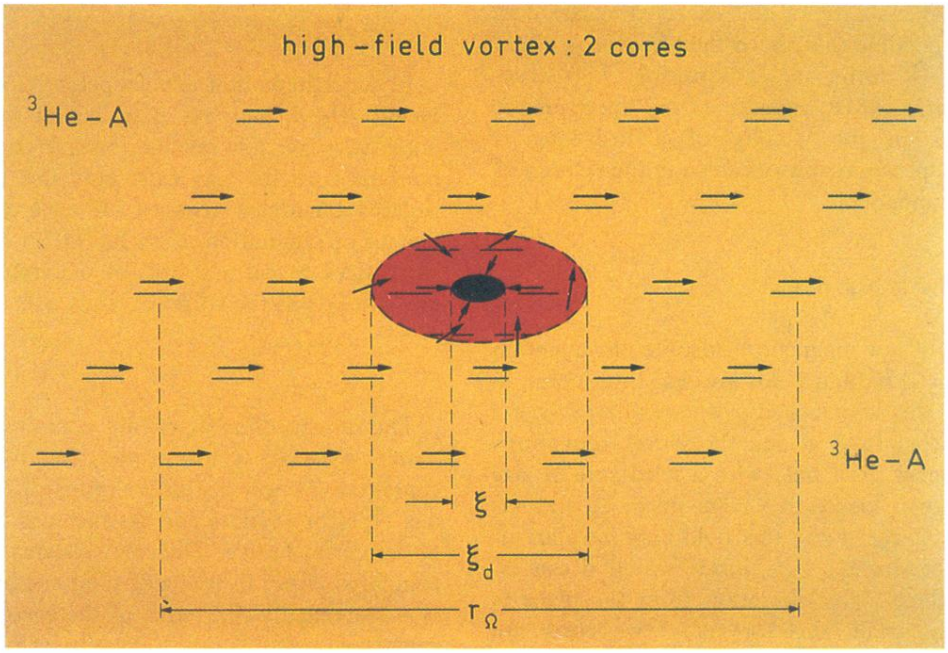

FIG. 14. The singular one-quantum vortex in ^{3}He-A in a high magnetic field. Compare with the three-core structure in Fig. 11 (notations are the same in both figures). The region between ξ_d and ξ_{2H} is absent in high fields: only the dipole-unlocked soft core remains.

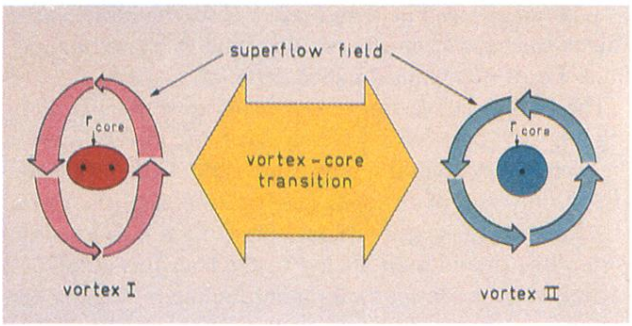

FIG. 2. Tentative identification of the two free-energy minima involved in the vortex-core transition of Fig. 1. At low pressures the nonaxisymmetric v vortex I with axi-planar core provides the free-energy minimum, while at high pressures the axisymmetric v vortex II with A-phase core becomes more advantageous. Circulation quantization escapes from real $\mathbf{r}$ space into momentum $\mathbf{k}$ space at the hard-core radius r_{core}. The axisymmetric v vortex has a round core, while the nonaxisymmetric v-vortex core is a "molecule," consisting of two half-quantum vortices. The vortex-core transition is a topological change between two inequivalent ways of accommodating vorticity (Volovik and Mineev, 1982; Salomaa and Volovik, 1986c). See Figs. 53 and 54.

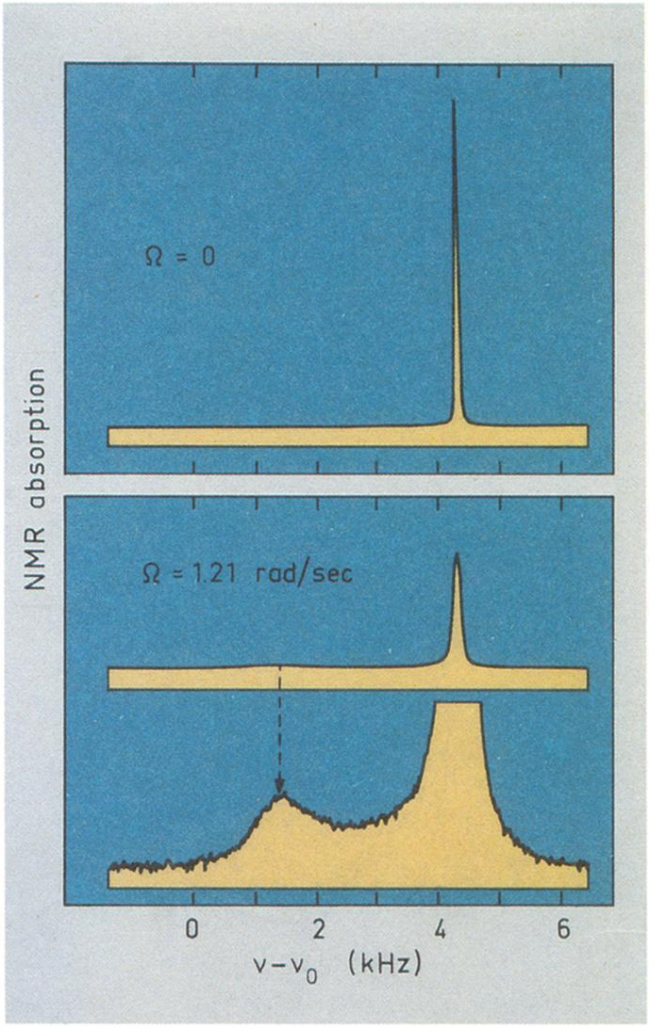

FIG. 26. Experimental NMR spectra of stationary and rotating ^{3}He-A (Hakonen, Ikkala, and Islander, 1982). The additional broadening of the main peak, due to rotation, is clearly apparent; the shift of this peak towards higher frequencies from the Larmor frequency is related to the spin-orbit coupling. The small satellite absorption peak, which appears in the NMR signal during rotation, is caused by the excitation of localized spin waves trapped by the continuous vortex textures.

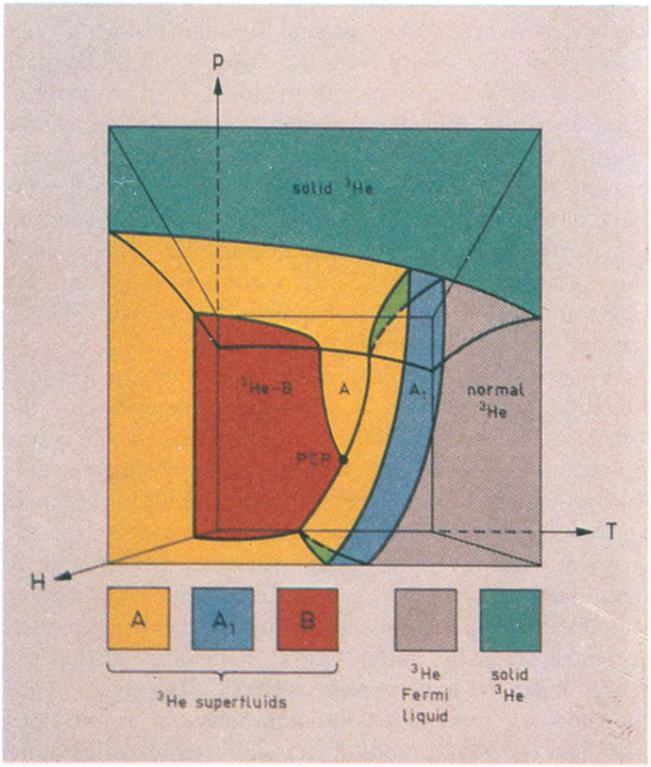

FIG. 3. Phase diagram of the low-temperature phases of stationary ^{3}He (Osheroff, Richardson, and Lee, 1972; Mermin and Lee, 1976). The zero-field cross section coincides with that in Fig. 1. Superfluid ^{3}He-B occurs at low temperatures and/or pressures, while superfluid ^{3}He-A is stabilized in a small region at high temperatures and pressures. With increasing magnetic field H, the A-phase regime increases at the expense of the B phase. In addition, the nonunitary superfluid ^{3}He-A_1 phase appears in a magnetic field between the A phase and the normal Fermi liquid in a narrow temperature regime. New superfluid phases nucleate inside the cores of quantized vortex lines in superfluid ^{3}He under rotation.

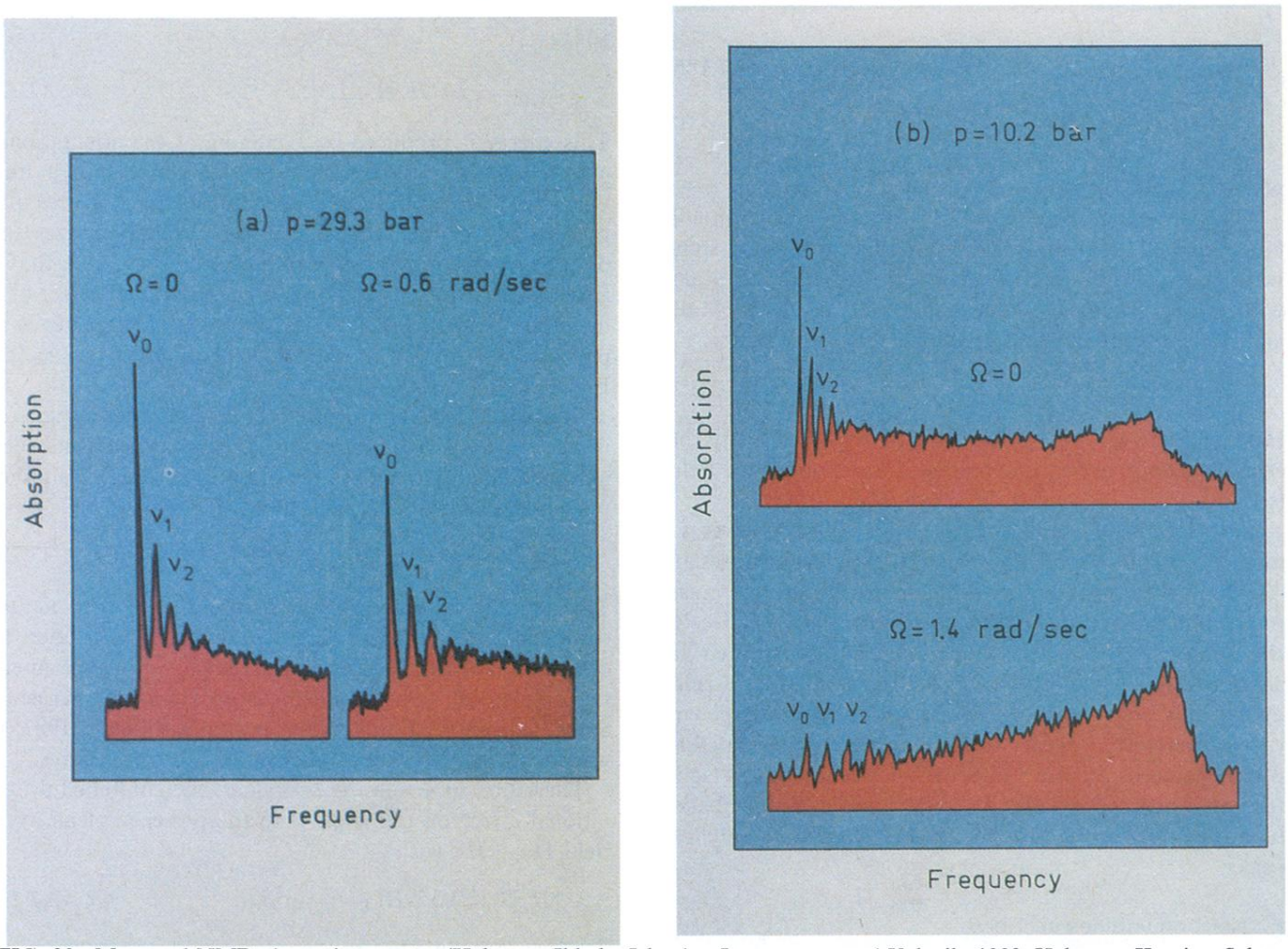

FIG. 30. Measured NMR absorption spectra (Hakonen, Ikkala, Islander, Lounasmaa, and Volovik, 1983; Hakonen, Krusius, Salmelin, Salomaa, Simola, Gongadze, Gurgenishvili, and Kharadze, 1987): (a) at $p=29.3$ bars for $T=0.45T_c$; (b) at $p=10.2$ bars for $T=0.50T_c$. Data are shown both in the stationary case and during rotation. The series of almost evenly spaced sharp spin-wave satellites results from the coherent nuclear motion of the Cooper-pair spins. The separation between the peaks at $\nu_0, \nu_1, \nu_2, \ldots$ is larger during rotation than in the stationary liquid. The envelope of the observed oscillatory curve corresponds to the flare-out textures in Fig. 29.

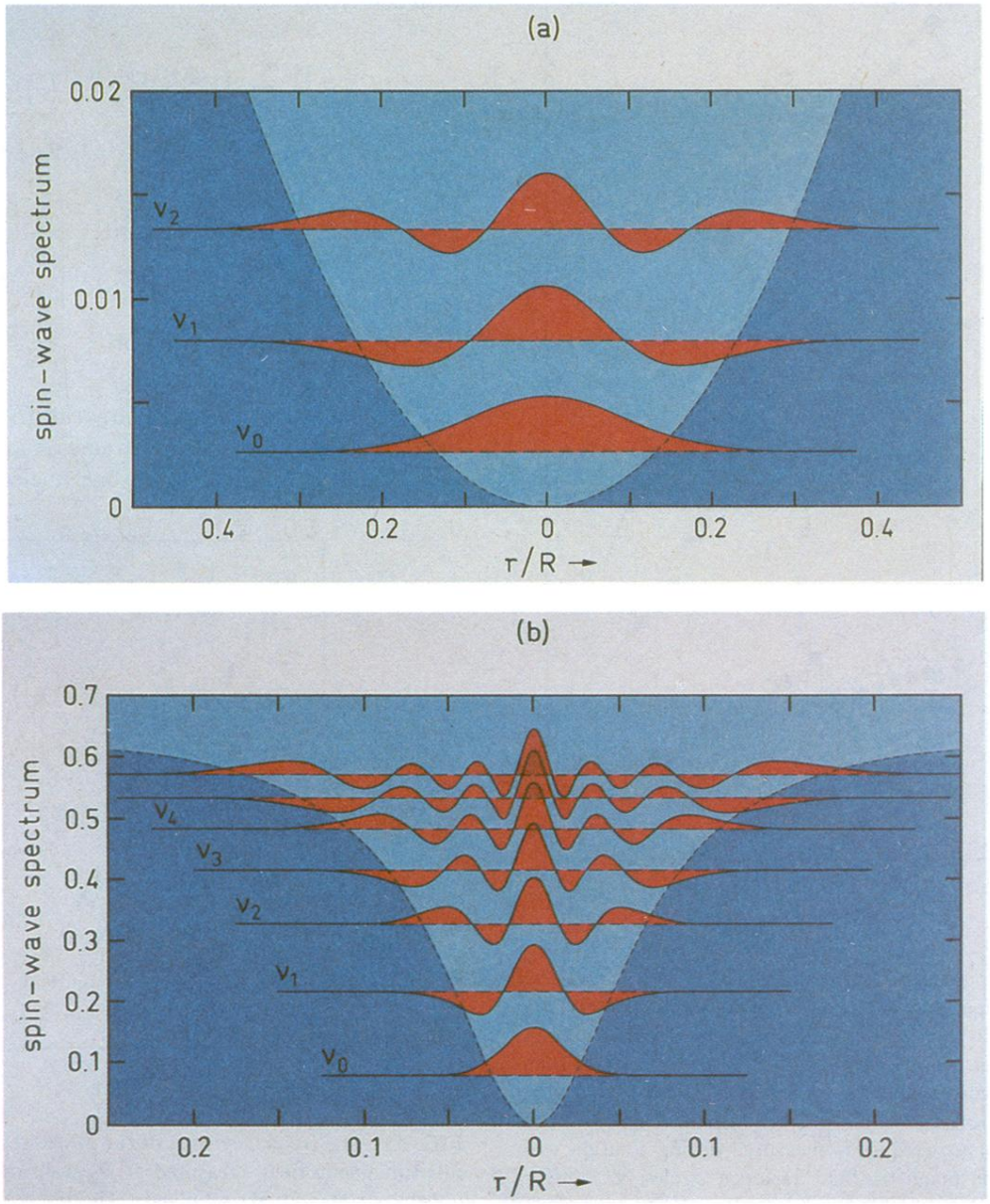

FIG. 31. The calculated spin-wave spectrum in the potential of the flare-out texture. (a) For $\lambda=0$ in the stationary state, the spectrum is very well approximated by that of a harmonic oscillator. (b) For large angular velocities of rotation (here $\lambda=10$), the $\beta(r)$ texture is strongly modified by rotation [see Fig. 29(b)], and the spectrum is no longer evenly spaced. [Dashed lines indicate $U(r)$, the spin-wave potential in Eq. (7.18c).]

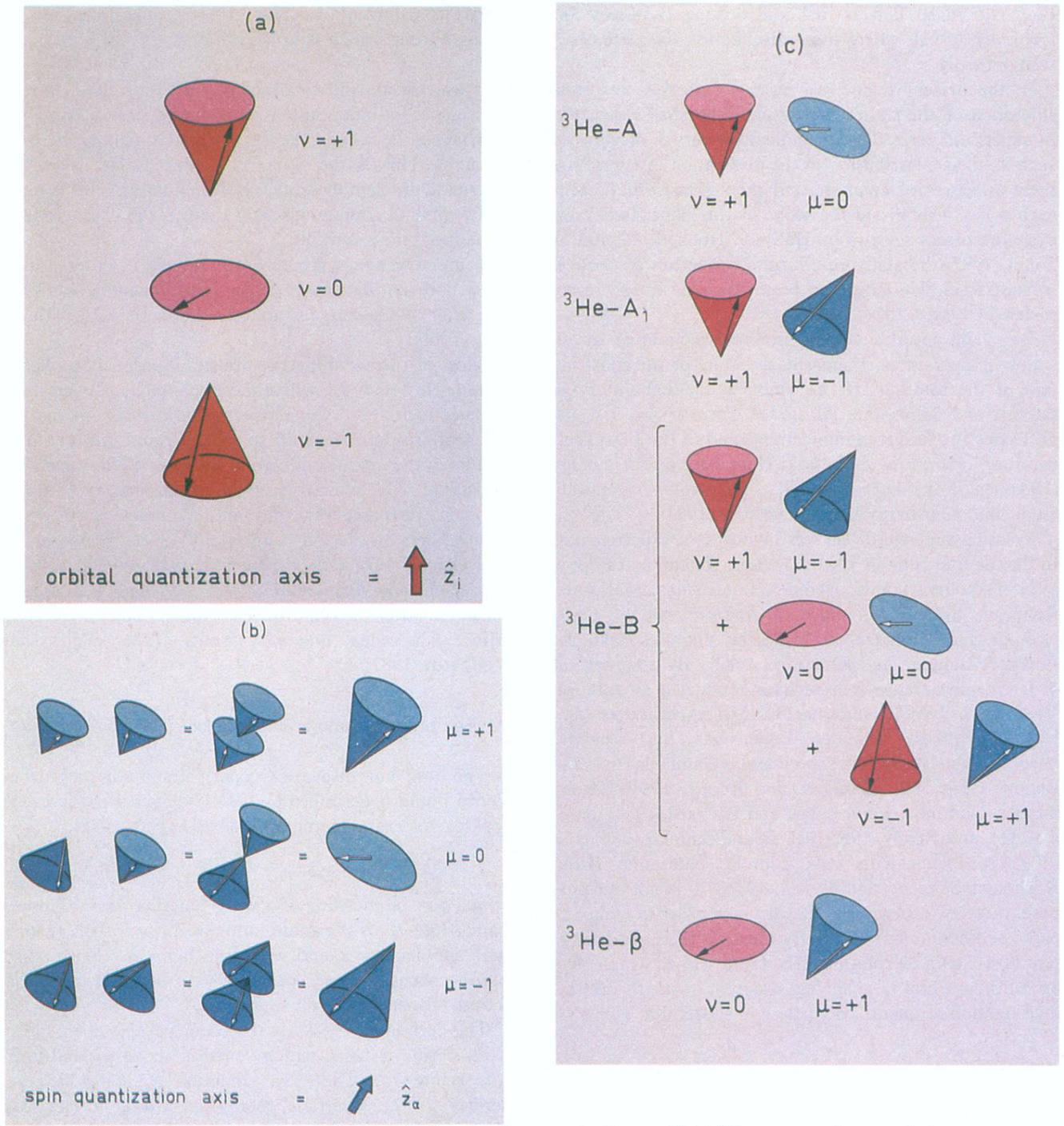

FIG. 4. (a) The relative motion of particles constituting the Cooper pairs in superfluid ^{3}He corresponds to a relative p-wave state ($L^{\text{int}}=1$), with the pair orbital angular-momentum projection L_z^{int} obtaining the three possible values $\nu=\pm1$ and 0. The orbital angular-momentum quantization axis is denoted by $\hat{z}_i$. (b) The Cooper-pair spins in superfluid ^{3}He are in a total triplet state ($S=1$). The projection S_z on the spin quantization axis $\hat{z}_\alpha$ may obtain the values $\mu=\pm1,0$. (c) The Cooper-pair structure in the superfluid A, A_1, B, and β phases of ^{3}He may be visualized as follows. In ^{3}He-A, the pair orbital-momentum projection is $\nu=+1$, while the pair spin projection is $\mu=0$; thus, the order parameter equals $\Psi=Y_{1,+1}\,|\uparrow\downarrow+\downarrow\uparrow\rangle$, where the first and second entries refer to the orbital and spin degrees of freedom, respectively, and $Y_{1,\nu}$ denote spherical harmonic eigenfunctions of $L^{\text{int}}=1$, with $L_z^{\text{int}}=\nu$. The direction of the pair orbital momentum defines the $\boldsymbol{l}$ vector in the A phase. The spin degrees of freedom are described by the magnetic anisotropy vector $\mathbf{d}$, on which the projection of the Cooper-pair spin is zero: $\mathbf{S}\cdot\mathbf{d}=0$. In ^{3}He-$A_1$, $\Psi=Y_{1,+1}\,|\uparrow\uparrow\rangle$, the pair orbital momentum projection $\nu=+1$, and only one spin projection is present, resulting in ferromagnetic nuclear spin alignment. In ^{3}He-B, $\Psi=Y_{1,+1}\,|\downarrow\downarrow\rangle+Y_{1,0}\,|\uparrow\downarrow+\downarrow\uparrow\rangle+Y_{1,-1}\,|\uparrow\uparrow\rangle$, the three possible orbital and spin projections occur with equal weight. Because of the broken relative spin-orbit symmetry, the quantization axes are coupled in equilibrium ^{3}He-B through an order-parameter matrix of rotation: $\hat{z}_\alpha=R_{\alpha i}\hat{z}_i$. In the spontaneously ferromagnetic β phase, $\Psi=Y_{1,0}\,|\uparrow\uparrow\rangle$, the roles of the orbital and spin degrees of freedom are conjugate to those in the A phase. This β phase has not been found to exist in the stationary bulk superfluid ^{3}He, but is theoretically found to nucleate in the axisymmetric v-vortex core in rotating ^{3}He-B. (See Fig. 38.)

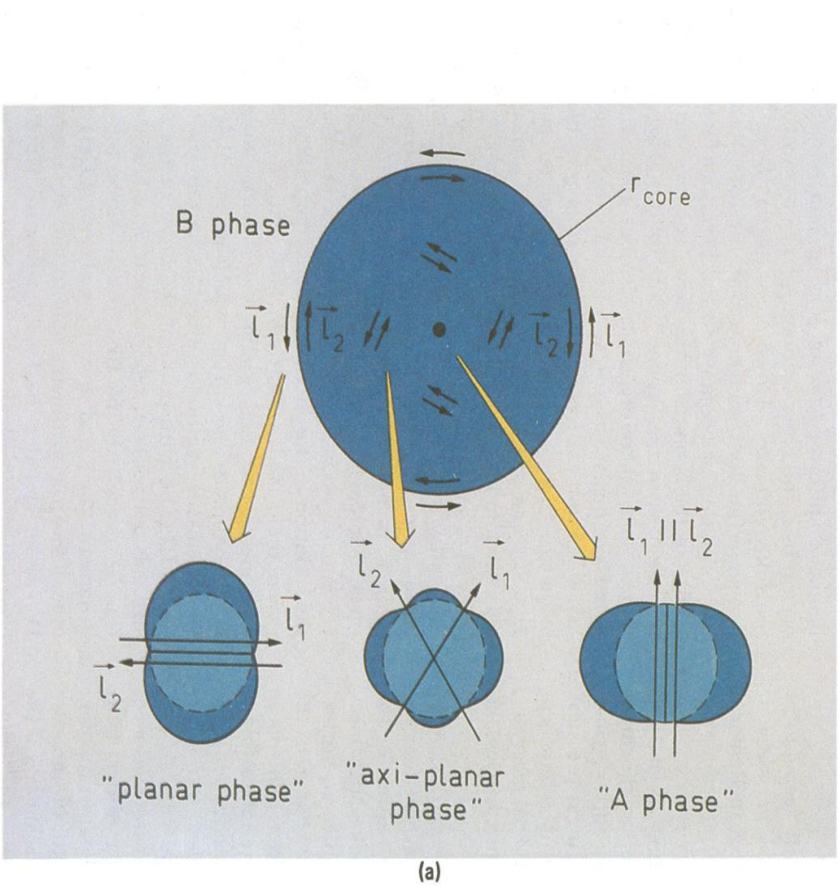

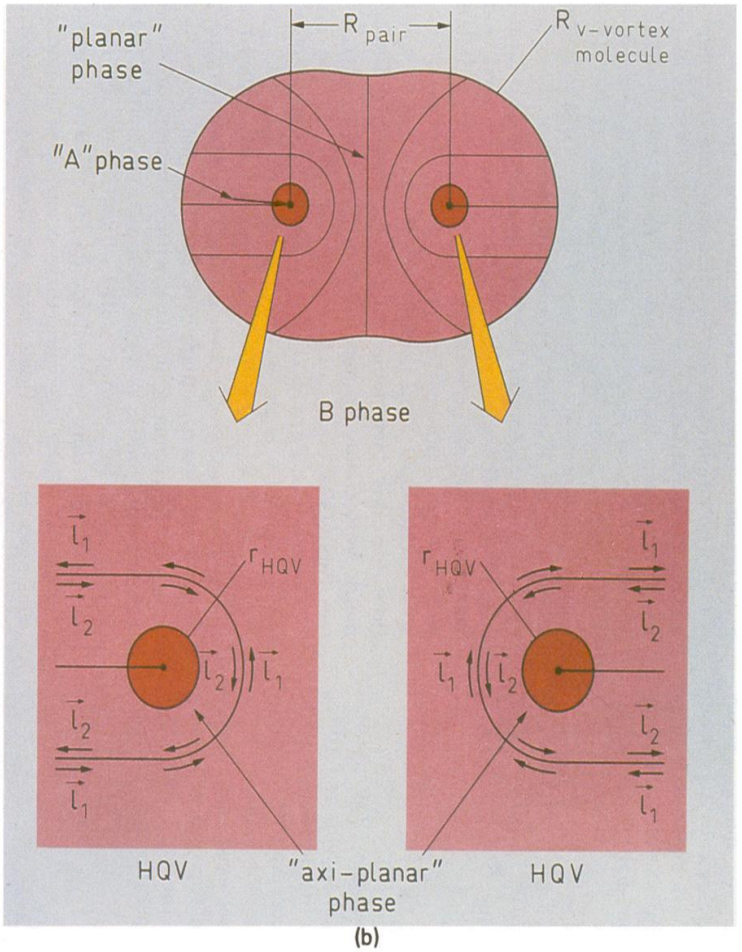

FIG. 53. Topological structure of the two vortices found to be stable in ^{3}He-B. (a) Topological structure of the energy gap in the cross-sectional plane of the axisymmetric v-vortex core (Salomaa and Volovik, 1985a), proposed to occur in rotating superfluid ^{3}He-B at high pressures. Point vortices, or boojums, on the Fermi sphere first appear in the "planarlike" phase at the distance r_{core}, signalling the radius at which the flaring out of vorticity from real space into momentum space first starts. Vorticity is supported in the core by the continuous winding—in the "axi-planar-like" phase—of the $\boldsymbol{l}$ vectors for the quasiparticles with spin projection up ($\boldsymbol{l}_1$) and for those with spin projection down ($\boldsymbol{l}_2$). As the $\boldsymbol{l}$ vectors "escape into the third dimension" (cf. Fig. 7 for an analogous situation in the MH texture), the vortex singularity "escapes into the fourth and fifth dimensions" in the $(\mathbf{r},\mathbf{k})$ space. They change from antiparallel at $r = r_{\text{core}}$ to parallel at $r = 0$ on the vortex axis, where the "A-phase-like" core occurs. This summarizes the inner structure of the core for vortex II in Fig. 2(b). The topological model for the core structure of the nonaxisymmetric v-vortex molecule (Salomaa and Volovik, 1986c), suggested to occur in rotating ^{3}He-B at low pressures (Thuneberg, 1986b; Volovik and Salomaa, 1985b). On the basis of their topological properties the two centers, separated by the distance R_{pair}, have been identified each as a half-quantum vortex (HQV) confined in the v-vortex molecule. Each HQV is accompanied by a disclination in the $\boldsymbol{l}$-vector field with half-integer winding number—or topological charge—which reverses $\boldsymbol{l}_1$ into $\boldsymbol{l}_2$ (and vice versa) on circling once around either HQV. The $\boldsymbol{l}$ vectors lie predominantly in the cross-sectional plane of the v-vortex molecule ("planarlike" phase). However, inside the inner cores of radius r_{HQV}, these vectors flare out of the plane, deviate from each other (in the "axi-planar-like" phase), and each covers one-quarter of the Fermi sphere. The spatial variation in the directions of the point vortices on the Fermi surface may be regarded as forming a string which topologically confines the HQV pair (vortex I in Fig. 2). This "bag" model of the v-vortex core "molecule" resembles the structure of hadrons with the half-quantum vortices corresponding to quarks.

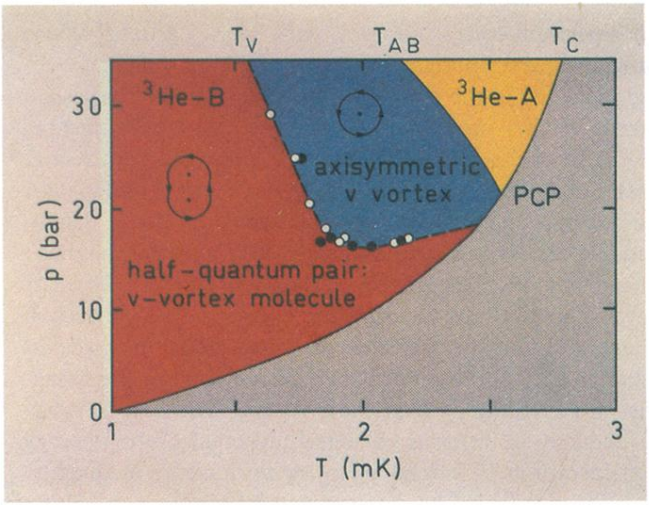

FIG. 54. Phase diagram of ^{3}He; compare with Fig. 1. According to our present understanding (Salomaa and Volovik, 1986c), we tend to identify the change in the vortex-core structure in ^{3}He-*B* as the *topological transition between two inequivalent ways in which vorticity can flare out* (Volovik and Mineev, 1982), illustrated in Figs. 53(a) and 53(b) for the axisymmetric and nonaxisymmetric vortices, both with v symmetry. The vortex-core transition signals this topological bifurcation in the escape of vorticity into the momentum space.